

Synthesis and Biomedical Applications of Gamma Peptide Nucleic Acid

Wei-Che Hsieh

*Submitted in Partial Fulfillment of the Requirements for the Degree of
Doctor of Philosophy*

Carnegie Mellon University

August 2018

Abstract

Nucleic acid is a promising material for biomedical applications due to its programmability and predictability of sequence binding. However, native nucleic acid itself could not be widely exploited in *in vivo* applications because of enzymatic degradation, weak and off-targeting binding and cellular delivery. Such issues could be potentially addressed by a novel synthetic nucleic acid analogue called Gamma Peptide Nucleic Acid (γ PNA), in which backbone is replaced with a gamma modified *N*-(2-aminoethyl)-glycine. Nonetheless, the biomedical applications of γ PNA will impede until the synthesis and binding properties are better investigated.

The presented work in this Dissertation first offers a robust synthetic strategy for preparing optically pure γ PNA monomers. The strategy utilizes a bulky temporary protecting group to shield the alpha proton of the aminoaldehyde intermediate and performs reductive amination to build the γ PNA backbone. As a result, the final monomers have enantiomeric excess more than 99.5% confirmed by HPLC and ^{19}F NMR. This methodology will facilitate the production of γ PNA for a wider range of applications.

Earlier, γ PNA is demonstrated to be preorganized into either right-handed (RH) or left-handed (LH) motifs by simply inverting the stereochemistry at γ position. The RH motif can bind to RH- γ PNA, unmodified PNA and native nucleic acid with exquisite binding affinity and sequence specificity, while the LH motif can only bind to LH- γ PNA and unmodified PNA. The second work presented in this Dissertation demonstrates that the sequence information embedded in conformationally orthogonal γ PNA can be interconverted by toehold-mediated strand displacement reaction. This work opens up the

opportunities for developing orthogonal molecular circuits to rapidly and sensitively detect genetic materials.

Designing a tight binding hybridization probe with high sequence specificity is challenging in that the probes are too stable to be sensitive to a base mispairing. Inspired by Nature's template-directed assembly, the third work presented in this Dissertation demonstrates a relatively weak binding MP γ PNA probe can be concatenated in the presence of disease-relevant RNA repeated expansions and becomes a tight binding and potentially selective hybridization probe. This work may benefit the development of future nucleic acid therapeutics.

Together, this Dissertation offers a robust synthetic strategy for preparing optically pure γ PNA monomers, systematically understands the binding relationships of γ PNA and provides a novel strategy to *in-situ* assemble tight binding probe with high sequence selectivity. This work envisions γ PNA as a versatile biomolecular self-assembly platform with control over sequence and helical sense and will hopefully facilitate the potential applications of γ PNA in diagnostics and therapeutics.

Acknowledgments

First of all, I would like to thank my advisor Prof. Danith Ly for his mentorship. His enthusiasm for novel science, hardworking, creativity and the “infamous” quotes affirm my belief for dedicating myself to improving people’s life. I would also like to thank my committee members Prof. Bruce Armitage, Prof. Kevin Noonan and Prof. James Schneider for their valuable and kind suggestions on my graduate work and my career.

Next, I would like to thank the Ly Lab family for their assistance and supports throughout my graduate study: Dr. Ashif Y. Shaikh for his diligence in testing different synthetic schemes; Dr. Gustavo R. Martinez for his great work in HPLC analysis and spectroscopic studies; Prof. Raman Bahal for his innovative work in γ PNA; Dr. Ramesh Batwal, Dr. Arunava Manna, Dr. Gopalsamy Sureshkumar, Dr. Shivaji A. Thadke, Dr. Anjan Banerjee, Dr. Alinakhi and Dinithi Perera for their suggestions in organic synthesis; Dr. Batool S. Haerian for her work in expressing RNA; Ashley Wang and Sharon Wu for their diligence in γ PNA synthesis; Raunaq Chamdia for his help in organic synthesis.

I would also like to thank all the collaborators who are willing to try our new ideas and materials in their research fields in the past 5 years,: Prof. Peter Glazer of Yale University and his lab members including Dr. Anisha Gupta and Dr. Adele Ricciardi; Prof. Hiroshi Sugiyama of Kyoto University and his graduate student Zutao Yu; Prof. James Schneider of Carnegie Mellon and his students Lingxiao (Bruce) Yan and Kimberly Hui; Prof. Fu-Sen Liang of University of New Mexico and his students including Dr. Umesh Bhattarai; Prof. Jennifer Grandis and Prof. Daniel Johnson of University of California, San Francisco; Prof. Alexander Deiters of University of Pittsburgh; Prof. David Zhang of Rice University and his students including Dr. Ping Song and Jin Bae.

I would like to thank staffs in Center for Molecular Analysis, CMU for their persistent efforts in maintaining core facilities, including Prof. Mark Bier, Logan Plath, Prof. Roberto Gil and Dr. Gayathri Withers. I also want to thank my neighboring groups for generously sharing chemicals and instruments for my studies, including the Achim group, the Noonan group, the Matyjaszewski group, the Bruchez group, the Das group, the Armitage group, the Collins group and the Bernhard group. I would also like to thank the Department office for their guidance throughout the graduate program, including Dr. Rea Freeland, Valerie Bridge, Brenda Chambers, Patsey Haddock, Beryl Omune, Tim Sager, Lorna Williams and Sara Wainer.

Lastly, I would like to appreciate my parents and my family for providing positive support and encouragement for my graduate work. I appreciate my wife Shao-Ling Wu for her willingness to join my journey in the USA and her enormous efforts in starting our family during my graduate study. I also appreciate my sons Finn and Ivan who did a great job at “conquering” my study desk and balancing my work with life.

Table of Contents

Abstract	ii
Acknowledgments	iv
Table of Contents	vi
List of Figures	ix
List of Schemes	xvii
List of Tables	xix
List of Appendices	xx
Chapter I: Introduction	1
1.1. Background	1
1.2. Chemically Modified Nucleic Acids	3
1.2.1. Modifications on Furanose	3
1.2.2. Modifications on Nucleobases	4
1.2.3. Modifications on Phosphodiester Backbone	5
1.3. Thesis Organization	11
1.3.1. Synthesis of γ PNA Monomers	11
1.3.2. Molecular Computing by γ PNA Platform	15
1.3.3. Design of Tight Binding Probes with High Sequence Specificity	17
1.4. References	18
Chapter II: A General Method for Preparing the Right- and Left- Handed Fmoc-MPyPNA Monomers with High Optical-Purity	29
2.1 Introduction	29
2.2. Results and Discussion	32
2.3. Conclusions	40
2.4. Experimental Sections	41
2.4.1. Material and Methods	41
2.4.2. Supplementary Schemes	42

2.4.3. Experimental Protocols	44
2.5. NMR, HRMS, GC and HPLC Data	63
2.6. References	104
Chapter III: Stereochemical Conversion of Nucleic Acid Circuits	107
via Strand Displacement	
3.1. Introduction	107
3.2. Design Rationale	110
3.3. Results	113
3.3.1. Recognition Orthogonality	113
3.3.2. Conformational Analysis	115
3.3.3. Thermal Stability	119
3.3.4. Strand Displacement Kinetics	122
3.3.5. Signal Transduction	126
3.4. Discussion	130
3.5. Experimental Protocols	132
3.5.1. PNA Monomer Synthesis	132
3.5.2. Oligomer Synthesis	132
3.5.3. UV-Melting Experiments	133
3.5.4. Circular dichroism analyses	133
3.5.5. Fluorescence Measurements	134
3.5.6. Gel Shift Assay	135
3.6. Appendices	136
3.7. References	146
Chapter IV: RNA-Templated Concatenation of Triplet Nucleic Acid Probe	150
4.1. Introduction	150
4.2. Results and Discussion	154
4.2.1. Probe Design	154
4.2.2. Synthesis of Probes	156

4.2.3. Conformational Flexibility	157
4.2.4. Concatenation in the Presence of RNA	161
4.3. Conclusions	165
4.4. Experimental Procedures	166
4.4.1. Solid-Phase Synthesis	166
4.4.2. HPLC Purification	168
4.4.3. MALDI-TOF MS Analysis	168
4.4.4. UV-Melting Experiments	168
4.5. Appendices	169
4.6. References	178

List of Figures

Chapter I: Introduction

- Figure I- 1. Watson-Crick base pairing. 2
- Figure I- 2. Common oligonucleotide structures with furanose modifications. **B:** Nucleobases. 4
- Figure I- 3. Representative examples of modified nucleobases. 5
- Figure I- 4. Representative examples of backbone modified nucleic acid analogues. 6
- Figure I- 5. Representative examples of cyclic PNA. 7
- Figure I- 6. Chemical Structures of α PNA and γ PNA. 8
- Figure I- 7. Backbone preorganization results in two helical motifs, the right-handed (RH) and the left-handed (LH)- γ PNA. Arrow directions: from *N*- to *C*- termini for γ PNA; from 5' to 3' ends for B-DNA. 9
- Figure I- 8. Representative Examples of γ PNA. 10

Chapter II: A General Method for Preparing the Right- and Left-Handed Fmoc-MP γ PNA Monomers with High Optical-Purity

- Figure II- 1. Fmoc-protected (*R*)- and (*S*)-MP γ PNA monomers being prepared by this method. 31
- Figure II- 2. Assessment of enantiomeric purity. ¹⁹F-NMR spectra of compounds **23** and **24**. The doublet pattern of each compound in **23** is the result of the formation of rotamers in d⁶-DMSO. 39
- Figure II- 3. Assessment of enantiomeric purity. HPLC chromatograms of compounds **23** and **24**. Undetectable peak overlapping was observed. HPLC Condition: C18 column (dimensions 4.6 mm X 250 mm), 1 mL/min flow rate, 60 °C oven temperature, 25 to 75% ACN/H₂O with 0.1% TFA in 30 min. 39
- Figure II-S 1. (A) ¹H NMR (500 MHz, DMSO) and (B) ¹³C NMR (125 MHz, DMSO) spectra of compound **4**. 63

Figure II-S 2. HRMS (ESI) spectrum of compound 4 .	64
Figure II-S 3. (A) ^1H NMR (500 MHz, DMSO) and (B) ^{13}C NMR (125 MHz, DMSO) spectra of compound 5 .	65
Figure II-S 4. HRMS (ESI) spectrum of compound 5 .	66
Figure II-S 5. (A) ^1H NMR (500 MHz, DMSO) and (B) ^{13}C NMR (125 MHz, DMSO) spectra of compound 8 .	67
Figure II-S 6. HRMS (ESI) spectrum of compound 8 .	68
Figure II-S 7. (A) ^1H NMR (500 MHz, DMSO) and (B) ^{13}C NMR (125 MHz, DMSO) spectra of compound 9 .	69
Figure II-S 8. HRMS (ESI) spectrum of compound 9 .	70
Figure II-S 9. (A) ^1H NMR (500 MHz, DMSO) and (B) ^{13}C NMR (125 MHz, DMSO) spectra of compound 10 .	71
Figure II-S 10. HRMS (ESI) spectrum of compound 10 .	72
Figure II-S 11. (A) ^1H NMR (500 MHz, DMSO) and (B) ^{13}C NMR (125 MHz, DMSO) spectra of compound 13 .	73
Figure II-S 12. GC chromatogram of compounds 12 (solid line) and 13 (dash line).	74
Figure II-S 13. (A) ^1H NMR (500 MHz, DMSO) and (B) ^{13}C NMR (125 MHz, DMSO) spectra of compound 15 .	75
Figure II-S 14. HRMS (ESI) spectrum of compound 15 .	76
Figure II-S 15. (A) ^1H NMR (500 MHz, DMSO) and (B) ^{13}C NMR (125 MHz, DMSO) spectra of compound 17 .	77
Figure II-S 16. HRMS (ESI) spectrum of compound 17 .	78
Figure II-S 17. (A) ^1H NMR (500 MHz, DMSO) and (B) ^{13}C NMR (125 MHz, DMSO) spectra of compound 19 .	79
Figure II-S 18. HRMS (ESI) spectrum of compound 19 .	80
Figure II-S 19. (A) ^1H NMR (500 MHz, DMSO) and (B) ^{13}C NMR (125 MHz, DMSO) spectra of compound 20a .	81
Figure II-S 20. HRMS (ESI) spectrum of compound 20a .	82
Figure II-S 21. (A) ^1H NMR (500 MHz, DMSO) and (B) ^{13}C NMR (125 MHz, DMSO) spectra of compound 20b .	83

Figure II-S 22. HRMS (ESI) spectrum of compound 20b .	84
Figure II-S 23. (A) ^1H NMR (500 MHz, DMSO) and (B) ^{13}C NMR (125 MHz, DMSO) spectra of compound 20c .	85
Figure II-S 24. HRMS (ESI) spectrum of compound 20c .	86
Figure II-S 25. (A) ^1H NMR (500 MHz, DMSO) and (B) ^{13}C NMR (125 MHz, DMSO) spectra of compound 20d .	87
Figure II-S 26. HRMS (ESI) spectrum of compound 20d .	88
Figure II-S 27. HRMS (ESI) spectra of (A) compound 20a-I and (B) compound 20b-I .	89
Figure II-S 28. HRMS (ESI) spectra of (A) compound 20c-I and (B) compound 20d-I .	90
Figure II-S 29. (A) ^1H NMR (500 MHz, DMSO) and (B) ^{13}C NMR (125 MHz, DMSO) spectra of compound 1a .	91
Figure II-S 30. HRMS (ESI) spectrum of compound 1a .	92
Figure II-S 31. (A) ^1H NMR (500 MHz, DMSO) and (B) ^{13}C NMR (125 MHz, DMSO) spectra of compound 1b .	93
Figure II-S 32. HRMS (ESI) spectrum of compound 1b .	94
Figure II-S 33. (A) ^1H NMR (500 MHz, DMSO) and (B) ^{13}C NMR (125 MHz, DMSO) spectra of compound 1c .	95
Figure II-S 34. HRMS (ESI) spectrum of compound 1c .	96
Figure II-S 35. (A) ^1H NMR (500 MHz, DMSO) and (B) ^{13}C NMR (125 MHz, DMSO) spectra of compound 1d .	97
Figure II-S 36. HRMS (ESI) spectrum of compound 1d .	98
Figure II-S 37. (A) ^1H NMR (500 MHz, DMSO) and (B) ^{13}C NMR (125 MHz, DMSO) spectra of compound 23 .	99
Figure II-S 38. (A) HRMS (ESI) and (B) ^{19}F NMR (470 MHz, DMSO) spectra of compound 23 .	100
Figure II-S 39. (A) ^1H NMR (500 MHz, DMSO) and (B) ^{13}C NMR (125 MHz, DMSO) spectra of compound 24 .	101
Figure II-S 40. (A) HRMS (ESI) and (B) ^{19}F NMR (470 MHz, DMSO) spectra of compound 24 .	102

Figure II-S 41. HPLC chromatograms of Mosher derivatives **S9** and **S10** made from Fmoc protected intermediates **S3** and **S7**. e.e. value= 95%. HPLC Condition: C18 column (dimensions 4.6 mm X 250 mm), 1 mL/min flow rate, 25 °C oven temperature, 25 to 75% ACN/H₂O with 0.1% TFA in 30 min. 103

Chapter III: Stereochemical Conversion of Nucleic Acid Circuits via Strand Displacement

Figure III- 1. Molecular design. Chemical structure of a (i) right-handed RH- γ PNA, (ii) left-handed LH- γ PNA, and (iii) non-helical NH-PNA. 110

Figure III- 2. (A) Strand displacement reactions involving (i) a contiguous template, and (ii) a template with a disrupted PEG-spacer. TS: Template Strand (15-nts), DS: Displacement Strand (10-nts), and IS: Invading Strand (15-nts). (B) Predicted helical senses of TS-DS molecular converters containing (i) a contiguous template, and (ii) a template with PEG-spacer. 111

Figure III- 3. Chemical compositions of TS, DS, and IS. DNA oligonucleotides D1, D2, and D3 were included for comparison. 112

Figure III- 4. Recognition orthogonality. (A) Depiction of HCR components. (B) HCR cascade. (C) Sequence compositions of hairpins and initiators. 113

Figure III- 5. Result of HCR following the addition of I1 (lanes 5 and 6), I3 (lanes 7 and 8), and I2 (lanes 9 and 10) to a mixture containing an equimolar ratio of H1A and H1B (lane 4) and incubation at 25 °C for 16 hrs. The concentrations of H1A and H1B were 1 μ M each. The samples were prepared in a PBS buffer (50 mM Na₂HPO₄, 138 mM NaCl, 2.7 mM KCl, pH 7.4), separated on a 10% non-denaturing PAGE, and stained with SYBR-Gold. 114

Figure III- 6. UV-absorption profiles of P1a, P1b, P2a, P2b, P3a, P3b, P3c, and P3d at 5 μ M strand concentration each recorded at 95 °C. 115

- Figure III- 7. Conformational preorganization. **(A)** CD spectra of DS and IS components, along with that of the corresponding TS-DS (P1a-P2a and P1a-P2b) and TS-IS (P1a-P3a, P1a-P3c, and P1a-P3d) duplexes (*Inset*). **(B)** CD profiles of P1a, P1b, and P3a at 5 μ M strand concentration each, recorded at room temperature. Notice that these oligomers did not have backbone modifications. 116
- Figure III- 8. **(A)** UV-absorption profiles of P1a-P2a, P1b-P2a, P1a-P2b, and P1b-P2b duplexes at equimolar (5 μ M) strand concentration each recorded at 95 $^{\circ}$ C. Conformational preorganization **(B)** Comparison of the CD spectra of TS-DS duplexes without (P1a-P2a and P1a-P2b) and with PEG-spacer (P1b-P2a and P1b-P2b) in the template. *Inset*: TS-IS duplexes without (P1a-P3c and P1a-P3d) and with PEG-spacer (P1b-P3c and P1b-P3d) in the template. The samples were prepared in a PBS buffer, and the data were recorded at 25 $^{\circ}$ C. The concentration of each strand was 5 μ M. 118
- Figure III- 9. Representative UV-melting profiles TS-DS (P1a-P2a) and TS-IS (P1a-P3a and P1a-P3c) duplexes. Depiction of TS-IS and TS-DS duplexes without PEG-spacer, along with their T_{ms} . The samples were prepared in PBS buffer and annealed at 95 $^{\circ}$ C for 5 min prior to subjecting to heating runs and determination of their T_{ms} . 119
- Figure III- 10. UV-melting profiles of P1a-P2b and P1b-P2b duplexes at equimolar (1 μ M) strand concentration. This demonstrated the introduction of a PEG-spacer in TS has little effect on the thermal stability of TS-DS. 120
- Figure III- 11. UV-melting profiles of P1a-P3a, P1a-P3b, P1b-P3a and P1b-P3b duplexes. The samples were prepared in PBS buffer and annealed at 95 $^{\circ}$ C for 5 min prior to subjecting to heating runs and determination of their T_{ms} . 120
- Figure III- 12. Strand displacement reactions. **(A)** Electrophoretic mobility of TS (P1a), DS (P2a and P2b), and IS (P3a and P3c) in 2% agarose gel 121

and after staining with SYBR-Gold. Values in the parentheses indicate the number of nucleotides in each strand and the helical sense. **(B)** Results of strand displacement reactions. The concentration of each component was 10 μM , prepared in a physiologically relevant buffer. Strand displacement was allowed to take place for 1 hr at 37 $^{\circ}\text{C}$.

Figure III- 13. Representative strand displacement reactions of TS-DS (P1a-P2b) 122
by IS (P3a, P3c, and P3d).

Figure III- 14. The kinetics of strand displacements. **(A)** Fluorescent 123
measurements of the strand displacement reactions as a function of time. *Inset:* Result showing that a DNA invading strand (D3) was unable to displace P2b from P1a. **(B)** Comparison of the strand displacement reactions between the conformationally-matched (1 and 2) and mismatched (3 and 4) IS and DS. The concentrations of TS-DS duplexes were 100 nM and those of IS were 1 μM (10-fold excess). The samples were prepared in PBS buffer, and the reactions were carried out at 37 $^{\circ}\text{C}$. Excitation was made 344 nm, and the emissions were recorded at 480 nm.

Figure III- 15. The effects of PEG-spacer and temperature on the rates of strand 125
displacement. Kinetic profiles of strand displacement **(A)** with and without PEG-spacer, and **(B)** at variable temperatures. The samples were prepared the same way as mentioned in **Figure III- 14** caption.

Figure III- 16. Signal transduction by molecular converter. **(A)** Sequences of 127
DNA reporter and off-target DNA DQ1. **(B)** Illustration of molecular conversion in the presence of DQ1 by an LH-input. **(C)** Fluorescent profiles of signal transduction. The reactions were carried out at 20 $^{\circ}\text{C}$ to minimize the dissociation of DQ1. Wavelengths ($\lambda_{\text{ex}}= 648 \text{ nm}$ and $\lambda_{\text{em}}= 668 \text{ nm}$) and slit sizes ($\text{Ex}= 5 \text{ nm}$ and $\text{Em}= 5 \text{ nm}$).

Figure III- 17. Signal transduction with RH- γ PNA. (A) Sequences of DNA reporter and off-target DNA DQ2. (B) Illustration of molecular conversion in the presence of DQ2 by an RH-input. (C) Fluorescent profiles of signal transduction. The reactions were carried out at 20 °C. Wavelengths (λ_{ex} = 648 nm and λ_{em} = 668 nm) and slit sizes (Ex= 5 nm and Em= 5 nm).	129
---	-----

Chapter IV: RNA-Templated Concatenation of Triplet Nucleic Acid Probe

Figure IV- 1. Mechanism of native chemical ligation reaction.	152
Figure IV- 2. Concatenation of two MP γ PNA units to form a product with a native amide backbone.	153
Figure IV- 3. Chemical Structures of (A) MP γ PNA probes and (B) CUG RNA repeat expansions.	155
Figure IV- 4. MALDI-TOF spectrum of P2 at 1 μ M concentration after incubation with DTT (100 μ M) at an ambient temperature for 1 hr. <i>Inset</i> : MS spectrum of P2 (M = 1468 Daltons). The M-120 peak corresponds to the reduced acyclic P2*, and the 1128-Dalton peak to the cyclic cP2.	158
Figure IV- 5. MALDI-TOF spectra of (A) P2 and (B) P3 at 1 μ M each, following the incubation with DTT (100 μ M) at 37 °C. The samples were analyzed at the indicated time-points. Square: parent P2 and P3 probes, opened circle: reduced acyclic P2* and P3*, and filled circle: cyclic cP2 and cP3 products. Each chemical entity has two masses, corresponding to that of the parent probe and that containing a potassium ion (+39 Dalton).	159
Figure IV- 6. MALDI-TOF spectrum of P2 probe. The sample was analyzed after incubation with DTT (100 μ M) at 37 °C for 5 hrs. Notice that only the cyclic product was observed.	160
Figure IV- 7. UV-melting profiles of RNA targets. The concentrations of RNAs were as followed 12 μ M (T1), 6 (T2), 3 (T4), 1.5 (T8), and 1	161

(T12), prepared in a physiologically relevant buffer. Note that the concentration of CUG-binding sites in each sample was the same (12 μM).

- Figure IV- 8. UV-melting profiles of T12 and [T12+P2+DTT] samples, with the latter recorded after incubation at an ambient temperature and at 37 °C for 1 hr. The concentration of T12 was 1 μM (corresponding to 12 μM binding sites of P2); P2, 12 μM ; and DTT, 100 μM . The samples were prepared by incubating the pre-annealed T12 with P2 and DTT at the indicated temperatures for 1 hr before subjecting to UV-melting analyses. *Inset*: UV-melting profiles of the negative controls carried out under identical conditions 162
- Figure IV- 9. UV-melting profiles of T12 with P4 and P5 in the presence of DTT. The concentrations of T12, P4, P5, and DTT were 1, 12, 12, and 100 μM , respectively. The mixtures were incubated at 37 °C for 1 hr prior to subjecting to UV-melting analyses. 163
- Figure IV- 10. MALDI-TOF spectrum of T12 with P2 and DTT after their incubation at 37 °C for 1 hr. The concentrations of T12, P2, and DTT were 1, 12, and 100 μM , respectively. 164

List of Schemes

Chapter I: Introduction

- Scheme I- 1. Synthesizing γ PNA monomers by Mitsunobu-Fukuyama condition with a representative example of Boc-L-MP γ PNA. 12
- Scheme I- 2. Synthesizing γ PNA monomers by *N*-alkylation reaction with a representative example Boc-L- γ -(*S*)-amPNA. 13
- Scheme I- 3. Synthesizing γ PNA monomers by reductive amination with a representative example Boc-L-alanine-based γ PNA. 13

Chapter II: A General Method for Preparing the Right- and Left-Handed Fmoc-MP γ PNA Monomers with High Optical-Purity

- Scheme II- 1. Synthesis of Boc-protected MP γ PNA monomer by Mitsunobu-mediated reaction. 33
- Scheme II- 2. Synthesis of intermediate **10** from L-serine methyl ester **3**. 35
- Scheme II- 3. Synthesis of (**A**) 9-(4-bromophenyl)-9-fluorenyl bromide (**13**) and (**B**) 2-(2-(tert-butoxy)ethoxy)ethyl 4-methylbenzenesulfonate (**17**). 36
- Scheme II- 4. Synthesis of Fmoc-protected MP γ PNA from intermediate (**10**). 37
- Scheme II-S 1. An attempt to use Fmoc protecting group for preparing γ PNA monomers. The final product **S9** and **S10** exhibited 95% ee. See **Figure II-S 39** for optical purity results. 42
- Scheme II-S 2. An attempt to use Dibenzyl protecting group for preparing γ PNA monomers. The hydrogenation condition cannot be applied to cytosine due to over reduction. 43

Chapter IV: RNA-Templated Concatenation of Triplet Nucleic Acid Probe

Scheme IV- 1. Reaction pathways of the triplet MP γ PNA probe. **(A)** Probe in the oxidized state (in the extracellular environments). **(B)** Probe in the reduced state (in the intracellular environments) in the presence of RNA target. **(C)** Probe in the reduced state in the absence of target.

List of Tables

Chapter II: A General Method for Preparing the Right- and Left-Handed Fmoc-MPyPNA Monomers with High Optical-Purity

Table II- 1. Screened conditions for Buchwald amination. All reactions were performed with 0.06 eq of Pd(OAc)₂ in toluene (0.1M) for 22 hr with the above indicated reagents in the table. Temperature was set at 80 °C to mitigate racemization issue. ^a: TLC yield. 35

List of Appendices

Chapter III: Stereochemical Conversion of Nucleic Acid Circuits

via Strand Displacement

Appendix III- 1. (A) HPLC profile and (B) MALDI-TOF MS spectrum of P1a.	136
Appendix III- 2. (A) HPLC profile and (B) MALDI-TOF MS spectrum of P1b.	137
Appendix III- 3. (A) HPLC profile and (B) MALDI-TOF MS spectrum of P2a.	138
Appendix III- 4. (A) HPLC profile and (B) MALDI-TOF MS spectrum of P2b.	139
Appendix III- 5. (A) HPLC profile and (B) MALDI-TOF MS spectrum of P3a.	140
Appendix III- 6. (A) HPLC profile and (B) MALDI-TOF MS spectrum of P3b.	141
Appendix III- 7. (A) HPLC profile and (B) MALDI-TOF MS spectrum of P3c.	142
Appendix III- 8. (A) HPLC profile and (B) MALDI-TOF MS spectrum of P3d.	143
Appendix III- 9. UV-absorption profiles of P1a-P2a, P1a-P2b, P1a-P3a, P1a-P3c, and P1a-P3d duplexes at equimolar (5 μ M) strand concentration, recorded at 95 $^{\circ}$ C. The high temperature was employed to dissociate the indicated duplexes.	144
Appendix III- 10. Fluorescence spectra of P1a-P2a and P1a-P3d duplexes. Concentrations: P1a= 60 nM, P2a= 72 nM, P3d= 120 nM. Samples were annealed at 95 $^{\circ}$ C and followed by gradual cooling to room temperature in 1 hr. The samples were then incubated at 37 $^{\circ}$ C for 5 min before fluorescent measurements with wavelengths (λ_{ex} = 350 nm and λ_{em} = 480 nm) and slit sizes (Ex= 5 nm and Em= 10 nm).	145

Chapter IV: RNA-Templated Concatenation of Triplet Nucleic

Acid Probe

Appendix IV- 1. Synthesis of cysteine-containing C and X monomers.	169
Appendix IV- 2. Inverted deletions occur due to the flexibility of the achiral PNA backbone unit, which permits rapid intramolecular cyclization reaction.	170
Appendix IV- 3. On-resin synthesis of a representative P2 probe. In Step (D), after TFA deprotection and solvent rinses, coupling solution	171

was directly agitated with resin for 15 min without pyridine rinse.

- Appendix IV- 4. MALDI-TOF spectra of (A) P2, (B) P3, (C) P4, and (D) P5. 172
(E) Chemical structures of P2 through 5. Calc. M.W. (M.W. found): P2, 1468 Daltons (1465 Daltons); P3, 1659 (1657); P4, 1451 (1448); and P5, 1459 (1457).
- Appendix IV- 5. HPLC trace of crude P2. *Inset*: reinjection of purified P2. 173
- Appendix IV- 6. Reaction sequence of P2 probe. 174
- Appendix IV- 7. Reaction progress of P2. P2, parent probe; P2*, reduced acyclic form of P2; cP2, cyclic product of P2. P2 and P2* (with the latter starting from 0.5 hr) followed exponential decays, and cP2 followed exponential growth. Square, opened circle, and filled circle: experimental data, line: curve-fitting. 175
- Appendix IV- 8. Reaction progress of P3. P3, parent probe; P3*, reduced acyclic form of P3; cP3, cyclic product of P3. P3 followed exponential decay, and P3* (starting from 1 hr) and cP3 followed sigmoidal decay and growth profiles, respectively. Square, opened circle, and filled circle: experimental data, line: curve-fitting. 176
- Appendix IV- 9. UV-melting profiles of RNAs with P2 and DTT. The concentration of RNAs were: 12 μ M (T1), 6 (T2), 3 (T4), 1.5 (T8), and 1 (T12); and that of P2 and DTT were 12 μ M and 100 μ M, respectively. The mixtures were incubated at 37 °C for 1 hr prior to subjecting to UV-melting analyses. 177

Chapter I: Introduction

1.1. Background

Nucleic acid, especially deoxynucleic acid (DNA), is an attractive biomedical material. Besides its evolutionary role for carrying genetic information, DNA holds great promise to rationally design biologically irrelevant macrostructures ranging from nanometers to millimeters. This success comes from two key elements: First, the double helical structure of DNA suggested by Watson and Crick provides the “code” to program macrostructures, which consists of hydrogen-bonding interactions between adenine (A) and thymine (T) and between guanine (G) and cytosine (C).^{1,2} (**Figure I- 1**) Second, the deep and quantitative understanding of DNA thermodynamics^{3,4} in conjunction with computational algorithms⁵⁻⁷ makes it possible to reliably predict how DNA fold and interact with one another. Since the seminal work of Chen and Seeman⁸ in the early 1980s for building DNA self-assembly crystals, DNA has been rationally utilized in the bottom-up construction of a variety of macromolecular systems, including macrostructures such as polymeric materials,^{9,10} nanoparticles,^{11,12} DNA tiles and origami¹³⁻²²; and dynamic devices such as molecular circuits,^{23,24} autonomous nanoscale machines,²⁵⁻²⁸ information storage²⁹⁻³¹ and molecular computation.³²⁻³⁶

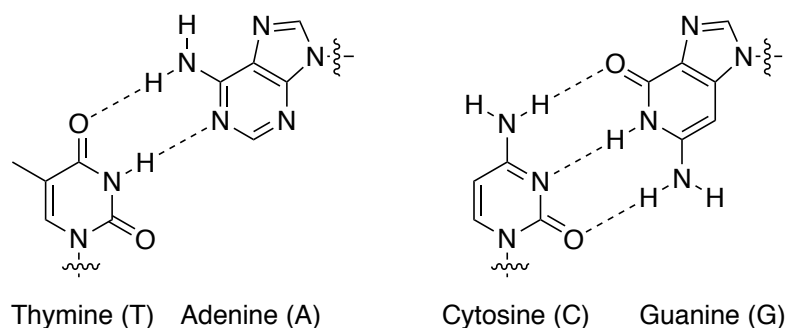


Figure I- 1. Watson-Crick base pairing.

On the other hand, nucleic acid has long been pursued as a molecular biology tool for target-responsive smart therapeutics^{37,38}, drug delivery systems^{39,40}, imaging⁴¹ and gene regulation.⁴² However, when applied to cellular environment, nucleic acid often faces issues such as enzymatic degradation, weak or off-target binding and cellular delivery. Interestingly, all these issues could be potentially solved by novel chemical modifications on nucleic acid structure. Therefore, the next section of this Chapter will provide a brief overview on how chemical modifications can impact the biophysical properties of nucleic acid. It will emphasize a unique nucleic acid analogue, called gamma peptide nucleic acid (γ PNA) for its innovatively endowed biophysical properties. The last section of this Chapter will outline three challenges faced when applying γ PNA to molecular self-assembly applications, which will be addressed by the next three Chapters of this Dissertation.

1.2. Chemically Modified Nucleic Acids

In attempts to modulate the properties of nucleic acid– nuclease stability, binding affinity and specificity and cellular uptake, nucleic acids are amenable to be chemically modified on the furanose sugar, the nucleobase and the phosphodiester backbone.

1.2.1. Modifications on Furanose

2'-Modified RNA. The two most commonly modifications at the 2'-OH position are 2'-*O*-methyl (2'-OMe) and 2'-*O*-methoxy ethyl (MOE).⁴³ (**Figure I- 2**) The 2' modifications with such electron-withdrawing groups induce the conformational equilibrium of the furanose ring toward the RNA-like C3'endo structure, which induces slightly better affinity toward complementary RNA. It has improved nuclease stability and less toxicity.⁴⁴

Locked Nucleic Acid (LNA). Similar to 2'-modified RNA, a methylene bridge introduced between the 2' oxygen of the ribose and the 4'-carbon locks the sugar conformation as the C3'endo structure. The modified nucleic acid is known as locked nucleic acid (LNA).⁴⁵ (**Figure I- 2**) The key linkage confers stronger binding affinity (+5 to +9 °C per incorporation), great enzymatic resistance and cellular uptake.^{46,47} However, it showed increasing risk for causing hepatotoxicity.^{48,49}

Mirror-Image Oligonucleotides. The (L)-(deoxy)ribonucleic acid exhibits similar solubility, hybridization kinetics and duplex thermal stability to the native (D)-form, but cannot be recognized by nucleases.⁵⁰⁻⁵³ (**Figure I- 2**) However, it was observed to bind to native nucleic acid under certain conditions, so careful considerations have to be made for sequence design.^{50,54}

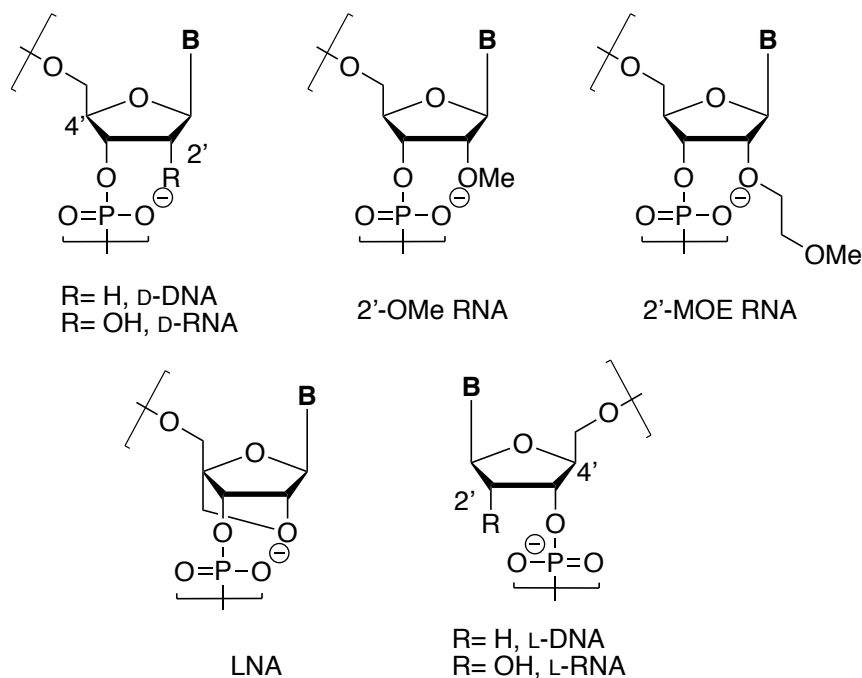


Figure I- 2. Common oligonucleotide structures with furanose modifications. **B:** Nucleobases.

1.2.2. Modifications on Nucleobases

The G-clamp base (X) is a cytosine analogue. (**Figure I- 3**) Unlike cytosine forming 3 H-bonds with guanine, G-clamp can form 5 H-bonds with guanine by the extra two through Hoogsteen base pairing.⁵⁵ Additionally, the tricyclic phenoxazine rings offers extended surface area for base stacking, which together significantly enhances thermal stability per incorporation.^{56,57} Besides G-clamp, diaminopurine (D) can form three H-bonds with thymine and enhance thermal stability by ~ 1.5 °C per incorporation.^{58,59} Other modified purines include the N^2 -imidazolylpropyl and N^2 -aminopropyl analogues of guanine. The cationic groups form electrostatic interactions with the phosphate backbone in the major groove of DNA and enhance duplex thermal stability by 1 to 3.3 °C per incorporation.^{60,61}

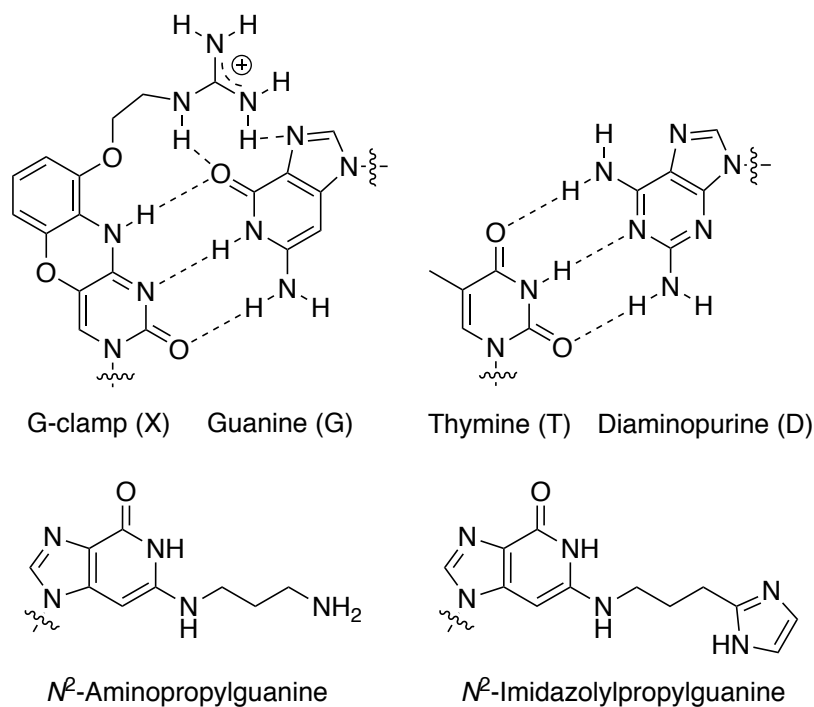


Figure I- 3. Representative examples of modified nucleobases.

1.2.3. Modifications on Phosphodiester Backbone

Phosphorothioate (PS). The phosphorothioate (PS) replaces the non-bridging oxygen in the phosphate group with a sulfur atom. (**Figure I- 4, left**) De Clercq et al. developed the first phosphorothioate analogs and showed improved enzymatic stability.⁶² However, phosphorothioates in general have a slightly lower binding affinity for complementary DNA or RNA targets as compared to the natural counterparts (– 0.5 °C per incorporation). Therefore, it requires a longer sequence to achieve a desired affinity for practical applications.⁶³ Additionally, incorporation of the sulfur atom introduces chirality at the phosphate group and causes heterogeneity in nuclease stability and binding affinity. The Sp form is more nuclease stable than the Rp form, but less thermally stable to complementary sequences.⁶⁴ Lastly, phosphorothioates have showed cytotoxic side effects due to the interactions with endogenous proteins.⁶⁵⁻⁶⁷

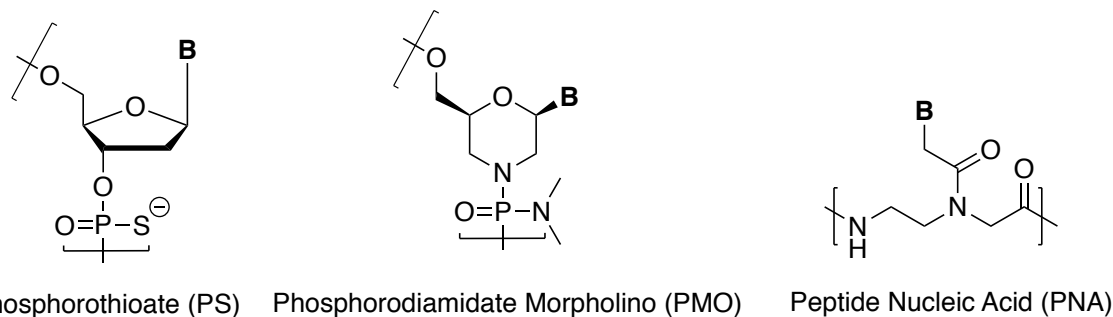


Figure I- 4. Representative examples of backbone modified nucleic acid analogues.

Phosphorodiamidate morpholino (PMO). Phosphorodiamidate morpholino oligomers replace the phosphodiester backbone with a phosphorodiamidate linkage and the ribofuranose ring with a morpholino ring.⁶⁸ (**Figure I- 4, middle**) The neutral backbone confers high enzymatic resistance and enhanced binding affinity as compared to the natural counterparts. However, it poorly traverses the cell membrane and requires other methods for cellular delivery.⁶⁹

Peptide nucleic acid (PNA). PNA replaces the natural sugar-phosphodiester backbone with the achiral *N*-(2-aminoethyl)glycine units, seminally reported by Nielsen et al. in 1991.⁷⁰ (**Figure I- 4, right**) PNA hybridizes to DNA and RNA with high affinity and sequence selectivity and resists enzymatic degradation.⁷¹ One unique feature of PNA is that it can invade double-stranded DNA when the target sequences are mostly purine- and pyrimidine-rich targets⁷¹, or when the mixed sequences are within unstable dsDNA helical regions.⁷²⁻⁷⁵ This opens up the opportunities to manipulate gene expression at the transcriptional level.^{76,77}

In real practice, PNA suffers from some limitations. PNA tends to fold into complex globular structures, presumably due to the collapse of the hydrophobic nucleobases.⁷⁸ Therefore, PNA tends to aggregate and nonspecifically adhere to surfaces and biomolecules. Additionally, the charge-neutral backbone confers poor cellular uptake for

in vivo applications.⁷⁹ Further synthetic efforts have been made to endow PNA with improved biophysical properties.⁸⁰⁻⁸² In general, the backbone modifications can be classified into two categories, cyclic and acyclic.

Cyclic backbone. Cyclic backbone has been pursued in order to preorganize the achiral flexible PNA backbone into helical structure.⁸⁰ (**Figure I- 5**) The tcypPNA replaces the ethylene portion of PNA with a *trans*-cyclopentyl group and restrains the backbone to better accommodate DNA and RNA.⁸³ Similarly, α/β dipeptide replaces the PNA backbone with a dimer of D-proline and a cyclic β -amino acid, resulting in strong mismatch discrimination and binding affinity.⁸⁴

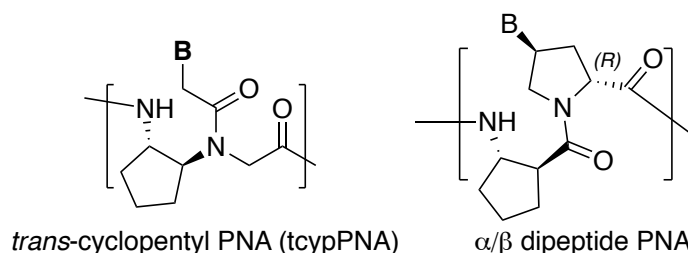


Figure I- 5. Representative examples of cyclic PNA.

Acyclic backbone.

α PNA. Introduction of stereogenic centers at alpha backbone results in α PNA. (**Figure I- 6, left**) In general, α PNA/DNA complexes have slightly less thermal stability than PNA/DNA complexes.⁸⁵ However, incorporation of cationic side chains, such as lysine and arginine, can enhance the thermal stability through electrostatic interactions with phosphate charge of DNA.^{86,87} Lastly, cellular uptake of α PNA can be improved by guanidium groups⁸⁸ and *N*-acetylgalactosamine.^{88,89}

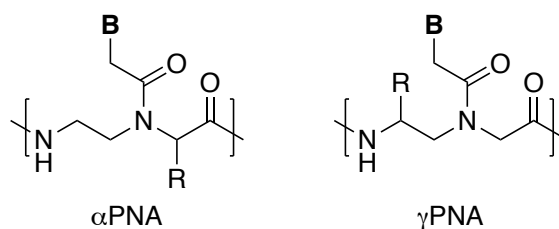


Figure I- 6. Chemical Structures of α PNA and γ PNA.

γ PNA. Among all chemically modified nucleic acids, γ PNA is perhaps the most promising analogue that can improve enzymatic resistance, binding affinity, sequence specificity and cellular delivery simultaneously by relatively simple chemical synthesis. (**Figure I- 6, right**) The substituents at gamma backbone positions induce steric clash with the substituents on the tertiary amines and preorganize backbone into either right-handed (RH) or left-handed (LH) motif.⁹⁰ (**Figure I- 7**) The LH motif cannot bind to physiologically relevant complementary B-DNA due to conformational mismatching.⁹¹ On the other hand, the RH motif can bind to RH- γ PNA, unmodified PNA and native nucleic acid with exquisite binding affinity and sequence specificity. Unlike unmodified PNA, the RH- γ PNA can invade double helical DNA or RNA without sequence restriction.^{92,93}

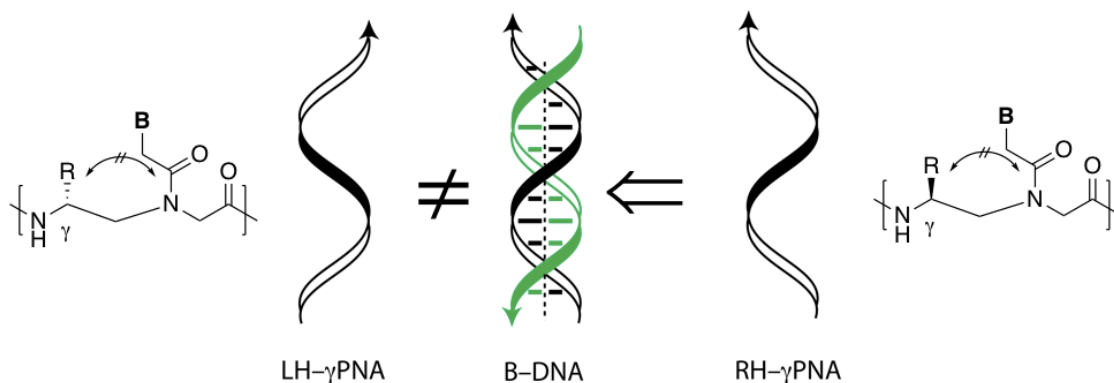


Figure I- 7. Backbone preorganization results in two helical motifs, the right-handed (RH) and the left-handed (LH)- γ PNA. Arrow directions: from *N*- to *C*- termini for γ PNA; from 5' to 3' ends for B-DNA.

The preorganization minimizes the entropic penalty upon duplex complexation, which affords high binding affinity and sequence discrimination as compared to unmodified PNA. On average, the T_m 's of the RH- γ PNA hybrid duplexes increased by ~ 3 °C for DNA and ~ 2 °C for RNA for every chiral unit incorporated into PNA oligomers. A single-base mismatch in PNA hybrid duplexes lowered T_m by 16–21 °C for DNA and 12–20 °C for RNA, depending on the mismatched pair, as compared to 10–14 °C and 11–18 °C respectively for unmodified PNA.⁸⁸ Additionally, a single-base mismatch in γ PNA duplexes lowered T_m by more than 27 °C.⁹¹

The size of γ modifications does not affect the backbone preorganization⁹⁴; therefore, a variety of side chains can be incorporated to improve the biophysical properties and provide new chemical functions. (**Figure I- 8**) Cationic groups (guanidinium and amine groups) can enhance the cellular uptake of γ PNA.⁹⁵⁻⁹⁷ Anionic groups (carboxylate and sulphate groups) can enhance water solubility and binding affinity toward DNA and RNA under medium to high salt concentrations.^{98,99} Diethylene glycol (commonly referred to as MiniPEG, or 'MP') moiety can enhance water solubility and biocompatibility of γ PNA without introducing charges.⁸⁸ L-Lysine-derived γ PNA monomers were prepared for post-synthesis modification with fluorescent dyes, peptides and bioactive ligands.^{100,101} L-Cysteine-derived γ PNA monomers were prepared to embody native chemical ligation for synthesizing long oligomers.¹⁰² These newly endowed properties of γ PNA have been exploited in a number of applications, including molecular assembly,^{91,103-109} gene editing,¹¹⁰⁻¹¹² antisense therapeutics,¹¹³⁻¹¹⁷ and diagnostics.¹¹⁸⁻¹²⁷

Despite the appeal, the wider range of γ PNA applications will impede until at least three challenges are addressed. The next section will discuss the three challenges addressed

by this Dissertation. It will turn γ PNA into a versatile biomolecular self-assembly platform with control over sequence and helical sense, and hopefully facilitate the potential applications in therapeutics and diagnostics.

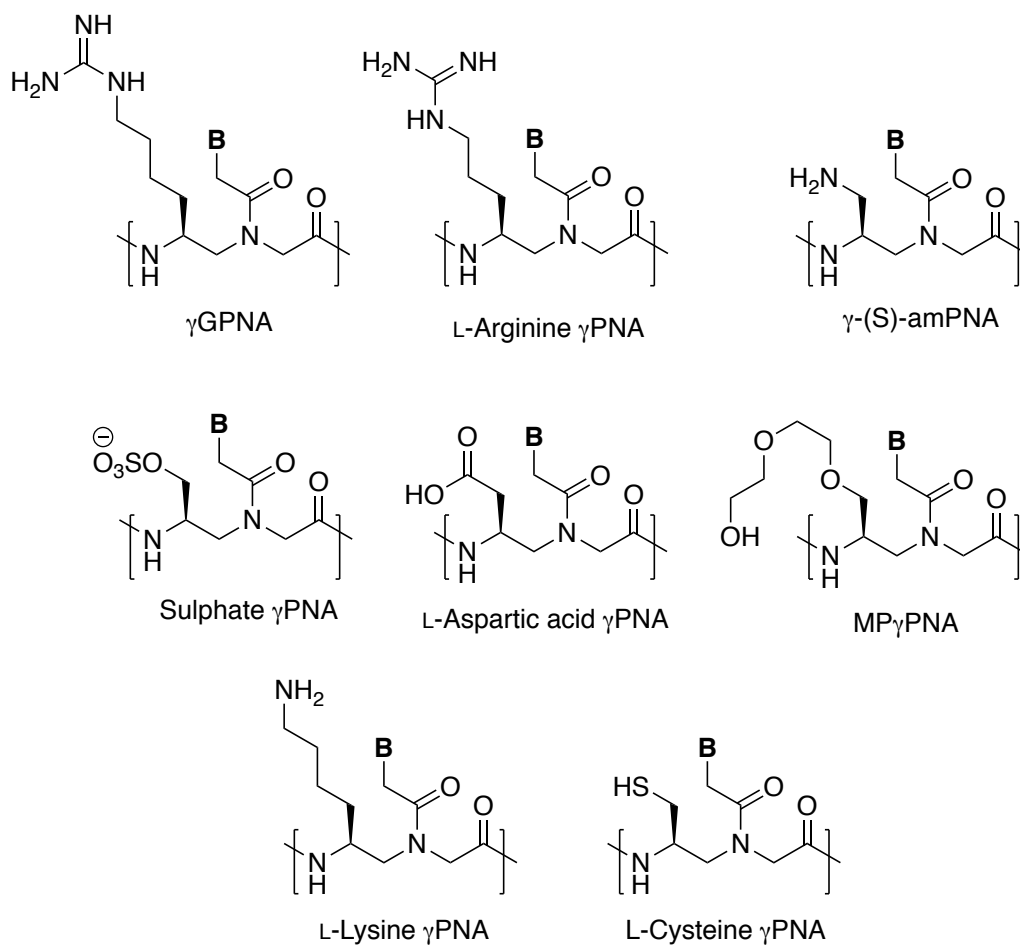


Figure I- 8. Representative Examples of γ PNA.

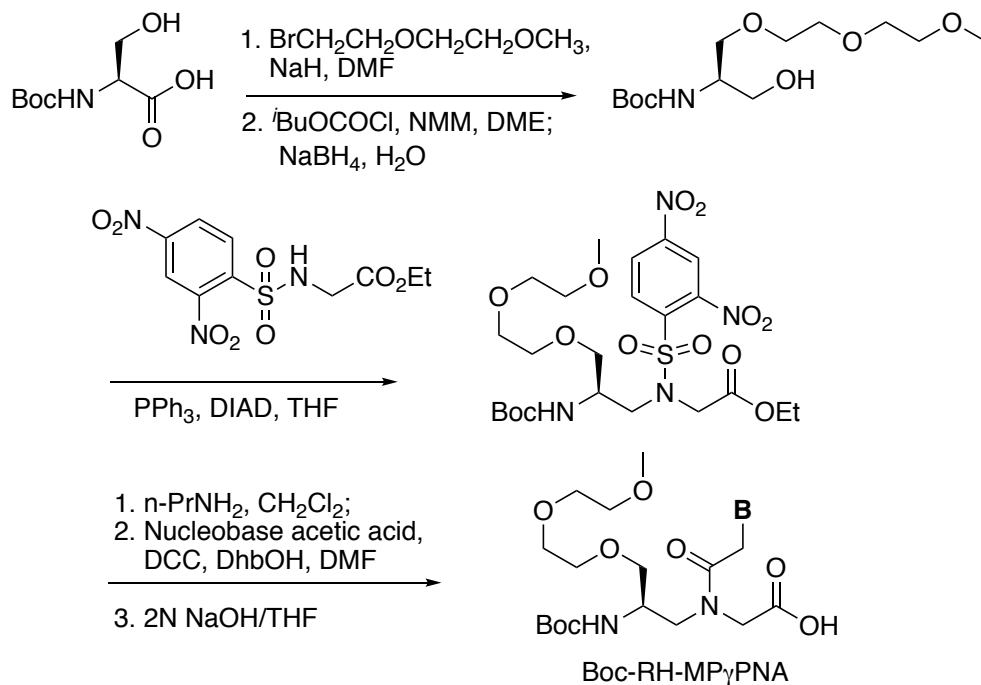
1.3. Thesis Organization

1.3.1. Synthesis of γ PNA Monomers

With the innovatively endowed biophysical properties, γ PNA has a unique role in several biomedical applications. Further implementation of γ PNA relies on the production of chemical building blocks that are optically-pure and that are compatible with the automated solid-phase peptide synthesis (SPPS). The former is essential since even the slightest amount of a racemate could have profound effects on the conformation and hybridization property of the oligonucleotide.¹²⁸ The latter is practical in that operating solid phase synthesizer with milder reagents would reduce the chance of corrosion and extend the lifetime of instrument. Therefore, it is foremost required to develop a robust method for scaling-up the production of enantiomerically-pure γ PNA monomers with mildly removable protecting groups.

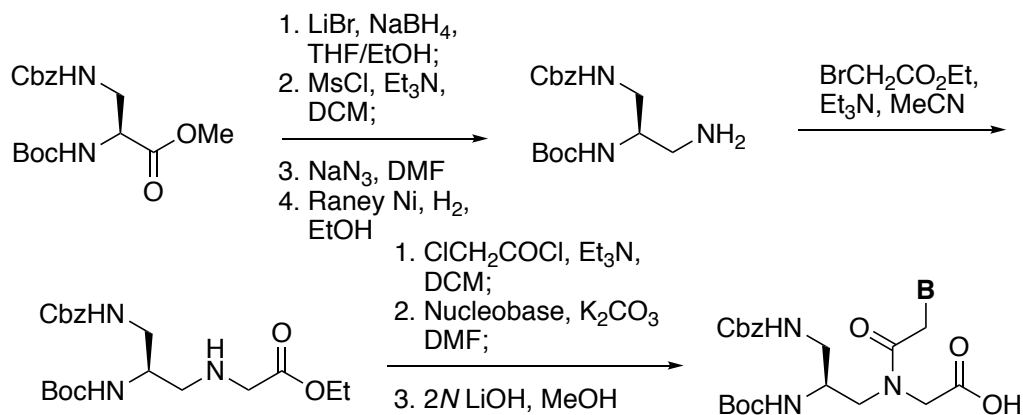
Currently, there are three general strategies to prepare γ PNA monomers. The first common strategy involves Mitsunobu-Fukuyama reaction that has been shown as a mild and epimerization-proof condition.¹²⁹ For example, in the preparation of MP γ PNA, Boc-protected L-serine was first alkylated with miniPEG side chain and followed by reduction to Boc-protected serinol.⁸⁸ The treatment of Mitsunobu-Fukuyama condition with dinitrophenylsulfonamide glycine and the mild basic removal of the sulfonamide group afforded MP γ PNA backbone. (**Scheme I- 1**) After coupling with nucleobase acetic acid and basic hydrolysis, the resulting γ PNA monomers were proved to be optically pure by ¹⁹F NMR.⁸⁸ However, this method generally suffers from tedious separation of byproducts such as triphenylphosphine oxide. Additionally, installation of the miniPEG side chain has

to compromise the yield with optical purity in a larger-scale set-up. Therefore, this method is generally not adopted for large-scale preparation.



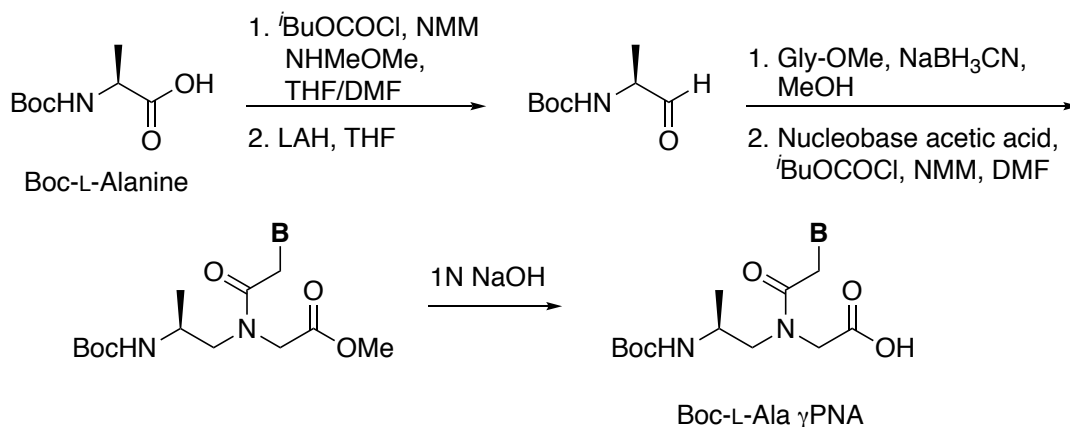
Scheme I- 1. Synthesizing γ PNA monomers by Mitsunobu-Fukuyama condition with a representative example of Boc-L-MP γ PNA.⁸⁸

The second general strategy to prepare γ PNA monomer involves preparing diamino derivatives from amino acids and then conducting *N*-alkylation to construct the chiral γ PNA backbones.^{96,130-134} (**Scheme I- 2**) While this strategy is generally epimerization-proof, the tricky *N*-alkylation afforded yields from 55% to 80% due to the chance of di-*N*-alkylation. Therefore, further investigations are required to optimize the reaction conditions.



Scheme I- 2. Synthesizing γ PNA monomers by *N*-alkylation reaction with a representative example Boc-L- γ -(*S*)-amPNA.⁹⁶

The third strategy to prepare γ PNA monomers involves the straight reduction of protected chiral amino acids to protected chiral amino aldehyde and then reductive amination to construct the corresponding chiral γ backbones.¹³⁵ (**Scheme I- 3**) This strategy is shorter and easier for purification as compared to the previous two strategies.



Scheme I- 3. Synthesizing γ PNA monomers by reductive amination with a representative example Boc-L-alanine-based γ PNA.¹³⁵

However, due to the presence of amino aldehyde, this strategy often suffered from epimerization even under mild experimental conditions such as rapid chromatography on silica gel.¹³⁶⁻¹³⁹ Manna et al. systematically studied epimerization under different reaction

conditions with Boc and 9-(9-phenylfluorenyl) (PhF) groups, and concluded that PhF can best secure the optical purity of γ PNA monomers in this reductive amination strategy.¹²⁸ This superior outcome resulted from two factors: (1) The bulky group twists the aldehyde structure into an unfavorable configuration and shields the alpha proton from removal¹⁴⁰; (2) PhF group prefers to be a leaving group following deprotonation over the inversion and reprotonation of the anion.¹⁴¹

While the PhF group can secure optical purity, the removal of this group requires strong acid or hydrogenation conditions, which is not compatible with acid-labile functional groups on monomers or pyrimidine bases, respectively. Chapter 2 of this Dissertation will address this challenge and provide a general method for synthesizing both RH- and LH- Fmoc-protected miniPEG containing γ PNA monomers.

1.3.2. Molecular Computing by γ PNA Platform

Currently, most dynamic nucleic acid nanodevices and circuits comprise native nucleic acids to achieve the desired manipulations in cell-free environment. However, when applied to *in vivo* environment, native nucleic acids could not achieve the desired goals due to the enzymatic degradation within a period of minutes.¹⁴² The half-lives of nucleic acid could be extended by chemical modification on the phosphodiester-sugar backbone. However, some of the modified nucleic acids has spurious binding with cellular components and induces cellular toxicity.¹⁴³ This problem could be potentially solved by bio-orthogonal nucleic acid analogues that cannot be recognized by cellular components. Furthermore, how to interface between the native and the bio-orthogonal forms is required to be investigated.

These two issues could be potentially addressed by using mirror-image oligonucleotide and toehold-mediated strand-displacement. (L)-DNA is a mirror-image of native DNA and known to have similar hybridization kinetics and duplex thermal stability to the native oligonucleotide.⁵⁰⁻⁵² It can bind to achiral PNA same as the native form. This common nature was exploited by Sczepanski et al. to develop a helical sense convertor to interface both forms by toehold-mediated strand-displacement.¹⁴⁴ The group demonstrated that PNA-mediated heterochiral circuits can detect endogenous microRNA. However, mirror-image oligonucleotides are not truly bio-orthogonal to endogenous nucleic acid^{50,54} and the signal integrity cannot be maintained in real *in vivo* applications. Therefore, it is necessary to find other materials for high signal-integrity molecular computing.

Earlier our group demonstrated that LH- γ PNA cannot bind to RH- γ PNA, DNA and RNA with the same complementary sequence, but can bind to achiral PNA similarly

to RH- γ PNA.⁹¹ Chapter 3 of this Dissertation demonstrates that the sequence information in the two orthogonal worlds can be interconverted through PNA-mediated strand displacement. Further integration of the γ PNA platform would facilitate the development of a rapid and sensitive method for *in-situ* detection of genetic materials.

1.3.3. Design of Tight Binding Probes with High Sequence Specificity

Designing a tight binding hybridization probe with high sequence specificity is challenging in that the probes are too stable to be sensitive to a base mispairing.¹⁴⁵ Nature has developed template-directed biopolymer synthesis to assemble low-affinity but highly sequence-specific building blocks to tightly and selectively bind to the template.¹⁴⁶ To mimic the process in the laboratory, one requires oligomeric monomers with mutually reactive functional groups, which are chemically stable in the absence of template, but are concatenated in the presence of template. However, this concept cannot be realized by traditional oligomeric monomers such as DNA and achiral PNA, because the flexible backbones allow the two reactive groups diffusively approaching each other and undergoing cyclization.^{147,148}

Chapter 4 of this Dissertation postulates that conformationally rigid oligomeric monomers, γ PNA in this study, can address this challenge. It demonstrates that a relatively short MP γ PNA probe did not immediately undergo intramolecular cyclization with a half-life of 1h. In the presence of targets consisting of RNA CUG repeats, the probe was concatenated to form long tight binding probes. While further investigations are needed to investigate the sequence-selectivity of such template-directed assemblies, this strategy provides a novel approach to design short nucleic-acid probes for targeting RNA-repeat expansions through template-directed oligomerization.

1.4. References

- (1) Watson, J. D.; Crick, F. H. C. Molecular Structure of Nucleic Acids: a Structure for Deoxyribose Nucleic Acid. *Nature* **1953**, *171*, 737–738.
- (2) Watson, J. D.; Crick, F. H. C. Genetical Implications of the Structure of Deoxyribonucleic Acid. *Nature* **1953**, *171* (4361), 964–967.
- (3) Bloomfield, V.; Crothers, D. M.; Tinoco, I., Jr. *Nucleic Acids: Structures, Properties and Functions.*; Univeristy Science Books, 2000.
- (4) SantaLucia, J.; Hicks, D. The Thermodynamics of DNA Structural Motifs. *Annu. Rev. Biophys. Biomol. Struct.* **2004**, *33* (1), 415–440.
- (5) Zuker, M. Mfold Web Server for Nucleic Acid Folding and Hybridization Prediction. *Nucleic Acids Res.* **2003**, *31* (13), 3406–3415.
- (6) Lorenz, R.; Bernhart, S. H.; Höner zu Siederdisen, C.; Tafer, H.; Flamm, C.; Stadler, P. F.; Hofacker, I. L. ViennaRNA Package 2.0. *Algorithms Mol. Biol.* **2011**, *6* (1), 26.
- (7) Zadeh, J. N.; Steenberg, C. D.; Bois, J. S.; Wolfe, B. R.; Pierce, M. B.; Khan, A. R.; Dirks, R. M.; Pierce, N. A. NUPACK: Analysis and Design of Nucleic Acid Systems. *J. Comput. Chem.* **2011**, *32* (1), 170–173.
- (8) Chen, J. H.; Seeman, N. C. Synthesis From DNA of a Molecule with the Connectivity of a Cube. *Nature* **1991**, *350* (6319), 631–633.
- (9) Pianowski, Z. L.; Winssinger, N. Nucleic Acid Encoding to Program Self-Assembly in Chemical Biology. *Chem. Soc. Rev.* **2008**, *37* (7), 1330–1336.
- (10) Seeman, N. C. DNA in a Material World. *Nature* **2003**, *421* (6921), 427–431.
- (11) Park, S. Y.; Lytton-Jean, A. K. R.; Lee, B.; Weigand, S.; Schatz, G. C.; Mirkin, C. A. DNA-Programmable Nanoparticle Crystallization. *Nature* **2008**, *451* (7178), 553–556.
- (12) Jones, M. R.; Seeman, N. C.; Mirkin, C. A. Programmable Materials and the Nature of the DNA Bond. *Science* **2015**, *347* (6224), 1260901.
- (13) Rothmund, P. W. K. Folding DNA to Create Nanoscale Shapes and Patterns. *Nature* **2006**, *440* (7082), 297–302.
- (14) Pinheiro, A. V.; Han, D.; Shih, W. M.; Yan, H. Challenges and Opportunities for Structural DNA Nanotechnology. *Nat. Nanotechnol.* **2011**, *6* (12), 763–772.
- (15) Aldaye, F. A.; Palmer, A. L.; Sleiman, H. F. Assembling Materials with DNA as the Guide. *Science* **2008**, *321* (5897), 1795–1799.
- (16) Douglas, S. M.; Dietz, H.; Liedl, T.; Högberg, B.; Graf, F.; Shih, W. M. Self-Assembly of DNA Into Nanoscale Three-Dimensional Shapes. *Nature* **2009**, *459* (7245), 414–418.
- (17) Dietz, H.; Douglas, S. M.; Shih, W. M. Folding DNA Into Twisted and Curved Nanoscale Shapes. *Science* **2009**, *325* (5941), 725–730.
- (18) Han, D.; Pal, S.; Nangreave, J.; Deng, Z.; Liu, Y.; Yan, H. DNA Origami with Complex Curvatures in Three-Dimensional Space. *Science* **2011**, *332* (6027), 342–346.
- (19) Wei, B.; Dai, M.; Yin, P. Complex Shapes Self-Assembled From Single-Stranded DNA Tiles. *Nature* **2012**, *485* (7400), 623–626.
- (20) Ke, Y.; Ong, L. L.; Shih, W. M.; Yin, P. Three-Dimensional Structures Self-Assembled From DNA Bricks. *Science* **2012**, *338* (6111), 1177–1183.

- (21) Veneziano, R.; Ratanalert, S.; Zhang, K.; Zhang, F.; Yan, H.; Chiu, W.; Bathe, M. Designer Nanoscale DNA Assemblies Programmed From the Top Down. *Science* **2016**, *352* (6293), 1534–1534.
- (22) Han, D.; Qi, X.; Myhrvold, C.; Wang, B.; Dai, M.; Jiang, S.; Bates, M.; Liu, Y.; An, B.; Zhang, F.; Yan, H.; Yin, P. Single-Stranded DNA and RNA Origami. *Science* **2017**, *358* (6369), eaao2648.
- (23) Bath, J.; Turberfield, A. J. DNA Nanomachines. *Nat. Nanotechnol.* **2007**, *2* (5), 275–284.
- (24) Gerling, T.; Wagenbauer, K. F.; Neuner, A. M.; Dietz, H. Dynamic DNA Devices and Assemblies Formed by Shape-Complementary, Non-Base Pairing 3D Components. *Science* **2015**, *347* (6229), 1446–1452.
- (25) Yurke, B.; Turberfield, A. J.; Mills, A. P., Jr; Simmel, F. C.; Neumann, J. L. A DNA-Fuelled Molecular Machine Made of DNA. *Nature* **2000**, *406* (6796), 605–608.
- (26) Omabegho, T.; Sha, R.; Seeman, N. C. A Bipedal DNA Brownian Motor with Coordinated Legs. *Science* **2009**, *324* (5923), 67–71.
- (27) Lund, K.; Manzo, A. J.; Dabby, N.; Michelotti, N.; Johnson-Buck, A.; Nangreave, J.; Taylor, S.; Pei, R.; Stojanovic, M. N.; Walter, N. G.; Winfree, E.; Yan, H. Molecular Robots Guided by Prescriptive Landscapes. *Nature* **2010**, *465* (7295), 206–210.
- (28) Gu, H.; Chao, J.; Xiao, S.-J.; Seeman, N. C. A Proximity-Based Programmable DNA Nanoscale Assembly Line. *Nature* **2010**, *465* (7295), 202–205.
- (29) Church, G. M.; Gao, Y.; Kosuri, S. Next-Generation Digital Information Storage in DNA. *Science* **2012**, *337* (6102), 1628.
- (30) Erlich, Y.; Zielinski, D. DNA Fountain Enables a Robust and Efficient Storage Architecture. *Science* **2017**, *355* (6328), 950–954.
- (31) Goldman, N.; Bertone, P.; Chen, S.; Dessimoz, C.; LeProust, E. M.; Sipos, B.; Birney, E. Towards Practical, High-Capacity, Low-Maintenance Information Storage in Synthesized DNA. *Nature* **2013**, *494* (7435), 77–80.
- (32) Adleman, L. M. Molecular Computation of Solutions to Combinatorial Problems. *Science* **1994**, *266* (5187), 1021–1024.
- (33) Benenson, Y. Biomolecular Computing Systems: Principles, Progress and Potential. *Nat. Rev. Genet.* **2012**, *13* (7), 455–468.
- (34) Stojanovic, M. N.; Stefanovic, D.; Rudchenko, S. Exercises in Molecular Computing. *Acc. Chem. Res.* **2014**, *47* (6), 1845–1852.
- (35) Qian, L.; Winfree, E. Scaling Up Digital Circuit Computation with DNA Strand Displacement Cascades. *Science* **2011**, *332* (6034), 1196–1201.
- (36) Qian, L.; Winfree, E.; Bruck, J. Neural Network Computation with DNA Strand Displacement Cascades. *Nature* **2011**, *475* (7356), 368–372.
- (37) Dittmer, W. U.; Reuter, A.; Simmel, F. C. A DNA-Based Machine That Can Cyclically Bind and Release Thrombin. *Angew. Chem. Int. Ed. Engl.* **2004**, *43* (27), 3550–3553.
- (38) Douglas, S. M.; Bachelet, I.; Church, G. M. A Logic-Gated Nanorobot for Targeted Transport of Molecular Payloads. *Science* **2012**, *335* (6070), 831–834.
- (39) Ko, S.; Liu, H.; Chen, Y.; Mao, C. DNA Nanotubes as Combinatorial Vehicles for Cellular Delivery. *Biomacromolecules* **2008**, *9* (11), 3039–3043.

- (40) Perrault, S. D.; Shih, W. M. Virus-Inspired Membrane Encapsulation of DNA Nanostructures to Achieve in Vivo Stability. *ACS nano* **2014**, *8* (5), 5132–5140.
- (41) Choi, H. M. T.; Beck, V. A.; Pierce, N. A. Next-Generation *In-Situ* Hybridization Chain Reaction: Higher Gain, Lower Cost, Greater Durability. *ACS nano* **2014**, *8* (5), 4284–4294.
- (42) Benenson, Y.; Gil, B.; Ben-Dor, U.; Adar, R.; Shapiro, E. An Autonomous Molecular Computer for Logical Control of Gene Expression. *Nature* **2004**, *429* (6990), 423–429.
- (43) Kurreck, J. Antisense Technologies. Improvement Through Novel Chemical Modifications. *Eur. J. Biochem.* **2003**, *270* (8), 1628–1644.
- (44) Crooke, S. T.; Lemonidis, K. M.; Neilson, L.; Griffey, R.; Lesnik, E. A.; Monia, B. P. Kinetic Characteristics of Escherichia Coli RNase H1: Cleavage of Various Antisense Oligonucleotide-RNA Duplexes. *Biochem. J.* **1995**, *312*, 599–608.
- (45) Wengel, J. Synthesis of 3'-C- and 4'-C-Branched Oligodeoxynucleotides and the Development of Locked Nucleic Acid (LNA). *Acc. Chem. Res.* **1998**, *32* (4), 301–310.
- (46) Birte Vester, A.; Wengel, J. LNA (Locked Nucleic Acid): High-Affinity Targeting of Complementary RNA and DNA. *Biochemistry* **2004**, *43* (42), 13233–13241.
- (47) Orum, H.; Wengel, J. Locked Nucleic Acids: a Promising Molecular Family for Gene-Function Analysis and Antisense Drug Development. *Curr. Opin. Mol. Ther.* **2001**, *3* (3), 239–243.
- (48) Swayze, E. E.; Siwkowski, A. M.; Wancewicz, E. V.; Migawa, M. T.; Wyrzykiewicz, T. K.; Hung, G.; Monia, B. P.; Bennett, C. F. Antisense Oligonucleotides Containing Locked Nucleic Acid Improve Potency but Cause Significant Hepatotoxicity in Animals. *Nucleic Acids Res.* **2007**, *35* (2), 687–700.
- (49) Hagedorn, P. H.; Yakimov, V.; Ottosen, S.; Kammler, S.; Nielsen, N. F.; Høg, A. M.; Hedtjærn, M.; Meldgaard, M.; Møller, M. R.; Ørum, H.; Koch, T.; Lindow, M. Hepatotoxic Potential of Therapeutic Oligonucleotides Can Be Predicted From Their Sequence and Modification Pattern. *Nucleic Acid Ther.* **2013**, *23* (5), 302–310.
- (50) Ashley, G. W. Modeling, Synthesis, and Hybridization Properties of (L)-Ribonucleic Acid. *J. Am. Chem. Soc.* **1992**, *114* (25), 9731–9736.
- (51) Urata, H.; Ogura, E.; Shinohara, K.; Ueda, Y.; Akagi, M. Synthesis and Properties of Mirror-Image DNA. *Nucleic Acids Res.* **1992**, *20* (13), 3325–3332.
- (52) Hauser, N. C.; Martinez, R.; Jacob, A.; Rupp, S.; Hoheisel, J. D.; Matysiak, S. Utilising the Left-Helical Conformation of L-DNA for Analysing Different Marker Types on a Single Universal Microarray Platform. *Nucleic Acids Res.* **2006**, *34* (18), 5101–5111.
- (53) Vater, A.; Klussmann, S. Turning Mirror-Image Oligonucleotides Into Drugs: the Evolution of Spiegelmer Therapeutics. *Drug Discov. Today* **2015**, *20* (1), 147–155.
- (54) Fujimori, S.; Shudo, K.; Hashimoto, Y. Enantio-DNA Recognizes Complementary RNA but Not Complementary DNA. *J. Am. Chem. Soc.* **1990**, *112* (20), 7436–7438.

- (55) Wilds, C. J.; Maier, M. A.; Tereshko, V.; Manoharan, M.; Egli, M. Direct Observation of a Cytosine Analogue That Forms Five Hydrogen Bonds to Guanosine: Guanidino G-Clamp. *Angew. Chem. Int. Ed. Engl.* **2002**, *41* (1), 115–117.
- (56) Flanagan, W. M.; Wolf, J. J.; Olson, P.; Grant, D.; Lin, K. Y.; Wagner, R. W.; Matteucci, M. D. A Cytosine Analog That Confers Enhanced Potency to Antisense Oligonucleotides. *Proc. Natl. Acad. Sci. U.S.A.* **1999**, *96* (7), 3513–3518.
- (57) Ortega, J.-A.; Blas, J. R.; Orozco, M.; Grandas, A.; Pedroso, E.; Robles, J. Binding Affinities of Oligonucleotides and PNAs Containing Phenoxazine and G-Clamp Cytosine Analogues Are Unusually Sequence-Dependent. *Org. Lett.* **2007**, *9* (22), 4503–4506.
- (58) Howard, F. B.; Miles, H. T. 2NH₂A-T Helices in the Ribo- and Deoxypolynucleotide Series. Structural and Energetic Consequences of 2NH₂A Substitution. *Biochemistry* **1984**, *23* (26), 6723–6732.
- (59) Lamm, G. M.; Blencowe, B. J.; Sparoat, B. S.; Iribarren, A. M.; Ryder, U.; Lamond, A. I. Antisense Probes Containing 2-Aminoadenosine Allow Efficient Depletion of U5 snRNP From HeLa Splicing Extracts. *Nucleic Acids Res.* **1991**, *19* (12), 3193–3198.
- (60) Ramasamy, K. S.; Zounes, M.; Gonzalez, C.; Freier, S. M.; Lesnik, E. A.; Cummins, L. L.; Griffey, R. H.; Monia, B. P.; Dan Cook, P. Remarkable Enhancement of Binding Affinity of Heterocycle-Modified DNA to DNA and RNA. Synthesis, Characterization and Biophysical Evaluation of N²-Imidazolylpropylguanine and N²-Imidazolylpropyl-2-Aminoadenine Modified Oligonucleotides. *Tetrahedron Lett.* **1994**, *35* (2), 215–218.
- (61) Manoharan, M.; Ramasamy, K. S.; Mohan, V.; Cook, P. D. Oligonucleotides Bearing Cationic Groups: N²-(3-Aminopropyl)Deoxyguanosine. Synthesis, Enhanced Binding Properties and Conjugation Chemistry. *Tetrahedron Lett.* **1996**, *37* (43), 7675–7678.
- (62) De Clercq, E.; Eckstein, F.; Merigan, T. C. Interferon Induction Increased Through Chemical Modification of a Synthetic Polyribonucleotide. *Science* **1969**, *165* (3898), 1137–1139.
- (63) Crooke, S. T. Progress in Antisense Technology: the End of the Beginning. *Meth. Enzymol.* **2000**, *313*, 3–45.
- (64) Oka, N.; Wada, T. Stereocontrolled Synthesis of Oligonucleotide Analogs Containing Chiral Internucleotidic Phosphorus Atoms. *Chem. Soc. Rev.* **2011**, *40* (12), 5829–5843.
- (65) Brown, D. A.; Kang, S. H.; Gryaznov, S. M.; Dedionisio, L.; Heidenreich, O.; Sullivan, S.; Xu, X.; Nerenberg, M. I. Effect of Phosphorothioate Modification of Oligodeoxynucleotides on Specific Protein-Binding. *J. Biol. Chem.* **1994**, *269* (43), 26801–26805.
- (66) Guvakova, M. A.; Yakubov, L. A.; Vlodaysky, I.; Tonkinson, J. L.; Stein, C. A. Phosphorothioate Oligodeoxynucleotides Bind to Basic Fibroblast Growth Factor, Inhibit Its Binding to Cell Surface Receptors, and Remove It From Low Affinity Binding Sites on Extracellular Matrix. *J. Biol. Chem.* **1995**, *270* (6), 2620–2627.

- (67) Rockwell, P.; O'Connor, W. J.; King, K.; Goldstein, N. I.; Zhang, L. M.; Stein, C. A. Cell-Surface Perturbations of the Epidermal Growth Factor and Vascular Endothelial Growth Factor Receptors by Phosphorothioate Oligodeoxynucleotides. *Proc. Natl. Acad. Sci. U.S.A.* **1997**, *94* (12), 6523–6528.
- (68) Summerton, J.; Weller, D. Morpholino Antisense Oligomers: Design, Preparation, and Properties. *Antisense Nucleic Acid Drug Dev.* **1997**, *7* (3), 187–195.
- (69) Heasman, J. Morpholino Oligos: Making Sense of Antisense? *Dev. Biol.* **2002**, *243* (2), 209–214.
- (70) Nielsen, P. E.; Egholm, M.; Berg, R. H.; Buchardt, O. Sequence-Selective Recognition of DNA by Strand Displacement with a Thymine-Substituted Polyamide. *Science* **1991**, *254* (5037), 1497–1500.
- (71) Nielsen, P. E. Peptide Nucleic Acid, a Molecule with Two Identities. *Acc. Chem. Res.* **1999**, 624–630.
- (72) Janowski, B. A.; Kaihatsu, K.; Huffman, K. E.; Schwartz, J. C.; Ram, R.; Hardy, D.; Mendelson, C. R.; Corey, D. R. Inhibiting Transcription of Chromosomal DNA with Antisense Peptide Nucleic Acids. *Nat. Chem. Biol.* **2005**, *1* (4), 210–215.
- (73) Zhang, X.; Ishihara, T.; Corey, D. R. Strand Invasion by Mixed Base PNAs and a PNA-Peptide Chimera. *Nucleic Acids Res.* **2000**, *28* (17), 3332–3338.
- (74) Smolina, I. V.; Demidov, V. V.; Soldatenkov, V. A.; Chasovskikh, S. G.; Frank-Kamenetskii, M. D. End Invasion of Peptide Nucleic Acids (PNAs) with Mixed-Base Composition Into Linear DNA Duplexes. *Nucleic Acids Res.* **2005**, *33* (17), e146.
- (75) Lee, J.; Park, I.-S.; Jung, E.; Lee, Y.; Min, D.-H. Direct, Sequence-Specific Detection of dsDNA Based on Peptide Nucleic Acid and Graphene Oxide Without Requiring Denaturation. *Biosens. Bioelectron.* **2014**, *62*, 140–144.
- (76) Nielsen, P. E. *Chemical Biology of Peptide Nucleic Acids (PNAs)*; Mayer/The Chemical Biology of Nucleic Acids; Wiley-Blackwell: Chichester, UK, 2010; Vol. 254, pp 103–113.
- (77) Li, W.; Shi, H.; Dong, B.; Nie, K.; Liu, Z.; He, N. Recognition Mechanisms and Applications of Peptide Nucleic Acids Targeting Double-Stranded DNA. *Curr. Med. Chem.* **2016**, *23* (41), 4681–4705.
- (78) Tackett, A. J. Non-Watson-Crick Interactions Between PNA and DNA Inhibit the ATPase Activity of Bacteriophage T4 Dda Helicase. *Nucleic Acids Res.* **2002**, *30* (4), 950–957.
- (79) Nielsen, P. E. Addressing the Challenges of Cellular Delivery and Bioavailability of Peptide Nucleic Acids (PNA). *Q. Rev. Biophys.* **2005**, *38* (04), 345–350.
- (80) Kumar, V. A.; Ganesh, K. N. Conformationally Constrained PNA Analogues: Structural Evolution Toward DNA/RNA Binding Selectivity. *Acc. Chem. Res.* **2005**, *38* (5), 404–412.
- (81) Sugiyama, T.; Kittaka, A. Chiral Peptide Nucleic Acids with a Substituent in the N-(2-Aminoethyl)Glycine Backbone. *Molecules* **2012**, *18* (1), 287–310.

- (82) Moccia, M.; Adamo, M. F. A.; Saviano, M. Insights on Chiral, Backbone Modified Peptide Nucleic Acids: Properties and Biological Activity. *Artif. DNA PNA XNA* **2016**, *5* (3), e1107176.
- (83) Pokorski, J. K.; Witschi, M. A.; Purnell, B. L.; Appella, D. H. (S,S)-Trans-Cyclopentane-Constrained Peptide Nucleic Acids. a General Backbone Modification That Improves Binding Affinity and Sequence Specificity. *J. Am. Chem. Soc.* **2004**, *126* (46), 15067–15073.
- (84) Vilaivan, T.; Srisuwannaket, C. Hybridization of Pyrrolidinyl Peptide Nucleic Acids and DNA: Selectivity, Base-Pairing Specificity, and Direction of Binding. *Org. Lett.* **2006**, *8* (9), 1897–1900.
- (85) Nielsen, P. E. Peptide Nucleic Acids (PNA) in Chemical Biology and Drug Discovery. *Chem. Biodivers.* **2010**, *7* (4), 786–804.
- (86) Nielsen, P. E.; Haaima, G.; Lohse, A.; Buchardt, O. Peptide Nucleic Acids (PNAs) Containing Thymine Monomers Derived From Chiral Amino Acids: Hybridization and Solubility Properties of D-Lysine PNA. *Angew. Chem. Int. Ed. Engl.* **1996**, *35* (17), 1939–1942.
- (87) Zhou, P.; Dragulescu-Andrasi, A.; Bhattacharya, B.; O’Keefe, H.; Vatta, P.; Hyldig-Nielsen, J. J.; Ly, D. H. Synthesis of Cell-Permeable Peptide Nucleic Acids and Characterization of Their Hybridization and Uptake Properties. *Bioorg. Med. Chem. Lett.* **2006**, *16* (18), 4931–4935.
- (88) Sahu, B.; Sacui, I.; Rapireddy, S.; Zanolli, K. J.; Bahal, R.; Armitage, B. A.; Ly, D. H. Synthesis and Characterization of Conformationally Preorganized, (R)-Diethylene Glycol-Containing Gamma-Peptide Nucleic Acids with Superior Hybridization Properties and Water Solubility. *J. Org. Chem.* **2011**, *76* (14), 5614–5627.
- (89) Manna, A.; Rapireddy, S.; Sureshkumar, G.; Ly, D. H. Synthesis of Optically Pure γ PNA Monomers: a Comparative Study. *Tetrahedron* **2015**, *71* (21), 3507–3514.
- (90) Dragulescu-Andrasi, A.; Rapireddy, S.; Frezza, B. M.; Gayathri, C.; Gil, R. R.; Ly, D. H. A Simple Gamma-Backbone Modification Preorganizes Peptide Nucleic Acid Into a Helical Structure. *J. Am. Chem. Soc.* **2006**, *128* (31), 10258–10267.
- (91) Sacui, I.; Hsieh, W.-C.; Manna, A.; Sahu, B.; Ly, D. H. Gamma Peptide Nucleic Acids: as Orthogonal Nucleic Acid Recognition Codes for Organizing Molecular Self-Assembly. *J. Am. Chem. Soc.* **2015**, *137* (26), 8603–8610.
- (92) Bahal, R.; Sahu, B.; Rapireddy, S.; Lee, C.-M.; Ly, D. H. Sequence-Unrestricted, Watson-Crick Recognition of Double Helical B-DNA by (R)-miniPEG- γ PNAs. *Chembiochem* **2012**, *13* (1), 56–60.
- (93) Crawford, M. Structural Characterization of Γ -Modified PNAs and Invasion of microRNA (Doctoral Dissertation), Carnegie Mellon University, Pittsburgh, PA., 2011.
- (94) Crawford, M. J.; Rapireddy, S.; Bahal, R.; Sacui, I.; Ly, D. H. Effect of Steric Constraint at the Γ -Backbone Position on the Conformations and Hybridization Properties of PNAs. *J. Nucleic Acids* **2011**, *2011* (9), 1–10.
- (95) Sahu, B.; Chenna, V.; Lathrop, K. L.; Thomas, S. M.; Zon, G.; Livak, K. J.; Ly, D. H. Synthesis of Conformationally Preorganized and Cell-Permeable

- Guanidine-Based Γ -Peptide Nucleic Acids (γ GPNA). *J. Org. Chem.* **2009**, *74* (4), 1509–1516.
- (96) Mitra, R.; Ganesh, K. N. Aminomethylene Peptide Nucleic Acid (Am-PNA): Synthesis, Regio-/Stereospecific DNA Binding, and Differential Cell Uptake of (A/ Γ ,R/S)Am-PNA Analogues. *J. Org. Chem.* **2012**, *77* (13), 5696–5704.
- (97) Manicardi, A.; Fabbri, E.; Tedeschi, T.; Sforza, S.; Bianchi, N.; Brognara, E.; Gambari, R.; Marchelli, R.; Corradini, R. Cellular Uptakes, Biostabilities and Anti-miR-210 Activities of Chiral Arginine-PNAs in Leukaemic K562 Cells. *Chembiochem* **2012**, *13* (9), 1327–1337.
- (98) Huang, H.; Joe, G. H.; Choi, S. R.; Kim, S. N.; Kim, Y. T.; Pak, C. S.; Hong, J. H.; Lee, W. Synthesis of Enantiopure Gamma-Glutamic Acid Functionalized Peptide Nucleic Acid Monomers. *Korean Chem. Soc.* **2010**, *31* (7), 2054–2056.
- (99) Avitabile, C.; Moggio, L.; Malgieri, G.; Capasso, D.; Di Gaetano, S.; Saviano, M.; Pedone, C.; Romanelli, A. Γ Sulphate PNA (PNA S): Highly Selective DNA Binding Molecule Showing Promising Antigene Activity. *PLoS ONE* **2012**, *7* (5), e35774.
- (100) Englund, E. A.; Appella, D. H. Synthesis of Γ -Substituted Peptide Nucleic Acids: a New Place to Attach Fluorophores Without Affecting DNA Binding. *Org. Lett.* **2005**, *7* (16), 3465–3467.
- (101) Englund, E. A.; Appella, D. H. Γ -Substituted Peptide Nucleic Acids Constructed From L-Lysine Are a Versatile Scaffold for Multifunctional Display. *Angew. Chem. Int. Ed. Engl.* **2007**, *46* (9), 1414–1418.
- (102) Dose, C.; Seitz, O. Convergent Synthesis of Peptide Nucleic Acids by Native Chemical Ligation. *Org. Lett.* **2005**, *7* (20), 4365–4368.
- (103) Englund, E. A.; Wang, D.; Fujigaki, H.; Sakai, H.; Micklitsch, C. M.; Ghirlando, R.; Martin-Manso, G.; Pendrak, M. L.; Roberts, D. D.; Durell, S. R.; Appella, D. H. Programmable Multivalent Display of Receptor Ligands Using Peptide Nucleic Acid Nanoscaffolds. *Nat. Commun.* **2012**, *3* (1), 614.
- (104) Scheibe, C.; Bujotzek, A.; Dervede, J.; Weber, M.; Seitz, O. DNA-Programmed Spatial Screening of Carbohydrate-Lectin Interactions. *Chem. Sci.* **2011**, *2* (4), 770–775.
- (105) Scheibe, C.; Seitz, O. PNA-Sugar Conjugates as Tools for the Spatial Screening of Carbohydrate-Lectin Interactions. *Pure Appl. Chem.* **2012**, *84* (1), 77–85.
- (106) Scheibe, C.; Wedepohl, S.; Riese, S. B.; Dervede, J.; Seitz, O. Carbohydrate-PNA and Aptamer-PNA Conjugates for the Spatial Screening of Lectins and Lectin Assemblies. *Chembiochem* **2013**, *14* (2), 236–250.
- (107) Machida, T.; Novoa, A.; Gillon, É.; Zheng, S.; Claudinon, J.; Eierhoff, T.; Imbert, A.; Römer, W.; Winssinger, N. Dynamic Cooperative Glycan Assembly Blocks the Binding of Bacterial Lectins to Epithelial Cells. *Angew. Chem. Int. Ed. Engl.* **2017**, *56* (24), 6762–6766.
- (108) Yu, Z.; Hsieh, W.-C.; Asamitsu, S.; Hashiya, K.; Bando, T.; Ly, D. H.; Sugiyama, H. Orthogonal γ PNA Dimerization Domains Empower DNA Binders with Cooperativity and Versatility Mimicking That of Transcription Factor Pairs. *Chem. Eur. J.* **2018**, JustAccepted.
- (109) Rapireddy, S.; Nhon, L.; Meehan, R. E.; Franks, J.; Stolz, D. B.; Tran, D.; Selsted, M. E.; Ly, D. H. RTD-1Mimic Containing γ PNA Scaffold Exhibits

- Broad-Spectrum Antibacterial Activities. *J. Am. Chem. Soc.* **2012**, *134* (9), 4041–4044.
- (110) Bahal, R.; Quijano, E.; A McNeer, N.; Liu, Y.; C Bhunia, D.; Lopez-Giraldez, F.; J Fields, R.; M Saltzman, W.; H Ly, D.; M Glazer, P. Single-Stranded γ PNAs for in Vivo Site-Specific Genome Editing via Watson-Crick Recognition. *Curr. Gene Ther.* **2014**, *14* (5), 331–342.
- (111) Bahal, R.; Ali McNeer, N.; Quijano, E.; Liu, Y.; Sulkowski, P.; Turchick, A.; Lu, Y.-C.; Bhunia, D. C.; Manna, A.; Greiner, D. L.; Brehm, M. A.; Cheng, C. J.; López-Giráldez, F.; Ricciardi, A.; Beloor, J.; Krause, D. S.; Kumar, P.; Gallagher, P. G.; Braddock, D. T.; Mark Saltzman, W.; Ly, D. H.; Glazer, P. M. In Vivo Correction of Anaemia in B-Thalassemic Mice by γ PNA-Mediated Gene Editing with Nanoparticle Delivery. *Nat. Commun.* **2016**, *7*, 13304.
- (112) Ricciardi, A. S.; Bahal, R.; Farrelly, J. S.; Quijano, E.; Bianchi, A. H.; Luks, V. L.; Putman, R.; López-Giráldez, F.; Coskun, S.; Song, E.; Liu, Y.; Hsieh, W.-C.; Ly, D. H.; Stitelman, D. H.; Glazer, P. M.; Saltzman, W. M. In Utero Nanoparticle Delivery for Site-Specific Genome Editing. *Nat. Commun.* **2018**, *9*, 2481.
- (113) Bahal, R.; McNeer, N. A.; Ly, D. H.; Saltzman, W. M.; Glazer, P. M. Nanoparticle for Delivery of Antisense γ PNA Oligomers Targeting CCR5. *Artif. DNA PNA XNA* **2013**, *4* (2), 49–57.
- (114) Gupta, A.; Quijano, E.; Liu, Y.; Bahal, R.; Scanlon, S. E.; Song, E.; Hsieh, W.-C.; Braddock, D. E.; Ly, D. H.; Saltzman, W. M.; Glazer, P. M. Anti-Tumor Activity of miniPEG-G-Modified PNAs to Inhibit MicroRNA-210 for Cancer Therapy. *Mol. Ther. Nucleic Acids* **2017**, *9*, 111–119.
- (115) Oyaghire, S. N.; Cherubim, C. J.; Telmer, C. A.; Martinez, J. A.; Bruchez, M. P.; Armitage, B. A. RNA G-Quadruplex Invasion and Translation Inhibition by Antisense Gamma-Peptide Nucleic Acid Oligomers. *Biochemistry* **2016**, *55* (13), 1977–1988.
- (116) Hsieh, W.-C.; Bahal, R.; Thadke, S. A.; Bhatt, K.; Sobczak, K.; Thornton, C.; Ly, D. H. Design of a “Mini” Nucleic Acid Probe for Cooperative Binding of an RNA-Repeated Transcript Associated with Myotonic Dystrophy Type 1. *Biochemistry* **2018**, *57* (6), 907–911.
- (117) Thadke, S. A.; Perera, J. D. R.; Hridya, V. M.; Bhatt, K.; Shaikh, A. Y.; Hsieh, W.-C.; Chen, M.; Gayathri, C.; Gil, R. R.; Rule, G. S.; Mukherjee, A.; Thornton, C. A.; Ly, D. H. Design of Bivalent Nucleic Acid Ligands for Recognition of RNA-Repeated Expansion Associated with Huntington's Disease. *Biochemistry* **2018**, *57* (14), 2094–2108.
- (118) Goldman, J. M.; Zhang, L. A.; Manna, A.; Armitage, B. A.; Ly, D. H.; Schneider, J. W. High Affinity γ PNA Sandwich Hybridization Assay for Rapid Detection of Short Nucleic Acid Targets with Single Mismatch Discrimination. *Biomacromolecules* **2013**, *14* (7), 2253–2261.
- (119) Zhang, Y.; Rana, A.; Stratton, Y.; Czyzyk-Krzeska, M. F.; Esfandiari, L. Sequence-Specific Detection of MicroRNAs Related to Clear Cell Renal Cell Carcinoma at fM Concentration by an Electroosmotically Driven Nanopore-Based Device. *Anal. Chem.* **2017**, *89* (17), 9201–9208.

- (120) Sadhu, K. K.; Winssinger, N. Detection of miRNA in Live Cells by Using Templated Ru^{II}-Catalyzed Unmasking of a Fluorophore. *Chem. Eur. J.* **2013**, *19* (25), 8182–8189.
- (121) Chang, D.; Lindberg, E.; Winssinger, N. Critical Analysis of Rate Constants and Turnover Frequency in Nucleic Acid-Templated Reactions: Reaching Terminal Velocity. *J. Am. Chem. Soc.* **2017**, *139* (4), 1444–1447.
- (122) Chang, D.; Kim, K. T.; Lindberg, E.; Winssinger, N. Accelerating Turnover Frequency in Nucleic Acid Templated Reactions. *Bioconjug. Chem.* **2017**, *29* (1), 158–163.
- (123) Pham, H. H.; Murphy, C. T.; Sureshkumar, G.; Ly, D. H.; Opresko, P. L.; Armitage, B. A. Cooperative Hybridization of γ PNA Miniprobcs to a Repeating Sequence Motif and Application to Telomere Analysis. *Org. Biomol. Chem.* **2014**, *12* (37), 7345–7354.
- (124) Orenstein, A.; Berlyoung, A. S.; Rastede, E. E.; Pham, H. H.; Fouquerel, E.; Murphy, C. T.; Leibowitz, B. J.; Yu, J.; Srivastava, T.; Armitage, B. A.; Opresko, P. L. γ PNA FRET Pair Miniprobcs for Quantitative Fluorescent In Situ Hybridization to Telomeric DNA in Cells and Tissue. *Molecules* **2017**, *22* (12), 2117.
- (125) Singer, A.; Rapireddy, S.; Ly, D. H.; Meller, A. Electronic Barcoding of a Viral Gene at the Single-Molecule Level. *Nano Lett.* **2012**, *12* (3), 1722–1728.
- (126) Nölling, J.; Rapireddy, S.; Amburg, J. I.; Crawford, E. M.; Prakash, R. A.; Rabson, A. R.; Tang, Y.-W.; Singer, A. Duplex DNA-Invasive Γ -Modified Peptide Nucleic Acids Enable Rapid Identification of Bloodstream Infections in Whole Blood. *MBio* **2016**, *7* (2), e00345–e00316.
- (127) Morin, T. J.; Shropshire, T.; Liu, X.; Briggs, K.; Huynh, C.; Tabard-Cossa, V.; Wang, H.; Dunbar, W. B. Nanopore-Based Target Sequence Detection. *PLoS ONE* **2016**, *11* (5), e0154426.
- (128) Manna, A.; Rapireddy, S.; Sureshkumar, G.; Ly, D. H. Synthesis of Optically Pure γ PNA Monomers: a Comparative Study. *Tetrahedron* **2015**, *71*, 3507–3514.
- (129) Falkiewicz, B.; Kołodziejczyk, A. S.; Liberek, B.; Wiśniewski, K. Synthesis of Achiral and Chiral Peptide Nucleic Acid (PNA) Monomers Using Mitsunobu Reaction. *Tetrahedron* **2001**, *57* (37), 7909–7917.
- (130) Pensato, S.; D'Andrea, L. D.; Pedone, C.; Romanelli, A. New Synthetic Route to Gamma-Mercaptomethyl PNA Monomers. *Synth. Commun.* **2008**, *38* (15), 2499–2506.
- (131) Chouikhi, D.; Ciobanu, M.; Zambaldo, C.; Duplan, V.; Barluenga, S.; Winssinger, N. Expanding the Scope of PNA-Encoded Synthesis (PES): Mtt-Protected PNA Fully Orthogonal to Fmoc Chemistry and a Broad Array of Robust Diversity-Generating Reactions. *Chem. Eur. J.* **2012**, *18* (40), 12698–12704.
- (132) Jain, D. R.; Ganesh, K. N. Clickable C-Gamma-Azido(Methylene/Butylene) Peptide Nucleic Acids and Their Clicked Fluorescent Derivatives: Synthesis, DNA Hybridization Properties, and Cell Penetration Studies. *J. Org. Chem.* **2014**, *79* (14), 6708–6714.

- (133) Jain, D. R.; Anandi, L.; Lahiri, M.; Ganesh, K. N. Influence of Pendant Chiral C-Gamma-(Alkylideneamino/Guanidino) Cationic Side-Chains of PNA Backbone on Hybridization with Complementary DNA/RNA and Cell Permeability. *J. Org. Chem.* **2014**, *79* (20), 9567–9577.
- (134) Kumar, P.; Jain, D. R. C-Gamma-Aminopropylene Peptide Nucleic Acid (Amp-PNA): Chiral Cationic PNAs with Superior PNA:DNA/RNA Duplex Stability and Cellular Uptake. *Tetrahedron* **2015**, *71* (21), 3378–3384.
- (135) Kosynkina, L.; Wang, W.; Liang, T. C. A Convenient Synthesis of Chiral Peptide Nucleic Acid (PNA) Monomers. *Tetrahedron Lett.* **1994**, *35* (29), 5173–5176.
- (136) Rittle, K. E.; Homnick, C. F.; Ponticello, G. S.; Evans, B. E. A Synthesis of Statine Utilizing an Oxidative Route to Chiral Alpha-Amino Aldehydes. *J. Org. Chem.* **1982**, *47* (15), 3016–3018.
- (137) Stanfield, C. F.; Parker, J. E.; Kanellis, P. Preparation of Protected Amino Aldehydes. *J. Org. Chem.* **1981**, *46* (23), 4797–4798.
- (138) Miles, N. J.; Sammes, P. G.; Kennewell, P. D.; Westwood, R. On the Double Bond Isostere of the Peptide Bond: Preparation of Modified Di- and Tri-Peptides Incorporating Proline and Alanine Analogues. *J. Chem. Soc. Perkin Trans 1* **1985**, *0* (0), 2299–2305.
- (139) Dellaria, J. F., Jr.; Maki, R. G. The Enantio- and Diastereoselective Synthesis of the First Phospho-Statine Derivative. *Tetrahedron Lett.* **1986**, *27* (21), 2337–2340.
- (140) Paz, M. M.; Sardina, F. J. Enantiomerically Pure Dimethyl (2S)-N-(9-Phenylfluoren-9-Yl)-3,4-Didehydroglutamate as Chiral Educt. Chiroselective Synthesis of (+)-5-O-Carbamoylpolyoxamic Acid and 3-Alkylglutamates. *J. Org. Chem.* **1993**, *58* (25), 6990–6995.
- (141) Lubell, W. D.; Rapoport, H. Configurational Stability of N-Protected Alpha-Amino Aldehydes. *J. Am. Chem. Soc.* **1987**, *109* (1), 236–239.
- (142) Fisher, T. L.; Terhorst, T.; Cao, X.; Wagner, R. W. Intracellular Disposition and Metabolism of Fluorescently-Labeled Unmodified and Modified Oligonucleotides Microinjected Into Mammalian Cells. *Nucleic Acids Res.* **1993**, *21* (16), 3857–3865.
- (143) Bramsen, J. B.; Laursen, M. B.; Nielsen, A. F.; Hansen, T. B.; Bus, C.; Langkjaer, N.; Babu, B. R.; Højland, T.; Abramov, M.; Van Aerschot, A.; Odadzic, D.; Smicius, R.; Haas, J.; Andree, C.; Barman, J.; Wenska, M.; Srivastava, P.; Zhou, C.; Honcharenko, D.; Hess, S.; Müller, E.; Bobkov, G. V.; Mikhailov, S. N.; Fava, E.; Meyer, T. F.; Chattopadhyaya, J.; Zerial, M.; Engels, J. W.; Herdewijn, P.; Wengel, J.; Kjems, J. A Large-Scale Chemical Modification Screen Identifies Design Rules to Generate siRNAs with High Activity, High Stability and Low Toxicity. *Nucleic Acids Res.* **2009**, *37* (9), 2867–2881.
- (144) Kabza, A. M.; Young, B. E.; Szczepanski, J. T. Heterochiral DNA Strand-Displacement Circuits. *J. Am. Chem. Soc.* **2017**, *139* (49), 17715–17718.
- (145) Kolpashchikov, D. M. Binary Probes for Nucleic Acid Analysis. *Chem. Rev.* **2010**, *110* (8), 4709–4723.
- (146) Lutz, J.-F.; Ouchi, M.; Liu, D. R.; Sawamoto, M. Sequence-Controlled Polymers. *Science* **2013**, *341* (6146), 1238149–1238149.

- (147) Gartner, Z. J.; Liu, D. R. The Generality of DNA-Templated Synthesis as a Basis for Evolving Non-Natural Small Molecules. *J. Am. Chem. Soc.* **2001**, *123* (28), 6961–6963.
- (148) Gartner, Z. J.; Kanan, M. W.; Liu, D. R. Expanding the Reaction Scope of DNA-Templated Synthesis. *Angew. Chem. Int. Ed. Engl.* **2002**, *41* (10), 1796–1800.

Chapter II: A General Method for Preparing the Right- and Left-Handed Fmoc-MP γ PNA Monomers with High Optical-Purity

The work in this chapter is to be submitted as:

Hsieh, W.-C.; Shaikh, A. Y.; Ly, D. H. A General Method for Preparing Optically-Pure (*R*)- And (*S*)-Fmoc-MiniPEG-Containing Gamma Peptide Nucleic Acid Monomers.

Wei-Che Hsieh and Dr. Danith H. Ly designed the research. Wei-Che Hsieh and Dr. Ashif Yasin Shaikh developed the schemes. Wei-Che Hsieh and Dr. Danith H. Ly analyzed the data and wrote the paper.

2.1 Introduction

Synthetic oligonucleotides are valuable as molecular tools and reagents for biology, biotechnology, and medicine, as well as for molecular engineering and computation.¹⁻³ Paramount to the success of many of these applications is a reliance on their ability to recognize and bind the designated DNA or RNA targets, or their obligatory partners with high affinity and sequence-specificity. Other biophysical attributes, including cellular transduction, biodistribution, and metabolism, may be required for intracellular or *in vivo* applications; however, they are not necessary for *in vitro* experiments. It is therefore essential to be able to modify the structures and chemical functionalities of these molecular tools and reagents with ease so that they could be tailor-designed to suit the specific tasks

in hand, since there is no one particular design or chemical outfit that can fulfill all the requirements.

A particular class of nucleic acid mimic that is endowed with such synthetic flexibility is peptide nucleic acid (PNA). Developed by Nielsen and coworkers⁴ in the early 1990's, PNA comprises an entirely different backbone skeleton from that of DNA or RNA, made up of *N*-(2-aminoethyl) glycine units. PNA has several appealing features, including tight and sequence-specific binding with DNA or RNA, and resistance to enzymatic degradation.⁵ Furthermore, the acyclic and achiral backbone provides a convenient means for chemical modifications. However, it is not without shortcomings. The charge-neutral polyamide backbone that confers PNA with many of its attractive features renders it less water soluble than the natural counterparts. As a result, PNA tends to aggregate and adhere to surfaces and other macromolecules in a non-specific manner. While this issue has been addressed to some degree,⁶⁻⁸ further improvements in this and other areas, including synthetic methodology and recognition property, are needed in order to expand the scope and utility of PNA in the various research disciplines.

A promising approach involves installation of a chiral center at the gamma backbone. Such a stereochemical modification transforms PNA from a random-fold into either a right-handed (RH) or a left-handed (LH) helical motif, depending on the stereochemistry.⁹ The LH conformer is unable to hybridize to the RH, or to DNA or RNA, due to conformational mismatch.¹⁰ On the other hand, the RH hybridizes to DNA or RNA with exquisite affinity and specificity, and is able to invade double helical DNA or RNA without sequence restriction.¹¹ Furthermore, by incorporating diethylene glycol (commonly referred to as MiniPEG, or 'MP') moiety at the gamma backbone, the water

solubility and biocompatibility of PNA could be significantly improved without introducing charges.¹² These newly endowed properties of PNA have been exploited in a number of applications, including biosensing,¹³⁻¹⁵ gene editing,^{16,17} and molecular engineering.¹⁰ The challenge with this stereochemical approach, however, is in the production of chemical building blocks that are optically-pure and that are compatible with the automated solid-phase peptide synthesis (SPPS). The former is essential since even the slightest amount of a racemate could have profound effects on the conformation and hybridization property of the oligonucleotide.¹⁸ Herein, we report the development of a robust method for scaling-up the production of enantiomerically-pure, Fmoc-protected (*R*)- and (*S*)-MP γ PNA monomers from relatively cheap and commercially available starting materials for SPPS (**Figure II- 1**).

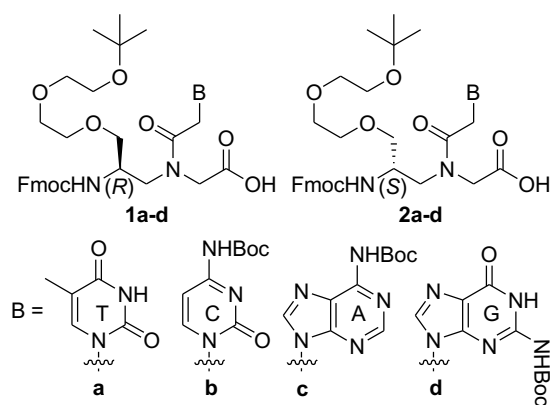
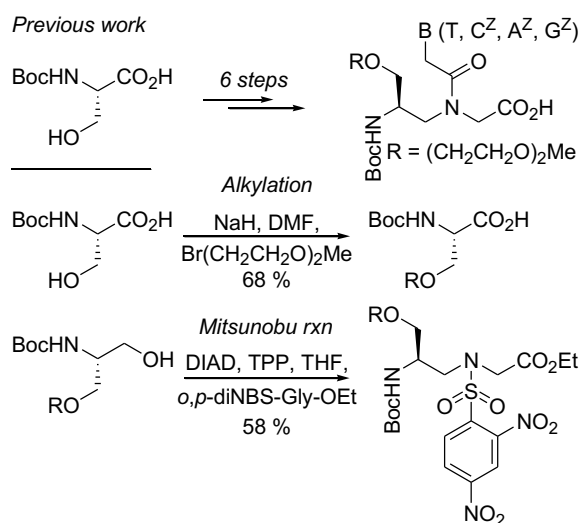


Figure II- 1. Fmoc-protected (*R*)- and (*S*)-MP γ PNA monomers being prepared by this method.

2.2. Results and Discussion

Most chiral PNA monomers were prepared through the reductive amination route, starting with Boc- or Fmoc-protected amino acids.¹⁹ However, such a coupling reaction is known to be configurationally unstable due to the propensity of Boc- and Fmoc-aminoaldehydes to undergo epimerization even under mild experimental conditions.²⁰⁻²³ We were able to minimize the extent of racemization by carrying out serine side chain-alkylation under a strict reaction condition and by employing Mitsunobu reaction in the preparation of MP γ PNA backbone (**Scheme II- 1**).¹² While we were able to produce small quantities of optically-pure MP γ PNA monomers for the initial proof-of-concept studies, it remains a challenge to scale-up monomer production without compromising optical purity. First, it requires the reaction to be performed at a low temperature and in a relatively short time to avoid racemization. Second, it requires a strenuous purification step that would be required to remove triphenylphosphine oxide from the desired backbone. Moreover, such a protocol is not compatible with Fmoc-chemistry due to the strong basicity employed in the alkylation step, which would lead to its removal.

To overcome these issues of scalability, optical purity, and harsh on-resin reaction conditions, we explored several protecting groups, including fluorenylmethyloxycarbonyl (Fmoc),²⁴ dibenzyl,²⁵ 9-phenylfluorenyl (PhF),²⁶ and 9-(4-bromophenyl)-9-fluorenyl (BrPhF),²⁷ along with numerous synthetic routes. Among these we found BrPhF to be the most robust and facile temporary protecting group, and the synthetic route outlined in **Scheme II- 2** through **4** to be the most economical in the production of monomers **1a-d** and **2a-d** (**Figure II- 1**). The other protecting groups were not as successful due to several setbacks (Refer to **Scheme II-S 1** and **Scheme II-S 2**).



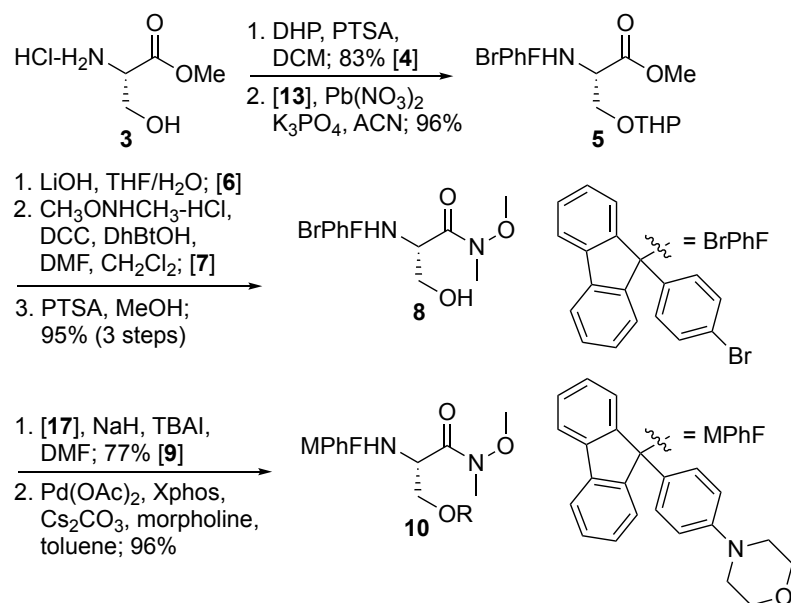
Scheme II- 1. Synthesis of Boc-protected MP γ PNA monomer by Mitsunobu-mediated reaction.¹²

Previously we have shown that PhF, a nitrogen protecting group originally developed by Rapoport²⁸ in the early 1980's, was effective in shielding the α -center of amino acids against epimerization under highly basic conditions.²⁹ The protective capacity of PhF has been largely attributed to its sterically demanding size and its preference as a leaving group. The demanding size forced the α -proton of ester to be in an unfavorable orientation for deprotonation.³⁰ Upon the extreme condition for deprotonation, namely the treatment of excess base and refluxing, the reprotionation of the α anion is slower than the elimination of the PhF group, which secured the optical purity of the intact PhF-protected ester.²⁸ Unfortunately, we found PhF to be difficult to remove in the subsequent steps, requiring either a strong acid or a prolonged hydrogenolysis—which could lead to undesired reactions, including reduction of the cytosine nucleobase.³¹ To avoid such harsh conditions, here we adopted its synthetic derivative, BrPhF,³² which

retains the full protection repertoire of PhF but can be selectively removed under a mild acidic condition following the insertion of an electron-donating group, such as morpholine.

The strategy for incorporating BrPhf and MPhf is outlined in **Scheme II- 2**. The hydroxyl group of L-serine methyl ester **3** was selectively protected by tetrahydropyranyl acetal (THP) group and followed by the *N*-alkylation of BrPhF group. We found the THP protection³³ instead of *in-situ* trimethylsilylation²⁶ was necessary to provide high yield of conversion to ester **5**. The conversion of ester **5** to Weinreb amide **8** was performed by the three-step process with basic hydrolysis, Weinreb amide formation and removal of THP group with 95% overall yield. This conversion could have been performed in a one-pot manner by employing Lewis acid Me₂AlCl and *N,O*-dimethylhydroxylamine hydrochloride;³⁴ however, the latter method could only remove the THP group even with excess of Me₂AlCl. (Data not shown)

Next, in the conversion of **8** to **10**, the hydroxyl group was *O*-alkylated with miniPEG tosylate **17** with addition of TBAI and NaH, followed by Buchwald amination with yields 77% and 96% respectively. For the amination, Cs₂CO₃ and Xphos were found to be the best combination due to higher conversion and presumably less elimination product found. (**Table II- 1**) Overall, the alkylated Weinreb amide (**10**) was prepared in seven steps with greater than 55% overall yield, with several reaction steps carried out in nearly quantitative yields. (**Scheme II- 2**)

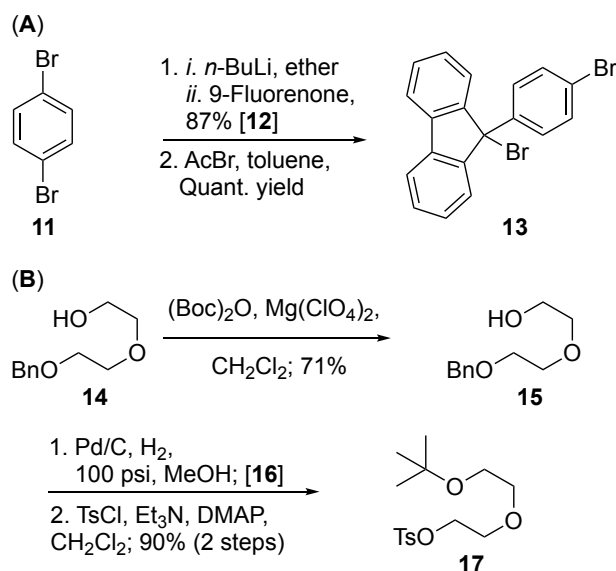


Scheme II- 2. Synthesis of intermediate **10** from L-serine methyl ester **3**.

Entry	Ligand (0.06 eq)	Base (5 eq)	Yield ^a
1	Xphos	NaO ^t Bu	<5%
2	Johnphos	NaO ^t Bu	<5%
3	BINAP	NaO ^t Bu	<5%
4	Xanthphos	NaO ^t Bu	<5%
5	Davephos	NaO ^t Bu	<5%
6	Xphos	Cs ₂ CO ₃	>90%
7	Johnphos	Cs ₂ CO ₃	~70%
8	BINAP	Cs ₂ CO ₃	~80%
9	Xanthphos	Cs ₂ CO ₃	<10%
10	Davephos	Cs ₂ CO ₃	~70%

Table II- 1. Screened conditions for Buchwald amination. All reactions were performed with 0.06 eq of Pd(OAc)₂ in toluene (0.1M) for 2 hr with the indicated reagents in the table. Temperature was set at 80 °C to mitigate racemization issue. ^a: TLC yield.

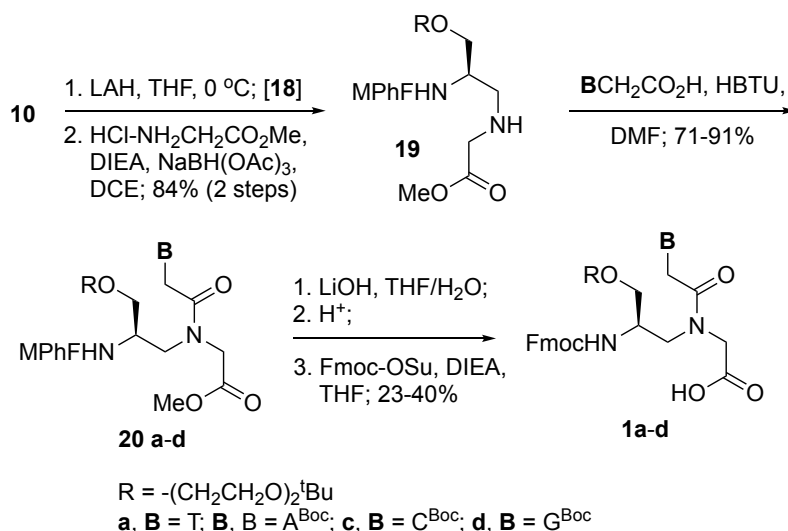
The BrPhF precursor and MP-sidechain were prepared as shown in **Scheme II- 3**. In **Scheme II- 3A**, the BrPhF hydroxyl precursor **12** was brominated with acetyl bromide³⁵ in toluene with quantitative yield, instead of HBr aqueous solution.³⁶ The latter condition resulted in rapid solvolysis of **13**. In **Scheme II- 3B**, the benzyl diethylene glycol was first converted to tert-Butyl ether by the treatment of magnesium perchlorate and Boc anhydride.³⁷ The relatively low yield resulted from the impurity benzyl monoethylene glycol from starting material. The tert-Butyl ether was then subjected to nearly neat high-pressure hydrogenation and tosylation to afford miniPEG tosylate **17**.



Scheme II- 3. Synthesis of (A) 9-(4-bromophenyl)-9-fluorenyl bromide (**13**)³² and (B) 2-(2-(tert-butoxy)ethoxy)ethyl 4-methylbenzenesulfonate (**17**).

Once prepared, the Weinreb amide **10** was converted to an aldehyde, followed by reductive amination³⁸ to produce the backbone intermediate **19**. (**Scheme II- 4**) Coupling the backbone with nucleobase acetic acids yielded the desired monomer esters **20a-d**. Subsequent hydrolysis and a replacement of MPhF with Fmoc produced the right-handed (*R*)-MP γ PNA monomers **1a-d**. During the workup of basic hydrolysis, we found the MPhF was removed by prolonged stirring with heterogenous Dowex resin at 0 °C. This condition

didn't remove the *tert*-butyl- or Boc-protecting group as crude ESI-MS data suggested. (Figure II-S 27 and Figure II-S 28) However, the Fmoc protection with the treatment of Fmoc-OSu and DIEA could not afford satisfactory yield (up to 40%) even with excess of reagents and prolonged stirring. An attempt to utilize Fmoc-Cl resulted in undesired cyclized product most likely due to the chlorination of carboxylic acid and then intramolecular *N*-acylation. (Data not shown) Further investigations with other Fmoc reagents may enhance the final yield.³⁹ Similarly, the left-handed version was prepared with a relatively cheap D-serine methyl ester.



Scheme II- 4. Synthesis of Fmoc-protected MP γ PNA from intermediate (**10**).

Their optical purities were confirmed by converting Fmoc groups of monomers **1a** (RH) and **2a** (LH) to Mosher derivatives **23** and **24**, respectively. On the ¹H-NMR spectra, both derivatives **23** and **24** formed rotamers with ratio ~ 1:1. (See **Figure II-S 37** and **Figure II-S 39**) However, on the ¹⁹F-NMR spectra (**Figure II- 2**), the RH derivative **23** exhibited double peaks, while the LH derivative **24** only exhibited a singlet as previously noted.¹² The discrepancy of ¹⁹F NMR patterns presumably resulted from the different chemical environments with the neighboring substituents; therefore, the rotamers of the LH derivative **24** were not separable.

In this study, the double peak pattern of the RH derivative was not observed on the spectrum of the LH derivative, indicating enantiomeric excess is greater than 99.5%, the detection limit of ¹⁹F-NMR.⁴⁰ A more rigorous analysis by HPLC also showed that the e.e. value is more than 99.5 % for both derivatives. (**Figure II- 3**) These results suggested that with BrPhF and MPhF as the protecting groups, the optical purity of final monomers was secured even under conditions with strong bases and elevated temperatures.

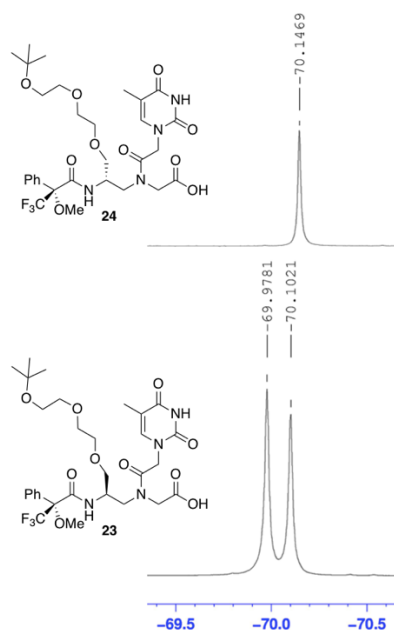


Figure II- 2. Assessment of enantiomeric purity. ^{19}F -NMR spectra of compounds **23** and **24**. The doublet pattern of each compound in **23** is the result of the formation of rotamers in d^6 -DMSO.

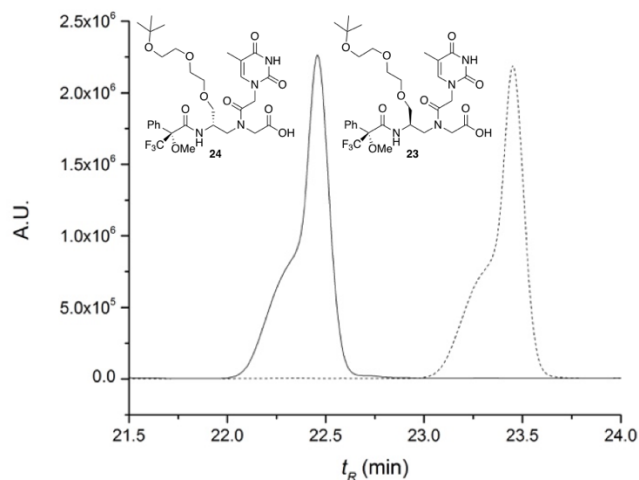


Figure II- 3. Assessment of enantiomeric purity. HPLC chromatograms of compounds **23** and **24**. Undetectable peak overlapping was observed. HPLC Condition: C18 column (dimensions 4.6 mm X 250 mm), 1 mL/min flow rate, 60 °C oven temperature, 25 to 75% ACN/ H_2O with 0.1% TFA in 30 min.

2.3. Conclusions

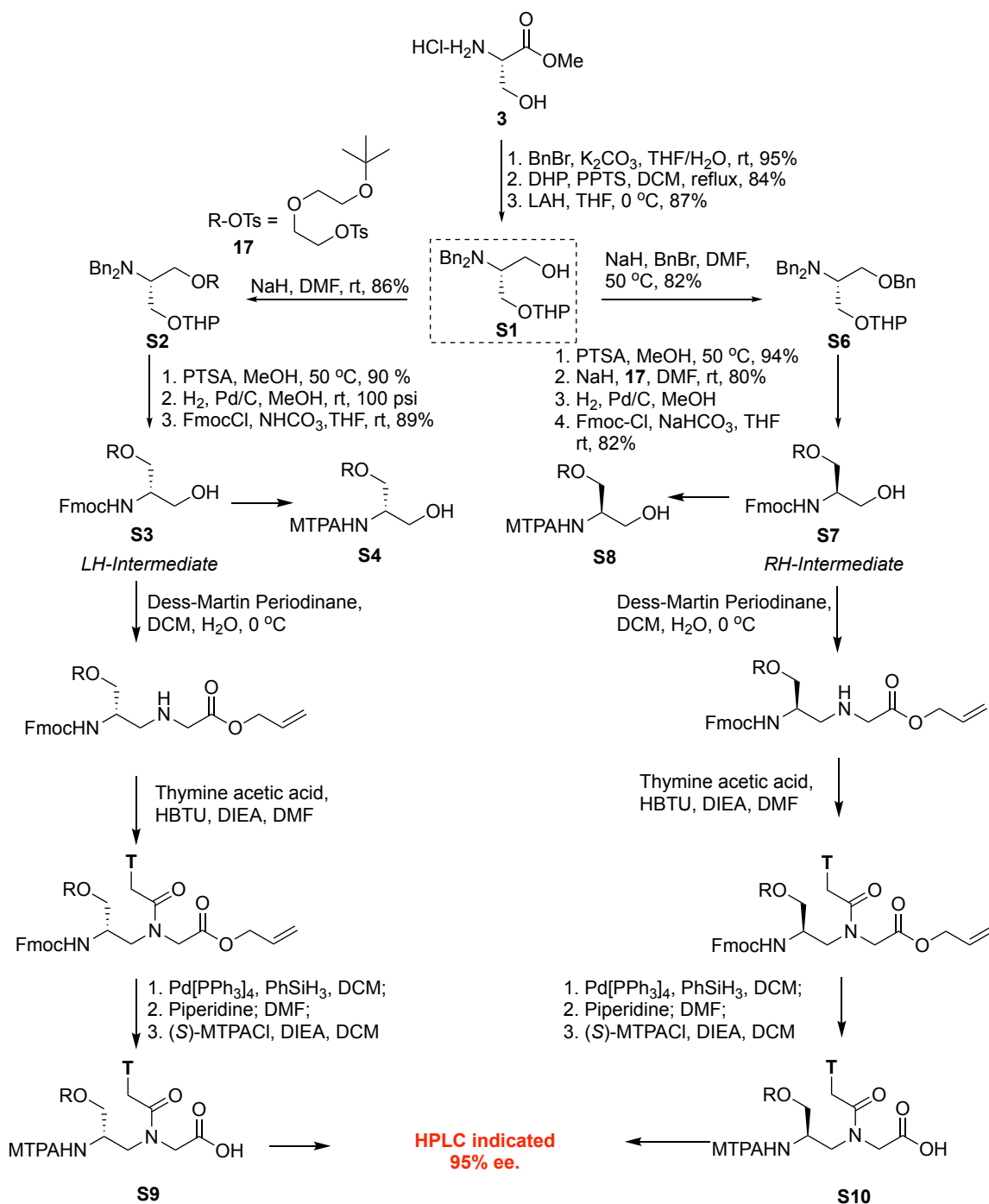
Overall, we developed a general and robust synthetic method for scaling-up the production of enantiomerically-pure, Fmoc-protected (*R*)- and (*S*)-MP γ PNA monomers. The work employed a safety-catch BrPhF-protecting group and its morpholine derivative for shielding the α -proton from undergoing epimerization in the alkylation and reductive amination steps. The ee values of these monomers were determined to be greater than 99.5% by HPLC and ^{19}F -NMR. Although the synthetic route is relatively lengthy in comparison to the published report,¹² many of these reaction steps provided excellent chemical yields and were used in the subsequent steps without purification. Upon the insertion of morpholine, the resulting MPhF-protecting group can be removed *in situ* with the ester group, during acid-neutralization following hydrolysis, without affecting the *tert*-butyl- or Boc-protecting group. The resulting amine can be readily protected with Fmoc or any other functional groups as desired. This is in direct contrast to all the other routes that we have examined,^{12,29} which were prone to racemization and required strenuous column chromatography for purification in every step. This method could be potentially applied to prepare monomers with novel chemical modifications at gamma backbone positions.

2.4. Experimental Sections

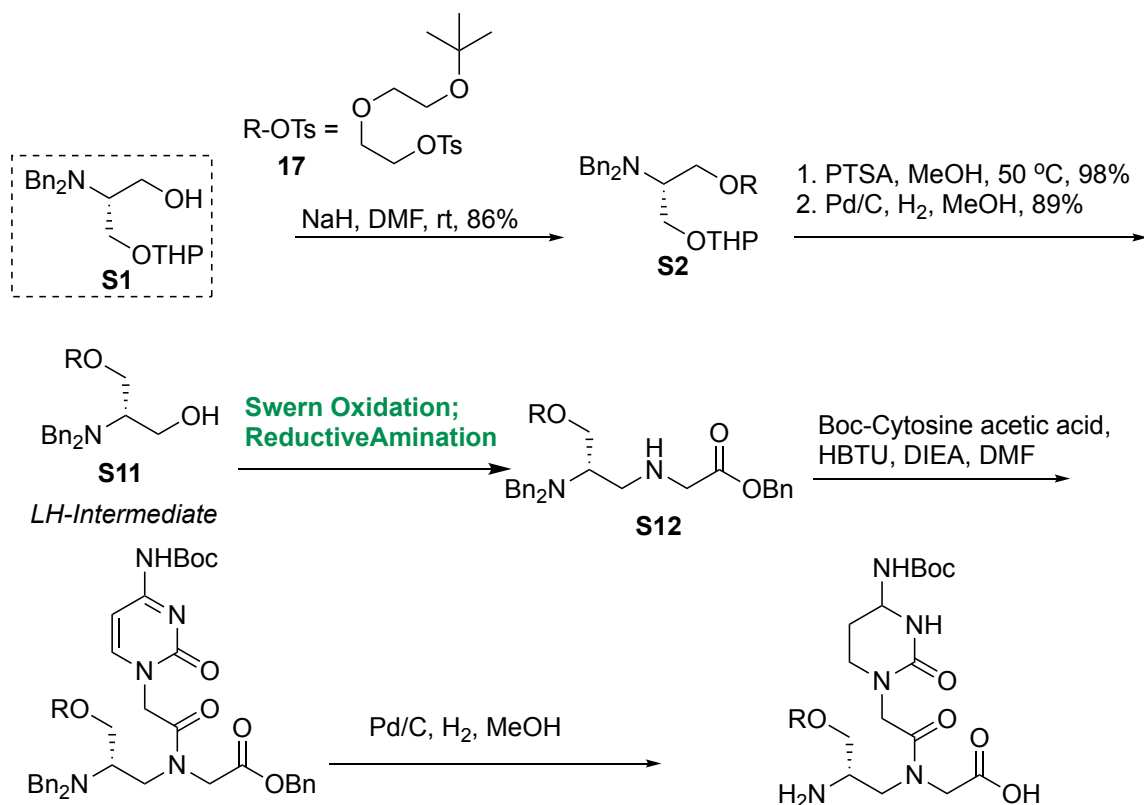
2.4.1. Material and Methods

All commercial reagents were used without further purification. Solvents were dried by standard methods and distilled freshly prior to use. ^1H -, ^{13}C - and ^{19}F -NMR spectra were recorded on a Bruker 500 MHz Avance NMR spectrometer using standard Bruker software. The ^1H NMR spectra were referenced to d^6 -DMSO (2.50 ppm) or TMS in CDCl_3 (0.00 ppm). The ^{13}C NMR spectra were referenced to CDCl_3 (77.23 ppm) or d^6 -DMSO (39.52 ppm). The ^{19}F NMR spectra were referenced to TFA in d^6 -DMSO (-76.55 ppm). Flash chromatography was performed using standard silica gel (60Å, 63-200 μm) or NH_2 silica gel (100 Å, 40-75 μm). TLC was generally performed with silica gel 60 F-254 precoated plates or NH_2 HPTLC plate plate. High Resolution Mass Spectrometry (HRMS) was performed with a Thermo Scientific Exactive Plus EMR Orbitrap ESI mass spectrometer. GC-MS analysis was performed on a Hewlett-Packard Agilent 6890-5973 GC-MS workstation with a Hewlett-Packard fused silica capillary column cross-linked with 5% phenylmethylsiloxane and Helium as the carrier gas. The following conditions were used for all GC-MS analyses: injector temperature, 250 °C; initial temperature, 70 °C; temperature ramp, 10 °C/min; final temperature, 280 °C. High-performance liquid chromatography was performed by Shimadzu UFLC system with a C18 column (dimensions 4.6 mm X 250 mm) and 1 mL/min flow rate. Gradients and temperature were indicated with figures.

2.4.2. Supplementary Schemes

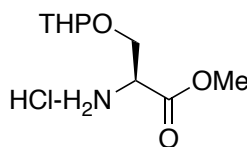


Scheme II-S 1. An attempt to use Fmoc protecting group for preparing γ PNA monomers. The final product **S9** and **S10** exhibited 95% ee. See **Figure II-S 41** for optical purity results.



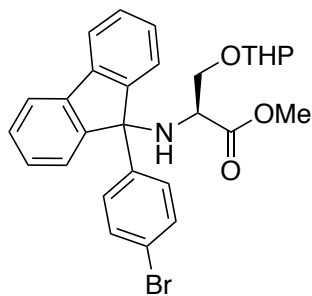
Scheme II-S 2. An attempt to use Dibenzyl protecting group for preparing γ PNA monomers. The hydrogenation condition cannot be applied to cytosine due to over reduction.

2.4.3. Experimental Protocols



*O*³-(Tetrahydropyran-2-yl)-L-serine methyl ester hydrochloride (**4**)³³

To a suspension of L-serine methyl ester hydrochloride (19.5 g, 127.3 mmol) in anhydrous CH₂Cl₂ (100 mL) was added 3,4-dihydro-1-H-pyran (17.1 mL, 187.8 mmol) and *p*-toluenesulfonic acid monohydrate (0.476 g, 2.5 mmol). The reaction mixture was allowed to stir at room temperature for 20 h. The resulting precipitates were chilled with ice bath, filtered and washed with chilled CH₂Cl₂ to afford white powder without further purification (25.7 g, 83%). C₉H₁₈ClNO₄; white solid; TLC (MeOH/CH₂Cl₂, 10:90) *R*_f = 0.6; diastereomeric ratio: 83:17; ¹H NMR (500 MHz, DMSO) δ 8.77 (3H, s), 4.63–4.57 (1H, m), 4.33–4.28 (1H, m), 4.04–3.99 (1H, m), 3.82–3.75 (4H, m), 3.63–3.58 (1H, m), 3.46–3.44 (1H, m), 1.79–1.41 (6H, m); ¹³C NMR (125 MHz, DMSO) δ 168.1, 98.3/97.7, 64.6/64.4, 61.3/61.0, 52.8, 52.3/52.2, 29.7/28.5, 24.8, 18.5. HRMS (ESI) calcd for C₉H₁₈NO₄: 204.1236; found: *m/z* 204.1223 [M – HCl + H]⁺.



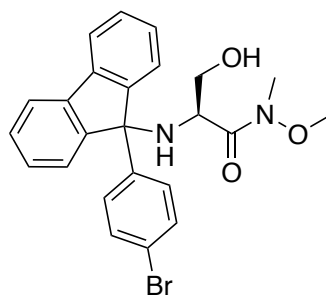
5

N-(9-(4-Bromophenyl)-9-Fluorenyl)-*O*³-(Tetrahydropyran-2-yl)-serine methyl ester (**5**)

9-(4-Bromophenyl)-9-Fluorenyl bromide (**13**): To an anhydrous solution of 9-(4-Bromophenyl)-9-Fluorenyl bromide (**12**)³² (14.1 g, 41.8 mmol) in toluene (208.0 mL) was added acetyl bromide (61.9 mL, 835.1 mmol) at 0 °C and refluxed at 120 °C for 2h. After the reaction completion was confirmed by GC-MS, the reaction mixture was concentrated under reduced pressure and co-evaporated with toluene for three more times. The residue was dried *in vacuo* for 12 h to afford the bromide compound (**13**) as yellowish syrup. It was directly used for the next step without further purification. For analytical sample: ¹H NMR (500 MHz, CDCl₃) δ 7.66 (2H, d, *J* = 7.7 Hz), 7.47 (2H, d, *J* = 7.4 Hz), 7.41 (2H, d, *J* = 8.6 Hz), 7.37–7.34 (4H, m), 7.29–7.26 (2H, m); ¹³C NMR (125 MHz, CDCl₃) δ 149.1, 140.4, 138.0, 131.4, 129.2 (2x), 128.6, 125.9, 122.2, 120.4, 66.5. GC-MS *t*_R = 17.8 min.

To a solution of serine ester (**4**) (8.00 g, 33.4 mmol) in anhydrous ACN (110.0 mL) was added Pb(NO₃)₂ (55.32 g, 167.0 mmol) and K₃PO₄ (35.5 g, 167.0 mmol) and stirred for 30 min. To the suspension was transferred bromide compound (**13**) in CH₂Cl₂ (44 mL) and allowed to stir at room temperature for 24 hr. The reaction was quenched by MeOH (10 mL). The mixture was then filtered by Celite pad. The filtrate was concentrated *in vacuo* and purified by flash chromatography on silica gel (EtOAc/hexane, 8:92 to 15:85) to afford yellow syrup as product. (16.7 g, 96% from serine ester (**4**)). C₂₈H₂₈BrNO₄; TLC (EtOAc/hexane, 15:85) *R*_F = 0.4; diastereomeric ratio: 83:17; ¹H NMR (500 MHz, DMSO)

δ 7.85 (2 H, t, $J = 8.0$ Hz), 7.43–7.35 (4 H, m), 7.32–7.22 (5 H, m), 7.18 (1 H, d, $J = 7.5$ Hz), 4.42 (0.17H, m), 4.32 (0.83H, t, $J = 3.4$ Hz), 3.55–3.51 (3H, m), 3.35–3.30 (2H, m), 3.17 (2.49H, s), 3.15 (0.51H, s), 2.76–2.71 (1 H, m), 1.57–1.28 (6 H, m); ^{13}C NMR (125 MHz, DMSO) δ 173.8/173.6, 148.5/148.4, 148.2/148.1, 144.1, 140.0, 139.9, 131.0, 128.6/128.5, 128.1, 128.0, 127.6, 125.5, 124.7, 120.3, 120.1, 98.0/96.8, 72.0, 68.4/67.7, 61.2/60.5, 55.9/55.6, 51.1/51.0, 29.9/29.7, 24.8, 18.8/18.4; HRMS (ESI) calcd for $\text{C}_{28}\text{H}_{29}^{81}\text{BrNO}_4$: 524.1259.; found: m/z 524.1252 $[\text{M} + \text{H}]^+$.



8

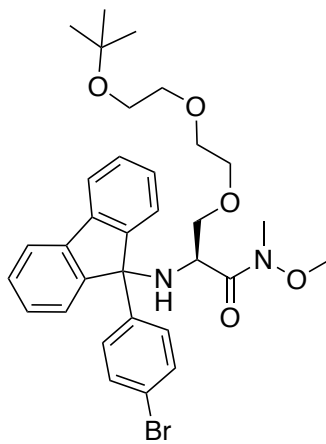
2-N-(9-(4-Bromophenyl)-9-Fluorenyl)-3-hydroxy-N-methoxy-N-methylpropanamide (8)

To a chilled solution of methyl ester (**5**) (10.0 g, 19.1 mmol) in a co-solvent of ethanol and water (400 mL, 1:1) was added LiOH-H₂O (3.21 g, 76.6 mmol) portionwisely at 0 °C with ice bath. The reaction mixture was allowed to gradually warm up to and stir at ambient temperature for 12 h. The mixture was neutralized by Dowex resin and filtered. The filtrate was concentrated *in vacuo* and coevaporated with toluene (3x) to afford acid (**6**) as white solid. The crude was used for the next step without further purification.

To the above acid was added anhydrous DMF and CH₂Cl₂ (200 mL, 3:1), followed by DCC (5.93 g, 28.7 mmol) and DhBtOH (4.68 g, 28.7 mmol) at 0 °C with ice bath. After 1h of stirring, a mixture of *N,O*-dimethylhydroxylamine (2.80 g, 28.7 mmol), DIEA (5.00 mL, 28.7 mmol) in anhydrous DMF and CH₂Cl₂ (200 mL, 3:1) was transferred to the above

reaction mixture at 0 °C. The resulting reaction mixture was allowed to stir for 2 h at ambient temperature. The reaction was then quenched by methanol and concentrated *in vacuo*. The resulting syrup was then diluted with EtOAc (50 mL). The organic layer was washed with sat. NaHCO₃ (3x) and brine (3x), dried over Na₂SO₄, and concentrated *in vacuo* to afford weinreb amide (**7**) as yellowish foaming solid. The crude was used for the next step without further purification.

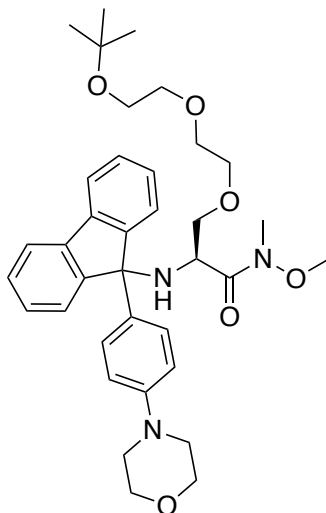
To the above amide was added methanol (95.7 mL) and *p*-toluenesulfonic acid monohydrate (3.64 g, 19.1 mmol) at 0 °C and allowed to stir at ambient temperature for 18 h. The reaction mixture was neutralized with sat. NaHCO₃ and concentrated *in vacuo*. The resulting solid was diluted with EtOAc and H₂O. The aqueous layer was washed with EtOAc (2x). The combined organic layer was washed with brine, dried over Na₂SO₄, and concentrated *in vacuo*. The residue was then purified by column chromatography (EtOAc: Hexane= 40:60 to 85:15) to afford alcohol (**8**) (8.50 g, 95% for three steps). Colorless syrup; C₂₄H₂₃BrN₂O₃; TLC (EtOAc/hexane, 65:35) *R*_f 0.4; ¹H NMR (500 MHz, DMSO) δ 7.83 (2 H, d, *J* = 8.1 Hz), 7.43–7.35 (5 H, m), 7.30–7.24 (4 H, m), 7.10 (1 H, d, *J* = 7.6 Hz), 4.63 (1H, t, *J* = 5.9 Hz), 3.33–3.24 (3H, m), 2.95 (4H, br), 2.72 (3H, br); ¹³C NMR (125 MHz, DMSO) δ 173.8, 149.0, 148.2, 144.5, 140.5, 139.5, 131.1, 128.4, 128.1, 127.9, 127.5, 125.7, 125.7, 120.1, 72.1, 64.0, 59.9, 53.8, 31.5; HRMS (ESI) calcd for C₂₄H₂₄BrN₂O₃: 467.0970; found: *m/z* 467.0954 [M + H]⁺.



9

2-N-(9-(4-Bromophenyl)-9-Fluorenyl)-3-(2-(2-(tert-butoxy)ethoxy)ethoxy)-N-methoxy-N-methylpropanamide (9)

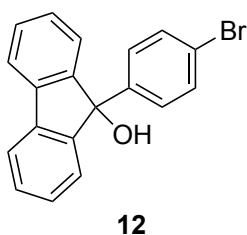
To a chilled solution of alcohol (**8**) (7.73g, 16.5 mmol eq) in DMF (0.2 M) at 0 °C with ice bath was added 60% NaH (1.00 g, 25.0 mmol) and allowed to stir at the same temperature. After 30 min, tetrabutylammonium iodide (0.10 g, 0.17 mmol) and tosylate (**17**) (10.5 g, 19.9 mmol) were added to the above suspension. After 12 h, the reaction was quenched by sat. NH₄Cl. The mixture was concentrated *in vacuo* and followed by stirring with EtOAc and water. The aqueous layer was washed with EtOAc (2x). The combined organic layer was then washed with brine, dried over Na₂SO₄, and concentrated *in vacuo*. The residue was purified by column chromatography on silica gel (EtOAc/hexane, 22:78 to 53:47) to afford colorless syrup (7.80 g, 77%). C₃₂H₃₉BrN₂O₅; TLC (EtOAc/hexane, 50:50) *R_f* = 0.4; ¹H NMR (500 MHz, DMSO) δ 7.83 (2 H, d, *J* = 6.3 Hz), 7.42–7.34 (5 H, m), 7.29–7.23 (4 H, m), 7.10 (1 H, d, *J* = 7.5 Hz), 3.40–3.27 (11H, m), 3.17 (1H, br), 2.99 (3H, br), 2.71 (3 H, br), 1.09 (9 H, s); ¹³C NMR (125 MHz, DMSO) δ 173.5, 148.8, 148.2, 140.4, 139.6, 131.1, 128.5, 128.0, 127.9, 127.5, 125.6, 124.9, 120.2, 73.1, 72.2, 72.0, 70.4, 70.0, 69.6, 60.6, 60.0, 51.4, 31.5, 27.2; HRMS (ESI) calcd for C₃₂H₄₀⁸¹BrN₂O₅: 613.2100; found: *m/z* 613.2085 [M + H]⁺.



10

3-(2-(2-(tert-butoxy)ethoxy)ethoxy)-N-methoxy-N-methyl-2-N-(9-(4-morpholinophenyl)-9-Fluorenyl)-propanamide (10)

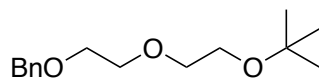
To a solution of bromide (**9**) (7.50 g, 12.2 mmol) in degassed toluene (24 mL) was added Pd(OAc)₂ (137.7 mg, 0.61 mmol), XPhos (292.31 mg, 0.61 mmol), cesium carbonate (20.0 g, 61.3 mmol) and morpholine (1.29 mL, 14.7 mmol). The resulting mixture was heated up to 80 °C for 2 hr. After gradual cooling to ambient temperature, the reaction mixture was filtered through Celite pad. The filtrate was concentrated *in vacuo* and directly purified by flash column chromatography on NH₂ silica gel (EtOAc/hexane, 18:72 to 63:37) to afford product (**10**) as colorless syrup (7.27 g, 96%). C₃₆H₄₇N₃O₆; TLC (EtOAc/hexane, 50:50) *R_f* = 0.2; ¹H NMR (300 MHz, DMSO) δ 7.82–7.78 (2 H, m), 7.38–7.07 (8 H, m), 6.78 (2H, d, *J* = 9.0 Hz), 3.68 (4H, t, *J* = 4.7 Hz), 3.38–3.22 (11 H, m), 3.11 (1H, br), 3.03–2.97 (7 H, m), 2.72 (3H, br), 1.10 (9H, s); ¹³C NMR (125 MHz, DMSO) δ 173.7, 150.0, 149.7, 148.8, 140.3, 139.4, 135.0, 128.1, 127.7, 127.2, 126.3, 125.6, 124.9, 120.0, 114.7, 73.3, 72.2, 72.0, 70.4, 70.0, 69.6, 66.0, 60.6, 59.3, 51.5, 48.3, 31.5, 27.2; HRMS (ESI) calcd for C₃₆H₄₇N₃NaO₆: 640.3363; found: *m/z* 643.3338 [M + Na]⁺.



*9-(4-Bromophenyl)-9-Fluorenone (12)*³²

To a solution of 1,4-dibromobenzene (72.1 g, 305.5 mmol) in 1L of ether at – 50 °C by ACN-dry ice bath, was added n-butyllithium (1M, 25 mL) over a period of 1h and stirred for another 30 min. To the above suspension was transferred fluorenone (38.5 g, 213.8 mmol) in 400 mL of ether under N₂ atmosphere and allowed to stir at the same temperature for another 1h. The reaction mixture then gradually warmed up to ambient temperature and stirred for 2 h. After reaction was complete, the mixture was cooled to 0 °C and quenched by water (200 mL). The aqueous layer was then washed with ether (300 mL 2x). The combined organic layer was washed with brine (300 mL 2x), dried over MgSO₄, and concentrated *in vacuo* to afford crude as yellow syrup. The residue was purified by flash column chromatography on silica gel (EtOAc/hexane, 1:49 to 1:9) to afford product (62.6 g, 87% yield from fluorenone).

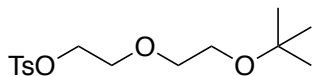
C₁₉H₁₃BrO; white solid; TLC (EtOAc/hexane, 15:85) *R_f* = 0.4; ¹H NMR (500 MHz, CDCl₃) δ 7.65 (2 H, d, *J* = 7.8 Hz), 7.38–7.35 (4H, m), 7.28–7.22 (6H, m), 2.41 (1H, br); ¹³C NMR (125 MHz, CDCl₃) δ 150.0, 142.3, 139.5, 131.3, 129.3, 128.6, 127.3, 124.7, 121.2, 120.2, 83.3.



15

((2-(2-(tert-butoxy)ethoxy)ethoxy)methyl)benzene (15)

To a chilled solution of ethylene glycol monobenzyl ether (157.0 g, 0.80 mol) in CH_2Cl_2 (1.0 L) at $-50\text{ }^\circ\text{C}$ by ACN/dry ice bath was added Boc anhydride (401.6 g, 1.84 mol) and $\text{Mg}(\text{ClO}_4)_2$ (17.9 g, 0.80 mol). The reaction mixture was allowed to gradually warm up to room temperature and refluxed for 36 hr. The reaction was quenched by adding sat. NaHCO_3 (200 mL). The aqueous layer was washed with CH_2Cl_2 (200 mL 2x). The combined organic layer was washed with brine, dried over Na_2SO_4 and concentrated *in vacuo*. The crude was purified by flash column chromatography on silica gel (EtOAc/hexane, 1:99 to 16:84) to afford product **(15)** (144.3 g, 71%) and mixture with ((2-(tert-butoxy)ethoxy)methyl)benzene (22.1 g). $\text{C}_{15}\text{H}_{24}\text{NO}_3$; colorless syrup; TLC (EtOAc/hexane, 15:85) $R_f = 0.6$; ^1H NMR (300 MHz, CDCl_3) δ 7.35–7.26 (5 H, m), 4.58 (2 H, s), 3.69–3.53 (8 H, m), 1.20 (9H, s); ^{13}C NMR (75 MHz, CDCl_3) δ 138.3, 128.3, 127.8, 127.5, 73.2, 72.5, 71.2, 70.7, 69.4, 61.2, 27.4; HRMS (ESI) calcd for $\text{C}_{15}\text{H}_{24}\text{NaO}_3$: 275.1623; found: m/z 275.1606 $[\text{M} + \text{Na}]^+$.

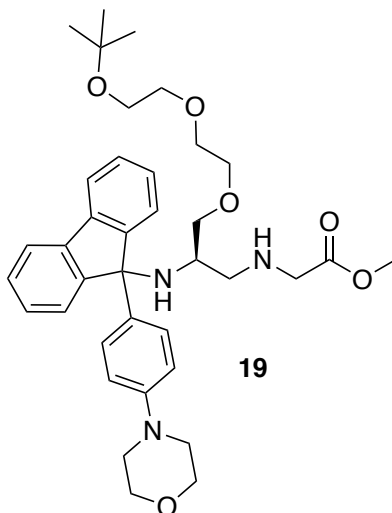


17

2-(2-(tert-butoxy)ethoxy)ethyl 4-methylbenzenesulfonate (17)

To a chilled solution of *tert*-butyl ether (**15**) (144.3 g, 0.57 mol) in MeOH (50 mL) at 0 °C was added Pd/C (608.5 mg, 0.57 mmol). The reaction was stirred with 100 psi of H₂ gas for 12 hr at ambient temperature. The reaction mixture was then cooled down to 0 °C and filtered through Celite. The filtrate was concentrated *in vacuo* to afford alcohol (**16**) and directly used for the next step without purification.

To a chilled solution of alcohol (**16**) in CH₂Cl₂ (1.0 L) at 0 °C was added DMAP (41.9 g, 0.34 mol), Et₃N (79.7 mL, 9.57 mol) and tosyl chloride (130.8 g, 0.69 mol). The reaction mixture was allowed to stir at ambient temperature for 12 hr before quenched with 10% citric acid (200 mL). The organic layer was further washed with 10% citric acid (200 mL) and brine, dried over Na₂SO₄ and concentrated *in vacuo*. The crude was purified by flash column chromatography on silica gel (EtOAc/hexane, 1:99 to 35:65) to afford tosylate (**17**) (163.1 g, 90%) as colorless syrup. C₁₅H₂₄O₅S; colorless syrup; TLC (EtOAc/hexane, 22:78) *R*_f = 0.4; ¹H NMR (500 MHz, CDCl₃) δ 7.80 (2H, t, *J* = 8.2 Hz), 7.34 (2H, t, *J* = 8.2 Hz), 4.16 (2H, t, *J* = 9.8 Hz), 3.70 (2H, t, *J* = 9.8 Hz), 3.53 (2H, t, *J* = 10.3 Hz), 3.44 (2H, t, *J* = 10.3 Hz) 2.44 (3H, s), 1.17 (9H, s); ¹³C NMR (125 MHz, CDCl₃) δ 144.7, 133.1, 129.8, 128.0, 73.0, 71.4, 69.3, 68.7, 61.2, 27.4, 21.6; HRMS (ESI) calcd for C₁₅H₂₄NaO₅S: 339.1242; found: *m/z* 339.1228 [M + Na]⁺.



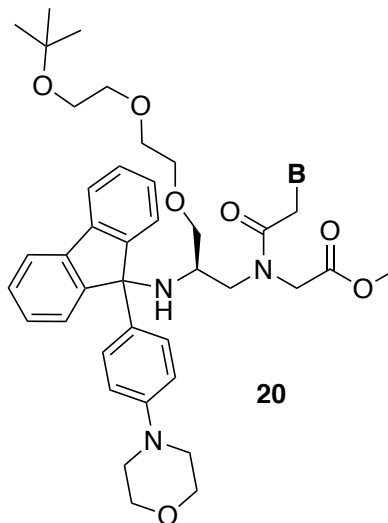
3-(2-(2-(tert-butoxy)ethoxy)ethoxy-2-N-(9-(4-morpholinophenyl)-9-Fluorenyl))-serine-Ψ
[CH₂N]Gly-OMe (19)

To a chilled solution of amide (**10**) (7.12 g, 11.5 mmol) in anhydrous THF (115 mL) at 0 °C was added lithium aluminum hydride (437.64 mg, 11.5 mmol). The reaction was allowed to stir for 1h before quenched with sat. Na₂SO₄ and further diluted with ether. The aqueous layer was then extracted with ether (2x). The combined organic layer was washed with brine, dried over Na₂SO₄ and concentrated *in vacuo* to afford aldehyde (**18**). The residue was directly used for the next step without purification.

To a chilled solution of aldehyde in anhydrous dichloroethane (115.3 mL) at 0 °C was added glycine methyl ester hydrochloride salt (1.38 g, 11.0 mmol), *N,N*-diisopropylethylamine (4.02 mL, 23.1 mmol) and sodium triacetoxyborohydride (3.67 g, 17.3 mmol). The reaction mixture was stirred at ambient temperature for 20 h before quenched with sat. NaHCO₃. The mixture was then diluted with ether. The aqueous layer was extracted with ether (2x). The combined organic layer was washed brine, dried over Na₂SO₄ and concentrated *in vacuo*. The residue was purified by flash column chromatography on silica gel gel (EtOAc/hexane, 24:76 to 99:1) to afford backbone (**19**)

as colorless syrup (5.84 g, 84% for two steps). $C_{37}H_{49}N_3O_6$; TLC (EtOAc/hexane, 80:20) $R_f=0.4$; 1H NMR (500 MHz, DMSO) δ 7.81–7.79 (2 H, m), 7.37–7.32 (4 H, m), 7.37–7.32 (2 H, m), 7.18 (2H, d, $J=9.0$ Hz), 6.78 (2H, d, $J=9.0$ Hz), 3.68 (4H, t, $J=4.8$ Hz), 3.60 (3H, s), 3.37–3.31 (6 H, m), 3.14 (2H, t, $J=4.8$ Hz), 3.06 (1H, d, $J=17.2$ Hz), 3.01–2.92 (7 H, m), 2.25 (1H, dd, $J=11.5, 5.3$ Hz), 2.16–2.09 (2 H, m), 1.08 (9H, s); ^{13}C NMR (125 MHz, DMSO) δ 172.5, 150.5, 150.1, 149.9, 139.7(2x), 136.1, 127.9(2x), 127.5(2x), 126.4, 125.3, 125.0, 120.0, 119.9, 114.7, 72.2, 72.0(2x), 70.4, 69.5, 69.4, 66.0, 60.6, 51.3, 51.2, 50.8, 50.0, 48.4, 27.2; HRMS (ESI) calcd for $C_{37}H_{50}N_3O_6$: 632.3700; found: m/z 632.3681 $[M + H]^+$.

A general procedure for nucleobase coupling:



To a solution of amine (1.0 eq) in anhydrous DMF (0.1 M) was added *N,N*-diisopropylethylamine (2.0 eq), nucleobase (2.0 eq) and HBTU (1.8 eq). The reaction was allowed to stir for 12 h before quenched by MeOH. The reaction mixture was concentrated *in vacuo*. The residue was diluted with EtOAc, washed with sat. NaHCO₃ and brine, dried over Na₂SO₄ and concentrated *in vacuo*. The crude was purified by flash column chromatography on NH₂ silica gel (MeOH/EtOAc, 1:99 to 15:85).

3-(2-(2-(Tert-butoxy)ethoxy)ethoxy)- 2-N-(9-(4-morpholinophenyl)-9-Fluorenyl)-L-serine Thymine methyl ester (20a)

91% yield; C₄₄H₅₅N₅O₉; colorless syrup; TLC (MeOH/EtOAc, 5:95) *R*_f = 0.5 with NH₂ Silica gel; rotamer ratio=4:1; ¹H NMR (500 MHz, DMSO) δ 11.27 (0.20 H, s), 11.22 (0.80 H, s), 7.84–7.78 (2 H, m), 7.50–7.11 (9 H, m), 6.79–6.76 (2 H, m), 4.40 (1.6 H, s), 3.94 (0.4 H, s), 3.69–3.67 (4 H, m), 3.66 (0.80 H, s), 3.57 (1H, d, *J* = 17.2 Hz), 3.54 (2.20 H, s), 3.48–3.22 (9 H, m), 3.15–3.04 (3 H, m), 3.01–2.99 (4 H, m), 2.92–2.90 (1 H, m), 2.88–2.63 (1 H, m), 2.22–2.16 (0.20 H, m), 2.07 (0.80 H, br), 1.76–1.75 (0.60 H, m), 1.72

(2.40 H, s), 1.08 (1.80 H, s), 1.06 (7.20 H, s); ^{13}C NMR (125 MHz, DMSO) δ 169.5/169.0, 167.8/167.4, 164.4/164.3, 150.9/150.8, 150.5/150.2, 150.0/149.9, 149.8/149.5, 142.1/141.9, 140.1/139.9, 139.6/139.5, 135.6/135.2, 128.2, 128.1/128.0, 127.8, 127.7/127.6, 126.5/126.4, 125.5/125.4, 125.3/125.2, 120.2, 120.1/119.9, 114.7, 108.1/107.9, 72.2 (2x), 71.2, 70.4/70.3, 69.9/69.6, 69.5/69.4, 66.0, 60.6/60.5, 52.1/51.6, 51.0/50.6, 50.4/50.1, 48.4, 47.8/47.6, 47.2, 27.3/27.2, 11.9; HRMS (ESI) calcd for $\text{C}_{44}\text{H}_{56}\text{N}_5\text{O}_9$: 798.4078; found: 798.4051 m/z $[\text{M} + \text{H}]^+$.

3-(2-(2-(Tert-butoxy)ethoxy)ethoxy)- 2-N-(9-(4-morpholinophenyl)-9-Fluorenyl)-L-serine Adenine(Boc) methyl ester (20b)

84 % yield; $\text{C}_{49}\text{H}_{62}\text{N}_8\text{O}_9$; colorless syrup; TLC (MeOH/ CHCl_3 , 5:95) R_f = 0.4; rotamer ratio=16:84; ^1H NMR (500 MHz, DMSO) δ 10.04–10.02 (1 H, m), 8.50–8.47 (1 H, m), 8.23–8.21 (1 H, m), 7.84–7.73 (2 H, m), 7.48–6.70 (10 H, m), 5.10 (1.68 H, s), 4.11 (0.32 H, s), 3.72–3.53 (8H, m), 3.42–3.28 (9 H, m), 3.24–2.71 (9 H, m), 2.19 (1 H, br), 1.48 (9 H, s), 1.07 (1.4 H, s), 1.01 (7.6 H, s); ^{13}C NMR (125 MHz, DMSO) δ 169.6/169.0, 167.3/166.8, 152.2, 151.6/151.3, 151.4/151.1, 150.6/150.3, 150.1/149.9, 149.8/149.5, 149.7/149.6, 144.8, 140.1/139.9, 139.6/139.5, 135.5/135.2, 128.3, 128.1, 127.8, 127.7, 127.6, 126.6/126.3, 125.4, 125.3, 123.0/122.9, 120.1, 114.7, 80.1/80.0, 72.3/72.2, 72.1/72.0, 71.1, 70.4/70.3, 70.1/69.7, 69.5/69.4, 66.0, 60.6/60.4, 52.2/51.6, 51.0/50.7, 50.6/50.2, 48.4, 47.3, 44.0/43.5, 27.8, 27.2; HRMS (ESI) calcd for $\text{C}_{49}\text{H}_{63}\text{N}_8\text{O}_9$: 907.4718; found: m/z 907.4685 $[\text{M} + \text{H}]^+$.

*3-(2-(2-(Tert-butoxy)ethoxy)ethoxy)- 2-N-(9-(4-morpholinophenyl)-9-Fluorenyl)-L-serine
Cytosine(Boc) methyl ester (20c)*

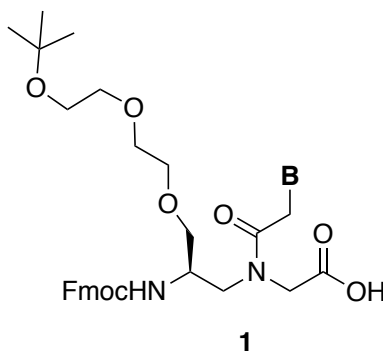
92% yield; C₄₈H₆₂N₆O₁₀; colorless syrup; TLC (MeOH/CHCl₃, 15:85) R_f= 0.5; rotamer ratio=4:1; ¹H NMR (500 MHz, DMSO) δ 10.26–10.24 (1 H, m), 7.83–7.71 (3 H, m), 7.45–7.18 (8 H, m), 7.13–6.75 (4 H, m), 4.49 (1.6 H, s), 3.96 (0.4 H, s), 3.69–3.66 (4.80 H, m), 3.56–3.53 (3.20 H, m), 3.49–3.33 (9 H, m), 3.26 (2H, t, J = 5.5 Hz), 3.20–2.63 (7 H, m), 2.23–2.16 (0.20 H, m), 2.09 (0.80 H, br), 1.45 (9 H, s), 1.08 (1.80 H, s), 1.06 (7.20 H, s); ¹³C NMR (125 MHz, DMSO) δ 169.5/169.0, 167.8/167.3, 163.2, 154.9, 152.1, 150.5, 150.4/150.2, 150.0/149.9, 149.7/149.5, 140.1/139.9, 139.6/139.4, 135.6/135.2, 128.2, 128.1, 127.8, 127.6, 126.6/126.4, 125.4/125.2, 120.2, 120.1/119.9, 114.8/114.7, 93.7, 80.8, 72.2 (2x), 71.1, 70.4/70.3, 69.9/69.6, 69.5/69.4, 66.0, 60.6/60.4, 52.1/51.6, 51.0/50.6, 50.4, 49.3/48.8, 48.4, 47.3, 27.8, 27.3/27.2; HRMS (ESI) calcd for C₄₈H₆₂N₆O₁₀: 883.4606; found: m/z 883.4580 [M + H]⁺.

*3-(2-(2-(tert-butoxy)ethoxy)ethoxy)- 2-N-(9-(4-morpholinophenyl)-9-Fluorenyl)-L-serine
Guanine(Boc) methyl ester (20d)*

71% yield; C₄₉H₆₂N₈O₁₀; colorless syrup; TLC (MeOH/CHCl₃, 10:90) R_f= 0.2 with NH₂ Silica gel; rotamer ratio=1:3; ¹H NMR (500 MHz, DMSO) δ 11.4 (2 H, br), 7.85–7.78 (2 H, m), 7.65–7.64 (1 H, m), 7.47–7.09 (8 H, m), 6.80–6.73 (2 H, m), 4.82 (2 H, m), 4.15–4.01 (1 H, m), 3.70–3.68 (6 H, m), 3.54–2.78 (19 H, m), 2.21–2.20 (1 H, m), 1.48–1.47 (9 H, m), 1.07 (2.52 H, s), 1.02 (6.48 H, s); ¹³C NMR (125 MHz, DMSO) δ 169.6/169.0, 167.3/166.8, 155.5, 150.5, 150.3, 150.1, 149.9, 149.8, 149.4, 139.9, 140.1/139.9, 139.7/139.4, 135.6/135.1, 128.3, 128.2/128.1, 127.9, 127.7, 126.5/126.3,

125.4/125.3, 125.2, 120.2/120.1, 120.0, 118.8, 114.7, 81.8, 72.3/72.2, 72.2/72.0, 71.0, 70.4/70.2, 70.0/69.7, 69.5/69.4, 66.0, 60.6/60.3, 52.2/51.7, 51.1/50.6, 50.4, 48.4, 47.3, 43.7/43.3, 27.8, 27.2/27.1; HRMS (ESI) calcd for C₄₉H₆₃N₈O₁₀: 923.4667; found: *m/z* 923.4650 [M + H]⁺.

A general method to convert monomer methyl ester **20 a-d to the final monomer **1** a-d.**



To a chilled solution of methyl ester **20** (1 eq) in a co-solvent of THF and water (1:1, 0.05 M) was added LiOH-H₂O (4 eq) portionwisely at 0 °C with ice bath. The reaction mixture was allowed to gradually warm up to and stir at ambient temperature for 12 h. The mixture was neutralized by Dowex resin to pH 4~5 at 0 °C and filtered. The filtrate was concentrated *in vacuo* and coevaporated with toluene (3X) to afford PNA amino acid crude without the need for further purification.

To a solution of PNA amino acid crude in THF (0.1M) was added Fmoc-OSu (1.2 eq) and DIEA (2.2 eq) and allowed to stir at room temperature for 18h. The reaction mixture was then stirred with methanol and concentrated *in vacuo* with silica gel. The crude was then purified by column chromatography (A= EtOAc, B= ACN/MeOH/H₂O= 2:1:1, A:B= 3:97 to 34:66) to afford final Fmoc miniPEG γ PNA monomers **1**.

Fmoc-3-(2-(2-(tert-butoxy)ethoxy)ethoxy)-L-serine thymine monomer (1a)

40% yield; C₃₅H₄₄N₄O₁₀; white powder; TLC (EtOAc/ACN/MeOH/H₂O, 6:1:1:1) *R*_f = 0.5; rotamer ratio=2:3; ¹H NMR (500 MHz, DMSO) δ 12.9 (1 H, br), 11.3–11.2 (1 H, m), 7.88 (2 H, *J* = 7.6 Hz, d), 7.69 (2 H, *J* = 7.4 Hz, d), 7.43–7.22 (5 H, m), 4.72–4.64 (1 H, m), 4.46 (1 H, s), 4.35–4.28 (2 H, m), 4.23–4.22 (1 H, m), 4.11 (1 H, m), 4.02–3.80 (2 H, m), 3.60–3.07 (13 H, m), 1.72 (3 H, m), 1.09–1.08 (9 H, m); ¹³C NMR (125 MHz, DMSO) δ 170.9/170.4, 168.0/167.5, 164.4, 155.9/155.8, 151.0/150.9, 143.9/143.8, 142.1/142.0, 140.7, 127.6, 127.0, 125.2, 120.1, 108.1/108.0, 72.2, 70.5, 70.4/69.9, 69.8/69.6, 65.6/65.4, 60.6/60.5, 49.8/49.4, 48.5/48.1, 47.8/47.7, 46.7, 27.3/27.2, 11.9; HRMS (ESI) calcd for C₃₅H₄₄N₄NaO₁₀: 703.2955; found: *m/z* 703.2919 [M + H]⁺.

Fmoc-3-(2-(2-(tert-butoxy)ethoxy)ethoxy)-L-serine adenine(Boc) monomer (1b)

29% yield; C₄₀H₅₁N₇O₁₀; white powder; TLC (EtOAc/ACN/MeOH/H₂O, 6:1:1:1) *R*_f = 0.4; rotamer ratio=2:3; ¹H NMR (500 MHz, DMSO) δ 12.8 (1 H, br), 10.0 (1 H, s), 8.51–8.50 (1 H, m), 8.27 (1 H, s), 7.88 (2 H, *J* = 7.3 Hz, d), 7.72–7.69 (2 H, m), 7.51–7.14 (5 H, m), 5.42–5.10 (2 H, m), 4.38–4.21 (4 H, m), 4.06–3.81 (2 H, m), 3.70–3.12 (10 H, m), 1.48 (9 H, m), 1.08 (3.6 H, s), 1.04 (5.4 H, s); ¹³C NMR (125 MHz, DMSO) δ 170.7/170.1, 167.4/166.9, 155.9/155.8, 152.2, 151.4, 151.1, 149.7, 144.9/144.8, 143.9/143.8, 140.7, 137.3, 128.9, 128.2, 127.6, 127.0, 125.3/125.2, 122.9, 120.1, 80.0, 72.2, 70.5, 70.4, 70.0, 69.8, 69.7, 69.6, 65.7, 65.6/65.4, 60.6/60.5, 49.8/49.3, 48.5, 49.6, 48.0, 46.7, 44.0/43.8, 27.8, 27.2; HRMS (ESI) calcd for C₄₀H₅₂N₇O₁₀: 790.3776; found: *m/z* 790.3736 [M + H]⁺.

Fmoc-3-(2-(2-(tert-butoxy)ethoxy)ethoxy)-L-serine cytosine(Boc) monomer (1c)

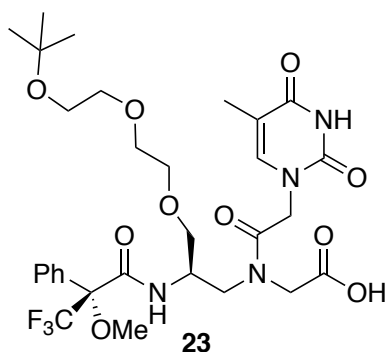
32% yield; C₃₉H₅₁N₅O₁₁; white powder; TLC (EtOAc/ACN/MeOH/H₂O, 6:1:1:1) *R_f* = 0.5; rotamer ratio=1:1; ¹H NMR (500 MHz, DMSO) δ 10.3 (1 H, br), 7.88 (2 H, J= 7.6 Hz, d), 7.84–7.79 (1 H, m), 7.71–7.68 (2 H, m), 7.44–7.40 (2 H, m), 7.34–7.27 (2 H, m), 6.67–6.95 (1 H, m), 4.87–4.77 (1 H, m), 4.62 (1 H, s), 4.33–4.20 (3 H, m), 4.03–3.79 (3 H, m), 3.58–3.00 (14 H, m), 1.45 (9 H, s), 1.09–1.08 (9 H, m); ¹³C NMR (125 MHz, DMSO) δ 171.2, 167.9/167.3, 163.2, 155.9/155.8, 155.1/155.0, 152.1, 150.5, 143.9/143.8, 140.7, 127.6, 127.0, 125.2, 120.1, 94.0/93.9, 80.9, 72.2, 70.4, 69.9/69.8, 69.6, 65.5/65.4, 60.6/60.5, 51.1/49.8, 49.6/49.5, 49.4/48.5, 48.3/47.9, 46.7, 27.8, 27.3/27.2; HRMS (ESI) calcd for C₃₉H₅₂N₅O₁₁: 766.3663; found: *m/z* 766.3643 [M + H]⁺.

Fmoc-3-(2-(2-(tert-butoxy)ethoxy)ethoxy)-L-serine guanine(Boc) monomer (1d)

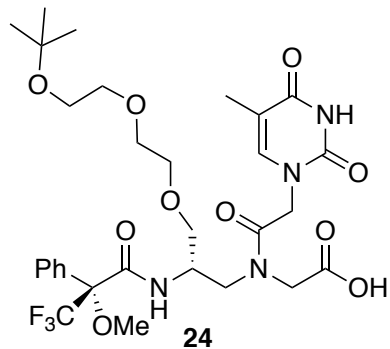
23% yield; C₄₀H₅₁N₇O₁₁; white powder; TLC (EtOAc/ACN/MeOH/H₂O, 6:1:1:1) *R_f* = 0.3; rotamer ratio=1:1; ¹H NMR (500 MHz, DMSO) δ 11.3–10.7 (2 H, br), 7.88–7.60 (5 H, m), 7.42–7.21 (4 H, m), 5.15–4.84 (2 H, m), 4.37–3.08 (20 H, m), 1.44–1.38 (9 H, m), 1.07–1.05 (9 H, m); ¹³C NMR (125 MHz, DMSO) δ 171.1/170.6, 167.4/166.7, 156.1/155.8, 155.1/155.0, 153.8/153.6, 149.6/149.5, 147.5/147.4, 143.8, 143.6, 140.7, 140.3, 127.6, 127.5/127.3, 127.0, 125.2/125.0, 121.3, 120.2/120.1, 118.9, 82.5/82.4, 72.2, 70.6, 70.4/70.0, 69.8/69.7, 65.6/65.4, 60.6/60.5, 51.4/50.3, 49.5/48.8, 48.6/47.9, 46.8/46.7, 43.9/43.8, 27.7/27.6, 27.2; HRMS (ESI) calcd for C₄₀H₅₂N₇O₁₁: 806.3725; found: *m/z* 806/3693 [M + H]⁺.

Determination of Optical Purities.

To a stirred, cold solution of thymine monomers (**1a and 2a**) (1.0 eq) in DMF was added piperidine (10 eq). After 2 hr, the reaction mixture was concentrated and co-evaporated with toluene for three times. The residue was then stirred in chilled CH₂Cl₂, followed by addition of DIEA (2 eq) and (*S*)-(+)- α -methoxy- α -(trifluoromethyl) phenylacetyl chloride (MTPACl; 1.1 equiv). The reaction mixture was allowed to stir at room temperature for 3 hr. After completion, the solution was diluted with CH₂Cl₂ and washed with water (2x) and brine. The organic layer was dried on Na₂SO₄ and concentrated *in vacuo*. The crude sample was directly injected into HPLC to analyze enantiomeric excess. For NMR analysis, the crude sample was purified by flash column chromatography.



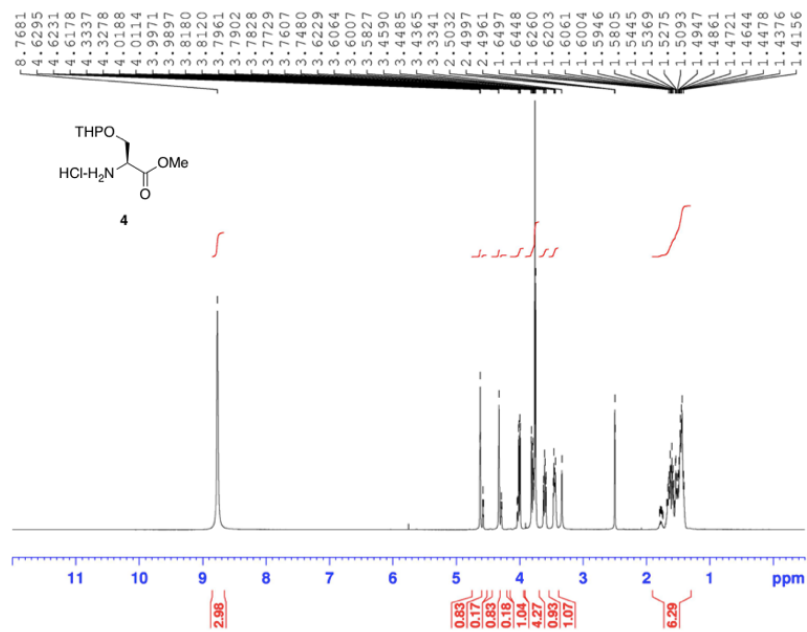
Compound **23**: C₃₀H₄₁F₃N₄O₁₀; colorless syrup TLC (EtOAc/ACN/MeOH/H₂O, 6:1:1:1) *R_f* = 0.5; rotamer ratio=1:1; ¹H NMR (500 MHz, DMSO) δ 12.9 (1 H, br), 11.3 (1 H, m), 8.27–8.14 (1 H, m), 7.55–7.41 (5 H, m), 7.13–7.07 (1 H, m), 4.61–4.27 (3 H, m), 3.94–3.11 (17 H, m), 1.74–1.72 (3 H, m), 1.11 (9 H, m); ¹³C NMR (125 MHz, DMSO) δ 170.5/170.2, 168.1/167.5, 165.8/165.5, 164.4/164.3, 158.4/158.1, 150.9, 141.9, 133.4/133.2, 129.4, 128.4, 127.2, 127.0, 124.9, 122.6, 108.1/108.0, 83.7/83.5, 72.3, 70.4, 70.0/69.7, 69.7/69.3, 60.6, 55.0/54.9, 49.2, 47.8/47.7, 47.7/47.6, 47.4/47.2, 27.3/27.2, 11.9/11.8); ¹⁹F NMR (470 MHz, DMSO) δ -70.0/-70.1; HRMS (ESI) calcd for C₃₀H₄₁F₃N₄NaO₁₀: 697.2672; found: *m/z* 679.2649 [M + Na]⁺.



Compound **24**: C₃₀H₄₁F₃N₄O₁₀; colorless syrup TLC (EtOAc/ACN/MeOH/H₂O, 6:1:1:1) *R_f*= 0.5; rotamer ratio=1:1; ¹H NMR (500 MHz, DMSO) δ 13.1 (1 H, br), 11.3 (1 H, m), 8.35–8.05 (1 H, m), 7.53–7.42 (5 H, m), 7.27–7.22 (1 H, m), 4.76–4.63 (1 H, m), 4.48 (1 H, s), 4.35–4.20 (2 H, m), 4.03–3.92 (1 H, m), 3.65–3.34 (15 H, m), 1.75 (3 H, m), 1.11–1.10 (9 H, m); ¹³C NMR (125 MHz, DMSO) δ 171.1/170.7, 168.9/168.0, 166.2/166.0, 164.9/164.8, 158.5, 151.4, 142.5/142.3, 133.6/133.2, 130.0, 129.8, 128.9, 128.7, 128.0, 127.8, 127.5, 108.7/108.6, 72.7, 70.9, 70.8, 70.2, 70.1, 69.5, 61.0, 55.5/55.4, 49.6, 48.3, 48.2, 48.0, 47.9, 47.4, 27.7, 12.3; ¹⁹F NMR (470 MHz, DMSO) δ -70.1; HRMS (ESI) calcd for C₃₀H₄₁F₃N₄NaO₁₀: 697.2672; found: *m/z* 697.2643 [M + Na]⁺.

2.5. NMR, HRMS, GC and HPLC Data

(A)



(B)

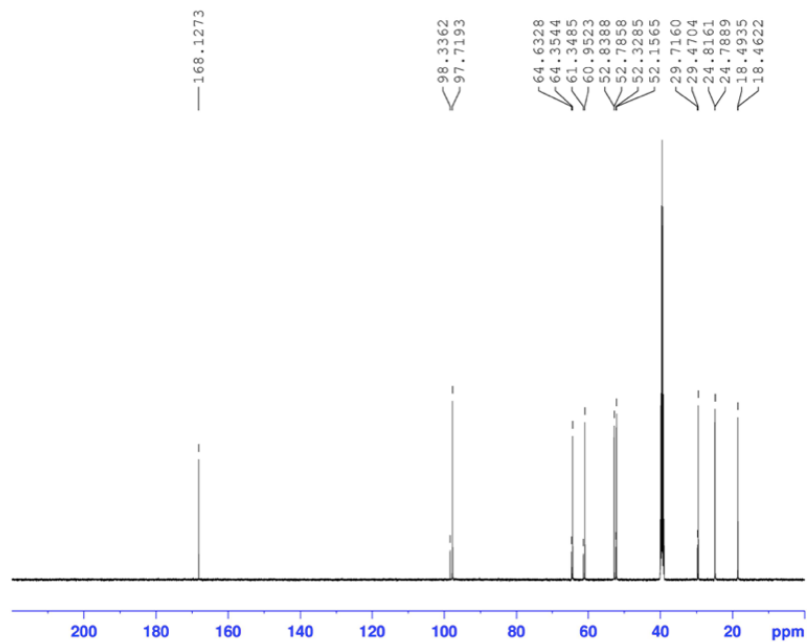


Figure II-S 1. (A) ^1H NMR (500 MHz, DMSO) and (B) ^{13}C NMR (125 MHz, DMSO) spectra of compound 4.

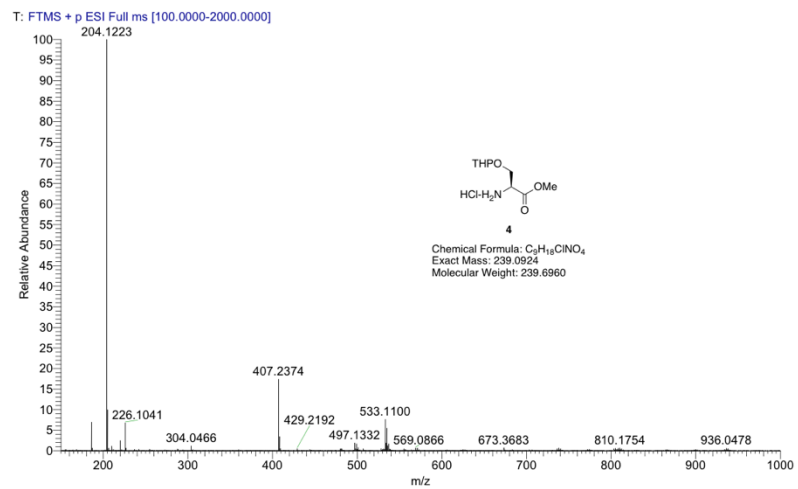
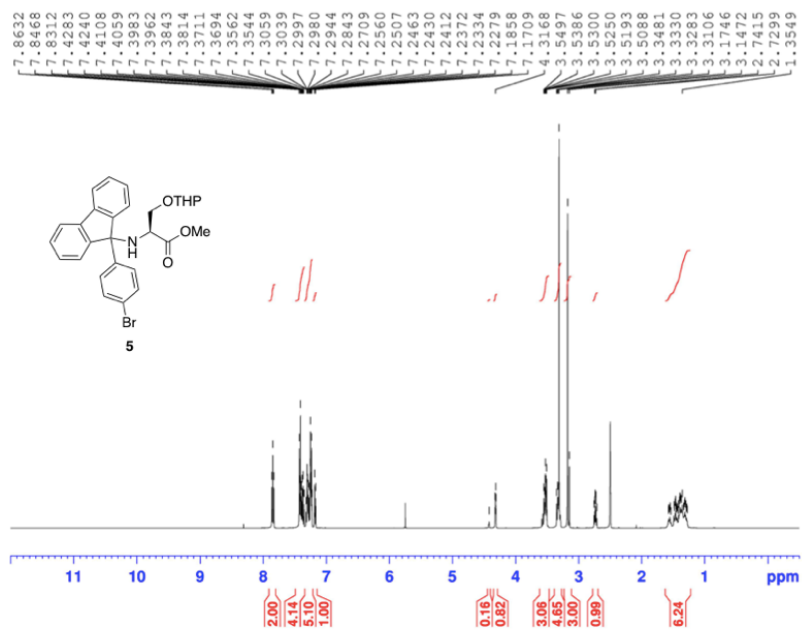


Figure II-S 2. HRMS (ESI) spectrum of compound **4**.

(A)



(B)

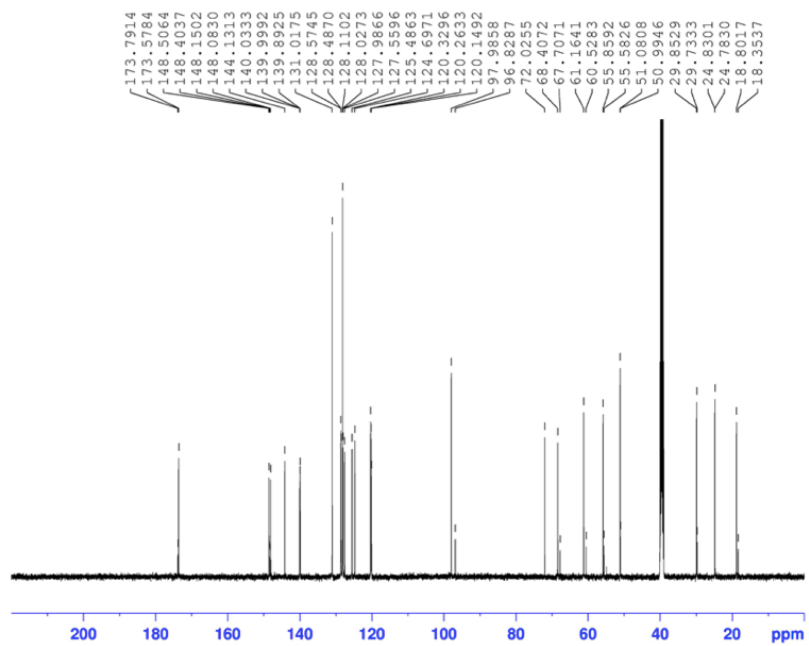


Figure II-S 3. (A) ^1H NMR (500 MHz, DMSO) and (B) ^{13}C NMR (125 MHz, DMSO) spectra of compound 5.

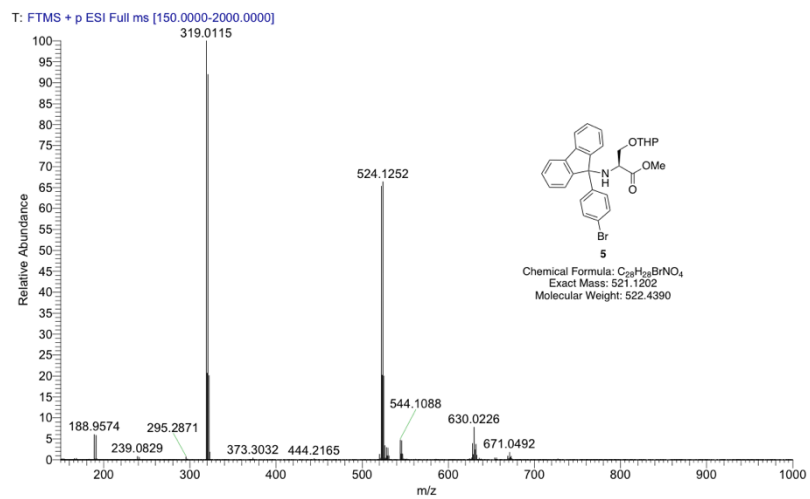
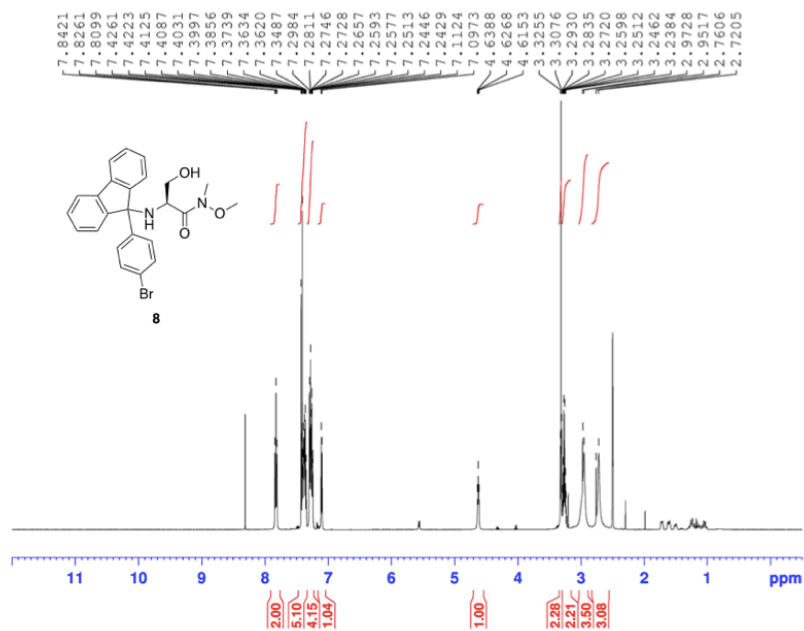


Figure II-S 4. HRMS (ESI) spectrum of compound **5**.

(A)



(B)

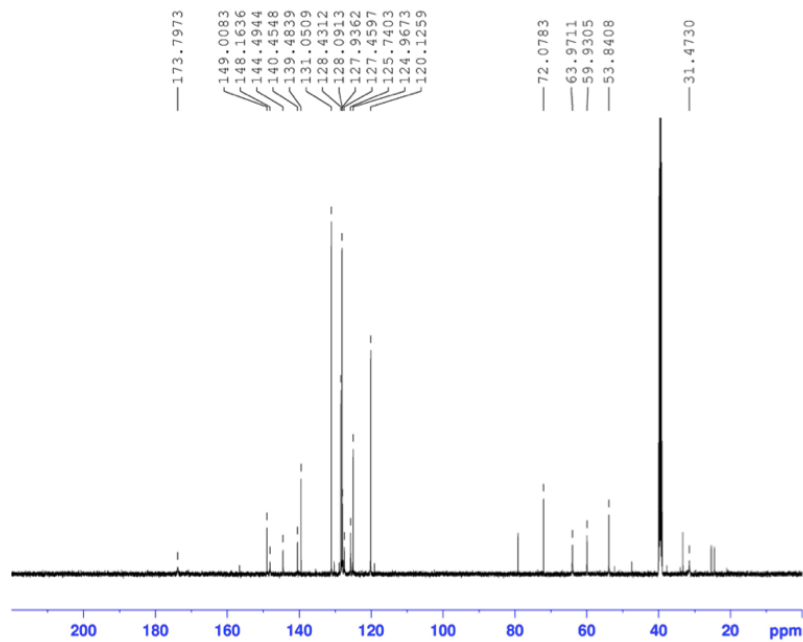


Figure II-S 5. (A) ¹H NMR (500 MHz, DMSO) and (B) ¹³C NMR (125 MHz, DMSO) spectra of compound **8**.

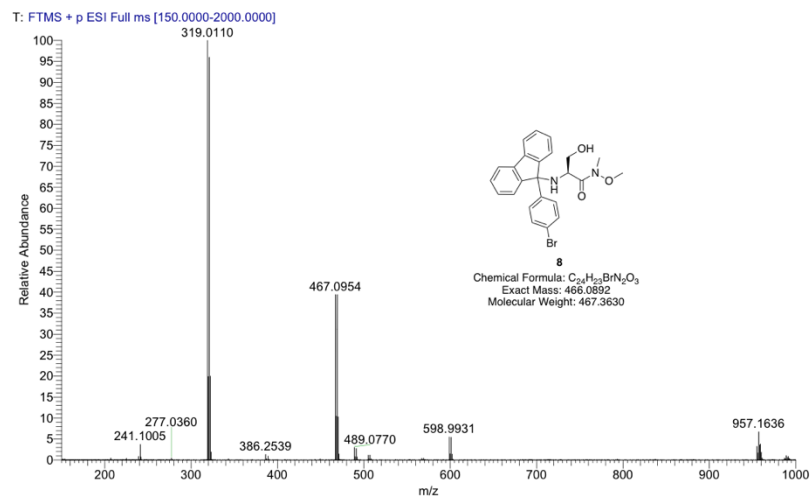
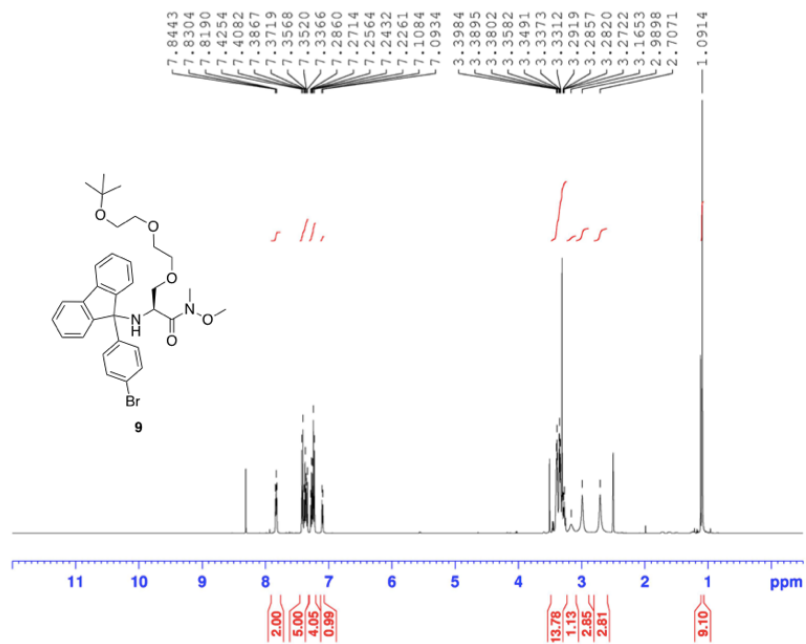


Figure II-S 6. HRMS (ESI) spectrum of compound **8**.

(A)



(B)

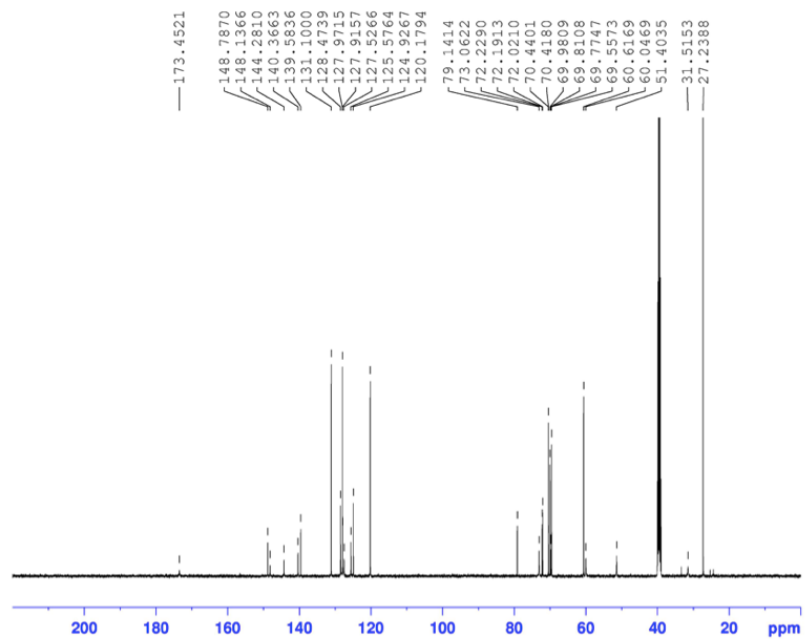


Figure II-S 7. (A) ¹H NMR (500 MHz, DMSO) and (B) ¹³C NMR (125 MHz, DMSO) spectra of compound 9.

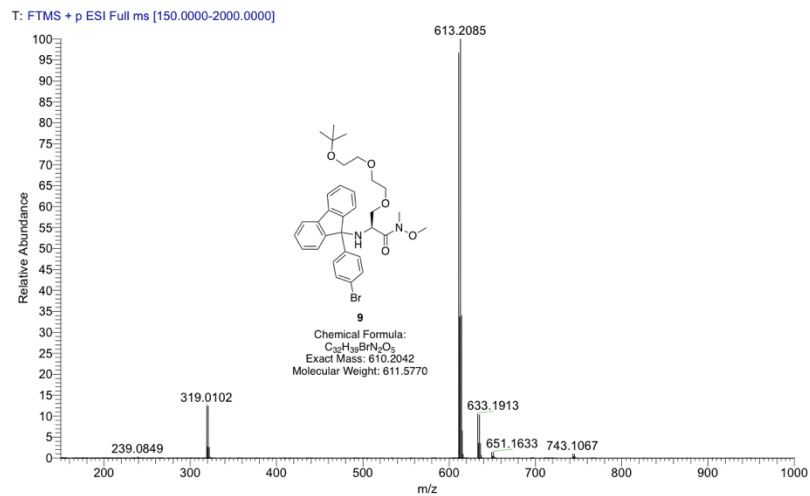
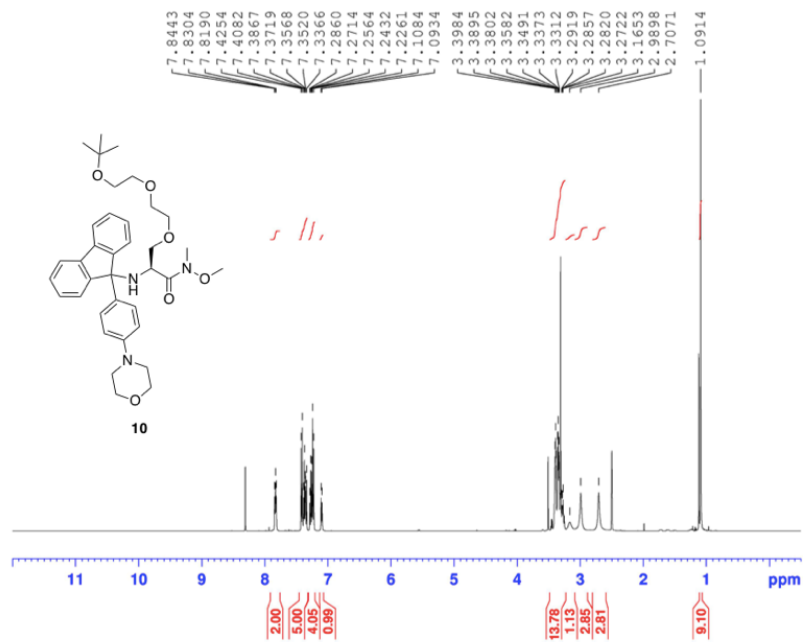


Figure II-S 8. HRMS (ESI) spectrum of compound **9**.

(A)



(B)

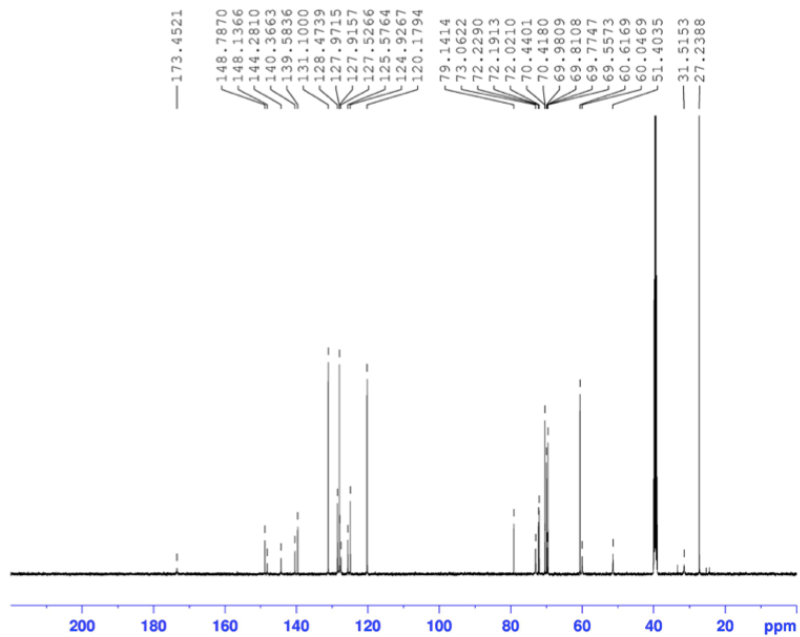


Figure II-S 9. (A) ¹H NMR (500 MHz, DMSO) and (B) ¹³C NMR (125 MHz, DMSO) spectra of compound **10**.

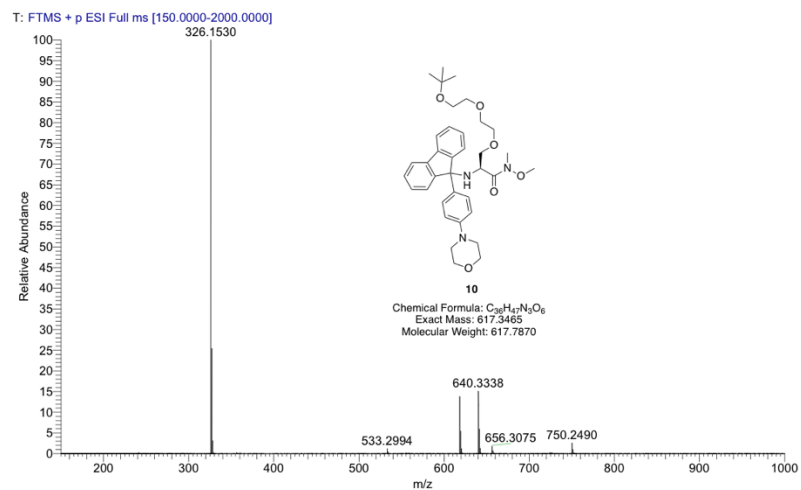
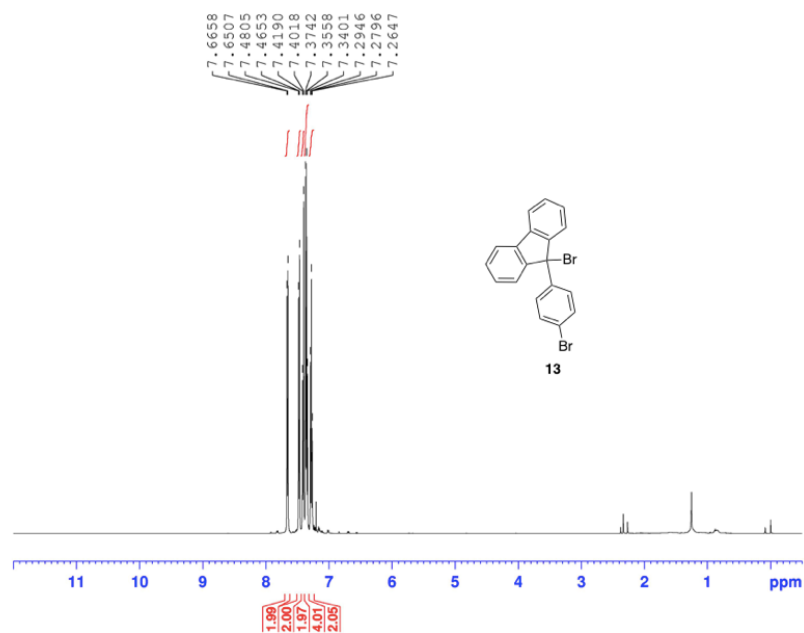


Figure II-S 10. HRMS (ESI) spectrum of compound **10**.

(A)



(B)

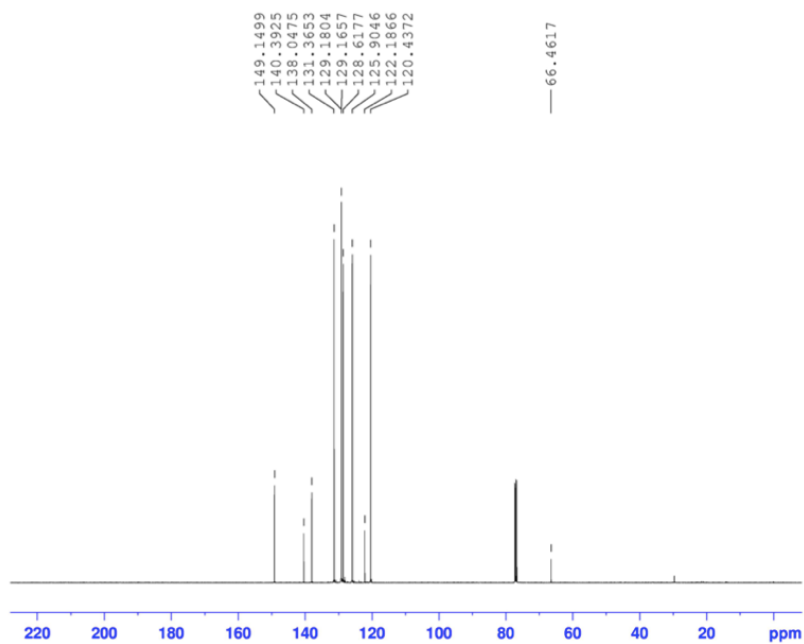


Figure II-S 11. (A) ¹H NMR (500 MHz, DMSO) and (B) ¹³C NMR (125 MHz, DMSO) spectra of compound **13**.

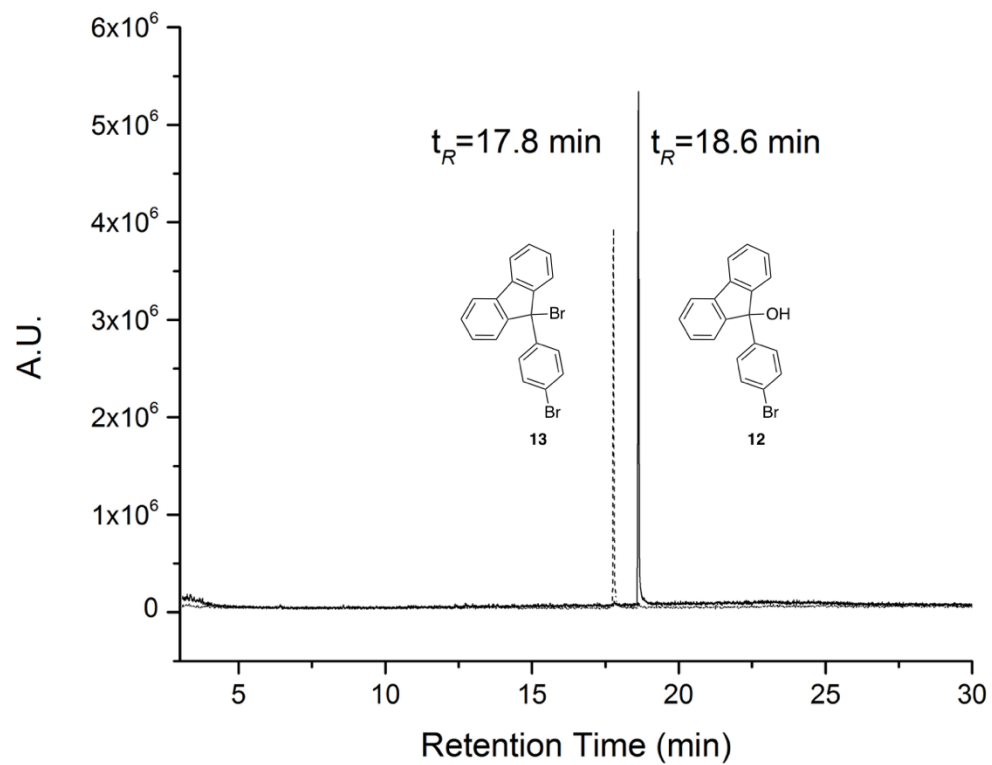
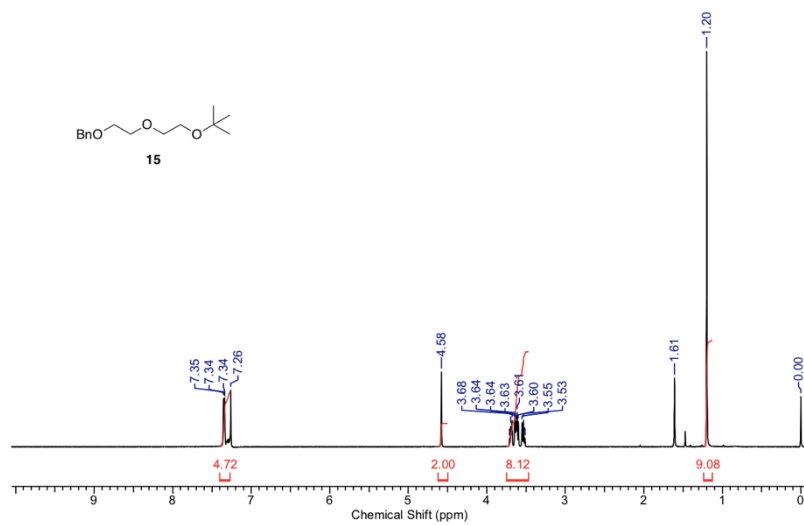


Figure II-S 12. GC chromatogram of compounds **12** (solid line) and **13** (dash line).

(A)



(B)

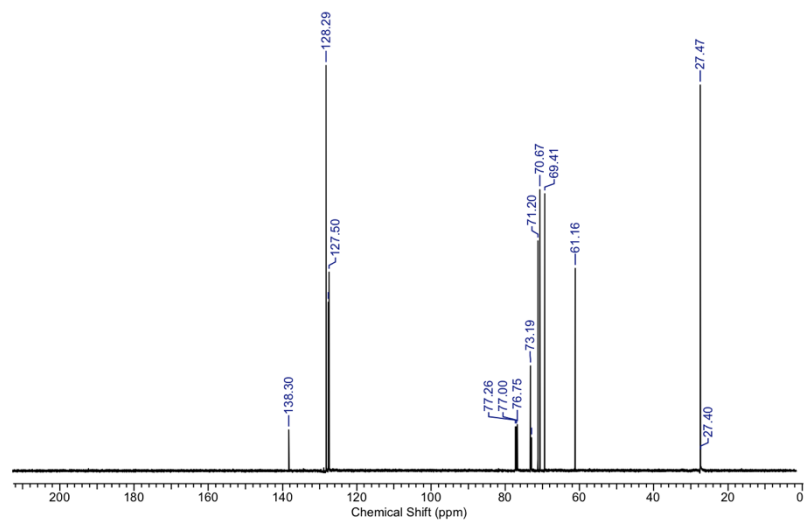


Figure II-S 13. (A) ¹H NMR (500 MHz, CDCl₃) and (B) ¹³C NMR (125 MHz, CDCl₃) spectra of compound **15**.

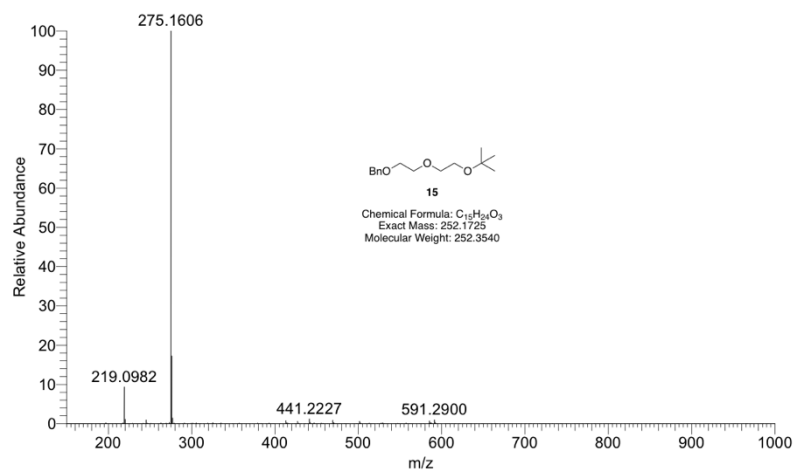
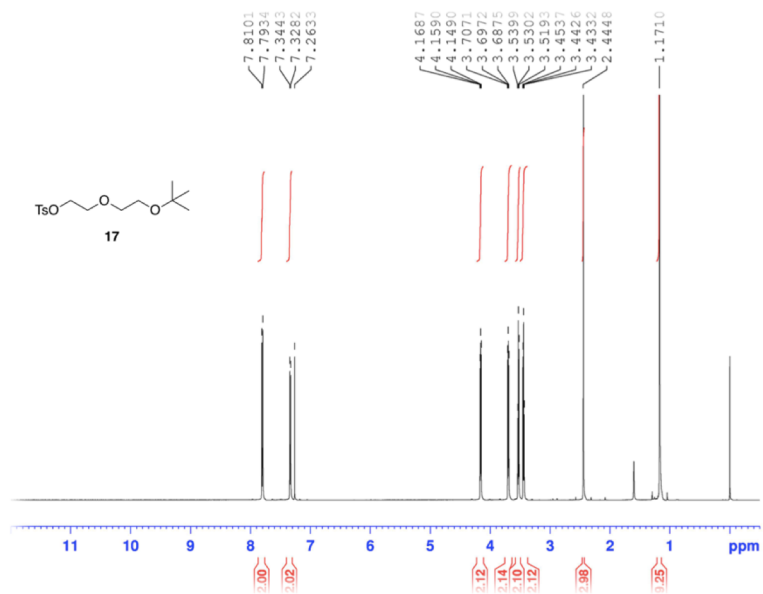


Figure II-S 14. HRMS (ESI) spectrum of compound **15**.

(A)



(B)

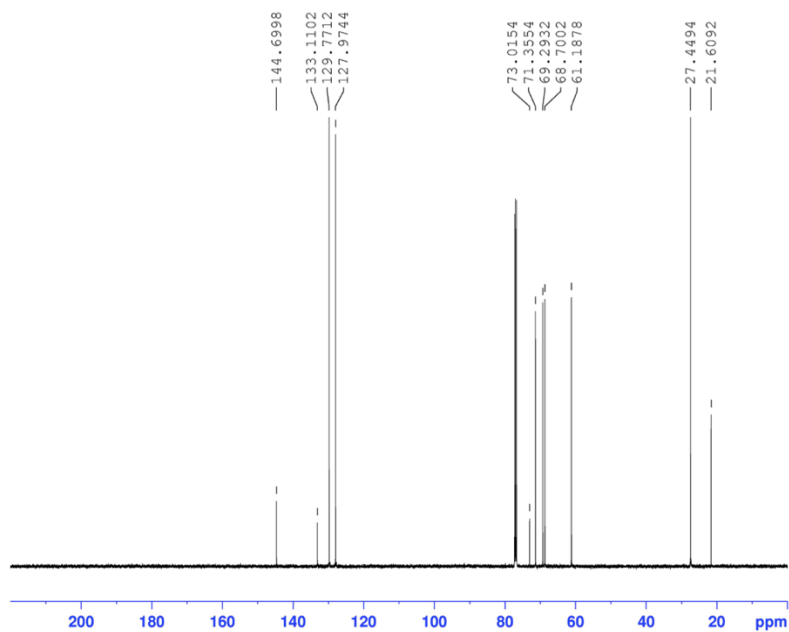


Figure II-S 15. (A) ¹H NMR (500 MHz, CDCl₃) and (B) ¹³C NMR (125 MHz, CDCl₃) spectra of compound 17.

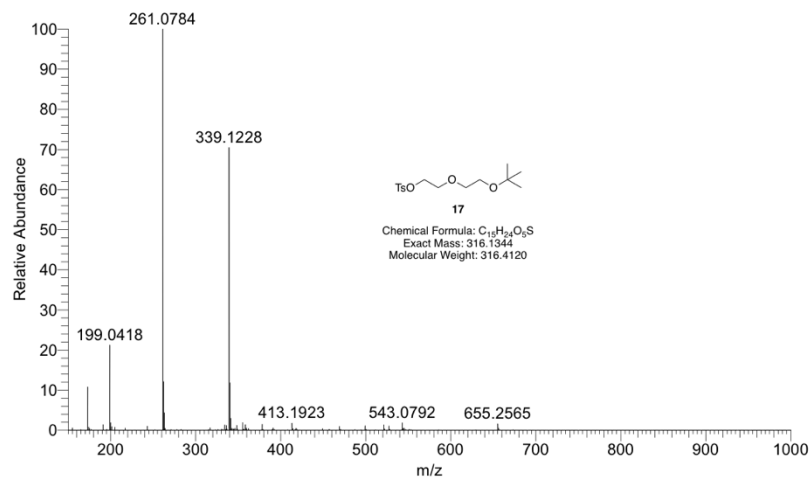
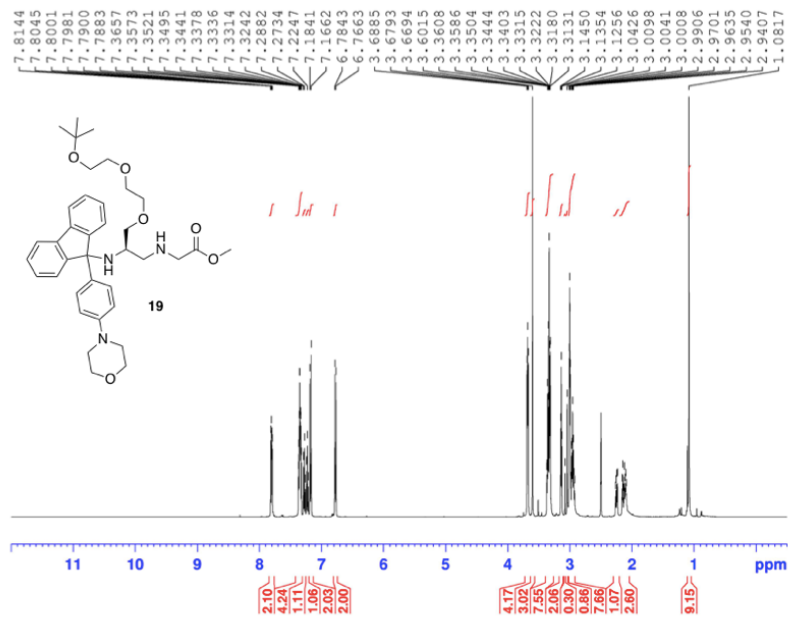


Figure II-S 16. HRMS (ESI) spectrum of compound 17.

(A)



(B)

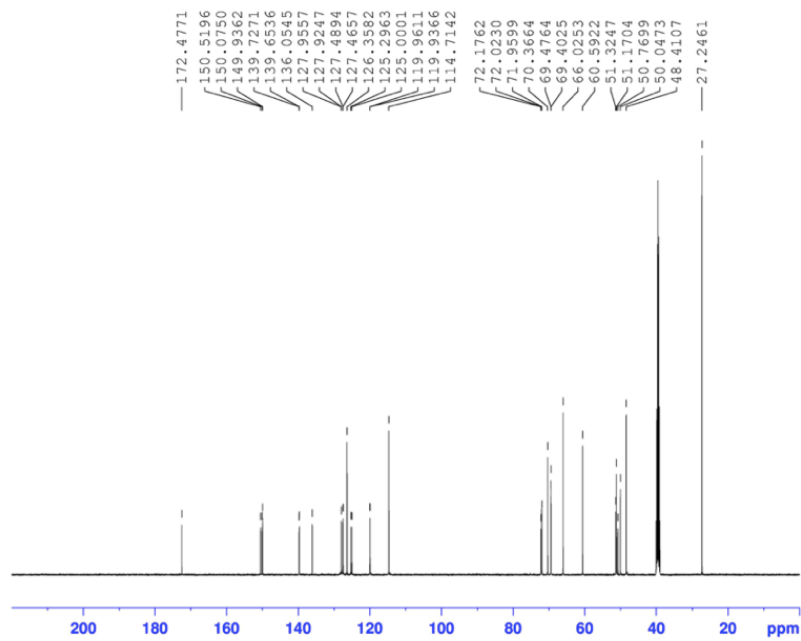


Figure II-S 17. (A) ^1H NMR (500 MHz, DMSO) and (B) ^{13}C NMR (125 MHz, DMSO) spectra of compound 19.

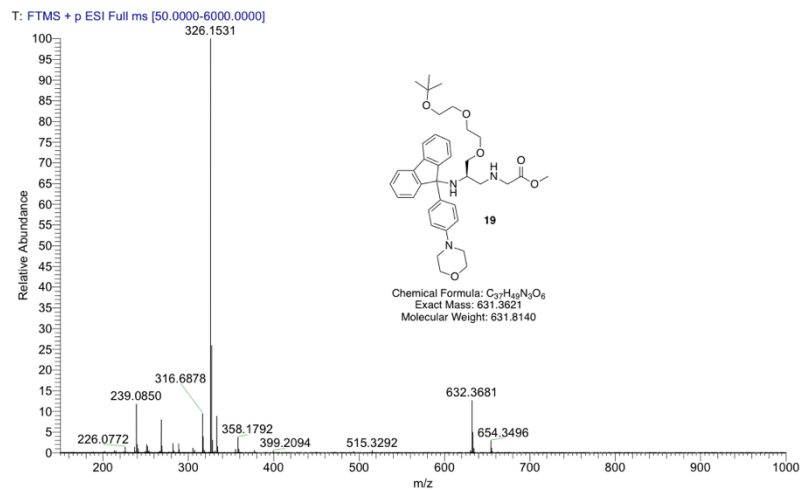
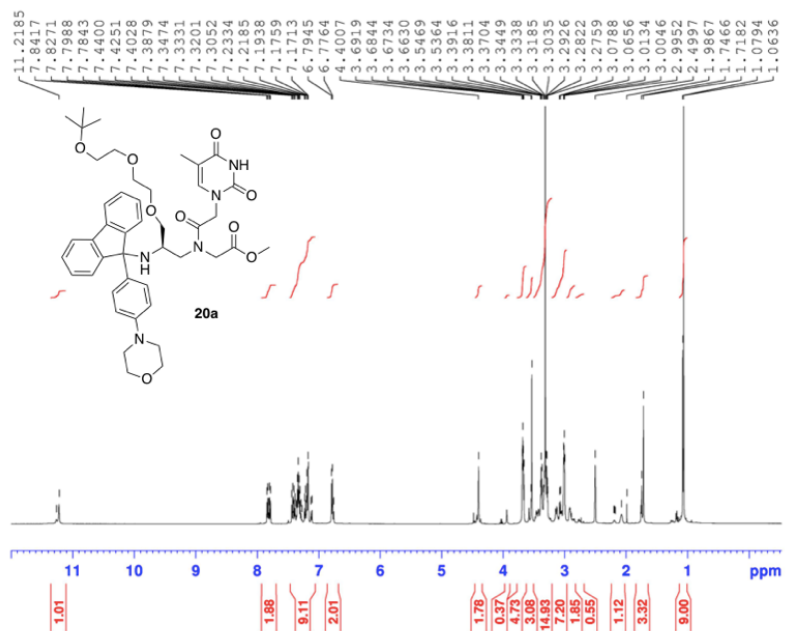


Figure II-S 18. HRMS (ESI) spectrum of compound 19.

(A)



(B)

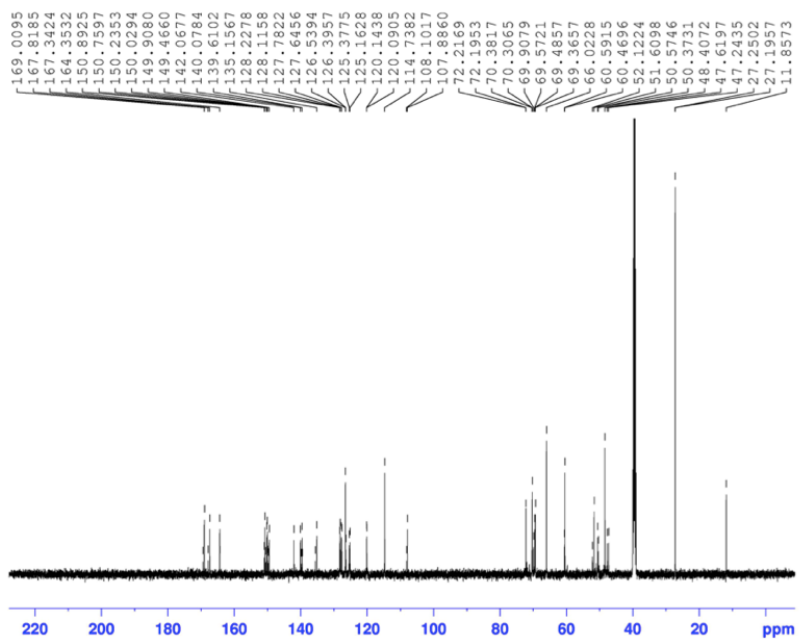


Figure II-S 19. (A) ¹H NMR (500 MHz, DMSO) and (B) ¹³C NMR (125 MHz, DMSO) spectra of compound 20a.

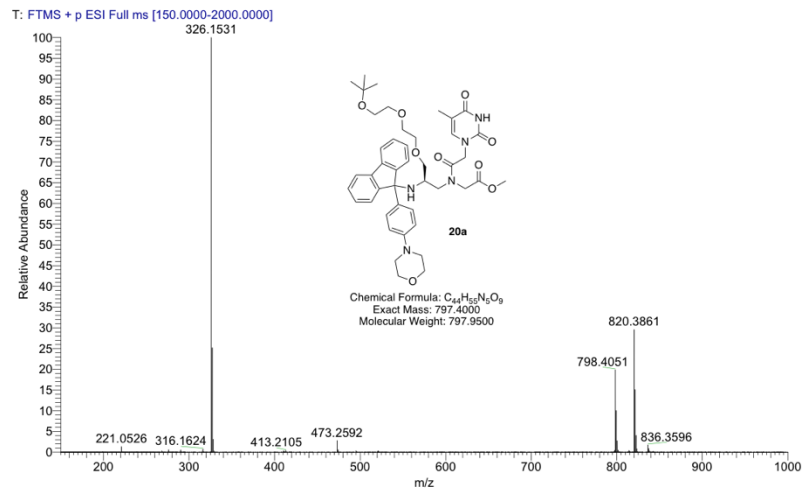


Figure II-S 20. HRMS (ESI) spectrum of compound **20a**.

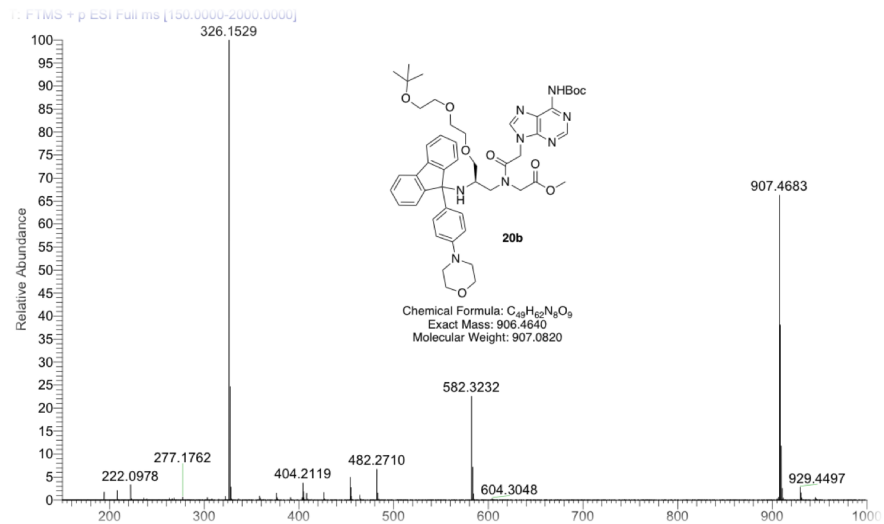


Figure II-S 22. HRMS (ESI) spectrum of compound **20b**.

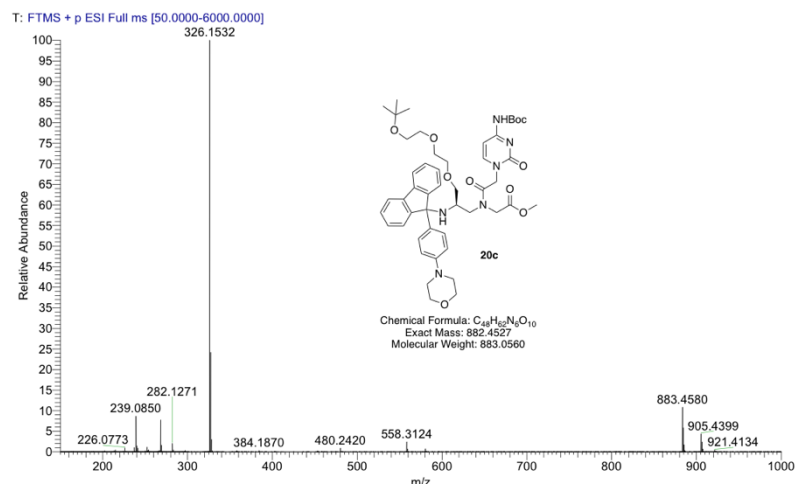
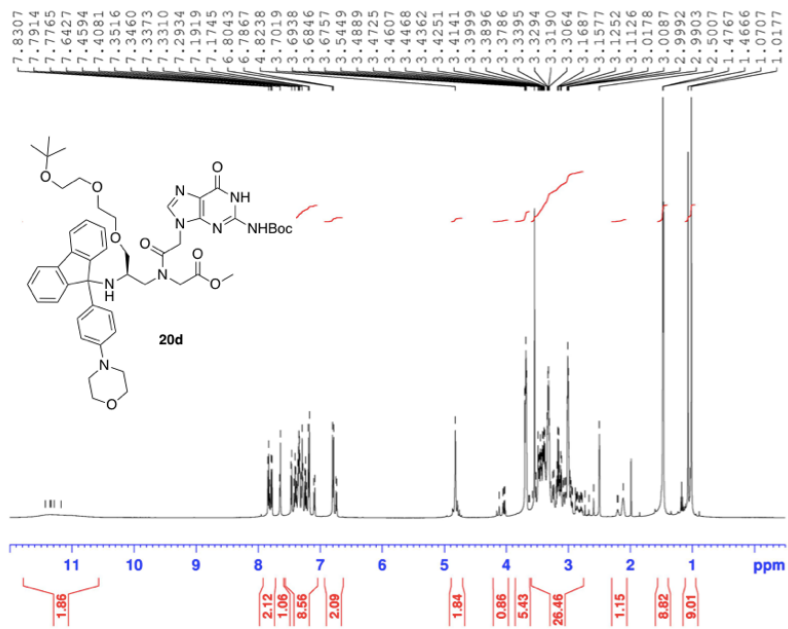


Figure II-S 24. HRMS (ESI) spectrum of compound **20c**.

(A)



(B)

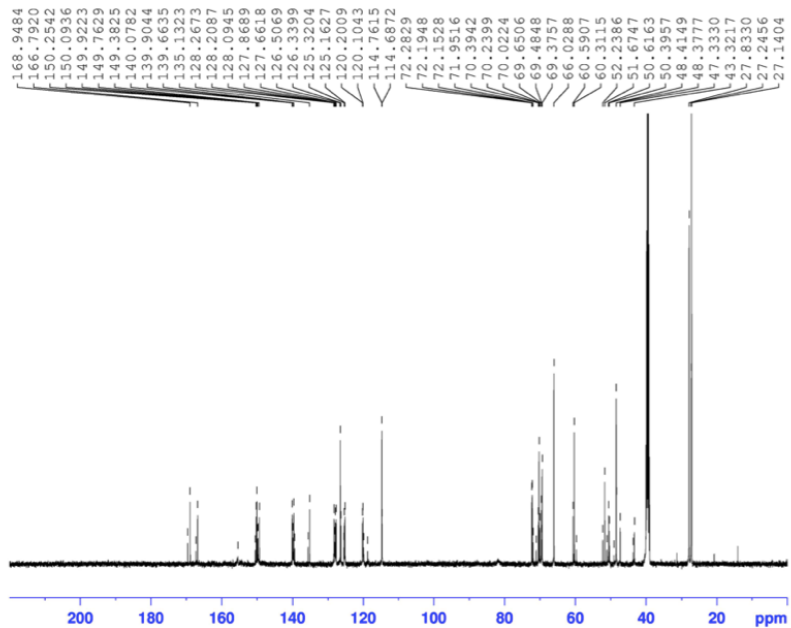


Figure II-S 25. (A) ¹H NMR (500 MHz, DMSO) and (B) ¹³C NMR (125 MHz, DMSO) spectra of compound **20d**.

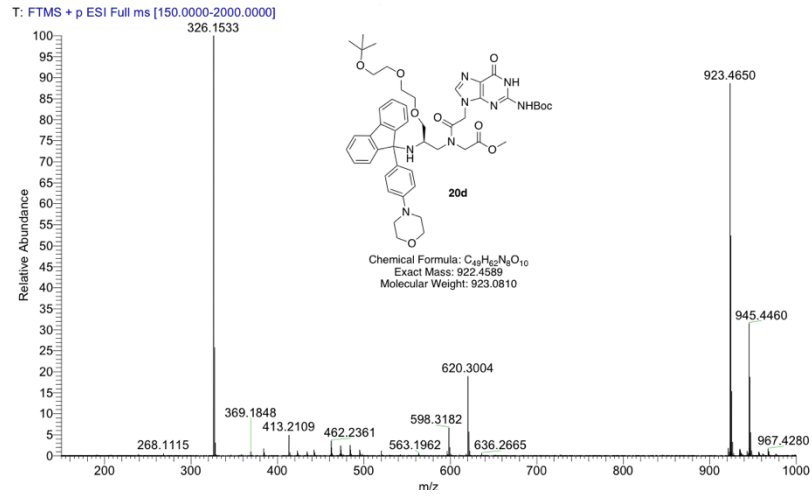
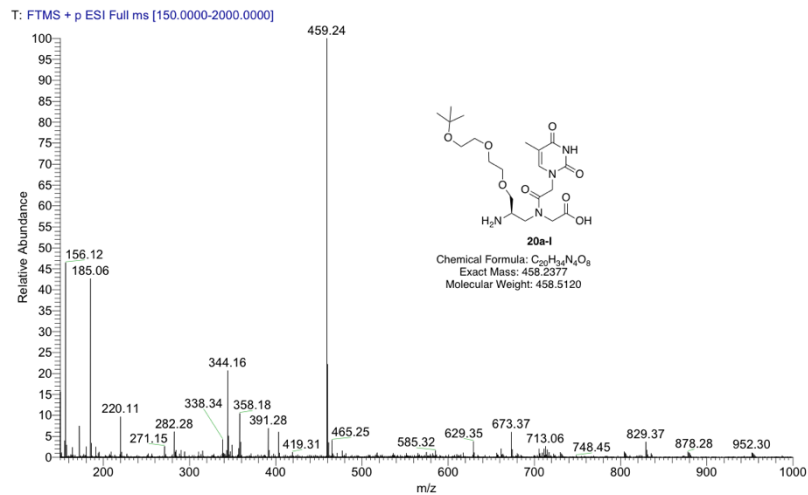


Figure II-S 26. HRMS (ESI) spectrum of compound **20d**.

(A)



(B)

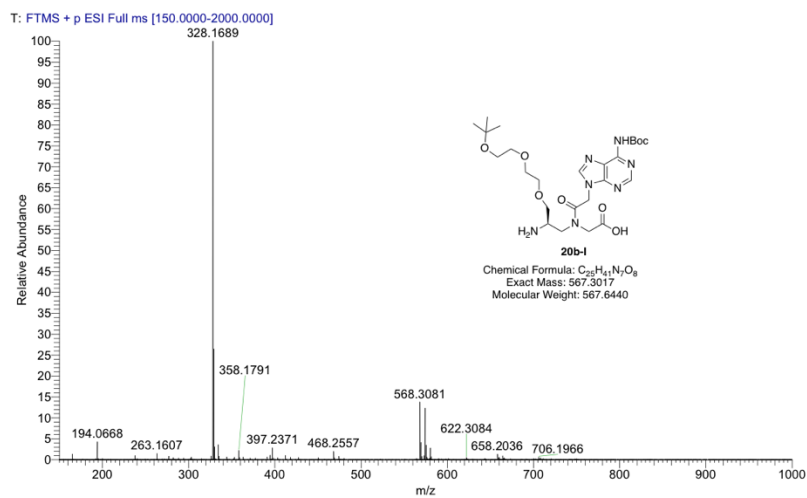
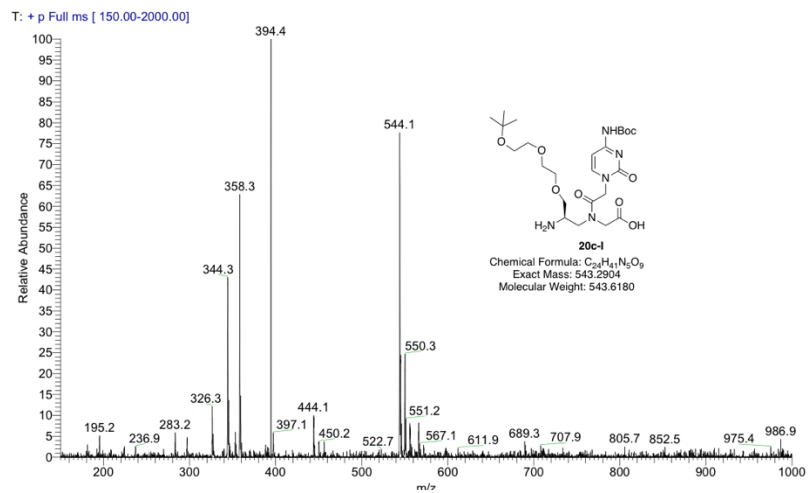


Figure II-S 27. HRMS (ESI) spectra of (A) compound **20a-I** and (B) compound **20b-I**.

(A)



(B)

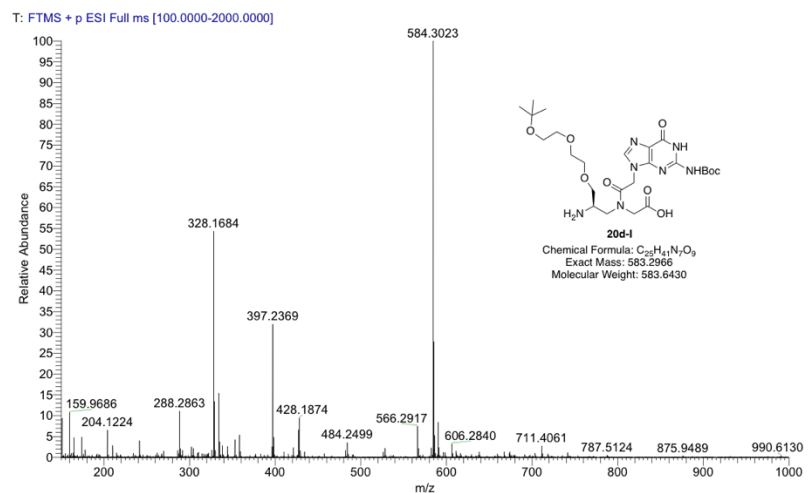
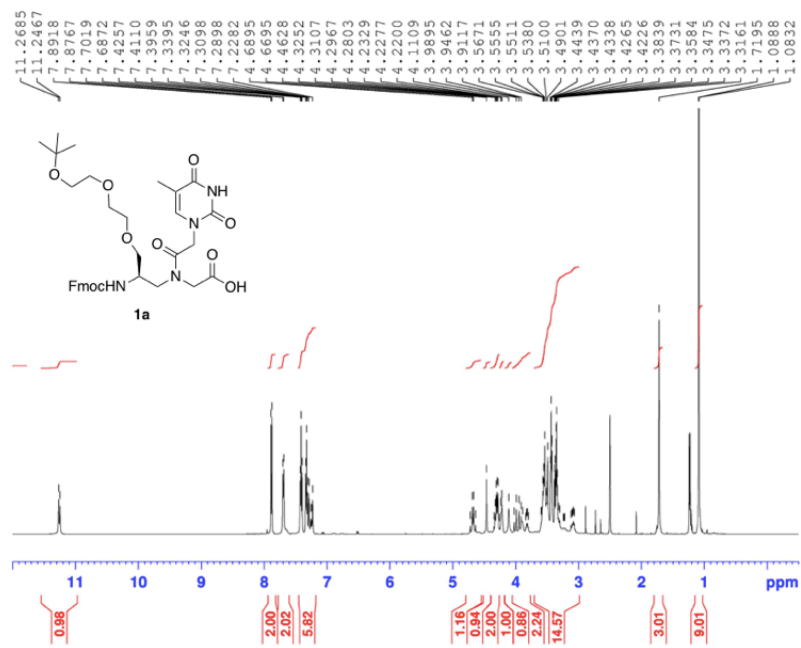


Figure II-S 28. HRMS (ESI) spectra of (A) compound **20c-I** and (B) compound **20d-I**.

(A)



(B)

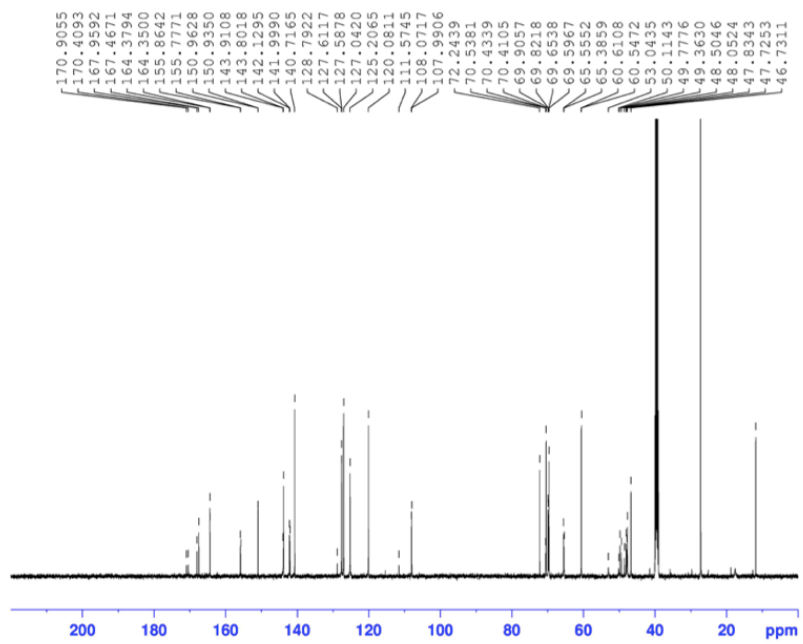


Figure II-S 29. (A) ¹H NMR (500 MHz, DMSO) and (B) ¹³C NMR (125 MHz, DMSO) spectra of compound **1a**.

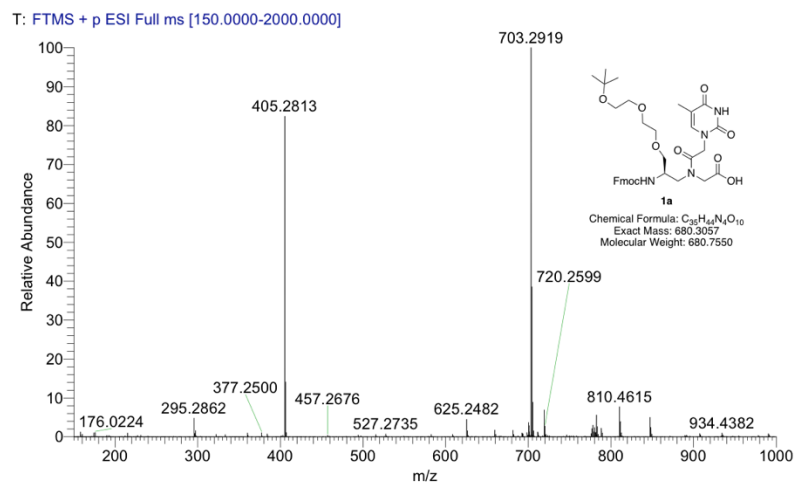
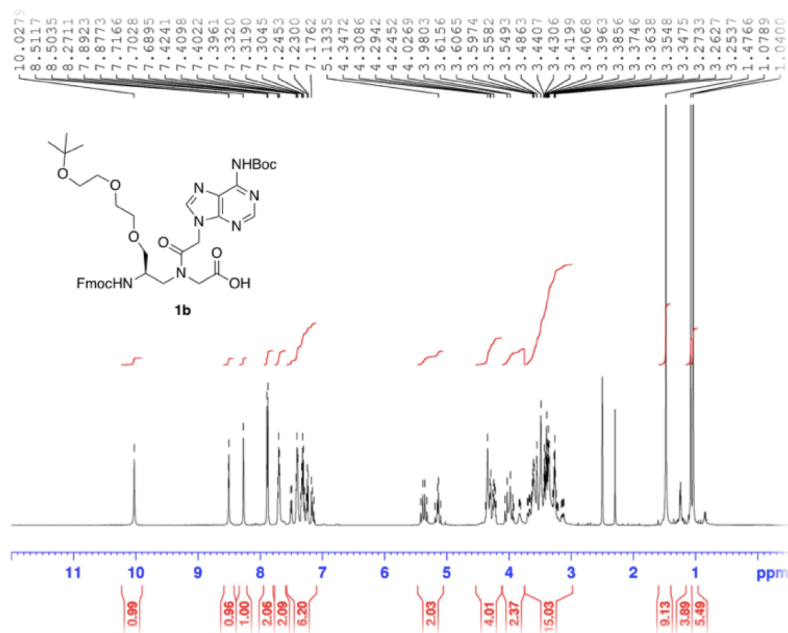


Figure II-S 30. HRMS (ESI) spectrum of compound **1a**.

(A)



(B)

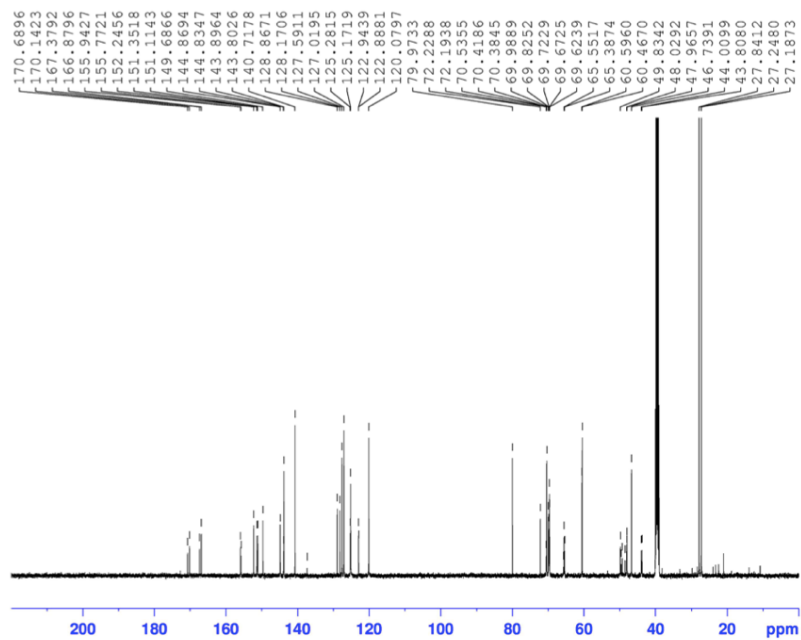


Figure II-S 31. (A) ¹H NMR (500 MHz, DMSO) and (B) ¹³C NMR (125 MHz, DMSO) spectra of compound **1b**.

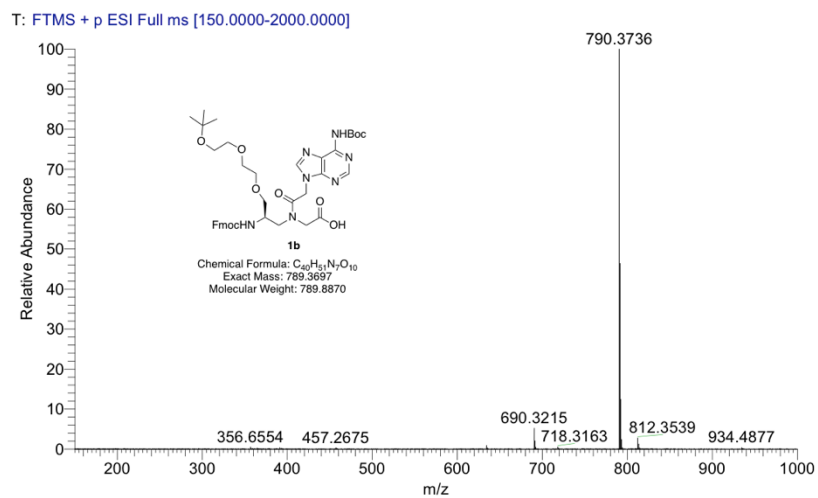
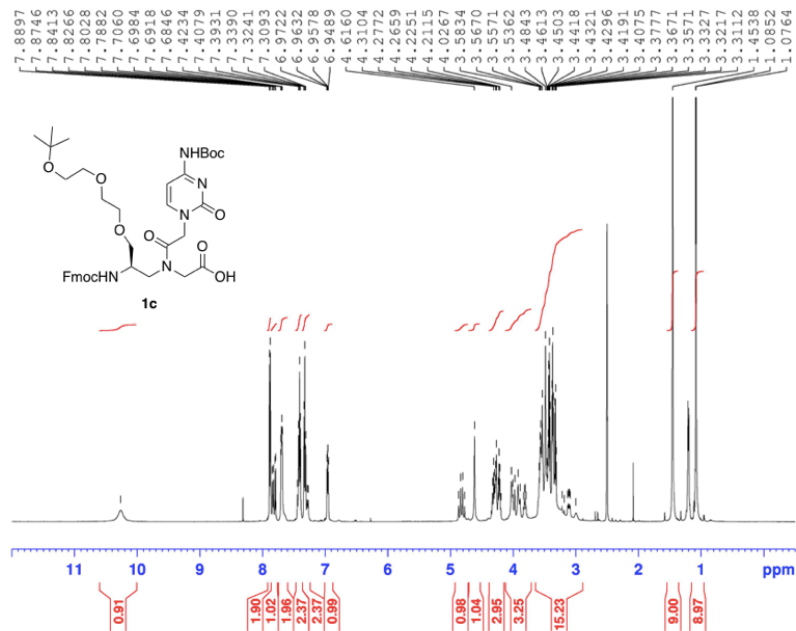


Figure II-S 32. HRMS (ESI) spectrum of compound **1b**.

(A)



(B)

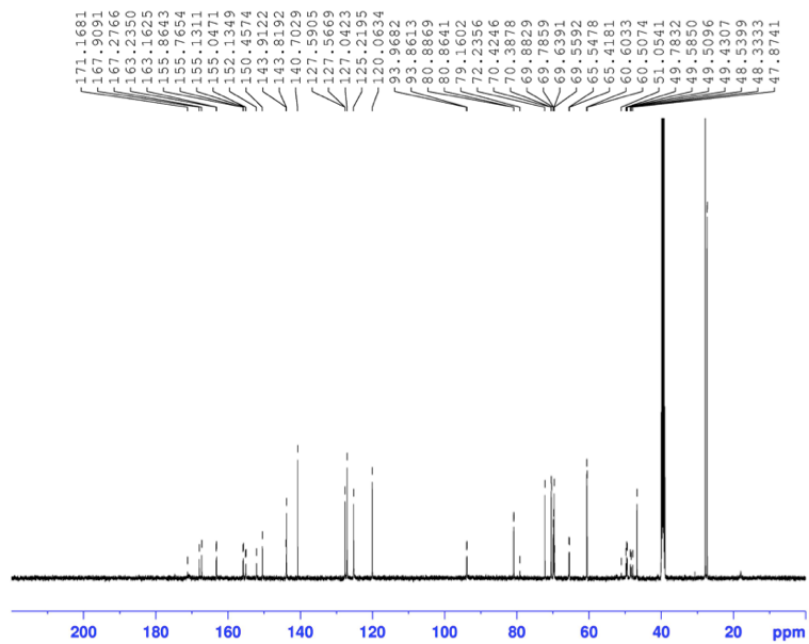


Figure II-S 33. (A) ¹H NMR (500 MHz, DMSO) and (B) ¹³C NMR (125 MHz, DMSO) spectra of compound **1c**.

T: FTMS + p ESI Full ms [150.0000-2000.0000]

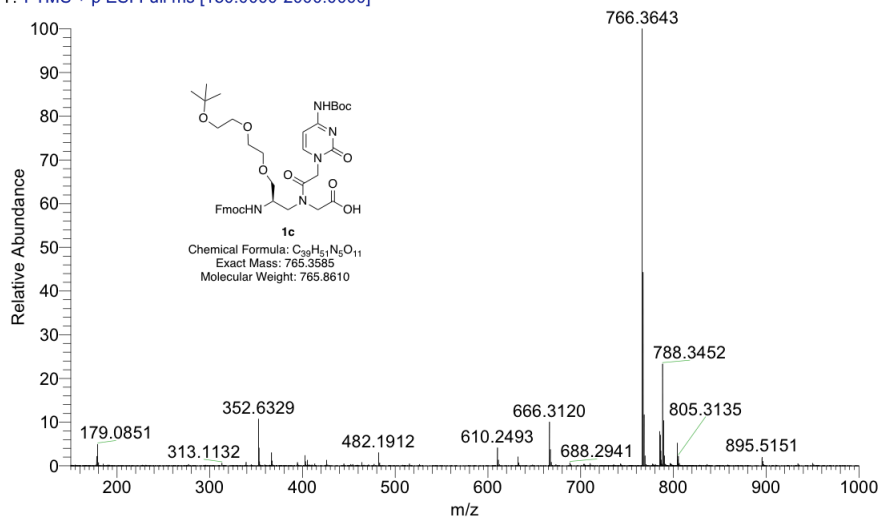
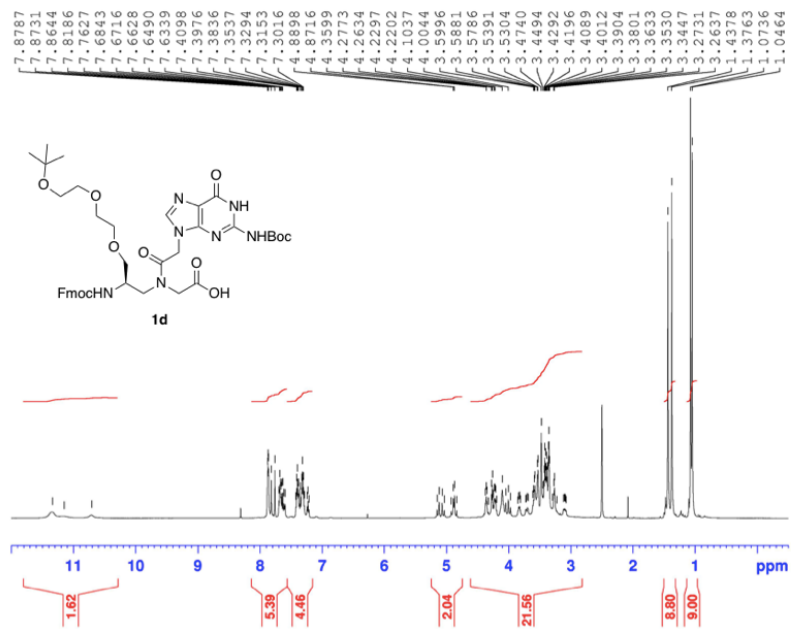


Figure II-S 34. HRMS (ESI) spectrum of compound **1c**.

(A)



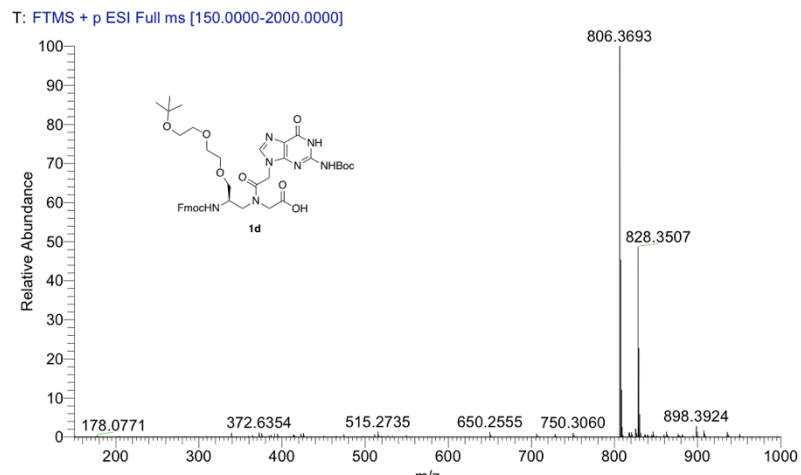
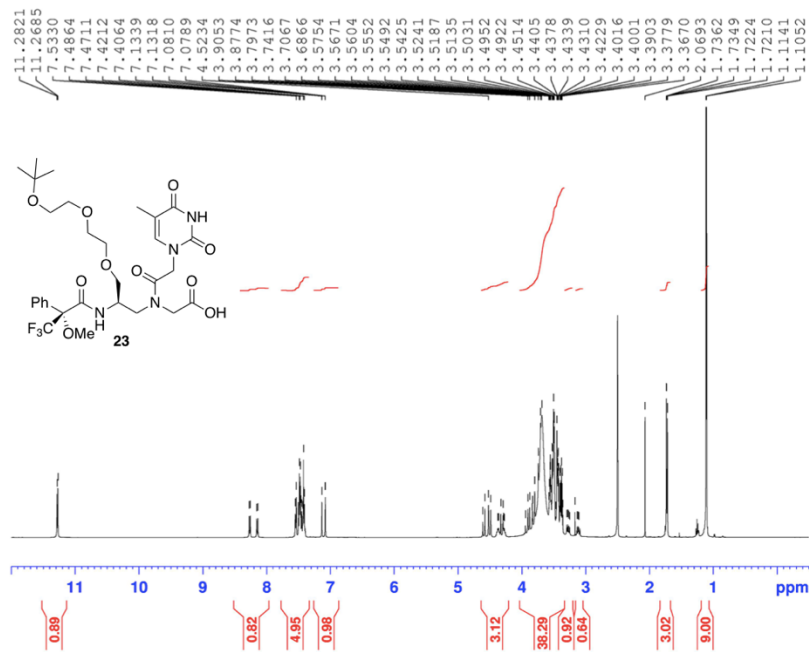


Figure II-S 36. HRMS (ESI) spectrum of compound **1d**.

(A)



(B)

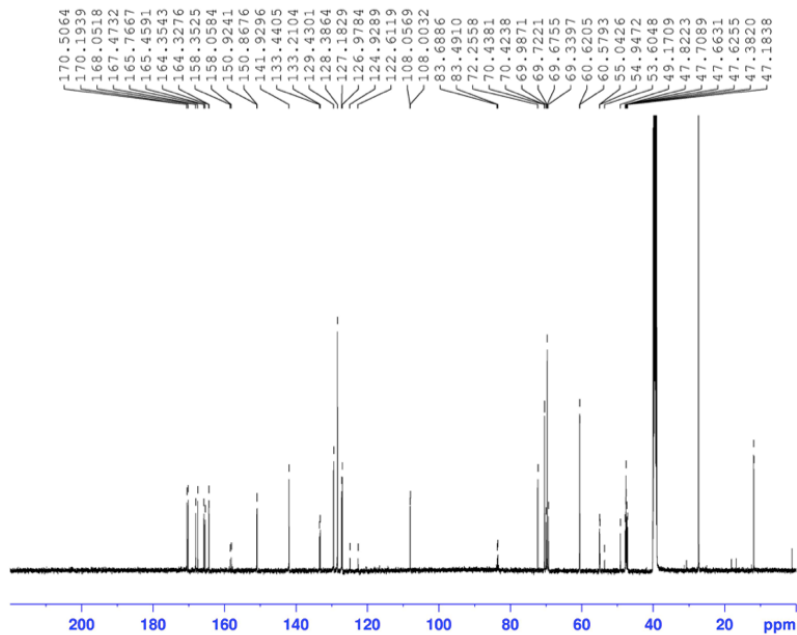
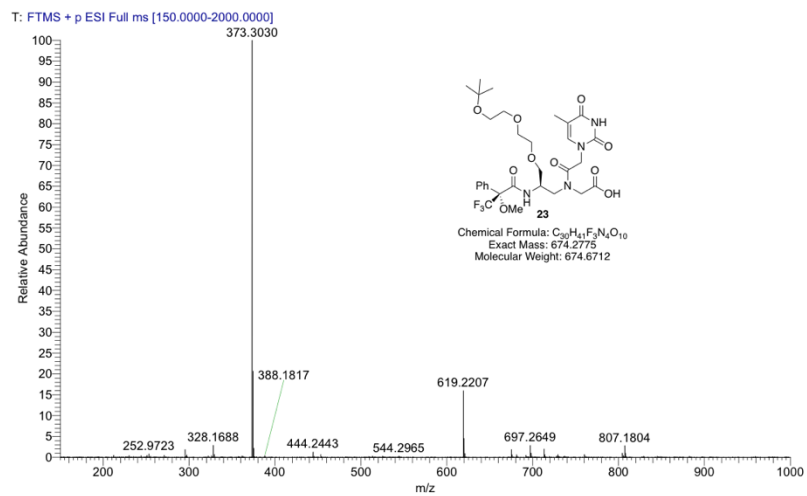


Figure II-S 37. (A) ¹H NMR (500 MHz, DMSO) and (B) ¹³C NMR (125 MHz, DMSO) spectra of compound **23**.

(A)



(B)

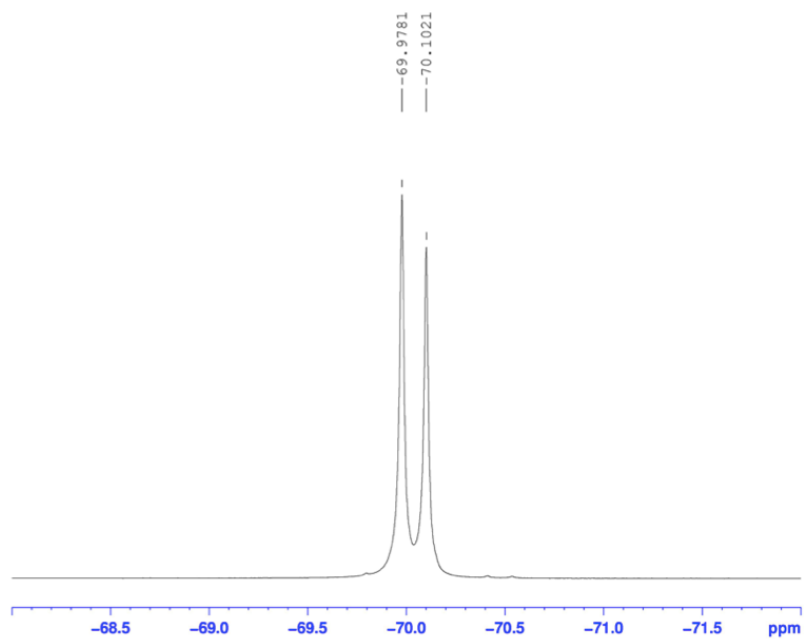
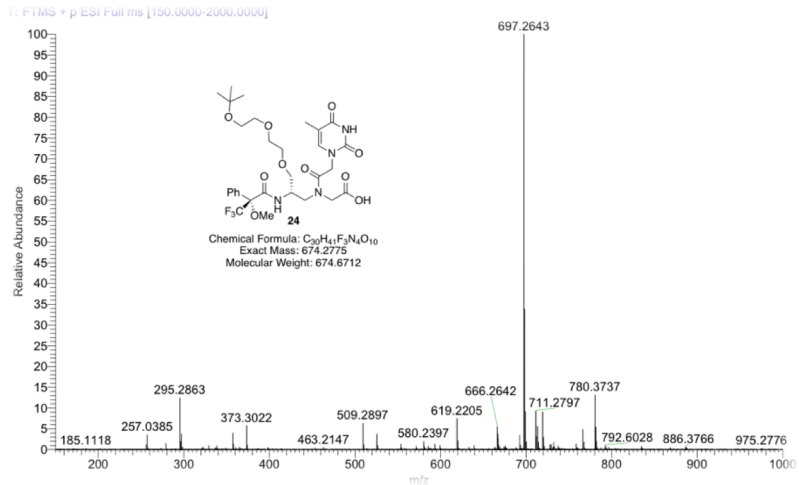


Figure II-S 38. (A) HRMS (ESI) and (B) ^{19}F NMR (470 MHz, DMSO) spectra of compound **23**.

(A)



(B)

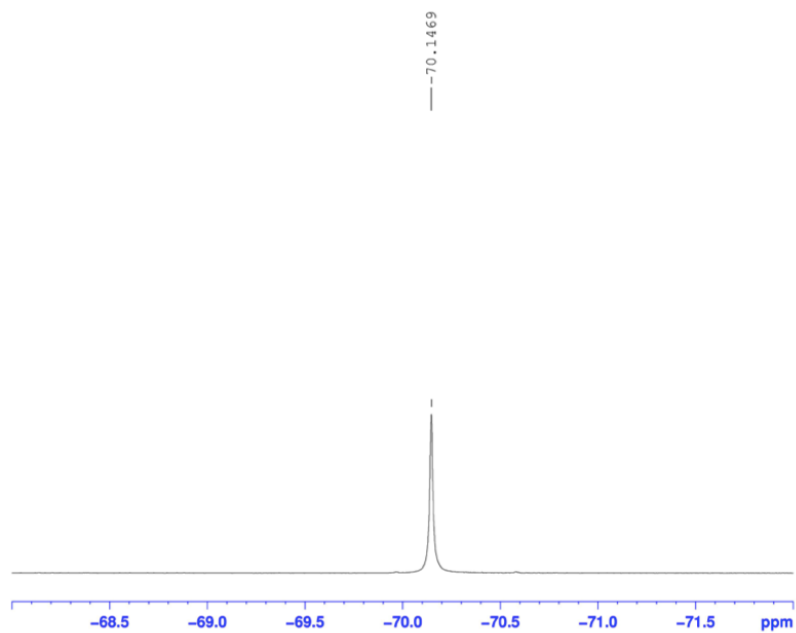


Figure II-S 40. (A) HRMS (ESI) and (B) ¹⁹F NMR (470 MHz, DMSO) spectra of compound **24**.

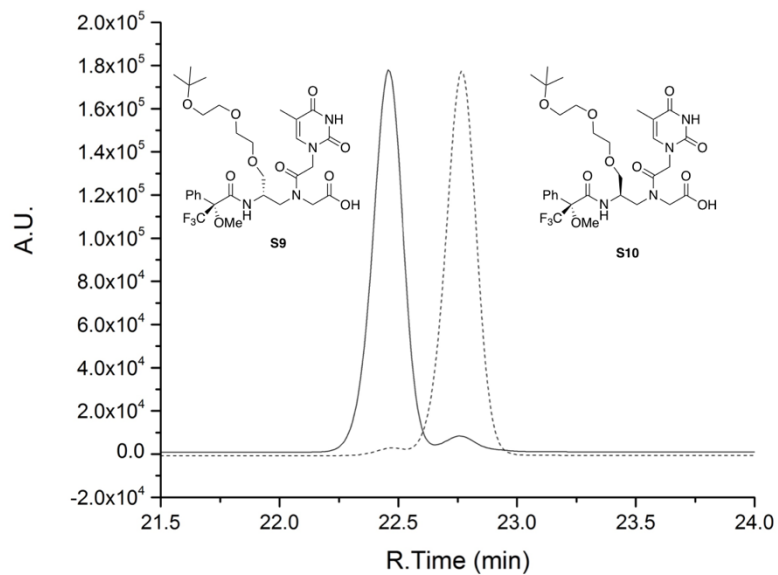


Figure II-S 41. HPLC chromatograms of Mosher derivatives **S9** and **S10** made from Fmoc protected intermediates **S3** and **S7**. e.e. value= 95%. HPLC Condition: C18 column (dimensions 4.6 mm X 250 mm), 1 mL/min flow rate, 25 °C oven temperature, 25 to 75% ACN/H₂O with 0.1% TFA in 30 min.

2.6. References

- (1) Khvorova, A.; Watts, J. K. The Chemical Evolution of Oligonucleotide Therapies of Clinical Utility. *Nat. Biotechnol.* **2017**, *35* (3), 238–248.
- (2) Jones, M. R.; Seeman, N. C.; Mirkin, C. A. Nanomaterials. Programmable Materials and the Nature of the DNA Bond. *Science* **2015**, *347* (6224), 1260901–1260901.
- (3) Adleman, L. M. Molecular Computation of Solutions to Combinatorial Problems. *Science* **1994**, *266* (5187), 1021–1024.
- (4) Nielsen, P. E.; Egholm, M.; Berg, R. H.; Buchardt, O. Sequence-Selective Recognition of DNA by Strand Displacement with a Thymine-Substituted Polyamide. *Science* **1991**, *254* (5037), 1497–1500.
- (5) Nielsen, P. E. Peptide Nucleic Acid. a Molecule with Two Identities. *Acc. Chem. Res.* **1999**, 624–630.
- (6) Egholm, M.; Buchardt, O.; Nielsen, P. E.; Berg, R. H. Peptide Nucleic-Acids (PNA) - Oligonucleotide Analogs with an Achiral Peptide Backbone. *J. Am. Chem. Soc.* **1992**, *114* (5), 1895–1897.
- (7) Haaima, G.; Lohse, A.; Buchardt, O.; Nielsen, P. E. Peptide Nucleic Acids (PNAs) Containing Thymine Monomers Derived From Chiral Amino Acids: Hybridization and Solubility Properties of D-Lysine PNA. *Angew. Chem. Int. Ed. Engl.* **1996**, *35* (17), 1939–1942.
- (8) Sforza, S.; Tedeschi, T.; Corradini, R.; Marchelli, R. Induction of Helical Handedness and DNA Binding Properties of Peptide Nucleic Acids (PNAs) with Two Stereogenic Centres. *Eur. J. Org. Chem.* **2007**, *2007* (35), 5879–5885.
- (9) Dragulescu-Andrasi, A.; Rapireddy, S.; Frezza, B. M.; Gayathri, C.; Gil, R. R.; Ly, D. H. A Simple Gamma-Backbone Modification Preorganizes Peptide Nucleic Acid Into a Helical Structure. *J. Am. Chem. Soc.* **2006**, *128* (31), 10258–10267.
- (10) Sacui, I.; Hsieh, W.-C.; Manna, A.; Sahu, B.; Ly, D. H. Gamma Peptide Nucleic Acids: as Orthogonal Nucleic Acid Recognition Codes for Organizing Molecular Self-Assembly. *J. Am. Chem. Soc.* **2015**, *137* (26), 8603–8610.
- (11) Bahal, R.; Sahu, B.; Rapireddy, S.; Lee, C.-M.; Ly, D. H. Sequence-Unrestricted, Watson-Crick Recognition of Double Helical B-DNA by (R)-miniPEG- γ PNAs. *Chembiochem* **2012**, *13* (1), 56–60.
- (12) Sahu, B.; Sacui, I.; Rapireddy, S.; Zanotti, K. J.; Bahal, R.; Armitage, B. A.; Ly, D. H. Synthesis and Characterization of Conformationally Preorganized, (R)-Diethylene Glycol-Containing Gamma-Peptide Nucleic Acids with Superior Hybridization Properties and Water Solubility. *J. Org. Chem.* **2011**, *76* (14), 5614–5627.
- (13) Singer, A.; Rapireddy, S.; Ly, D. H.; Meller, A. Electronic Barcoding of a Viral Gene at the Single-Molecule Level. *Nano Lett.* **2012**, *12* (3), 1722–1728.
- (14) Nölling, J.; Rapireddy, S.; Amburg, J. I.; Crawford, E. M.; Prakash, R. A.; Rabson, A. R.; Tang, Y.-W.; Singer, A. Duplex DNA-Invading Γ -Modified

- Peptide Nucleic Acids Enable Rapid Identification of Bloodstream Infections in Whole Blood. *MBio* **2016**, *7* (2), e00345–e00316.
- (15) Morin, T. J.; Shropshire, T.; Liu, X.; Briggs, K.; Huynh, C.; Tabard-Cossa, V.; Wang, H.; Dunbar, W. B. Nanopore-Based Target Sequence Detection. *PLoS ONE* **2016**, *11* (5), e0154426.
- (16) Bahal, R.; Ali McNeer, N.; Quijano, E.; Liu, Y.; Sulkowski, P.; Turchick, A.; Lu, Y.-C.; Bhunia, D. C.; Manna, A.; Greiner, D. L.; Brehm, M. A.; Cheng, C. J.; López-Giráldez, F.; Ricciardi, A.; Beloor, J.; Krause, D. S.; Kumar, P.; Gallagher, P. G.; Braddock, D. T.; Mark Saltzman, W.; Ly, D. H.; Glazer, P. M. In Vivo Correction of Anaemia in B-Thalassaemic Mice by γ PNA-Mediated Gene Editing with Nanoparticle Delivery. *Nat. Commun.* **2016**, *7*, 13304.
- (17) Ricciardi, A. S.; Bahal, R.; Farrelly, J. S.; Quijano, E.; Bianchi, A. H.; Luks, V. L.; Putman, R.; López-Giráldez, F.; Coskun, S.; Song, E.; Liu, Y.; Hsieh, W.-C.; Ly, D. H.; Stitelman, D. H.; Glazer, P. M.; Saltzman, W. M. In Utero Nanoparticle Delivery for Site-Specific Genome Editing. *Nat. Commun.* **2018**, *9*, 2481.
- (18) Manna, A.; Rapireddy, S.; Sureshkumar, G.; Ly, D. H. Synthesis of Optically Pure γ PNA Monomers: a Comparative Study. *Tetrahedron* **2015**, *71*, 3507–3514.
- (19) Kosynkina, L.; Wang, W.; Liang, T. C. A Convenient Synthesis of Chiral Peptide Nucleic Acid (PNA) Monomers. *Tetrahedron Lett.* **1994**, *35* (29), 5173–5176.
- (20) Rittle, K. E.; Homnick, C. F.; Ponticello, G. S.; Evans, B. E. A Synthesis of Statine Utilizing an Oxidative Route to Chiral Alpha-Amino Aldehydes. *J. Org. Chem.* **1982**, *47* (15), 3016–3018.
- (21) Stanfield, C. F.; Parker, J. E.; Kanellis, P. Preparation of Protected Amino Aldehydes. *J. Org. Chem.* **1981**, *46* (23), 4797–4798.
- (22) Miles, N. J.; Sammes, P. G.; Kennewell, P. D.; Westwood, R. On the Double Bond Isostere of the Peptide Bond: Preparation of Modified Di- and Tri-Peptides Incorporating Proline and Alanine Analogues. *J. Chem. Soc. Perkin Trans 1* **1985**, *0* (0), 2299–2305.
- (23) Dellaria, J. F., Jr.; Maki, R. G. The Enantio- and Diastereoselective Synthesis of the First Phospho-Statine Derivative. *Tetrahedron Lett.* **1986**, *27* (21), 2337–2340.
- (24) Myers, A. G.; Zhong, B.; Movassaghi, M.; Kung, D. W.; Lanman, B. A.; Kwon, S. Synthesis of Highly Epimerizable N-Protected α -Amino Aldehydes of High Enantiomeric Excess. *Tetrahedron Lett.* **2000**, *41* (9), 1359–1362.
- (25) Reetz, M. T. Synthesis and Diastereoselective Reactions of N,N-Dibenzylamino Aldehydes and Related Compounds. *Chem. Rev.* **1999**, *99* (5), 1121–1162.
- (26) Lubell, W.; Rapoport, H. Surrogates for Chiral Aminomalondialdehyde - Synthesis of N-(9-Phenylfluoren-9-Yl)Serinal and N-(9-Phenylfluoren-9-Yl)Vinylglycinal. *J. Org. Chem.* **1989**, *54* (16), 3824–3831.

- (27) Gosselin, F.; Van Betsbrugge, J.; Hatam, M.; Lubell, W. D. A Novel Linking-Protecting Group Strategy for Solid-Phase Organic Chemistry with Configurationally Stable Alpha-[N-(Phenylfluorenyl)]Amino Carbonyl Compounds: Synthesis of Enantiopure Norephedrine on Solid Support. *J. Org. Chem.* **1999**, *64* (7), 2486–2493.
- (28) Lubell, W. D.; Rapoport, H. Configurational Stability of N-Protected Alpha-Amino Aldehydes. *J. Am. Chem. Soc.* **1987**, *109* (1), 236–239.
- (29) Manna, A.; Rapireddy, S.; Sureshkumar, G.; Ly, D. H. Synthesis of Optically Pure γ PNA Monomers: a Comparative Study. *Tetrahedron* **2015**, *71* (21), 3507–3514.
- (30) Karppanen, E. J.; Koskinen, A. M. P. The 9-Phenyl-9-Fluorenyl Group for Nitrogen Protection in Enantiospecific Synthesis. *Molecules* **2010**, *15* (9), 6512–6547.
- (31) Pothukanuri, S.; Pianowski, Z.; Winssinger, N. Expanding the Scope and Orthogonality of PNA Synthesis. *Eur. J. Org. Chem.* **2008**, *2008* (18), 3141–3148.
- (32) Surprenant, S.; Lubell, W. D. 9-(4-Bromophenyl)-9-Fluorenyl as a Safety-Catch Nitrogen Protecting Group. *J. Org. Chem.* **2006**, *71* (2), 848–851.
- (33) Asahina, Y.; Takei, M.; Kimura, T.; Fukuda, Y. Synthesis and Antibacterial Activity of Novel Pyrido[1,2,3-De][1,4]Benzoxazine-6-Carboxylic Acid Derivatives Carrying the 3-Cyclopropylaminomethyl-4-Substituted-1-Pyrrolidinyl Group as a C-10 Substituent. *J. Med. Chem.* **2008**, *51* (11), 3238–3249.
- (34) Shimizu, T.; Osako, K.; Nakata, T. Efficient Method for Preparation of N-Methoxy-N-Methyl Amides by Reaction of Lactones or Esters with Me₂AlCl-MeONHMe-HCl. *Tetrahedron Lett.* **1997**, *38* (15), 2685–2688.
- (35) Beaudoin, D.; Grenon, O. L.; Maris, T.; Wuest, J. D. Building Giant Carbocycles by Reversible C-C Bond Formation. *Angew. Chem. Int. Ed. Engl.* **2016**, *55* (3), 894–898.
- (36) Christie, B. D.; Rapoport, H. Synthesis of Optically Pure Pipecolates From L-Asparagine - Application to the Total Synthesis of (+)-Apovincamine Through Amino-Acid Decarbonylation and Iminium Ion Cyclization. *J. Org. Chem.* **1985**, *50* (8), 1239–1246.
- (37) Bartoli, G.; Bosco, M.; Locatelli, M.; Marcantoni, E.; Melchiorre, P.; Sambri, L. Unusual and Unexpected Reactivity of T-Butyl Dicarboxylate (Boc₂O) with Alcohols in the Presence of Magnesium Perchlorate. a New and General Route to T-Butyl Ethers. *Org. Lett.* **2005**, *7* (3), 427–430.
- (38) Abdel-Magid, A. F.; Carson, K. G.; Harris, B. D.; Maryanoff, C. A.; Shah, R. D. Reductive Amination of Aldehydes and Ketones with Sodium Triacetoxyborohydride. Studies on Direct and Indirect Reductive Amination Procedures. *J. Org. Chem.* **1996**, *61* (11), 3849–3862.
- (39) Kumar, A.; Sharma, A.; Haimov, E.; El-Faham, A.; de la Torre, B. G.; Albericio, F. Fmoc-Amox, a Suitable Reagent for the Introduction of Fmoc. *Org. Process Res. Dev.* **2017**, *21* (10), 1533–1541.
- (40) Seco, J. M.; Quinoa, E.; Riguera, R. The Assignment of Absolute Configuration by NMR. *Chem. Rev.* **2004**, *104* (1), 17–117.

Chapter III: Stereochemical Conversion of Nucleic Acid

Circuits *via* Strand Displacement

The work in this chapter has been previously submitted as:

Hsieh, W.-C.; Martinez, G. R.; Wang, A.; Wu, S. F.; Chamdia, R.; H Ly, D.

Stereochemical Conversion of Nucleic Acid Circuits via Strand Displacement.

Wei-Che Hsieh and Dr. Danith H. Ly designed the research. Wei-Che Hsieh and Raunaq Chamdia synthesized the monomers. Wei-Che Hsieh, Ashley Wang, Sharon F. Wu, Dr. Gustavo R. Martinez and Dr. Danith H. Ly prepared the oligomers. Wei-Che Hsieh and Dr. Gustavo R. Martinez performed spectroscopic studies. Wei-Che Hsieh and Dr. Danith H. Ly performed the gel analysis. Wei-Che Hsieh and Dr. Danith H. Ly analyzed the data and wrote the paper.

3.1. Introduction

In addition to fulfilling their evolutionary roles as a medium for the storage and transmission of genetic information, nucleic acid biopolymers provide a convenient means for organizing molecular self-assembly because of their specific and predictable nucleobase interactions and defined length scale. Among them, synthetic DNA oligonucleotides have garnered considerable interest as building blocks for molecular engineering because of their chemical stability, ease of synthesis, and low cost of production. Since the seminal work of Chen and Seeman¹ more than two decades ago that demonstrated their utility in the construction of molecular frameworks for organizing

molecular self-assembly, DNA has been utilized in the bottom-up construction of a wide range of macro- and supra-molecular systems, including polymeric materials,^{2,3} nanoparticles,^{4,5} DNA tiles and origami,⁶⁻¹⁵ molecular circuits,^{16,17} and autonomous nanoscale machines,¹⁸⁻²¹ as well as in information storage²²⁻²⁴ and molecular computation.²⁵⁻²⁹ However, beyond the feasibility studies that were commonly carried out in test tubes, such an approach has not been extensively explored in the biological systems due, in part, to the concerns for enzymatic degradation and inadvertent hybridization of the chemical building blocks with the host's genetic materials, although earnest attempts have been made.³⁰⁻³⁴ Spurious binding is not only counterproductive, but could lead to adverse cellular and cytotoxic effects. Synthetic derivatives, such as α -DNA and α -RNA (or 'Spiegelmer')^{35,36} in principle, could be employed to address some of these concerns; however, there is no simple way to interface the genetic information encoded in such materials with that in natural nucleic acid biopolymers.

A particular interest in many biological applications involves dynamic assembly,³⁷ one that relies on the precise spatial and temporal control of the non-equilibrium dynamics to drive the hybridization process. These non-covalent reactions are driven by strand displacement, a biological phenomenon first recognized several decades ago³⁸ and recently pioneered by Yurke¹⁸ in nucleic acid programming, in which two strands of partial or full complementary DNA hybridize to each other, and, in the process, displace one or more of the pre-hybridized strands. Strand displacement is initiated upon hybridization of the complementary single-stranded regions, commonly referred to as 'toeholds,' where the rate of such a reaction can be controlled by varying the binding strength.³⁹

Of a myriad of molecular operations that have been developed, with most geared toward the construction of materials, one that holds considerable promise for molecular diagnostics is hybridization chain reaction (HCR). HCR was developed by Dirks and Pierce⁴⁰ more than a decade ago as a means for amplifying the transduction signals in a similar manner to that of polymerase chain reaction (PCR) but without the enzyme. The amplification process relies on the coexistence of two metastable hairpin species with complementary domains in the loops and toeholds. The two hairpins are unable to hybridize to each other because the former is kinetically trapped. HCR is triggered upon the addition of an initiator, causing a cascade reaction between the two hairpins. The power of HCR in signal amplification has been well-recognized and successfully applied in a number of biosensing applications^{41,42}; however, many of them were directed toward the detection of genetic materials in processed samples, such as fixed cells and tissues, but rarely in their native states.⁴³

Recently, we reported on the development of an orthogonal nucleic acid system that is comprised of three components: a right-handed (RH, **Figure III- 1, i**) and a left-handed γ PNA conformer (LH, **Figure III- 1, ii**), and non-helical PNA version (NH, **Figure III- 1, iii**). The first two are orthogonal to each other in recognition, while the third is compatible with both the RH and LH conformers, as well as with DNA and RNA. Unlike their natural counterparts, these chemical building blocks are impervious to enzymatic degradation. Moreover, they are relatively simple to chemically synthesize and structurally modify, as all three components share the same PNA backbone skeleton with the exception of the stereochemistry or the lack thereof at the gamma (γ)-position, which determines whether the resulting oligonucleotide adopts an RH, LH, or NH motif.

Herein, this work demonstrates that the genetic information encoded in the RH and LH conformers, as well as in natural nucleic acid biopolymers, can be interconverted through strand displacement. Strategic placement of the backbone spacer and systemic evaluation of the experimental conditions yielded insight into key parameters for the design of molecular circuits for the detection of genetic materials with improved recognition specificity, detection sensitivity, and conversion rate. The work has implications for the organization and assembly of materials and molecular computation in biological systems.

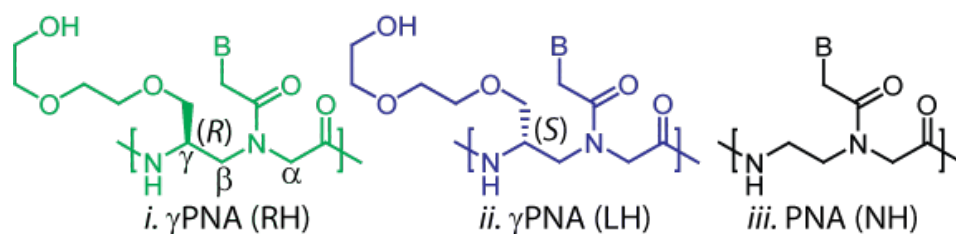


Figure III- 1. Molecular design. Chemical structure of a *(i)* right-handed RH- γ PNA, *(ii)* left-handed LH- γ PNA, and *(iii)* non-helical NH-PNA.

3.2. Design Rationale

A number of configurationally-inverted nucleic acid systems has been developed, including β - and α -DNA,³⁵ β - and α -RNA,³⁶ and LNA⁴⁴ and α -L-LNA.⁴⁵ Cross-hybridization still occurs between the two mirror-imaged partners, but to a lesser extent than with the conformationally-matched pairs. In contrast, the RH- and LH- γ PNA conformers are unable to hybridize to each other.⁴⁶ Such a feature could hinder or prevent the conversion process altogether.

To demonstrate the genetic information encoded in the RH- and LH- γ PNA can be interconverted, we designed two sets of molecular converters (**Figure III- 2A**), with each comprising a non-helical template strand (TS) and either an RH, LH, or NH displacement strand (DS). The first set contained a contiguous TS (**Figure III- 2A, i**), while the second contained TS with a flexible PEG-spacer between toehold and the stem (**Figure III- 2A, ii**). The role of the spacer was to decouple the helical induction in toehold from the stem, making the former conformationally more flexible and, thus, more accommodating to the invading strand (IS) with a mismatched helical sense (**Figure III- 2B**).

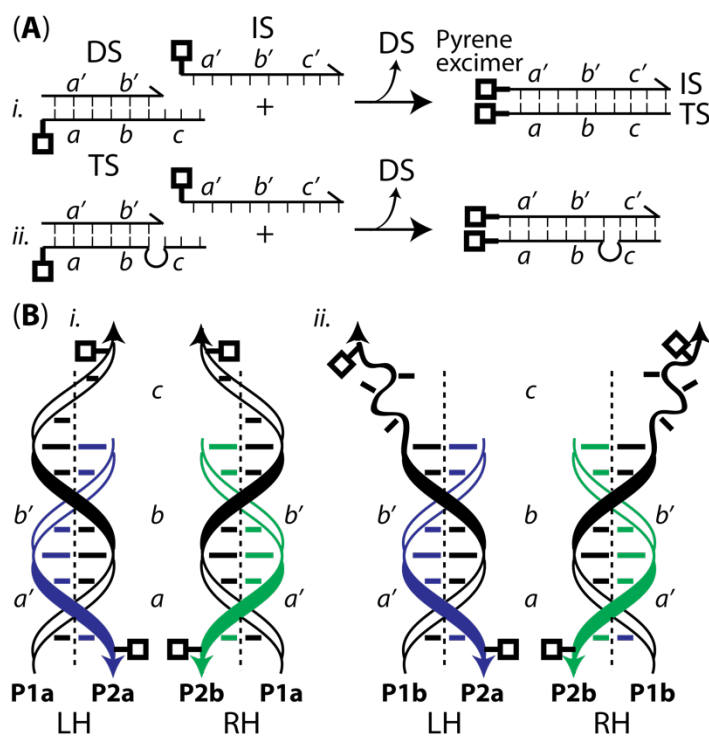


Figure III- 2. (A) Strand displacement reactions involving (i) a contiguous template, and (ii) a template with a disrupted PEG-spacer. TS: Template Strand (15-nts), DS: Displacement Strand (10-nts), and IS: Invading Strand (15-nts). (B) Predicted helical senses of TS-DS molecular converters containing (i) a contiguous template, and (ii) a template with PEG-spacer.

The chemical compositions of TS, DS, and IS are shown in **Figure III- 3**, along with their HPLC and MALDI-TOF spectra (**Appendix III- 1-8**). Glutamic acids were incorporated at the *N*-terminus of each component to improve water solubility and to enable their separation by gel electrophoresis. Pyrene was chosen as a reporter for monitoring strand displacement.⁴⁷ In its absence, excitation of pyrene monomers at 344 nm results in fluorescent emissions at 380 and 400 nm. In its presence, excitation of pyrenes at the same wavelength results in the emission of excimers at 485 nm. This ~ 100 nm red-shift in the fluorescent emission provides a convenient means for monitoring the strand displacement reaction.

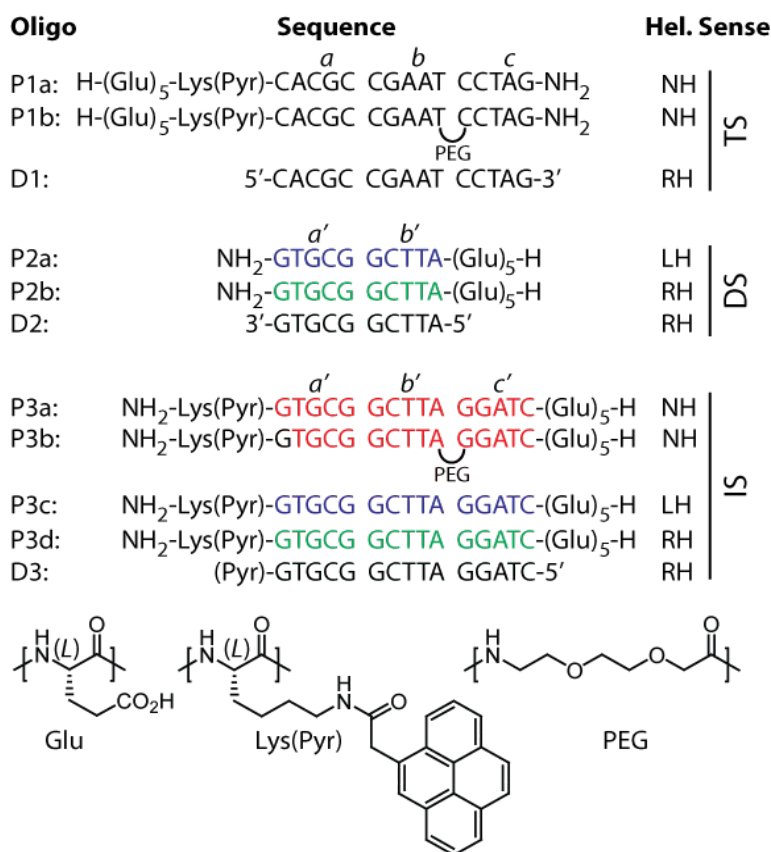


Figure III- 3. Chemical compositions of TS, DS, and IS. DNA oligonucleotides D1, D2, and D3 were included for comparison.

3.3. Results

3.3.1. Recognition Orthogonality

To further substantiate the recognition orthogonality of LH conformer with nucleic acid biopolymers, we adopted the HCR system as reported by Dirks and Pierce⁴⁸ (**Figure III- 4A and B**), and prepared the corresponding DNA (I1), LH- γ PNA (I2), and RH- γ PNA (I3) initiators (**Figure III- 4C**). The binding affinity of I3 with DNA is too high to be determined accurately by conventional spectroscopic techniques. Based on the previous findings⁴⁹, with the 10-mer RH- γ PNAs showing dissociation constants (K_{DS}) in the femtomolar range, we estimated the K_D value of I3 with DNA (or RNA) to be at least several orders of magnitude lower. We expected I1 and I3 to hybridize to H1A and initiate HCR (**Figure III- 4A and B**), but not I2, due to the conformational mismatch, unless cross-hybridization takes place between it and H2A.

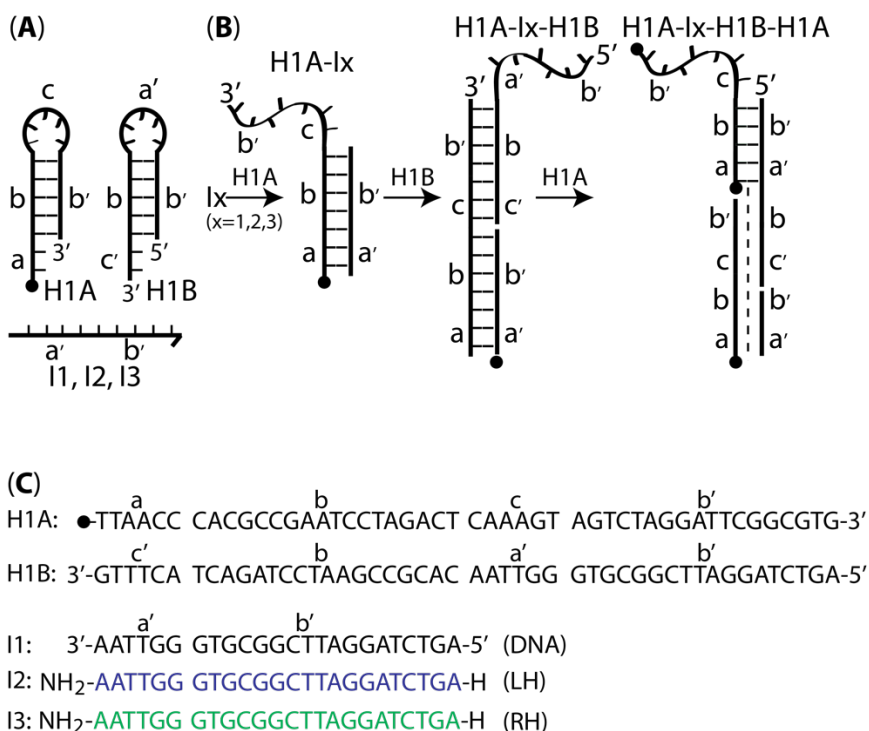


Figure III- 4. Recognition orthogonality. (A) Depiction of HCR components. (B) HCR cascade. (C) Sequence compositions of hairpins and initiators.

Consistent with this prediction, we observed HCR only upon the addition of I1 (Figure III- 5, lanes 5 and 6) and I3 (lanes 7 and 8), as apparent from the formation of shifted bands and from the inverse molecular weight distribution with respect to initiator concentration (compare lanes 6 to 5, and lanes 8 to 7). No evidence of HCR took place following the addition of I2 and incubation of the mixtures for 16 hrs. This result is consistent with the previous report that showed a high degree of recognition orthogonality of LH- γ PNA with DNA, and, *via* inference, RNA.⁴⁶

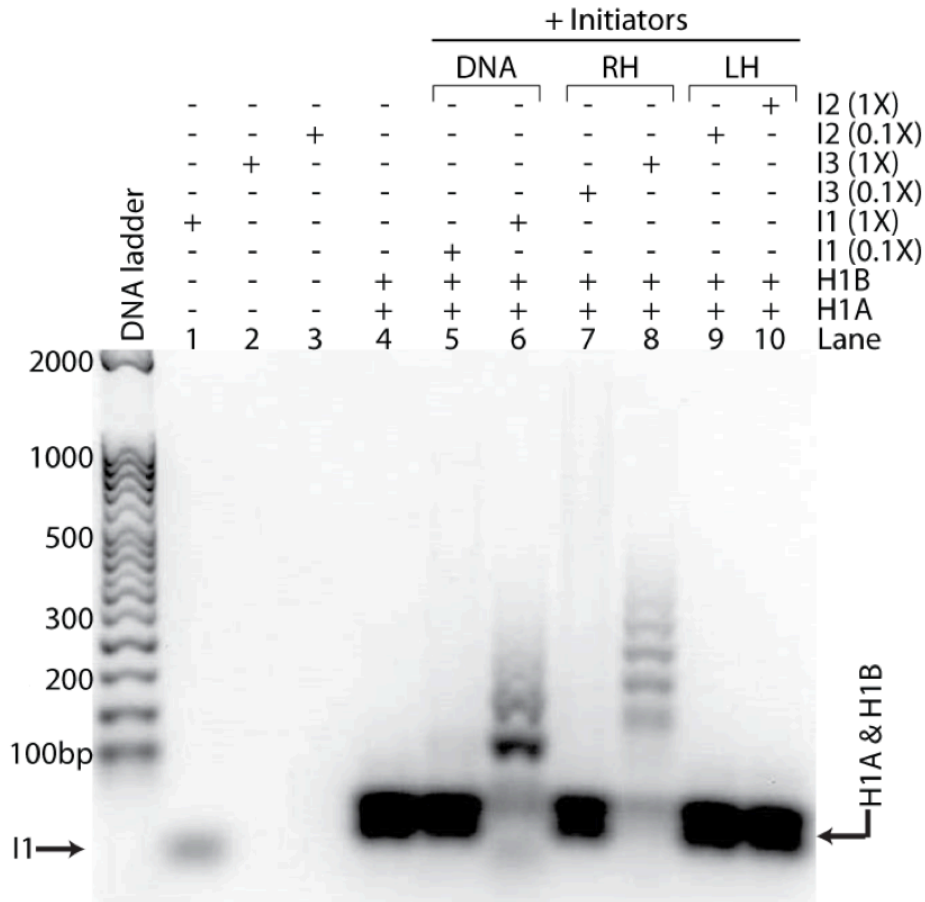


Figure III- 5. Result of HCR following the addition of I1 (lanes 5 and 6), I3 (lanes 7 and 8), and I2 (lanes 9 and 10) to a mixture containing an equimolar ratio of H1A and H1B (lane 4) and incubation at 25 °C for 16 hrs. The concentrations of H1A and H1B were 1 μ M each. The samples were prepared in a PBS buffer (50 mM Na_2HPO_4 , 138 mM NaCl, 2.7 mM KCl, pH 7.4), separated on a 10% non-denaturing PAGE, and stained with SYBR-Gold.

3.3.2. Conformational Analysis

Circular dichroism (CD) was employed to assess the conformations of DS and IS, along with that of the corresponding TS-DS and TS-IS duplexes. With the same concentration (**Figure III- 6**), the individual DS (P2a and P2b) and IS (P3c and P3d) components adopted either an RH or an LH motif as inferred from the CD spectral patterns (**Figure III- 7A**), as consistent with the earlier published literature.⁵⁰ This is in contrast to the weak CD signals observed with the achiral (and non-helical) P1a and P1b templates and P3a invading strand (**Figure III- 7B**).⁵¹

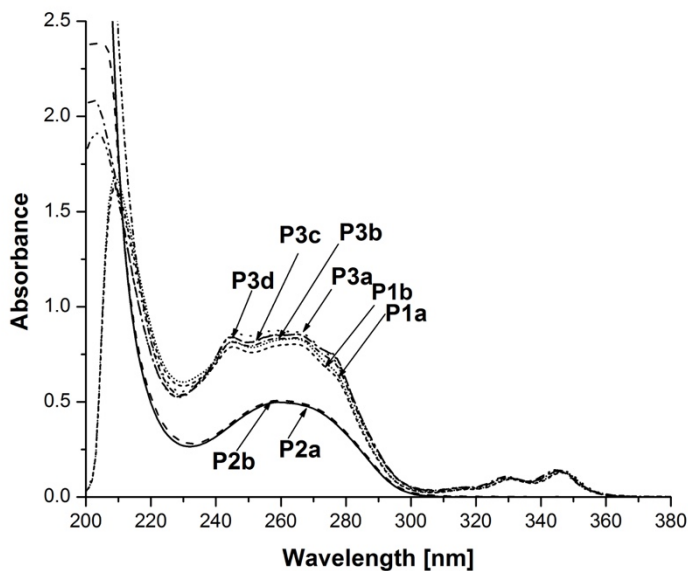


Figure III- 6. UV-absorption profiles of P1a, P1b, P2a, P2b, P3a, P3b, P3c, and P3d at 5 μ M strand concentration each recorded at 95 $^{\circ}$ C.

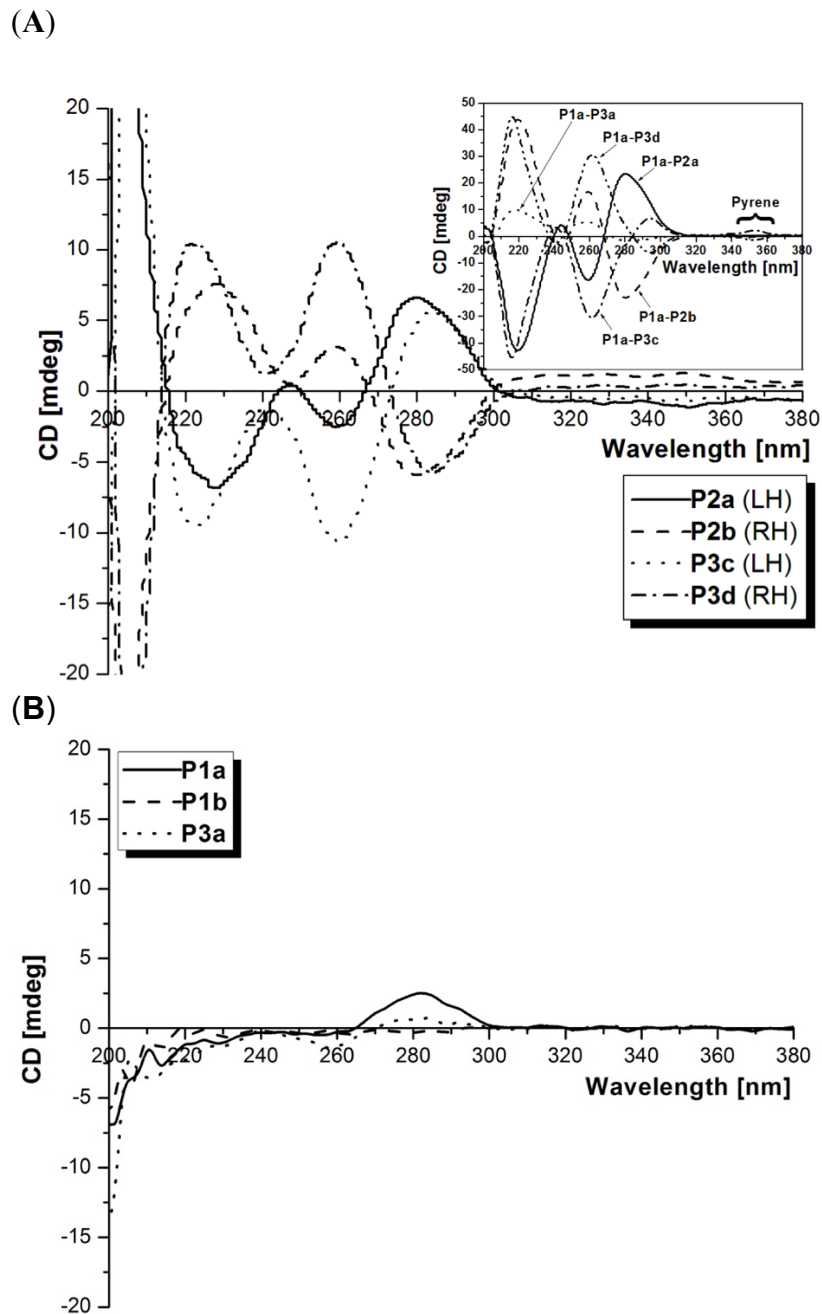


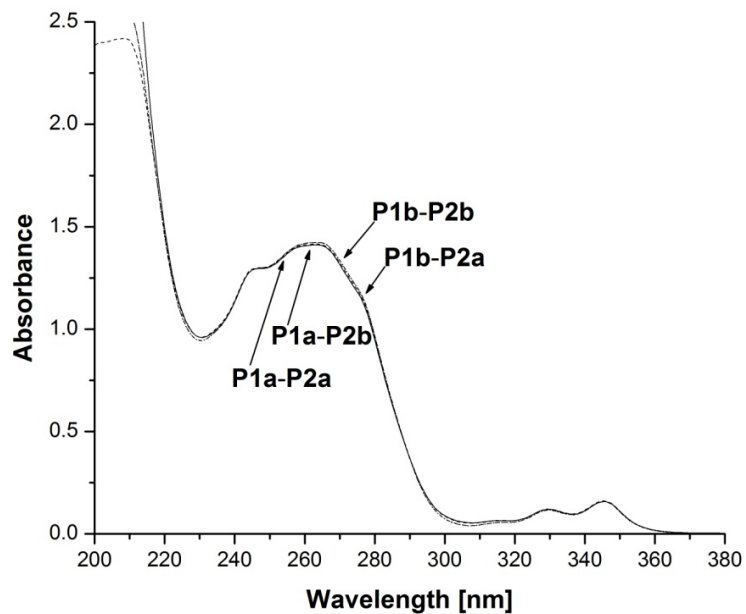
Figure III- 7. Conformational preorganization. (A) CD spectra of DS and IS components, along with that of the corresponding TS-DS (P1a-P2a and P1a-P2b) and TS-IS (P1a-P3a, P1a-P3c, and P1a-P3d) duplexes (*Inset*). (B) CD profiles of P1a, P1b, and P3a at 5 μ M strand concentration each, recorded at room temperature. Notice that these oligomers did not have backbone modifications.

Similar spectral patterns were observed with TS-DS and TS-IS duplexes (**Figure III- 7A**, *Inset*, and **Appendix III- 9**). Among the three duplexes with an identical length and concentration (**Appendix III- 9**), P1a-P3a exhibited the weakest CD signals, nearly five-fold lower than that of P1a-P3c and P1a-P3d. (**Figure III- 7A**, *Inset*) This large difference in the signal strength is reflected in the conformational homogeneity of the duplex, with P1a-P3a existing as both an RH and an LH conformer in different proportions, whereas the others were present in a single conformational state.

This observation is consistent with the X-ray crystallography data⁵², along with the findings by Nordén⁵³ and Green⁵⁴, which showed that the helical preference of a PNA-PNA duplex induced by chiral amino acids at the *C*-terminus does not exist in one predominant state, but rather as a mixture of both RH and LH, with one in slight excess over the other.

On the other hand, incorporation of a PEG-spacer in TS disrupted the helical induction in the toehold, as evident from the reduction in CD signals of P1b-P2a and P1b-P2b duplexes as compared to that of the respective P1a-P2a and P1a-P2b (**Figure III- 8**). However, its inclusion had little effect on the helical induction of the full-length TS-IS duplexes (**Figure III- 8B**, *Inset*), as it is mediated by IS. This result is consistent with our prediction that the introduction of a flexible PEG-spacer would disrupt base-stacking interactions in toehold, rendering it conformationally more flexible (**Figure III- 2B**).

(A)



(B)

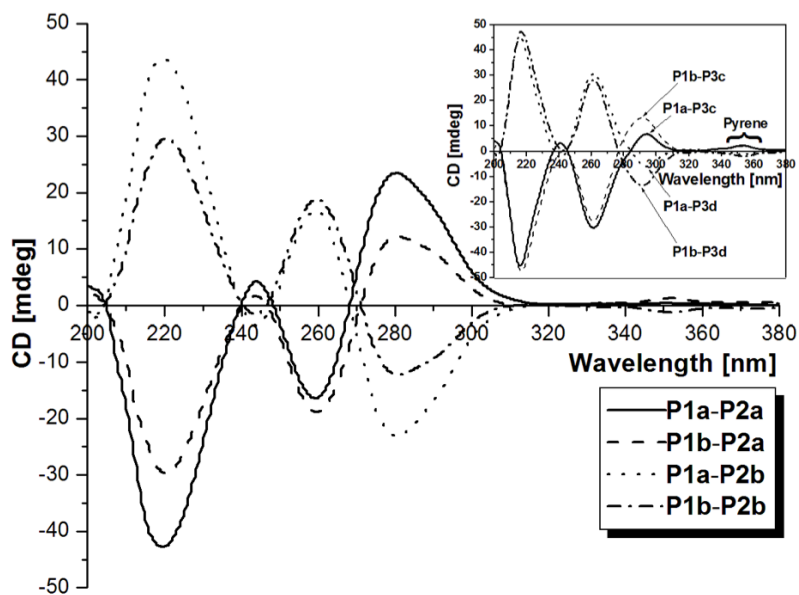


Figure III- 8. (A) UV-absorption profiles of P1a-P2a, P1b-P2a, P1a-P2b, and P1b-P2b duplexes at equimolar ($5 \mu\text{M}$) strand concentration each recorded at 95°C . Conformational preorganization (B) Comparison of the CD spectra of TS-DS duplexes without (P1a-P2a and P1a-P2b) and with PEG-spacer (P1b-P2a and P1b-P2b) in the template. *Inset:* TS-IS duplexes without (P1a-P3c and P1a-P3d) and with PEG-spacer (P1b-P3c and P1b-P3d) in the template. The samples were prepared in a PBS buffer, and the data were recorded at 25°C . The concentration of each strand was $5 \mu\text{M}$.

3.3.3. Thermal Stability

Next, we assessed the feasibility of TS-DS as molecular converters by measuring their thermal stability, along with that of the resulting TS-IS products. The displacement TS-IS products (P1a-P3a and P1a-P3c) are generally 10-15 °C higher in melting transition (T_m) than that of the TS-DS converters (P1a-P2a) as expected given the additional base pairs. (**Figure III- 9**) Introduction of a PEG-spacer in TS had little effect on the thermal stability of TS-DS, since backbone disruption is external to the stem region. (**Figure III- 10**) However, it had a moderate destabilizing effect on the thermal stability of TS-IS, lowering the T_m by ~ 10 °C (**Figure III- 11**). This finding implies that strand displacement is thermodynamically favorable. This suggestion was further corroborated by gel electrophoresis that showed the expected strand displacement reaction upon the addition of IS to TS-DS (**Figure III- 12**).

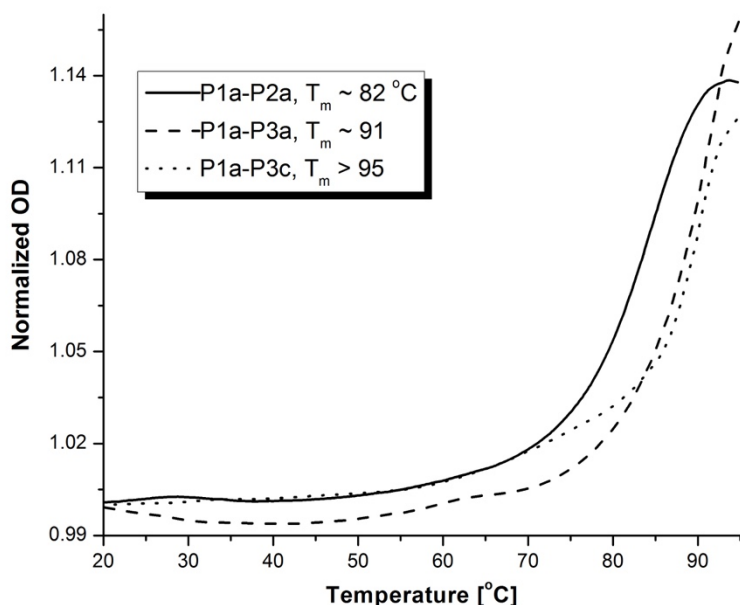


Figure III- 9. Representative UV-melting profiles TS-DS (P1a-P2a) and TS-IS (P1a-P3a and P1a-P3c) duplexes. Depiction of TS-IS and TS-DS duplexes without PEG-spacer, along with their T_m s. The samples were prepared in PBS buffer and annealed at 95 °C for 5 min prior to subjecting to heating runs and determination of their T_m s.

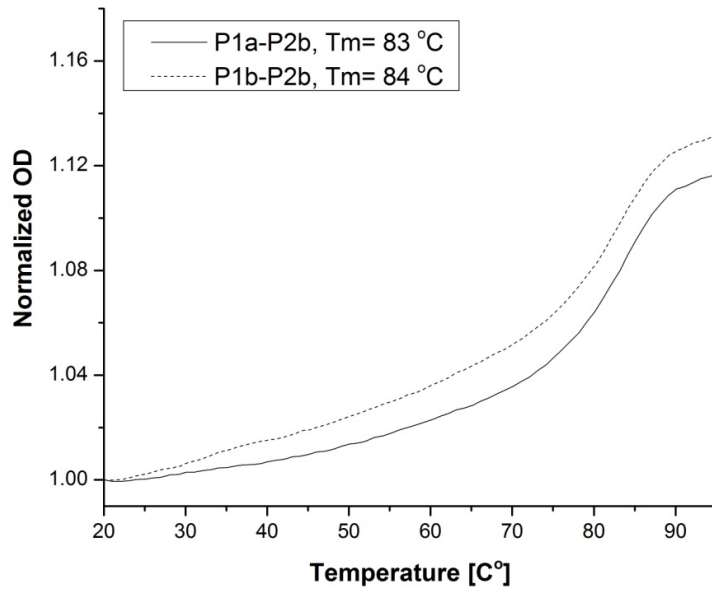


Figure III- 10. UV-melting profiles of P1a-P2b and P1b-P2b duplexes at equimolar (1 μ M) strand concentration. This demonstrated the introduction of a PEG-spacer in TS has little effect on the thermal stability of TS-DS.

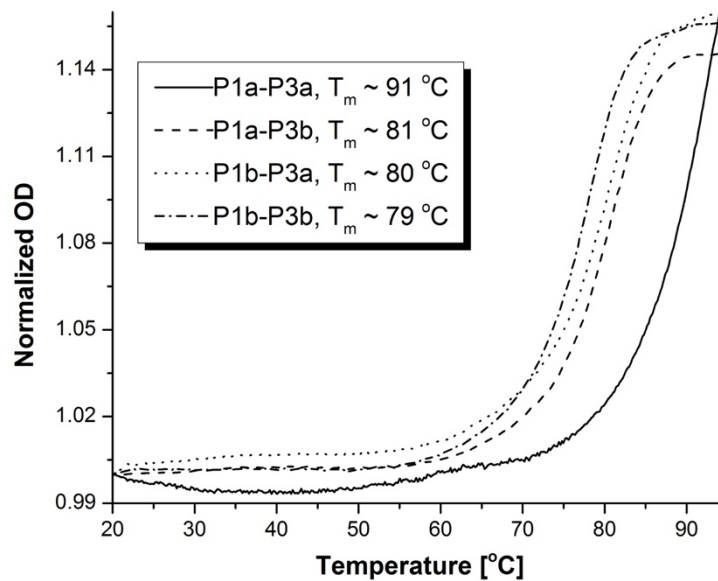


Figure III- 11. UV-melting profiles of P1a-P3a, P1a-P3b, P1b-P3a and P1b-P3b duplexes. The samples were prepared in PBS buffer and annealed at 95 °C for 5 min prior to subjecting to heating runs and determination of their T_m s.

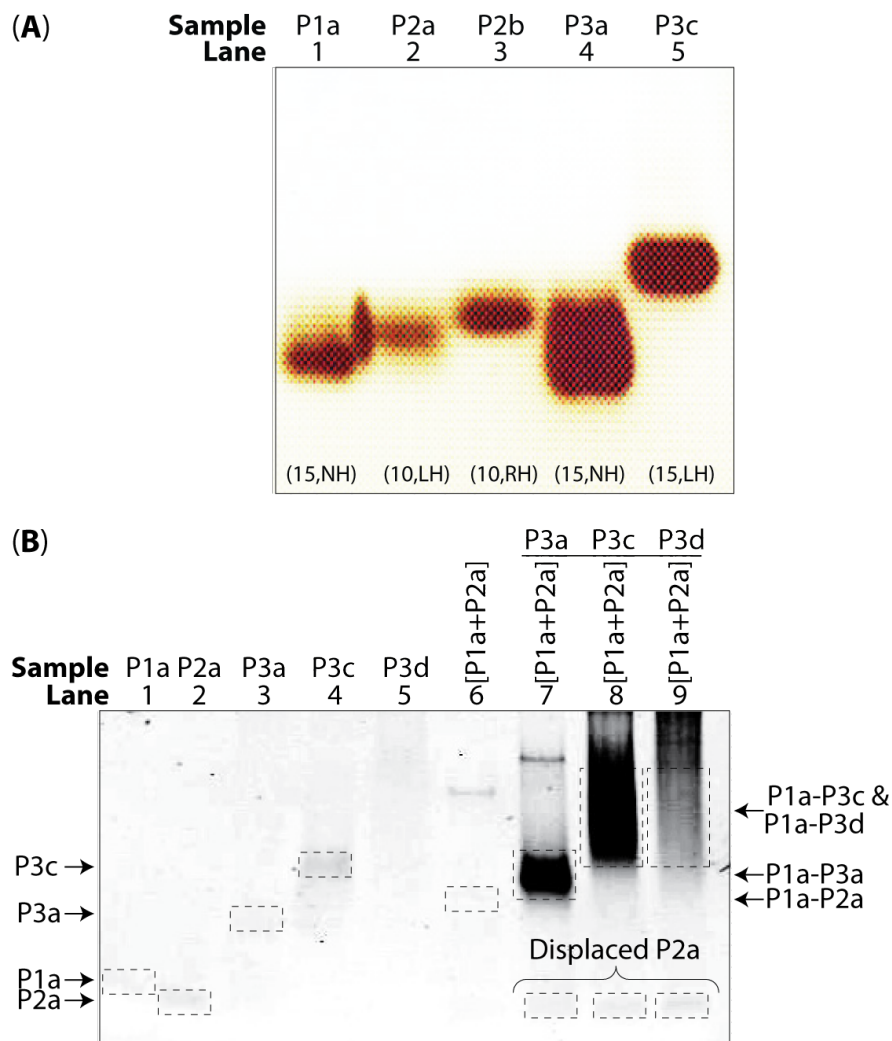


Figure III- 12. Strand displacement reactions. **(A)** Electrophoretic mobility of TS (P1a), DS (P2a and P2b), and IS (P3a and P3c) in 2% agarose gel and after staining with SYBR-Gold. Values in the parentheses indicate the number of nucleotides in each strand and the helical sense. **(B)** Results of strand displacement reactions. The concentration of each component was 10 μ M, prepared in a physiologically relevant buffer. Strand displacement was allowed to take place for 1 hr at 37 $^{\circ}$ C.

3.3.4. Strand Displacement Kinetics

Strand displacement brings the pyrene moieties on template and invading strands together and forms pyrene excimer, (**Figure III- 13**), which shifts fluorescent emission by ~ 100 nm for monitoring the hybridization kinetics. (**Appendix III- 10**) All samples were prepared at a physiologically relevant condition.⁵⁵ The reaction started with incubation of TS-DS at 37 °C for 5 min, followed by adding IS. A DNA counterpart was included for comparison and as a control in validating the mathematical treatment of the kinetics data. The rate constant for strand displacement of DNA was found to be $2.9 \times 10^4 \text{ M}^{-1}\text{s}^{-1}$, which is within the range as reported in the literature.³⁹ (**Figure III- 14A, 1**) Under identical conditions, the rate constants of displacing DS_{RH} by IS_{NH} and IS_{RH} were similar, 1.9×10^4 and $1.3 \times 10^4 \text{ M}^{-1}\text{s}^{-1}$ (**Figure III- 14A, 2 and 3**), respectively, which are slightly lower than that of DNA. We attributed the reduction in the rate to a decrease in water solubility (and possible aggregation of the stock solution) of γ PNAs and to an increase in the thermodynamic stability of the stem, in comparison to that of DNA. Interestingly, strand displacement did not take place with a DNA (D3) invading strand due to the resultant P1a-D3 being thermodynamically less stable than that of P1a-P2b (**Figure III- 14A, Inset**). The displacement rate of DS_{LH} by IS_{RH} , or DS_{RH} by IS_{LH} is further reduced by two-fold (**Figure III- 14B, compare 3 and 4 to 1 and 2, respectively**).

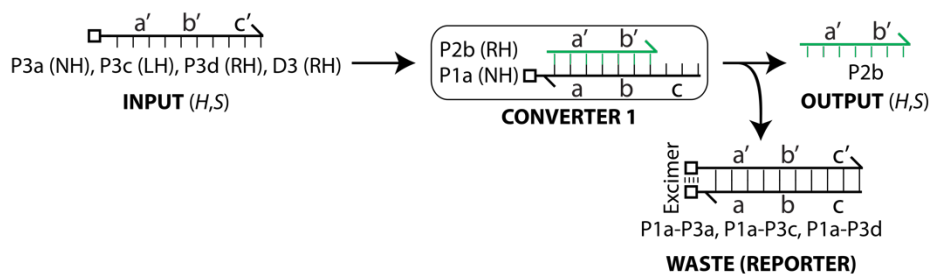


Figure III- 13. Representative strand displacement reactions of TS-DS (P1a-P2b) by IS (P3a, P3c, and P3d).

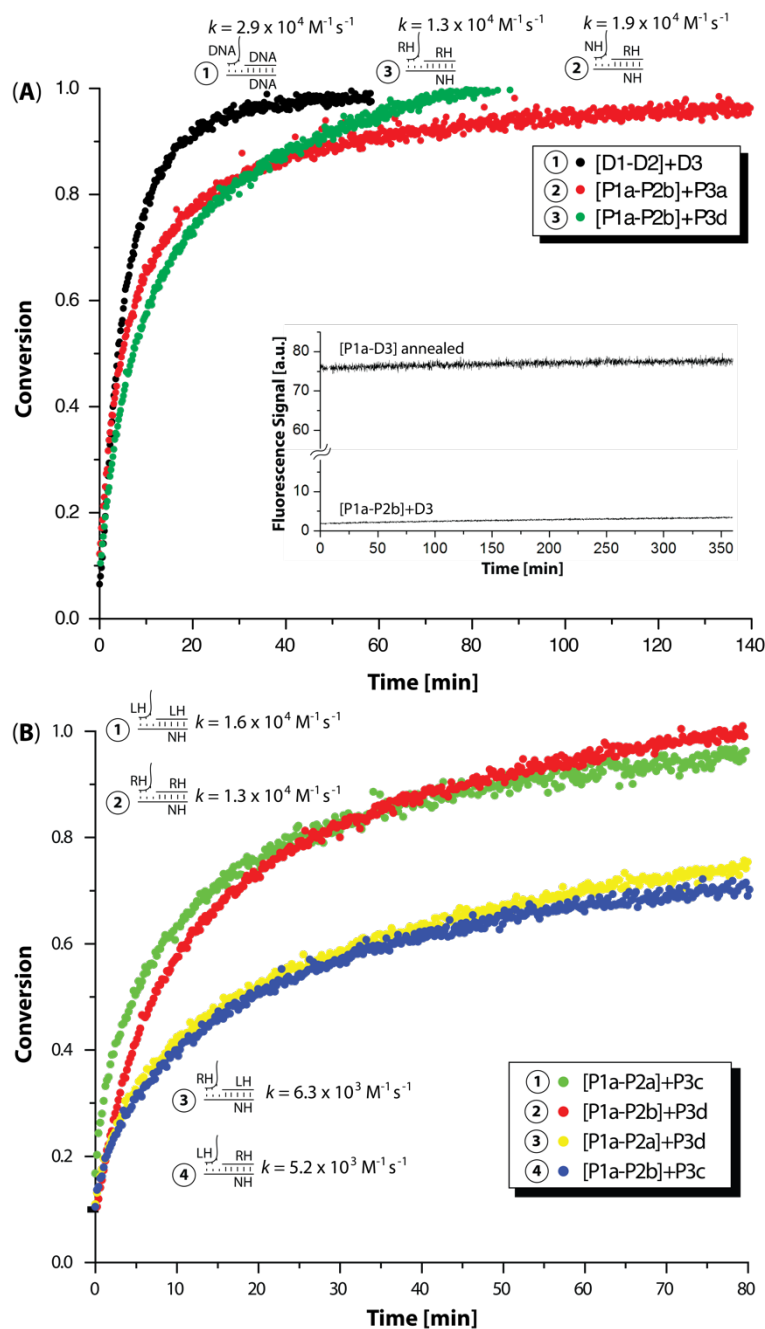


Figure III- 14. The kinetics of strand displacements. **(A)** Fluorescent measurements of the strand displacement reactions as a function of time. *Inset:* Result showing that a DNA invading strand (D3) was unable to displace P2b from P1a. **(B)** Comparison of the strand displacement reactions between the conformationally-matched (1 and 2) and mismatched (3 and 4) IS and DS. The concentrations of TS-DS duplexes were 100 nM and those of IS were 1 μM (10-fold excess). The samples were prepared in PBS buffer, and the reactions were carried out at 37 $^{\circ}\text{C}$. Excitation was made 344 nm, and the emissions were recorded at 480 nm.

Contrary to our prediction, introduction of a flexible PEG-spacer in TS (P1b) did not improve the rate of strand displacement. In fact, it lowered the rate by roughly three-fold in comparison to that without the spacer (**Figure III- 15**). Similar trends in the rates were observed with the spacer introduced in TS, IS, or in both (**Figure III- 15A**, *Inset*). We attributed the reduction in the rate to an additional internal diffusion for strand hybridization.⁵⁶

Figure III- 15B revealed the temperature-dependent rates of strand displacement. The low temperature rates were similar to those reported by Kabza and Sczepanski in the conversion of heterochiral D- and L-DNA by PNA.⁵⁷ Temperature-dependent measurements revealed that the rates of strand displacement increased proportionally with temperature. An Arrhenius plot of the rates as a function of temperature yielded an activation energy of 73 kJ/mol for strand displacement of a mismatched helical sense (or stereoconversion), which is nearly two-fold lower than that observed with DNA of a similar length but without the toehold.⁵⁸

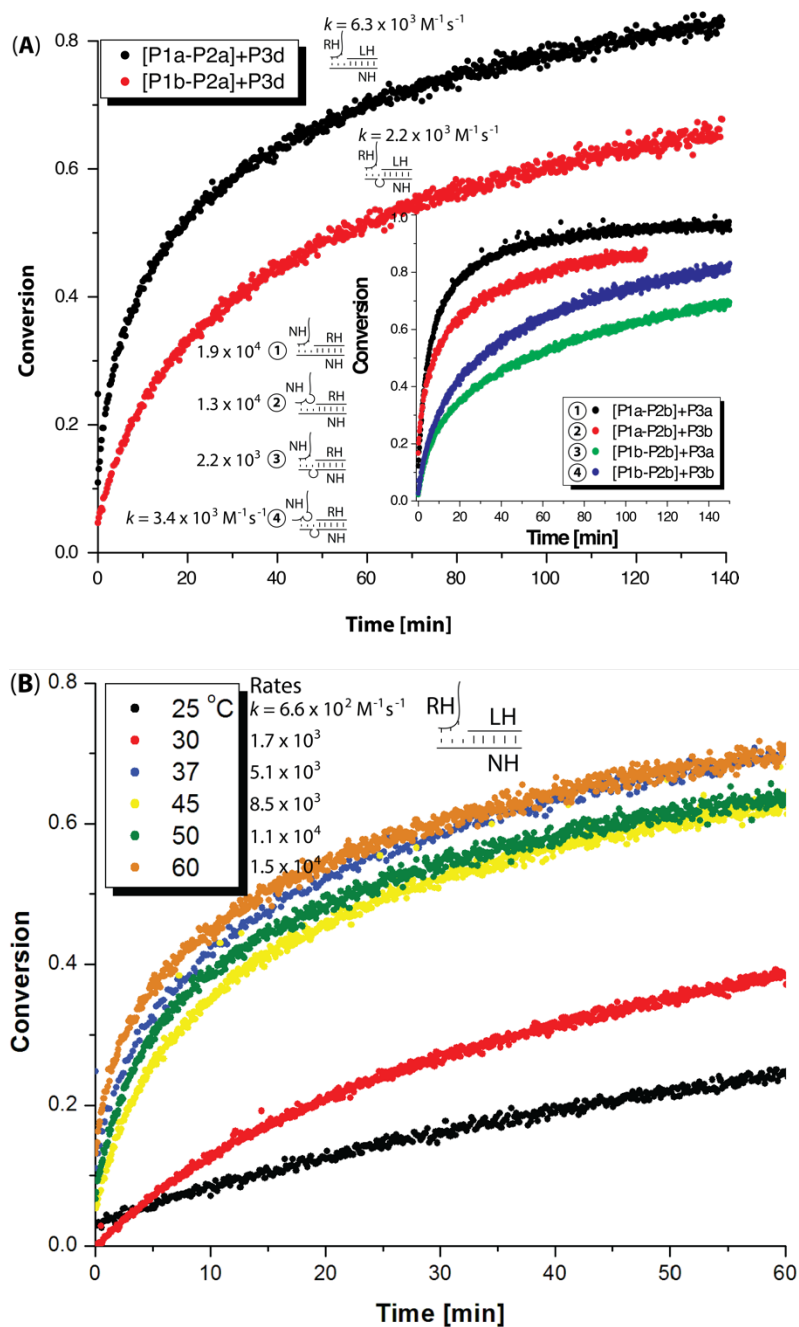


Figure III- 15. The effects of PEG-spacer and temperature on the rates of strand displacement. Kinetic profiles of strand displacement (A) with and without PEG-spacer, and (B) at variable temperatures. The samples were prepared the same way as mentioned in Figure III-14 caption.

3.3.5. Signal Transduction

To demonstrate that the sequence information stored in orthogonal LH- γ PNA can be converted to biologically relevant DNA sequence, we coupled the LH- γ PNA input (P3c) with the molecular converter and a DNA reporter. (**Figure III- 16**) Despite sequence complementarity, incubation of LH-input (P3c) with reporter did not yield any fluorescent signals, indicating that cross-hybridization between the two did not take place. (**Figure III- 16C, 4**). The fluorescent signals were observed only when all three components, input, converter, and reporter, were present. (**Figure III- 16C, 2**) The fluorescent signals were slightly dampened upon the addition of a DNA quencher (DQ1). (**Figure III- 16C, 3**) The reduction in the fluorescent signals, in this case, is not due to cross-hybridization of helically mismatched P3c with DQ1, but due to the inevitable dissociation of DQ1 and association of D1' with the right-handed output (P2b), even at a relatively low reaction temperature (20 °C). The dissociation of DQ1 resulted from the relatively low stability of such duplex (predicted T_m :~ 26.8 °C by IDT OligoAnalyzer).

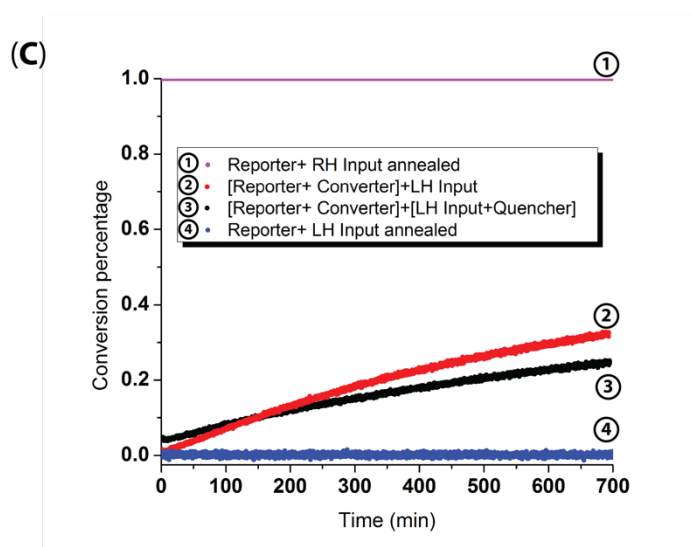
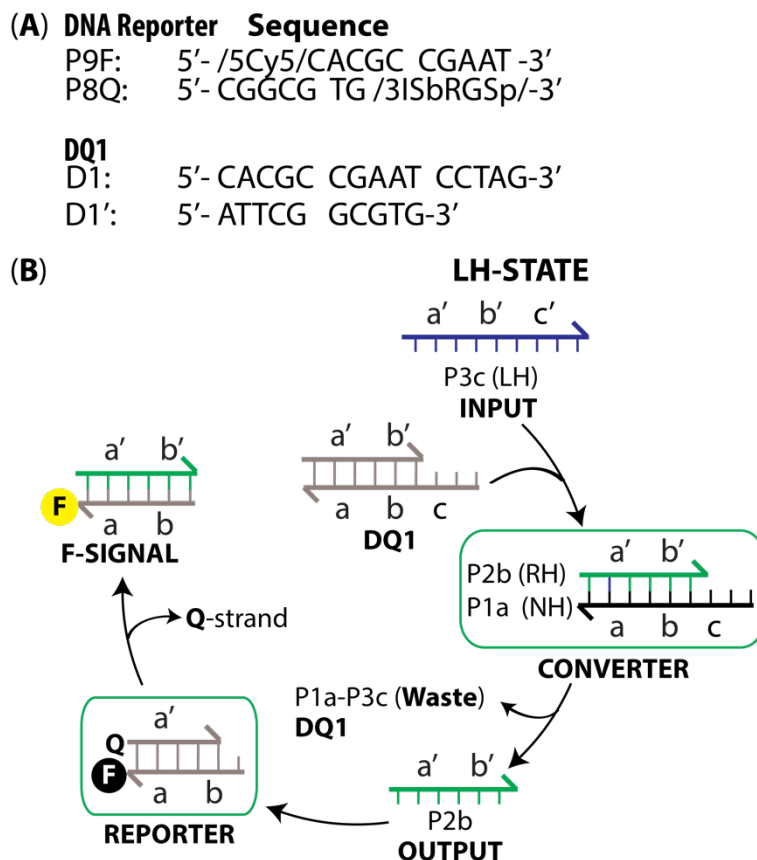


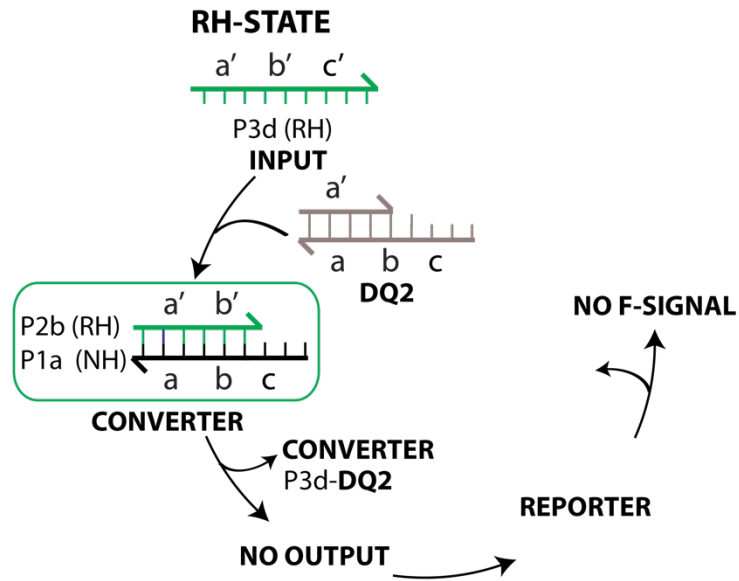
Figure III- 16. Signal transduction by molecular converter. **(A)** Sequences of DNA reporter and off-target DNA DQ1. **(B)** Illustration of molecular conversion in the presence of DQ1 by an LH-input. **(C)** Fluorescent profiles of signal transduction. The reactions were carried out at 20 °C to minimize the dissociation of DQ1. Wavelengths (λ_{ex} = 648 nm and λ_{em} = 668 nm) and slit sizes (E_x = 5 nm and E_m = 5 nm).

On the other hand, the right-handed input (P3d) can generate fluorescent signal faster than the left-handed input (P3d) because P3d can skip the molecular converter and directly react with DNA reporter. (**Figure III- 17C, red line**) However, the addition of a DNA quencher (DQ2) resulted in a complete quenching of the fluorescent signals. This result highlights the potential danger in employing natural or right-handed nucleic acid building blocks in molecular organization and self-assembly in biological systems in the presence of background genetic materials.

(A) DNA Reporter Sequence
P9F: 5'- /5Cy5/CACGC CGAAT -3'
P8Q: 5'- CGGCG TG /3ISbRGSsp/-3'

DQ2
D1: 5'- CACGC CGAAT CCTAG-3'
P8Q: 5'- CGGCG TG /3ISbRGSsp/-3'

(B)



(C)

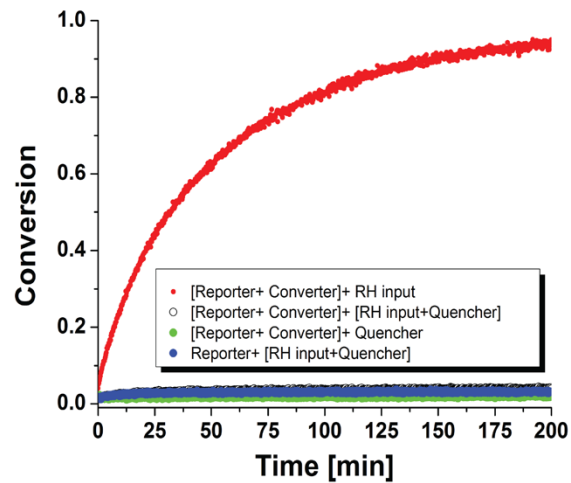


Figure III- 17. Signal transduction with RH- γ PNA. **(A)** Sequences of DNA reporter and off-target DNA DQ2. **(B)** Illustration of molecular conversion in the presence of DQ2 by an RH-input. **(C)** Fluorescent profiles of signal transduction. The reactions were carried out at 20 °C. Wavelengths (λ_{ex} = 648 nm and λ_{em} = 668 nm) and slit sizes (E_x = 5 nm and E_m = 5 nm).

3.4. Discussion

The emerging roles of nucleic acids as engineering materials and as molecular ‘processors’ and signaling mediums, in addition to their natural roles in the storage and transmission of genetic information, lend to the possibility for their integration. The interface would provide a more accessible means for controlling life processes. Such an undertaking, however, will require the delivery of these chemical building blocks into live cells and intact organisms, and that they are able to withstand the enzymatic assaults and be able to recognize their designated partners without cross-interference with the endogenous genetic materials. Natural building blocks, such as DNA oligonucleotides, are attractive in this regard and have been extensively utilized in molecular engineering and computation, but they are not well-suited for intracellular or *in vivo* applications due to the aforementioned concerns. Although synthetic counterparts, such as configurationally-inverted α -DNA and α -RNA, could be employed to alleviate some of these concerns, there is no simple way to ‘wire’ the genetic information encoded in these chemical building blocks with DNA or RNA. The development of a nucleic acid platform that has the potential to address these challenges will be crucial in the translation of *de novo* molecular engineering concepts and principles into the biological realm.

We have shown that by applying the appropriate chemistry⁴⁶, a randomly-folded PNA, as originally developed by Nielsen and coworkers⁵⁹ more than two decades ago, can be preorganized into either an RH or an LH motif. Due to conformational mismatch, the two conformers are unable to hybridize to each other. By employing PNA as an interfacing medium that is capable of recognizing the RH and LH conformers, as well as DNA and RNA, the genetic information encoded in any one of these nucleic acid systems can be

interconverted, with rates comparable to that of homochiral DNA.⁴⁶ Inclusion of conformational chirality provides another dimension in nucleic acid recognition, in addition to sequence information. A distinct advantage of this particular nucleic acid platform is that all three components, RH, LH, and NH, contain the same molecular scaffold, with the exception of the stereochemistry or the lack thereof at the (γ)-backbone that determines the conformations of the oligomers. They are relatively simple to chemically synthesize and structurally modify. They can be made cell-permeable, if necessary, by installing the appropriate chemical groups at the (γ)-backbone.⁵⁹ On the other hand, such a task is generally challenging to accomplish with natural nucleic acid biopolymers.

Overall, the work provides a foundation for the organization and assembly of materials, and for building molecular circuits in biological systems without the concerns for the erosion of chemical building blocks or degradation of signals as a result of cross-interference with the host's genetic materials. We envision further integration of this gamma peptide nucleic acid platform would facilitate the development of a rapid and sensitive method for *in-situ* detection of genetic materials, an essential step on the road to implement a global pathogen surveillance system (GPS2) for the monitoring and the containment of infectious pathogens.

3.5. Experimental Protocols

3.5.1. PNA monomer Synthesis

Regular Boc-protected PNA monomers were purchased from PolyOrg Inc. MiniPEG- γ PNA monomers were synthesized using Boc-protected L-serine as a starting material as previously reported by Sahu and coworkers.³⁹

3.5.2. Oligomer Synthesis

All oligomers were synthesized on solid-support using standard Boc-chemistry procedures. The oligomers were cleaved from resin using an m-cresol: thioanisole: trifluoromethanesulfonic acid (TFMSA): trifluoroacetic acid (TFA) (1:1:2:6) cocktail solution and precipitated with ether. PNA oligomers were purified by reverse-phase high performance liquid chromatography (RP-HPLC) in analytical mode (C18 column with dimensions 4.6 mm X 250 mm, 1 mL/min, 60 °C) or in semi-prep mode (C18 column with dimensions 19 mm X 100 mm, 5 mL/min, 55 °C), and characterized by MALDI-TOF MS with CHCA matrix. All PNA stock solutions were prepared using nanopure water, and the concentrations were determined at 90 °C on a Agilent Cary UV-Vis 300 spectrometer equipped using the following extinction coefficients: 13,700 M⁻¹cm⁻¹ (A), 6,600 M⁻¹cm⁻¹ (C), 11,700 M⁻¹cm⁻¹ (G), 8,600 M⁻¹cm⁻¹ (T) and 24,000 M⁻¹cm⁻¹ (Pyrene).^{49,60} All DNA oligomers were ordered from IDT without further purification.

3.5.3. UV-Melting Experiments

All UV-melting samples were prepared by mixing PNA oligomers at the indicated concentrations in a physiologically simulated buffer (137 mM NaCl, 2.7 mM KCl, 8 mM Na₂HPO₄, and 2 mM KH₂PO₄, pH= 7.4), and annealed by incubation at 95 °C for 5 min followed by a gradual cooling to room temperature. UV melting curves were collected using Agilent Cary UV-Vis 300 spectrometer equipped with a thermoelectrically controlled multi-cell holder. UV-melting spectra were collected by monitoring UV-absorption at 260 nm from 20 to 95 °C in the heating runs, and from 95 to 20 °C in the cooling runs, both at the rate of 0.2 °C per min. The cooling and heating curves were nearly identical, indicating that the hybridization process is reversible. The recorded spectra were smoothed using a 7-point adjacent averaging algorithm. The first derivatives of the melting curves were taken to determine the melting temperatures of the duplexes.

3.5.4. Circular Dichroism Analyses

CD samples were prepared at 5 μM strand concentrations in sodium phosphate buffer (137 mM NaCl, 2.7 mM KCl, 8 mM Na₂HPO₄, and 2 mM KH₂PO₄, pH= 7.4). The samples were heated to 95 °C and gradually cooled down to room temperature. CD experiments were performed on a JASCO J-715 spectropolarimeter using a quartz cuvette with 1cm path length. The samples were scanned from 320 to 200 nm with a scan rate of 100 nm/min and 15 scan accumulations at 25 °C. All spectra were baseline-subtracted, smoothed using a five-point adjacent averaging algorithm and replotted using Origin software.

3.5.5. Fluorescence Measurements

I. To perform kinetic experiments for nucleic acid conversions, two components were prepared separately in 1xPBS buffer*: (1) 216 nM of DS and 180 nM of TS; (2) 180 nM of IS. The two samples were annealed at 95 °C for 5 min before 1 h of gradual cooling to ambient temperature. On Cary Eclipse Fluorescence Spectrometer, DS-TS duplex was incubated at 37 °C for 5 min followed by addition of IS to reach final concentrations: [DS]= 72 nM, [TS]= 60 nM and [IS]= 120 nM. Real-time fluorescence data were collected with wavelengths (λ_{ex} = 350 nm and λ_{em} = 480 nm) and slit sizes (E_x = 5 nm and E_m = 10 nm).

To calculate rate constant for nucleic acid conversions, set the first collection point as $t = 0$. Calculate conversion percentage by equation (1):

$$x = \frac{F_{obs} - F_i}{F_f - F_i} \quad (1)$$

, where F_{obs} = real-time fluorescence intensity; F_i = fluorescence intensity of initial stage, DS-TS duplex; F_f = fluorescence intensity of final stage, DS-IS duplex.

Then use the linear relationship in equation (2) to calculate 2nd order kinetic rate constant k :

$$\frac{1}{IS_0 - TS_0} \ln \frac{(IS_0 - X) TS_0}{(TS_0 - X) IS_0} = k t \quad (2)$$

, where $X = TS_0 * x$.

*1x PBS buffer= 137 mM NaCl, 2.7 mM KCl, 8 mM Na₂HPO₄, and 2 mM KH₂PO₄, pH= 7.4.

To perform kinetic experiment for signal transduction, four components were prepared separately in 1xPBS buffer*: (1) 90 nM of P9F and 108 nM of P8Q; (2) 540 nM of P2b and P1a; (3) 2160 nM of D1 and D2; (4) 2160 nM of LH or RH input. The four

components were annealed at 95 °C for 5 min before 1 h of gradual cooling to ambient temperature.

On Cary Eclipse Fluorescence Spectrometer, component (1) was incubated at 20 or 37 °C followed by addition of other components or buffers. Real-time fluorescence data were collected with wavelengths ($\lambda_{\text{ex}}= 648 \text{ nm}$ and $\lambda_{\text{em}}= 668 \text{ nm}$) and slit sizes ($E_{\text{x}}= 5 \text{ nm}$ and $E_{\text{m}}= 5 \text{ nm}$). $t= 0$ is defined by the first observation after mixing all indicated components.

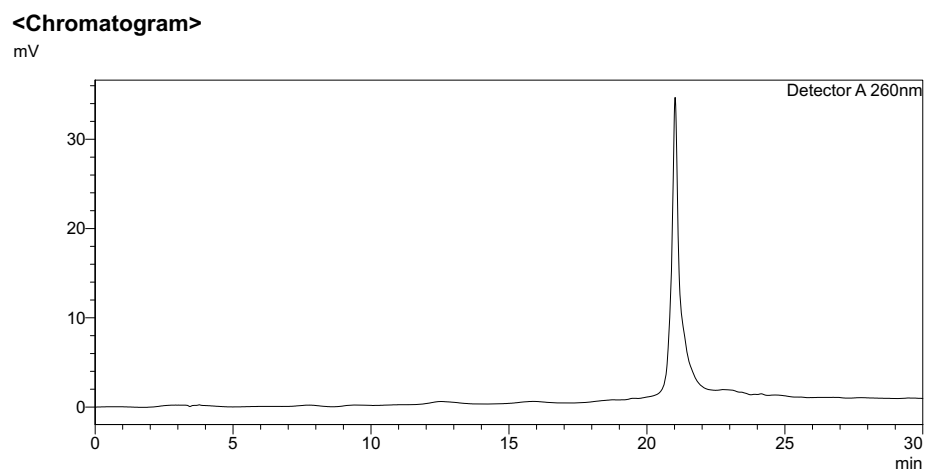
3.5.6. Gel Shift Assay

PNA strands were prepared as indicated concentration in 1xPBS buffer. For strand displacement reactions, TS-DS duplexes were annealed at 95 °C for 5 min and gradually cooled down to ambient temperature in 1 h. The duplexes were then incubated at 37 °C for 5 min before addition of IS oligomers. The reaction mixture were incubated at the same temperature for another 1 h before gel shift analysis. The samples were then loaded onto 2% agarose-gel containing 1xSYBR-Gold with 1xTris-borate buffer and electrophoretically separated at 100 V for 15 min. The bands were visualized by UV-Transilluminator. For the results shown in **Figure III- 12**, the samples were separated on a 10% non-denaturing PAGE for 1.5 h at 120 V/cm.

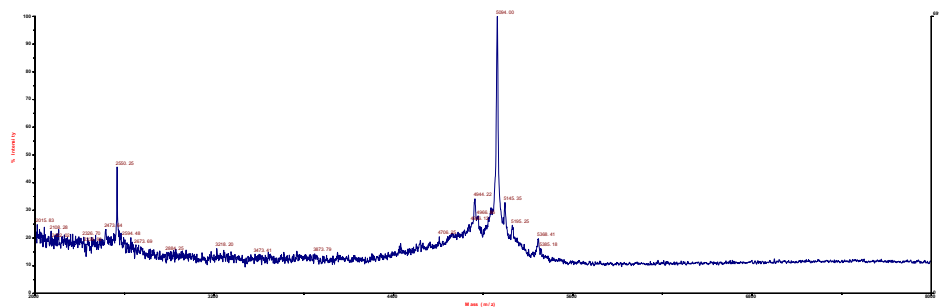
3.6. Appendices

Appendix III- 1. (A) HPLC profile and (B) MALDI-TOF MS spectrum of P1a.

(A)



(B)

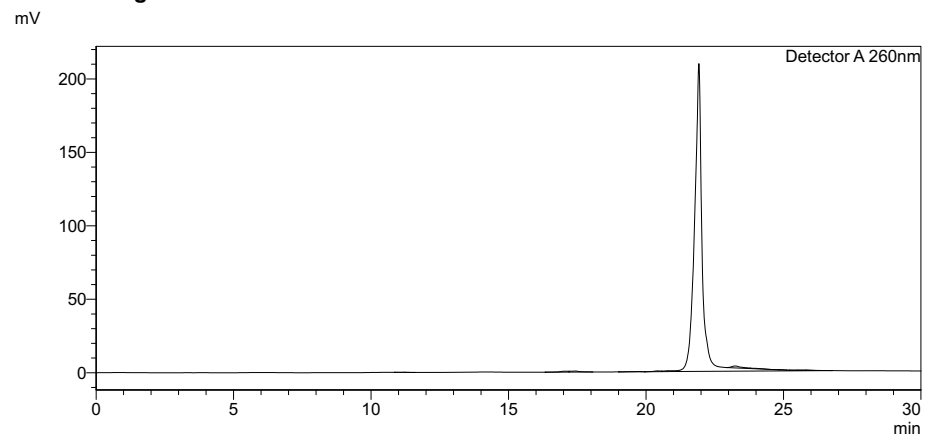


Calculated mass = 5089.99, observed mass = 5094.00.

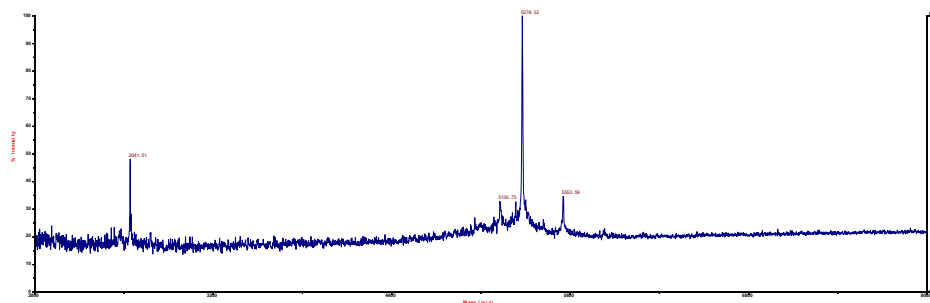
Appendix III- 2. (A) HPLC profile and (B) MALDI-TOF MS spectrum of P1b.

(A)

<Chromatogram>



(B)



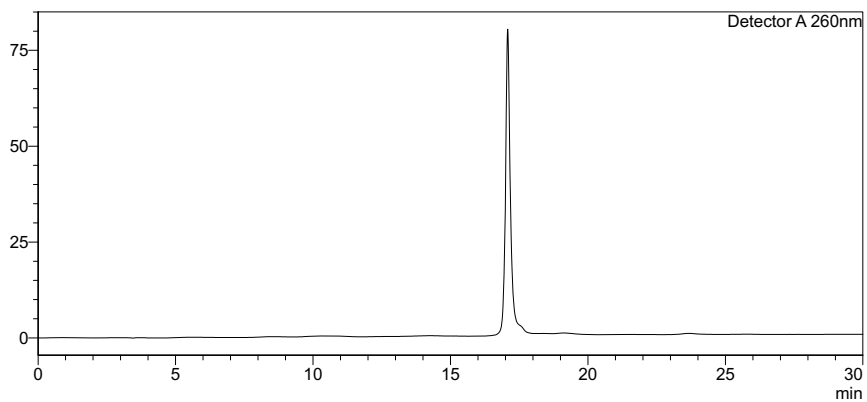
Calculated mass = 5279.20, observed mass = 5278.32.

Appendix III- 3. (A) HPLC profile and (B) MALDI-TOF MS spectrum of P2a.

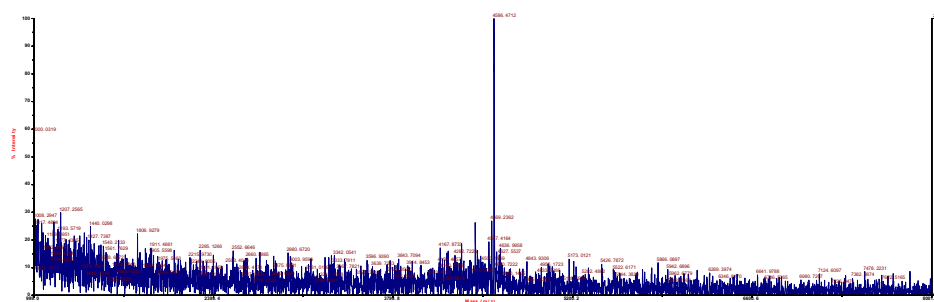
(A)

<Chromatogram>

mV



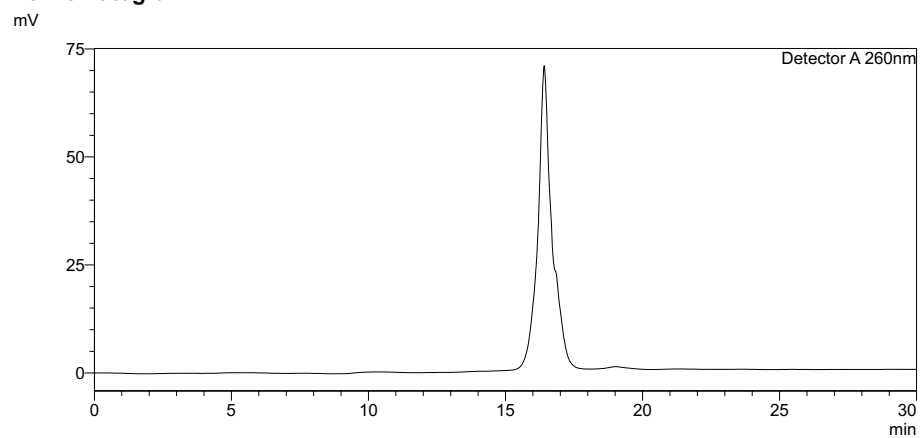
(B)



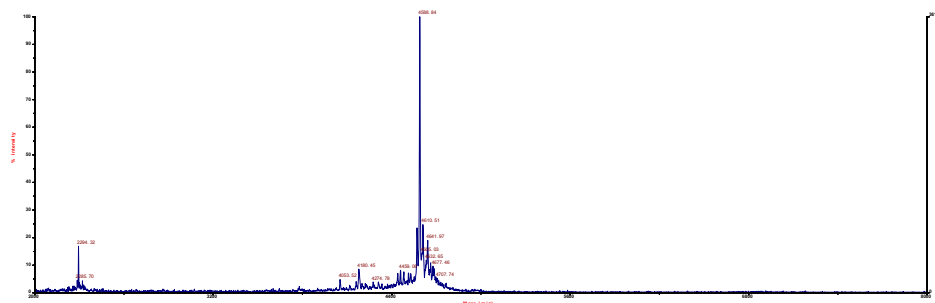
Appendix III- 4. (A) HPLC profile and (B) MALDI-TOF MS spectrum of P2b.

(A)

<Chromatogram>



(B)



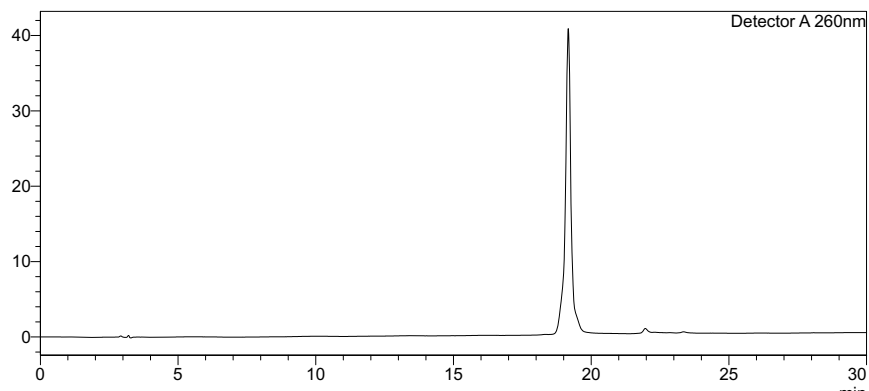
Calculated mass = 4585.55, observed mass = 4588.84.

Appendix III- 5. (A) HPLC profile and (B) MALDI-TOF MS spectrum of P3a.

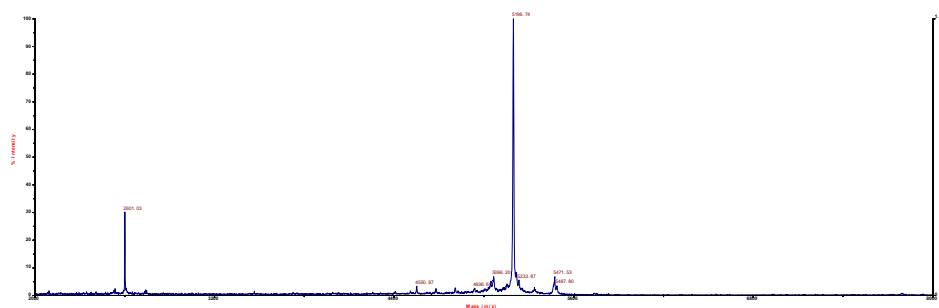
(A)

<Chromatogram>

mV



(B)



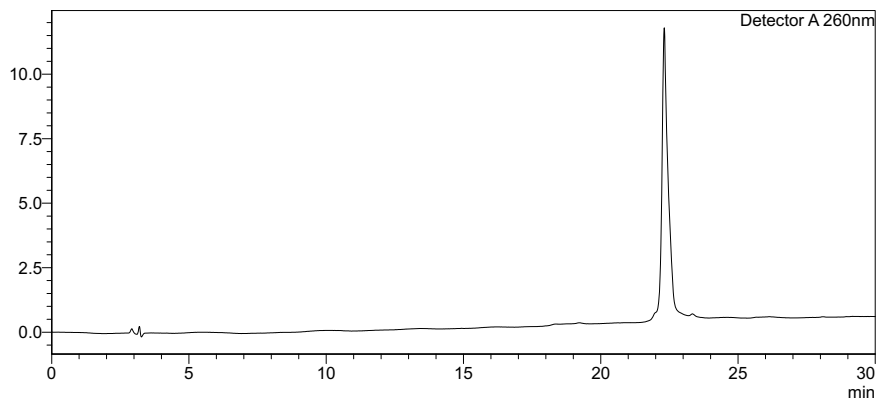
Calculated mass = 5192.03, observed mass = 5196.74.

Appendix III- 7. (A) HPLC profile and (B) MALDI-TOF MS spectrum of P3c.

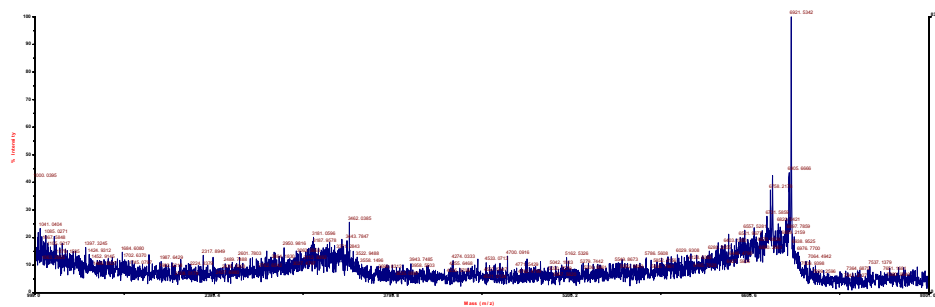
(A)

<Chromatogram>

mV



(B)



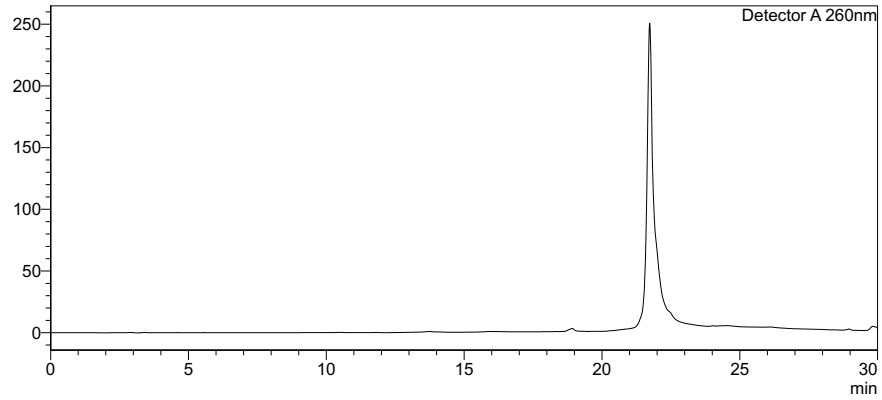
Calculated mass = 6921.97, observed mass = 6921.53.

Appendix III- 8. (A) HPLC profile and (B) MALDI-TOF MS spectrum of P3d.

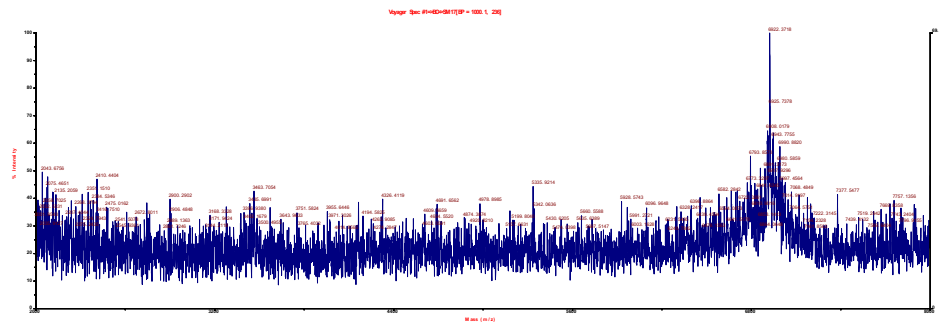
(A)

<Chromatogram>

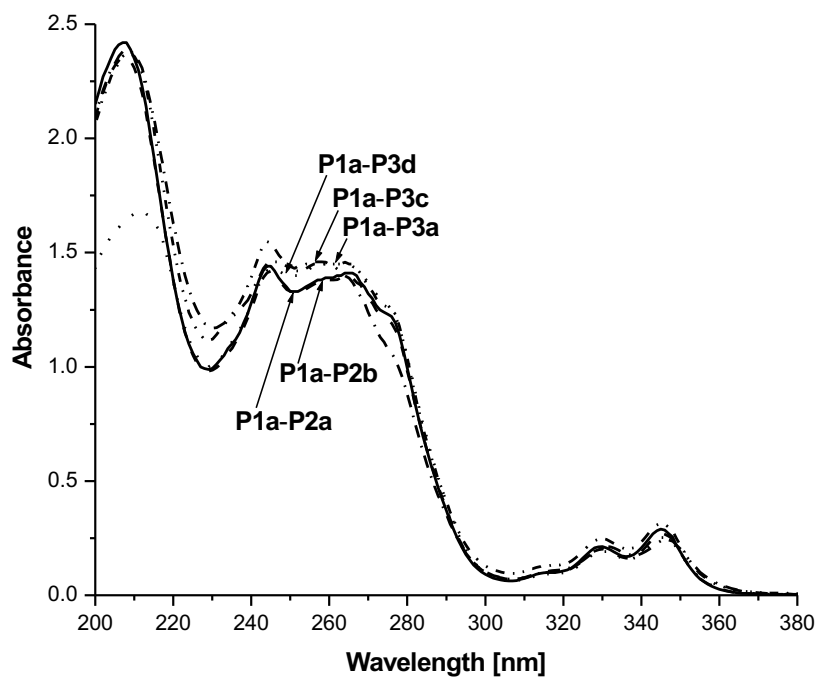
mV



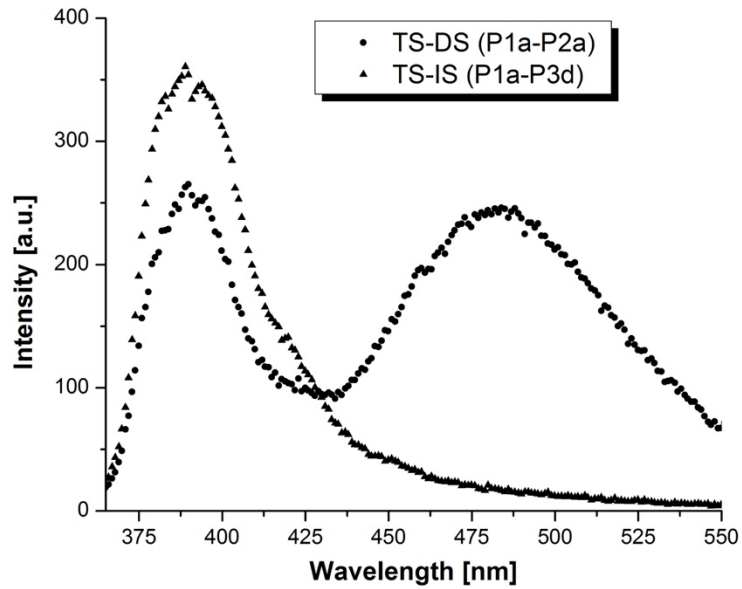
(B)



Appendix III- 9. UV-absorption profiles of P1a-P2a, P1a-P2b, P1a-P3a, P1a-P3c, and P1a-P3d duplexes at equimolar (5 μ M) strand concentration, recorded at 95 °C. The high temperature was employed to dissociate the indicated duplexes.



Appendix III- 10. Fluorescence spectra of P1a-P2a and P1a-P3d duplexes. Concentrations: P1a= 60 nM, P2a= 72 nM, P3d= 120 nM. Samples were annealed at 95 °C and followed by gradual cooling to room temperature in 1 hr. The samples were then incubated at 37 °C for 5 min before fluorescent measurements with wavelengths (λ_{ex} = 350 nm and λ_{em} = 480 nm) and slit sizes (E_x = 5 nm and E_m = 10 nm).



3.7. References

- (1) Chen, J. H.; Seeman, N. C. Synthesis From DNA of a Molecule with the Connectivity of a Cube. *Nature* **1991**, 350 (6319), 631–633.
- (2) Pianowski, Z. L.; Winssinger, N. Nucleic Acid Encoding to Program Self-Assembly in Chemical Biology. *Chem. Soc. Rev.* **2008**, 37 (7), 1330–1336.
- (3) Seeman, N. C. DNA in a Material World. *Nature* **2003**, 421 (6921), 427–431.
- (4) Park, S. Y.; Lytton-Jean, A. K. R.; Lee, B.; Weigand, S.; Schatz, G. C.; Mirkin, C. A. DNA-Programmable Nanoparticle Crystallization. *Nature* **2008**, 451 (7178), 553–556.
- (5) Jones, M. R.; Seeman, N. C.; Mirkin, C. A. Programmable Materials and the Nature of the DNA Bond. *Science* **2015**, 347 (6224), 1260901.
- (6) Rothmund, P. W. K. Folding DNA to Create Nanoscale Shapes and Patterns. *Nature* **2006**, 440 (7082), 297–302.
- (7) Pinheiro, A. V.; Han, D.; Shih, W. M.; Yan, H. Challenges and Opportunities for Structural DNA Nanotechnology. *Nat. Nanotechnol.* **2011**, 6 (12), 763–772.
- (8) Aldaye, F. A.; Palmer, A. L.; Sleiman, H. F. Assembling Materials with DNA as the Guide. *Science* **2008**, 321 (5897), 1795–1799.
- (9) Douglas, S. M.; Dietz, H.; Liedl, T.; Högberg, B.; Graf, F.; Shih, W. M. Self-Assembly of DNA Into Nanoscale Three-Dimensional Shapes. *Nature* **2009**, 459 (7245), 414–418.
- (10) Dietz, H.; Douglas, S. M.; Shih, W. M. Folding DNA Into Twisted and Curved Nanoscale Shapes. *Science* **2009**, 325 (5941), 725–730.
- (11) Han, D.; Pal, S.; Nangreave, J.; Deng, Z.; Liu, Y.; Yan, H. DNA Origami with Complex Curvatures in Three-Dimensional Space. *Science* **2011**, 332 (6027), 342–346.
- (12) Wei, B.; Dai, M.; Yin, P. Complex Shapes Self-Assembled From Single-Stranded DNA Tiles. *Nature* **2012**, 485 (7400), 623–626.
- (13) Ke, Y.; Ong, L. L.; Shih, W. M.; Yin, P. Three-Dimensional Structures Self-Assembled From DNA Bricks. *Science* **2012**, 338 (6111), 1177–1183.
- (14) Veneziano, R.; Ratanalert, S.; Zhang, K.; Zhang, F.; Yan, H.; Chiu, W.; Bathe, M. Designer Nanoscale DNA Assemblies Programmed From the Top Down. *Science* **2016**, 352 (6293), 1534.
- (15) Han, D.; Qi, X.; Myhrvold, C.; Wang, B.; Dai, M.; Jiang, S.; Bates, M.; Liu, Y.; An, B.; Zhang, F.; Yan, H.; Yin, P. Single-Stranded DNA and RNA Origami. *Science* **2017**, 358 (6369), eaao2648.
- (16) Bath, J.; Turberfield, A. J. DNA Nanomachines. *Nat. Nanotechnol.* **2007**, 2 (5), 275–284.
- (17) Gerling, T.; Wagenbauer, K. F.; Neuner, A. M.; Dietz, H. Dynamic DNA Devices and Assemblies Formed by Shape-Complementary, Non-Base Pairing 3D Components. *Science* **2015**, 347 (6229), 1446–1452.
- (18) Yurke, B.; Turberfield, A. J.; Mills, A. P., Jr; Simmel, F. C.; Neumann, J. L. A DNA-Fuelled Molecular Machine Made of DNA. *Nature* **2000**, 406 (6796), 605–608.

- (19) Omabegho, T.; Sha, R.; Seeman, N. C. A Bipedal DNA Brownian Motor with Coordinated Legs. *Science* **2009**, *324* (5923), 67–71.
- (20) Lund, K.; Manzo, A. J.; Dabby, N.; Michelotti, N.; Johnson-Buck, A.; Nangreave, J.; Taylor, S.; Pei, R.; Stojanovic, M. N.; Walter, N. G.; Winfree, E.; Yan, H. Molecular Robots Guided by Prescriptive Landscapes. *Nature* **2010**, *465* (7295), 206–210.
- (21) Gu, H.; Chao, J.; Xiao, S.-J.; Seeman, N. C. A Proximity-Based Programmable DNA Nanoscale Assembly Line. *Nature* **2010**, *465* (7295), 202–205.
- (22) Church, G. M.; Gao, Y.; Kosuri, S. Next-Generation Digital Information Storage in DNA. *Science* **2012**, *337* (6102), 1628.
- (23) Erlich, Y.; Zielinski, D. DNA Fountain Enables a Robust and Efficient Storage Architecture. *Science* **2017**, *355* (6328), 950–954.
- (24) Goldman, N.; Bertone, P.; Chen, S.; Dessimoz, C.; LeProust, E. M.; Sipos, B.; Birney, E. Towards Practical, High-Capacity, Low-Maintenance Information Storage in Synthesized DNA. *Nature* **2013**, *494* (7435), 77–80.
- (25) Adleman, L. M. Molecular Computation of Solutions to Combinatorial Problems. *Science* **1994**, *266* (5187), 1021–1024.
- (26) Benenson, Y. Biomolecular Computing Systems: Principles, Progress and Potential. *Nat. Rev. Genet.* **2012**, *13* (7), 455–468.
- (27) Stojanovic, M. N.; Stefanovic, D.; Rudchenko, S. Exercises in Molecular Computing. *Acc. Chem. Res.* **2014**, *47* (6), 1845–1852.
- (28) Qian, L.; Winfree, E. Scaling Up Digital Circuit Computation with DNA Strand Displacement Cascades. *Science* **2011**, *332* (6034), 1196–1201.
- (29) Qian, L.; Winfree, E.; Bruck, J. Neural Network Computation with DNA Strand Displacement Cascades. *Nature* **2011**, *475* (7356), 368–372.
- (30) Win, M. N.; Smolke, C. D. Higher-Order Cellular Information Processing with Synthetic RNA Devices. *Science* **2008**, *322* (5900), 456–460.
- (31) Chen, Y.-J.; Groves, B.; Muscat, R. A.; Seelig, G. DNA Nanotechnology From the Test Tube to the Cell. *Nat. Nanotechnol.* **2015**, *10* (9), 748–760.
- (32) Groves, B.; Chen, Y.-J.; Zurla, C.; Pochekailov, S.; Kirschman, J. L.; Santangelo, P. J.; Seelig, G. Computing in Mammalian Cells with Nucleic Acid Strand Exchange. *Nat. Nanotechnol.* **2016**, *11* (3), 287–294.
- (33) Douglas, S. M.; Bachelet, I.; Church, G. M. A Logic-Gated Nanorobot for Targeted Transport of Molecular Payloads. *Science* **2012**, *335* (6070), 831–834.
- (34) Delebecque, C. J.; Lindner, A. B.; Silver, P. A.; Aldaye, F. A. Organization of Intracellular Reactions with Rationally Designed RNA Assemblies. *Science* **2011**, *333* (6041), 470–474.
- (35) Fujimori, S.; Shudo, K.; Hashimoto, Y. Enantio-DNA Recognizes Complementary RNA but Not Complementary DNA. *J. Am. Chem. Soc.* **1990**, *112* (20), 7436–7438.
- (36) Ashley, G. W. Modeling, Synthesis, and Hybridization Properties of (L)-Ribonucleic Acid. *J. Am. Chem. Soc.* **1992**, *114* (25), 9731–9736.
- (37) Zhang, D. Y.; Seelig, G. Dynamic DNA Nanotechnology Using Strand-Displacement Reactions. *Nat. Chem.* **2011**, *3* (2), 103–113.

- (38) Meselson, M. S.; Radding, C. M. A General Model for Genetic Recombination. *Proc. Natl. Acad. Sci. U.S.A.* **1975**, *72* (1), 358–361.
- (39) Zhang, D. Y.; Winfree, E. Control of DNA Strand Displacement Kinetics Using Toehold Exchange. *J. Am. Chem. Soc.* **2009**, *131* (47), 17303–17314.
- (40) Dirks, R. M.; Pierce, N. A. Triggered Amplification by Hybridization Chain Reaction. *Proc. Natl. Acad. Sci. U.S.A.* **2004**, *101* (43), 15275–15278.
- (41) Choi, H. M. T.; Chang, J. Y.; Le A Trinh; Padilla, J. E.; Fraser, S. E.; Pierce, N. A. Programmable *In-Situ* Amplification for Multiplexed Imaging of mRNA Expression. *Nat. Biotechnol.* **2010**, *28* (11), 1208–1212.
- (42) Jung, C.; Ellington, A. D. Diagnostic Applications of Nucleic Acid Circuits. *Acc. Chem. Res.* **2014**, *47* (6), 1825–1835.
- (43) Wu, Z.; Liu, G.-Q.; Yang, X.-L.; Jiang, J.-H. Electrostatic Nucleic Acid Nanoassembly Enables Hybridization Chain Reaction in Living Cells for Ultrasensitive mRNA Imaging. *J. Am. Chem. Soc.* **2015**, *137* (21), 6829–6836.
- (44) Wengel, J. Synthesis of 3'-C- and 4'-C-Branched Oligodeoxynucleotides and the Development of Locked Nucleic Acid (LNA). *Acc. Chem. Res.* **1998**, *32* (4), 301–310.
- (45) Rajwanshi, V. K.; Håkansson, A. E.; Dahl, B. M.; Wengel, J. LNA Stereoisomers: Xylo- LNA (B- D - Xylo Configured Locked Nucleic Acid) and A- L -LNA (A- L -Ribo Configured Locked Nucleic Acid). *Chem. Commun.* **1999**, *0* (15), 1395–1396.
- (46) Sacui, I.; Hsieh, W.-C.; Manna, A.; Sahu, B.; Ly, D. H. Gamma Peptide Nucleic Acids: as Orthogonal Nucleic Acid Recognition Codes for Organizing Molecular Self-Assembly. *J. Am. Chem. Soc.* **2015**, *137* (26), 8603–8610.
- (47) Yang, C. J.; Jockusch, S.; Vicens, M.; Turro, N. J.; Tan, W. Light-Switching Excimer Probes for Rapid Protein Monitoring in Complex Biological Fluids. *Proc. Natl. Acad. Sci. U.S.A.* **2005**, *102* (48), 17278–17283.
- (48) Dirks, R. M.; Pierce, N. A. Triggered Amplification by Hybridization Chain Reaction. *Proc. Natl. Acad. Sci. U.S.A.* **2004**, *101* (43), 15275–15278.
- (49) Sahu, B.; Sacui, I.; Rapireddy, S.; Zanolli, K. J.; Bahal, R.; Armitage, B. A.; Ly, D. H. Synthesis and Characterization of Conformationally Preorganized, (R)-Diethylene Glycol-Containing Gamma-Peptide Nucleic Acids with Superior Hybridization Properties and Water Solubility. *J. Org. Chem.* **2011**, *76* (14), 5614–5627.
- (50) Dragulescu-Andrasi, A.; Rapireddy, S.; Frezza, B. M.; Gayathri, C.; Gil, R. R.; Ly, D. H. A Simple Gamma-Backbone Modification Preorganizes Peptide Nucleic Acid Into a Helical Structure. *J. Am. Chem. Soc.* **2006**, *128* (31), 10258–10267.
- (51) Wittung, P.; Nielsen, P. E.; Buchardt, O.; Egholm, M.; Nordén, B. DNA-Like Double Helix Formed by Peptide Nucleic Acid. *Nature* **1994**, *368* (6471), 561–563.

- (52) Rasmussen, H.; Kastrup, J. S.; Nielsen, J. N.; Nielsen, J. M.; Nielsen, P. E. Crystal Structure of a Peptide Nucleic Acid (PNA) Duplex at 1.7 Å Resolution. *Nat. Struct. Biol.* **1997**, *4* (2), 98–101.
- (53) Wittung, P.; Eriksson, M.; Lyng, R.; Nielsen, P. E.; Nordén, B. Induced Chirality in PNA-PNA Duplexes. *J. Am. Chem. Soc.* **1995**, *117* (41), 10167–10173.
- (54) Totsingan, F.; Jain, V.; Bracken, W. C.; Faccini, A.; Tedeschi, T.; Marchelli, R.; Corradini, R.; Kallenbach, N. R.; Green, M. M. Conformational Heterogeneity in PNA:PNA Duplexes. *Macromolecules* **2010**, *43* (6), 2692–2703.
- (55) Santoro, S. W.; Joyce, G. F. A General Purpose RNA-Cleaving DNA Enzyme. *Proc. Natl. Acad. Sci. U.S.A.* **1997**, *94* (9), 4262–4266.
- (56) Genot, A. J.; Zhang, D. Y.; Bath, J.; Turberfield, A. J. Remote Toehold: a Mechanism for Flexible Control of DNA Hybridization Kinetics. *J. Am. Chem. Soc.* **2011**, *133* (7), 2177–2182.
- (57) Kabza, A. M.; Young, B. E.; Sczepanski, J. T. Heterochiral DNA Strand-Displacement Circuits. *J. Am. Chem. Soc.* **2017**, *139* (49), 17715–17718.
- (58) Reynaldo, L. P.; Vologodskii, A. V.; Neri, B. P.; Lyamichev, V. I. The Kinetics of Oligonucleotide Replacements. *J. Mol. Biol.* **2000**, *297* (2), 511–520.
- (59) Nielsen, P. E.; Egholm, M.; Berg, R. H.; Buchardt, O. Sequence-Selective Recognition of DNA by Strand Displacement with a Thymine-Substituted Polyamide. *Science* **1991**, *254* (5037), 1497–1500.
- (60) Kholodar, S. A.; Novopashina, D. S.; Meschaninova, M. I.; Venyaminova, A. G. Multipyrene Tandem Probes for Point Mutations Detection in DNA. *J. Nucleic Acids* **2013**, *2013* (2), 860457.

Chapter IV: RNA-Templated Concatenation of Triplet Nucleic Acid Probe

The work in this chapter has been previously published as:

Bahal, R.; Manna, A.; Hsieh, W.-C.; Thadke, S. A.; Sureshkumar, G.; Ly, D. H. RNA-Templated Concatenation of Triplet Nucleic-Acid Probe. *Chembiochem* **2018**, *19* (7), 674–678.

Dr. Raman Bahal, Dr. Arunava Manna, Wei-Che Hsieh, and Dr. Danith H. Ly designed the research. Dr. Gopalsamy Sureshkumar synthesized gamma PNA monomers. Dr. Raman Bahal prepared the oligomers. Dr. Raman Bahal and Wei-Che Hsieh collected the MALDI-TOF data. Dr. Raman Bahal and Dr. Arunava Manna collected the UV-Vis data. Dr. Raman Bahal, Dr. Arunava Manna, Wei-Che Hsieh, Dr. Shivaji A. Thadke and Dr. Danith H. Ly analyzed the data and wrote the paper.

4.1. Introduction

The design of molecules for tight and selective binding of biological targets, such as proteins and nucleic acids, is the cornerstone of bioorganic and medicinal chemistry. Despite the heroic efforts made by synthetic chemists, achieving both of these properties at a high degree still remains a challenge owing to their discordance. However, nature has devised a creative solution to this dichotomy. Instead of partitioning synthesis from recognition, many biological processes couple the two steps tightly through macromolecule-templated synthesis.^{1,2} Template-directed synthesis, in general, modulates the effective molarity of reactants, enabling highly diluted components to react with

astonishing efficiency and selectivity. In the case of biological polymerization processes, which involve the conjugation of consecutively assembled chemical building blocks into larger oligomeric systems, proximity-based reactions modify the avidity of the reactants. This allows the low-affinity but highly selective components to coalesce and bind tightly and selectively to the templated target. Such an example is DNA replication, a template-directed polymerization reaction occurring in every living organism on earth with unparalleled rate and fidelity and exceptional affinity and selectivity of the copied (daughter) strand for the parent template.

The concept of template-directed synthesis has long been recognized by chemists³⁻⁵ and effectively exploited in the synthesis of organic molecules⁶ and in the organization and assembly of a variety of macro- and supramolecular systems.^{7,8} Despite the appeal, such an approach has rarely been applied to the *in-situ* assembly of mutually reactive nucleic-acid building blocks for recognition of genetic materials in live cells and intact organisms, except in the context of prebiotic chemical synthesis.⁹⁻¹¹

To enable this process, the mutually reactive nucleic acid components would need to be chemically stable for a defined period, such that in the presence of template they would undergo template-directed concatenation. On the other hand, in the absence of template they would self-deactivate by undergoing an intramolecular (cyclization) reaction. We postulate that natural nucleic-acid biopolymers, DNA and RNA are highly flexible in conformation^{12,13} and tend to self-deactivate before concatenation takes place. Therefore, conformationally rigid nucleic acid analogues could be exploited to achieve *in-situ* assembly of mutually reactive nucleic-acid building blocks.

Gamma peptide nucleic acid (γ PNA) is a nucleic acid analogue in which the natural sugar-phosphodiester backbone of DNA is replaced by the chiral N-(2-aminoethyl)glycine unit.^{14,15} The gamma modification preorganizes single-stranded γ PNA into a right-handed motif to enhance the binding affinity and sequence selectivity toward endogenous nucleic acids.¹⁶ Compared to other conformationally rigid nucleic acid synthetic analogues, such as locked nucleic acids (LNAs)¹⁷, γ PNA is easier to chemically synthesize. We envision the rigid nature of γ PNA could impede the mobility of terminal reactive groups and thereby reduce the rate of intramolecular reaction. To assess the feasibility of this design concept, native chemical ligation (NCL) was selected because of its appealing native backbone product formation within γ PNA (**Figure IV- 1** and **Figure IV- 2**), bio-orthogonality, fast reaction kinetics, and the fact that such a reaction has been successfully demonstrated both *in vitro* and *in vivo*.¹⁸⁻²⁰

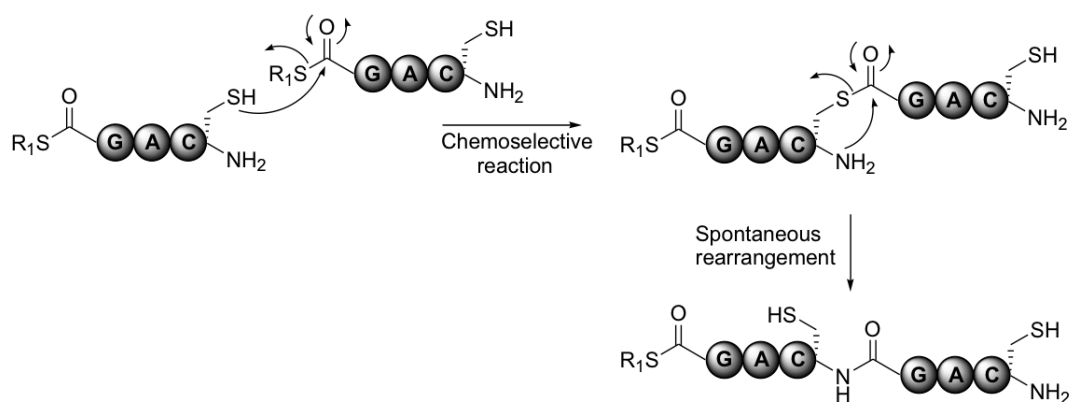


Figure IV- 1. Mechanism of native chemical ligation reaction.

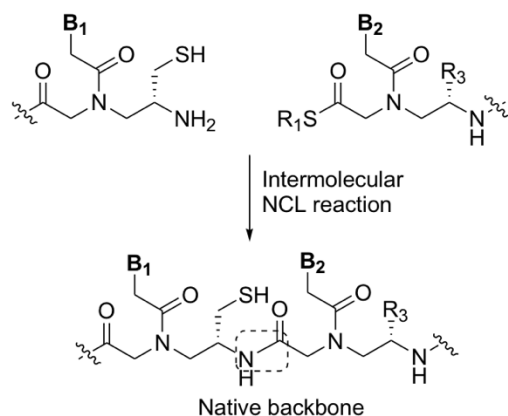
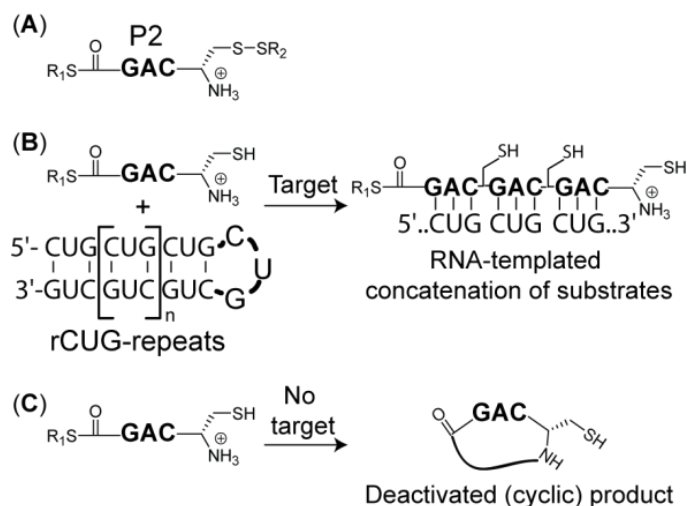


Figure IV- 2. Concatenation of two MP γ PNA units to form a product with a native amide backbone.

We selected 5'-G(CUG)_nC-3' as model RNA targets. This particular sequence is of biomedical interest because its expansion ($n > 40$ repeats) is responsible for the etiology of DM1, a debilitating neuromuscular disorder for which there is no effective treatment or cure. The pathogenicity of DM1 is largely attributed to RNA toxicity.²¹ Upon transcription, the expanded rCUG repeats (rCUG^{exp}) adopt an imperfect hairpin structure that sequesters the muscleblind-like protein 1 (MBNL1), an alternative RNA splicing factor, along with several other key regulators. Formation of the rCUG^{exp}-MBNL1 complex would not only prevent MBNL1 from performing its normal physiological function but would also trap the transcript in the nucleus, preventing its export to the cytoplasm for production of the essential DMPK protein. Thornton and co-worker showed that displacement of MBNL1 protein from rCUG_{exp} by a 25-nt morpholino oligonucleotide reversed the disease phenotypes in an animal model.²²

Here, we chose GAC γ PNA sequences to target the template rCUG repeats. (**Scheme IV- 1**) We demonstrated that the GAC γ PNA sequences are chemically stable in the oxidized state. Under simulated reducing environments, γ PNA oligomers were ready for RNA-templated concatenation, or self-deactivation within reasonable timeframe.



Scheme IV- 1. Reaction pathways of the triplet $MP\gamma$ PNA probe. (A) Probe in the oxidized state (in the extracellular environments). (B) Probe in the reduced state (in the intracellular environments) in the presence of RNA target. (C) Probe in the reduced state in the absence of target.

4.2. Results and Discussion

4.2.1. Probe Design

We designed a series of triplet miniPEG- γ -peptide nucleic-acid ($MP\gamma$ PNA)²³ probes containing a C-terminal thioester and an N-terminal cystine, along with the various controls (**Figure IV- 3A**). The N-terminal cystine was chosen to provide greater control of probe handling so that they would remain chemically stable until the disulfide bond was reduced—a chemical state mimicking that in the intracellular environments.²⁴ We selected 5'-G(CUG)_nC-3' as model RNA targets, for which $n= 1, 2, 4, 8,$ and 12 (**Figure IV- 3B**).

4.2.2. Synthesis of Probes

All Boc-MP γ PNA monomers were prepared from Boc-L-serine according to published procedures²³, except for the sulfhydryl-protected C and X monomers from Boc-Cys(Trt)-OH. (**Appendix IV- 1**) Probes were made on MBHA resin using Boc chemistry, purified by reversed-phase (RP) HPLC, and confirmed by MALDI-TOF. In the synthesis of probes containing a C-terminal thioester by conventional solid-phase peptide synthesis using Boc chemistry, there was concern for inverted deletions following removal of the Boc protecting group and neutralization of the amines (**Appendix IV- 2**). To mitigate this possibility, we performed the neutralization and coupling steps in-situ. (**Appendix IV- 3**) Such a condition provided reasonable chemical yields (~76%) and purities of P2 through 5 (**Appendix IV- 4**), with only minor deletion products. **Appendix IV- 5** shows a representative HPLC trace of crude P2.

However, under the identical conditions, we were not able to prepare P1. No precipitation occurred following the addition of diethyl ether to the cleavage mixture. Analysis of the crude sample by HPLC revealed several indiscernible baseline peaks (data not shown). We attribute the failure in the synthesis of P1 to the high conformational flexibility of achiral PNA, which presumably underwent rapid inverted deletions following the deprotection and neutralization steps (**Appendix IV- 2**).

4.2.3. Conformational Flexibility

We next determined the relative conformational flexibility of the probes by measuring the half-lives of the reactive intermediates following reduction of the disulfide bond. MALDI-TOF was chosen over HPLC and other analytical techniques in quantification of the reaction products because of the relatively short timescale of intramolecular NCL, which can be performed in less than 5 min. Dithiothreitol (DTT) was employed as a reducing agent. To assimilate the physiological conditions, all the experiments were performed at a physiologically relevant ionic strength (10 mM NaPi, 150 mM KCl, 2 mM MgCl₂; pH 7.4).²⁶

Initial experiments were performed at ambient temperature, at which P2 (1 μM) was incubated with DTT (100 μM, within the concentration range of glutathione in cells)²⁴ for 1 h. Under these conditions, we found that the disulfide bond was completely reduced, as evidenced by the loss of mass equal to 120 Da (**Figure IV- 4** and **Appendix IV- 6**). To our surprise, we noticed that the reduced acyclic form of P2 (P2*), with m/z of M-120 Da, remained intact without any trace of the cyclic P2 product (cP2) being formed. This was apparent from the absence of a chemical species with a mass of 1128 Da. This result is in line with the earlier finding that MPγPNA adopts an extended helical conformation,¹⁴ which significantly reduces the rate of intramolecular reaction in comparison to that of a more flexible achiral PNA.

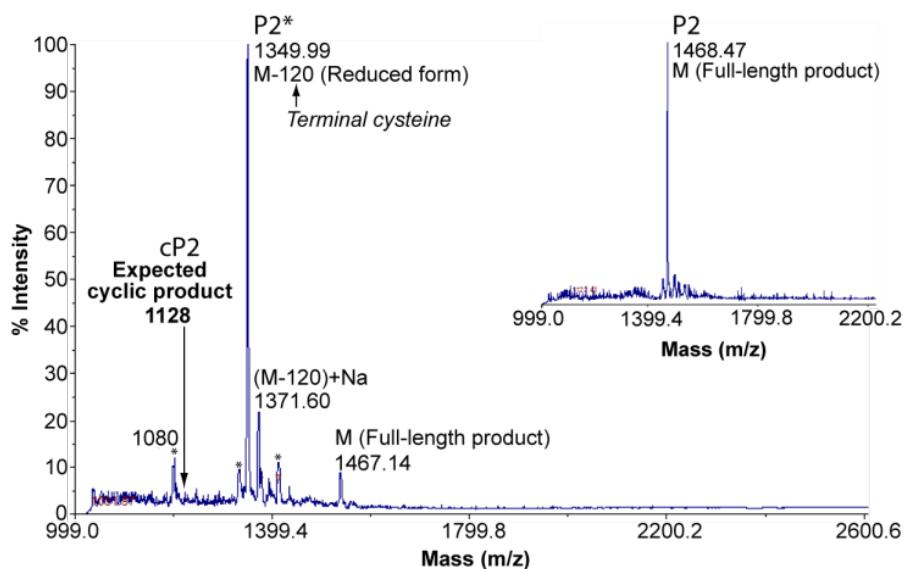


Figure IV- 4. MALDI-TOF spectrum of P2 at 1 μM concentration after incubation with DTT (100 μM) at an ambient temperature for 1 hr. *Inset:* MS spectrum of P2 ($M = 1468$ Daltons). The M-120 peak corresponds to the reduced acyclic P2*, and the 1128-Dalton peak to the cyclic cP2.

To assess the biological feasibility of this reaction, we monitored the progress of the reaction of P2 at physiological temperature (37 $^{\circ}\text{C}$) as a function of time and compared the results with those obtained with P3. The difference between the two probes is the degree of base-stacking interaction, which is more pronounced for P3 owing to the expanded tricyclic ring of G-clamp. Inspection of **Figure IV- 5A** reveals that the reduced acyclic P2* has $t_{1/2} \sim 1$ h. The conversion from an acyclic product into a cyclic product was complete within 3 h. On the other hand, examination of **Figure IV- 5B** shows that the reactive intermediate P3* has $t_{1/2} \sim 4$ h, which is four times longer than that of P2*. The kinetic profiles of the two probes are markedly different: those of P2* and cP2 follow exponential decay and growth (**Appendix IV- 7**), respectively, and those of P3* and cP3 follow sigmoidal profiles (**Appendix IV- 8**). The longer half-life of P3* is presumably attributed to the improved base-stacking interactions.

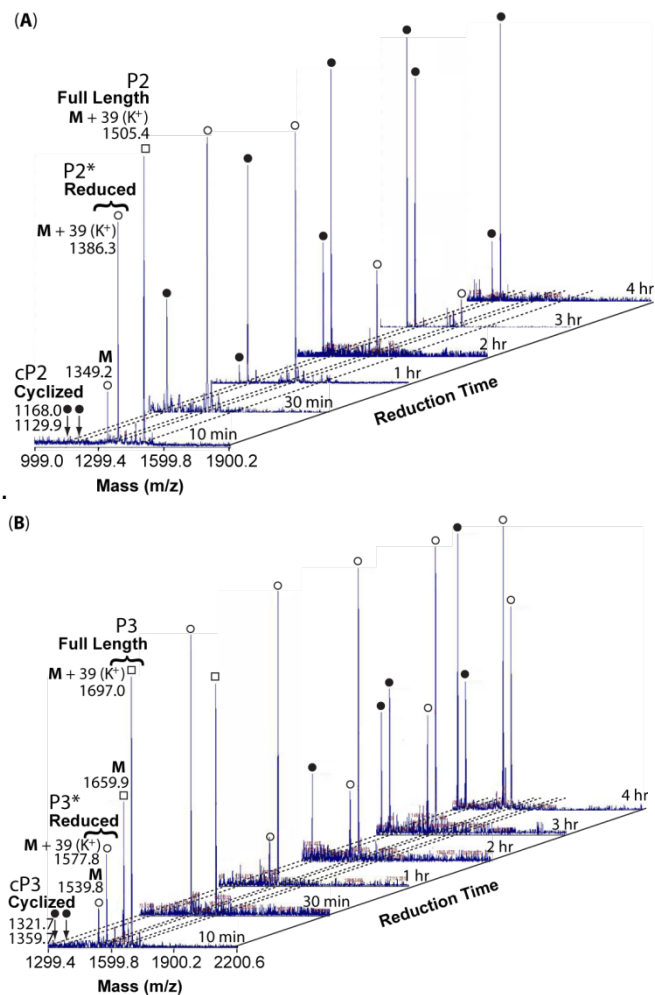


Figure IV- 5. MALDI-TOF spectra of (A) P2 and (B) P3 at 1 μ M each, following the incubation with DTT (100 μ M) at 37 $^{\circ}$ C. The samples were analyzed at the indicated time-points. Square: parent P2 and P3 probes, opened circle: reduced acyclic P2* and P3*, and filled circle: cyclic cP2 and cP3 products. Each chemical entity has two masses, corresponding to that of the parent probe and that containing a potassium ion (+39 Dalton).

Interestingly, even after 5 h we did not observe the formation of concatenated intermolecular P2 products in the absence of the RNA target (**Figure IV- 6**). One possibility could be due to the steric hindrance of the leucine residue at the C terminus and another could be due to the relatively low concentration of the probe. Overall, the data show that the lifetime of the reactive intermediate can be extended, if necessary, by increasing the degree of base-stacking interactions.

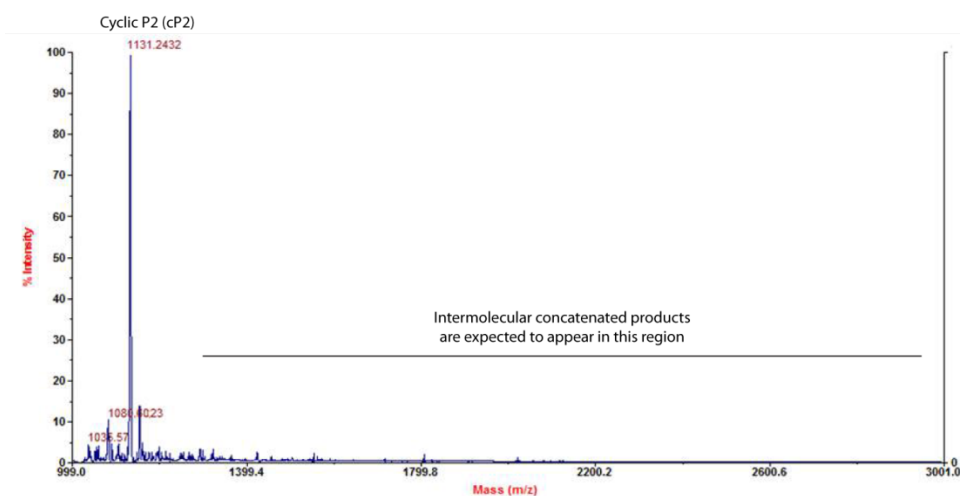


Figure IV- 6. MALDI-TOF spectrum of P2 probe. The sample was analyzed after incubation with DTT (100 μ M) at 37 $^{\circ}$ C for 5 hrs. Notice that only the cyclic product was observed.

4.2.4. Concatenation in the Presence of RNA

With this promising result, we next determined whether RNA could serve as a template for the concatenation of P2.

First, we determined the thermal stability of RNA. We found the thermal stability of $r(\text{CUG})_n$ remained fairly constant ($\sim 69^\circ\text{C}$) for $n=6, 8$ and 12 . (**Figure IV- 7**) This result was corroborated with literature: Beyond a repeat length of five, the thermal stability of $r(\text{CUG})_n$ remained fairly constant, with melting temperature (T_m) values in the $70\text{--}75^\circ\text{C}$ range.²⁷ This indicated that increasing the number of triplet repeats beyond five does not necessarily make the hairpin structure thermodynamically more stable. This finding suggests that rCUG repeats might be able to template P2 oligomerization.

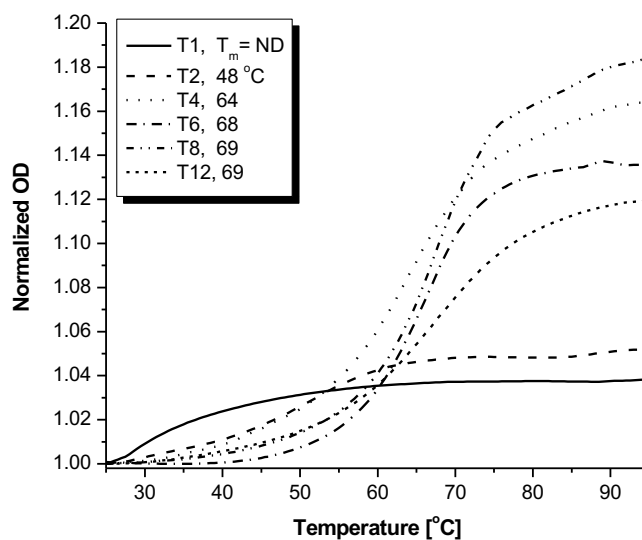


Figure IV- 7. UV-melting profiles of RNA targets. The concentrations of RNAs were as follows $12\ \mu\text{M}$ (T1), 6 (T2), 3 (T4), 1.5 (T8), and 1 (T12), prepared in a physiologically relevant buffer. Note that the concentration of CUG-binding sites in each sample was the same ($12\ \mu\text{M}$).

Next, we determined the effect of P2 on the thermal stability of RNA. **Figure IV-8** shows representative UV-melting profiles of T12 and its combination with P2 following their incubation with DTT at ambient temperature and at 37 °C for 1 h. At both incubation temperatures, the improvements in the thermal stability of T12 were similar, with ΔT_m values of approximately +20 °C, although the improvement was slightly less efficient at ambient temperature than at 37 °C, as inferred from the residual melting of unbound T12 in the 40–60 °C temperature regime. Neither DTT nor P2 alone had a notable effect on the T_m value of T12 (**Figure IV- 8, inset**). A similar experiment was performed with P3, but the T_m values were too high to be determined by UV-melting measurements (data not shown). In all of the experiments, we observed the T_m values of T4, T6, T8, and T12 to be significantly higher with DTT than without it (**Appendix IV- 9**).

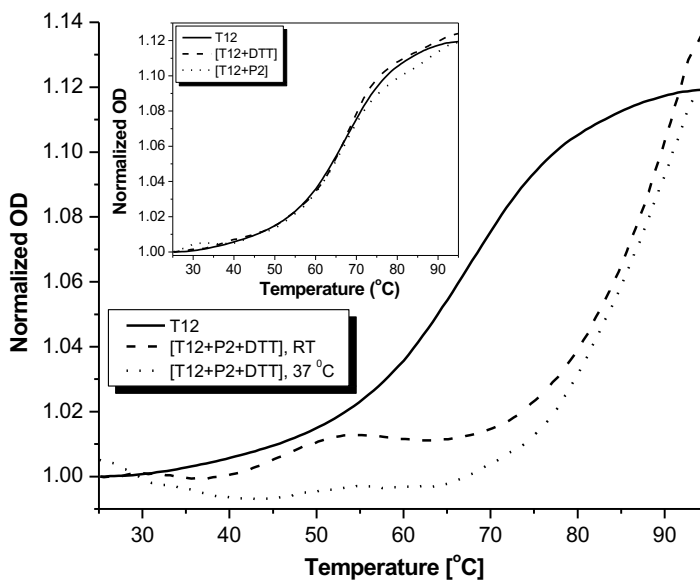


Figure IV- 8. UV-melting profiles of T12 and [T12+P2+DTT] samples, with the latter recorded after incubation at an ambient temperature and at 37 °C for 1 hr. The concentration of T12 was 1 μ M (corresponding to 12 μ M binding sites of P2); P2, 12 μ M; and DTT, 100 μ M. The samples were prepared by incubating the pre-annealed T12 with P2 and DTT at the indicated temperatures for 1 hr before subjecting to UV-melting analyses. *Inset*: UV-melting profiles of the negative controls carried out under identical conditions.

Similarly, neither the C-terminal amide probe P4 nor the single-base mismatched P5 had a net positive effect on the thermal stability of T12 following incubation with DTT (**Figure IV- 9**).

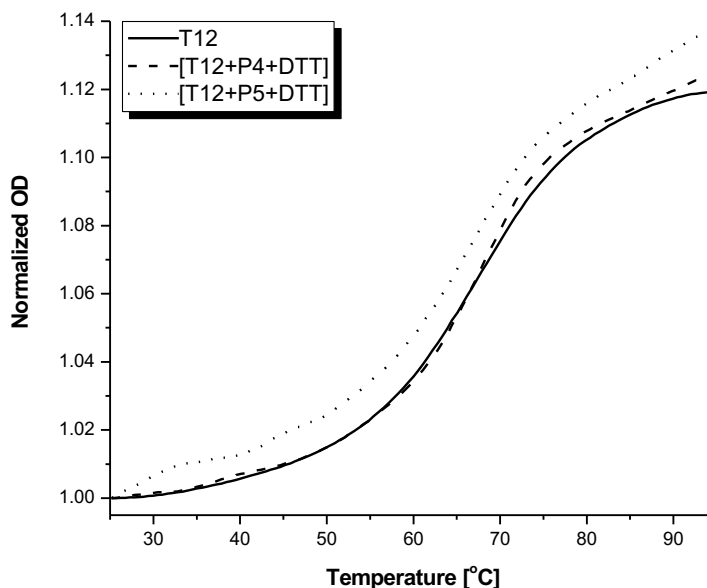


Figure IV- 9. UV-melting profiles of T12 with P4 and P5 in the presence of DTT. The concentrations of T12, P4, P5, and DTT were 1, 12, 12, and 100 μM , respectively. The mixtures were incubated at 37 $^{\circ}\text{C}$ for 1 hr prior to subjecting to UV-melting analyses.

The evidence for RNA-templated concatenation of P2 was further corroborated by MALDI-TOF analysis (**Figure IV- 10**), which showed new m/z signals corresponding to the concatenated products. However, we were not able to observe the formation of significant amounts of oligomeric products larger than a hexamer (6-concatenated probes). A likely possibility could be due to the unusually high binding affinity of this particular class of MP γ PNA molecules.¹⁴ Once formed, they remained bound to the RNA template, which could not be detected by MALDI-TOF, despite concerted efforts to dissociate the complex by addition of denaturants, such as urea and guanidine up to a certain point (4 mM), and by alkaline treatment. Nevertheless, the data show that the (CUG)₁₂-RNA hairpin

structure is capable of templating P2 concatenation, with the resulting products bound tightly and selectively to the RNA template.

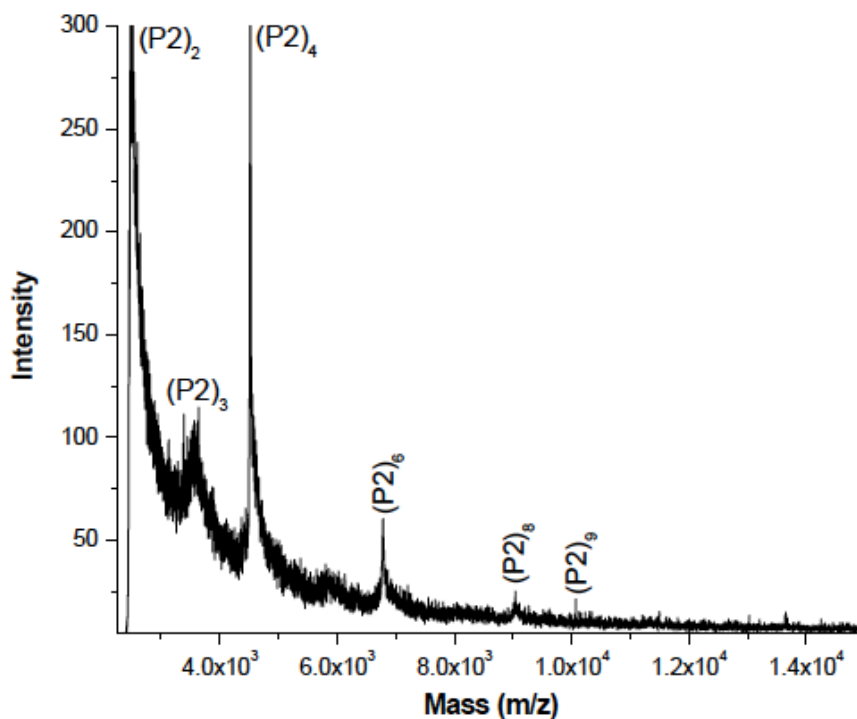


Figure IV- 10. MALDI-TOF spectrum of T12 with P2 and DTT after their incubation at 37 °C for 1 hr. The concentrations of T12, P2, and DTT were 1, 12, and 100 μ M, respectively.

4.3. Conclusions

A relatively short MP γ PNA probe, 3 nt in length, containing a *C*-terminal thioester and an *N*-terminal cystine, did not undergo immediate intramolecular NCL reaction upon reduction of the disulfide bond. The reactive acyclic P2* intermediate has a half-life of approximately 1 h at physiological temperature, which is well beyond a typical nucleic-acid hybridization timeframe.²⁸ The lifetime of the reactive species could be extended, if necessary, by increasing the π - π interactions of the nucleobases, as seen with P3. Despite the r(CUG)_n repeats (n>5) adopting their own secondary hairpin structures, the triplet nucleic-acid probe could still recognize the RNA targets and underwent template-directed concatenation.

Nucleic-acid-catalyzed oligomerization was previously demonstrated, in particular, by Lynn,²⁹ Liu,³⁰ and Seitz³¹; however, none of these systems contained mutually reactive *C*-terminal thioester and *N*-terminal cysteine moieties in the same nucleic-acid recognition module and none were designed to bind to biomedically relevant and structured RNA targets, such as CUG repeats. Overall, this work provides a proof of concept for the design of short nucleic-acid probes for targeting RNA-repeated expansions through template-directed oligomerization, lending possibility for the development of therapeutic interventions for DM1 and other related neuromuscular and neurodegenerative disorders. The potential benefits of such relatively small nucleic-acid probes for biological and biomedical applications are many, including the ease of chemical synthesis, structural and functional modifications, scale up (by solution as opposed to solid-phase chemistry), and improvements in pharmacokinetic properties relative to conventional antisense molecules.

4.4. Experimental Procedures

4.4.1. Solid-Phase Synthesis

Resin loading. 1 g of MBHA resin (1 mmol/g, Peptide International, RMB-2100-PI) was soaked in DCM in a reaction vessel for 1 hr, after which it was washed with DCM (3x) and then 5% DIEA in DCM (3x). The following solutions were prepared: (A) 30 mg of Boc-Leu-OH in 450 μ L DMF, (B) 55 mg HATU in 750 μ L NMP, and (C) 0.5 M DIEA in pyridine. The following coupling cocktail was prepared by adding 450 μ L of solution A into 3.5 mL NMP, followed by 460 μ L of solution C and 550 μ L of solution B, allowed to sit for 3 min, and then added to the resin. The coupling reaction was allowed to continue for 1 hr with gentle shaking. The solution was pushed out, and the resin was thoroughly washed with DMF (3x) and DCM (3x). The unreacted amino groups were capped by adding 5 mL of a solution containing (1:2:2, acetic anhydride:pyridine:NMP) to the resin and gently shaking the reaction vessel for 1 hr. After confirming by Kaiser test that the unreacted amino groups have been capped (colorless to pale yellow resin), the capping solution was pushed out and resin was thoroughly washed with DCM and then dried in an inline vacuum.

Coupling S-Trt mercaptopropionic (MPA) acid onto resin. Swell the resin (100 mg) in DCM for 1 hr. Boc was removed by treating resin with TFA:m-cresol (95:5) for 4 min (3x). Inert gas, argon in this case, was used to push the solvent out of the reaction vessel in order to minimize the prospect of oxidizing the thiol group. The resin was neutralized with pyridine washes (2x). The following coupling cocktail was prepared by mixing 150 μ L of 0.2 M MPA (in DMF) with 150 μ L of 0.2 M MDCHA (in pyridine) and 300 μ L of 0.1 M HBTU (in DMF), allowed to sit for 3 min and then added to the resin. The

coupling reaction was allowed to continue for 15 min with gentle shaking of the reaction vessel.

Coupling MP γ PNA building blocks onto the Leu-MPA-containing resin. Boc removal was performed under identical conditions as above, but the neutralization step was omitted for the rest of the oligomer synthesis to circumvent intramolecular cyclization and deletion of the subsequent units. In this case, neutralization was performed in-situ. After the treatment of resin with TFA:m-cresol and DMC (3x) and DMF (3x) washes, the following coupling cocktail was prepared by mixing 300 μ L of 0.2 M MP γ PNA (in DMF) with 150 μ L of 0.39 M HBTU (in DMF) and 150 μ L of 0.4 MDIEA (in DMF) and allowing to sit for 3 min, and then added to the resin. The reaction was allowed to proceed for 15 min by gentle shaking of the reaction vessel. The rest of the building blocks were coupled the same way.

Last coupling step. After coupling the MP γ PNA building block containing the cysteine side-chain (protected with Trt) at the γ -backbone, both Boc and Trt protecting groups were removed by treating resin with TFA:m-cresol (95:5) for 4 min (3x). Resin was thoroughly washed with DCM (3x) and DMF (3x). Argon was used to push out the solvent to prevent thiol oxidation. 300 μ L of 0.4 M Boc-Cys(Npys)-OH prepared in DMF was added to the resin, and the reaction permitted to take place for 2 hrs. Resin was then thoroughly washed with DMF (3x) and DCM (3x).

Deprotection and cleavage of oligos from resin. Boc was removed by treatment of the resin with TFA:m-cresol (95:5) for 4 min (3x). After removal of the last TFA:m-cresol (95:5) solution, 800 μ L of the cleavage cocktail consisting of TFMSA:TFA:m-cresol (2:8:1) was added to resin and the reaction vessel was gently shaken for 2 hrs. The solution

was collected in a 15-mL canonical tube, and the oligos were precipitated by adding 10 mL of ethyl ether into the mixture. Centrifugation, followed by 2 rounds of ethyl ether washes, the precipitate was air-dried and dissolved in 500 μ L of H₂O:ACN (85:15) solution.

4.4.2. HPLC Purification

PNA oligomer purification was done on Hitachi L-7000 series HPLC with C18 column at 40 °C. The purification conditions were: flow rate at 2 mL/min using water with 0.1% TFA and acetonitrile with 0.1% TFA.

4.4.3. MALDI-TOF MS Analysis

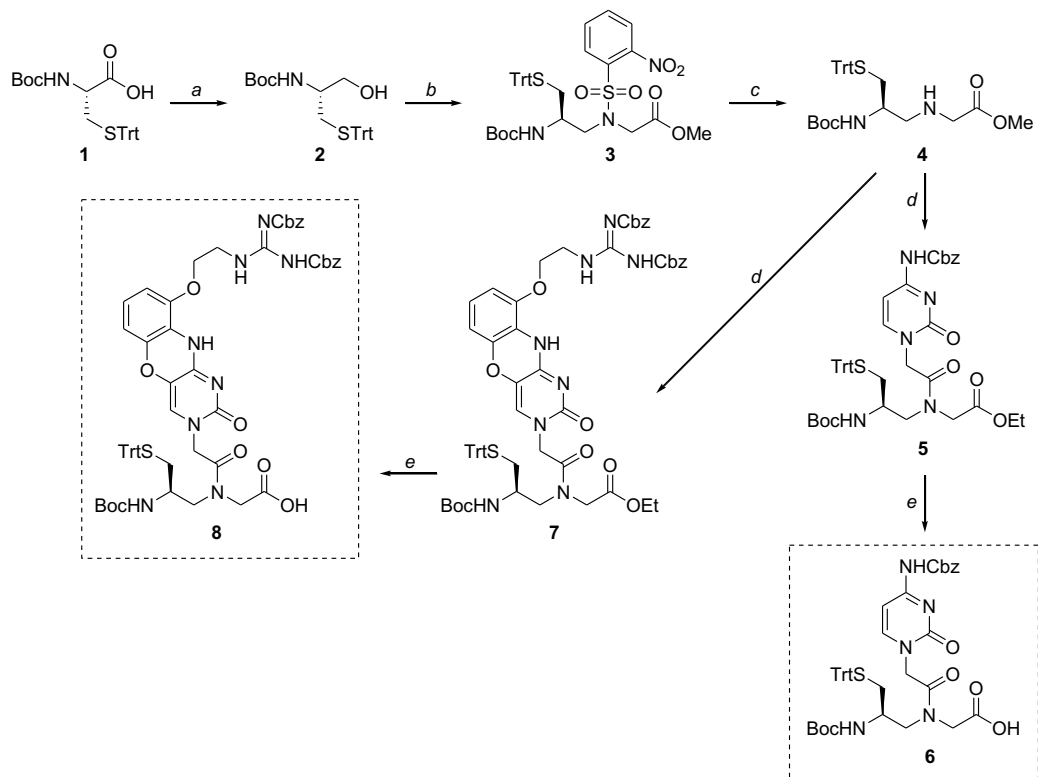
A solution of α -cyano-4-hydroxycinnamic acid (10 mg of α -cyano-4-hydroxycinnamic acid in 500 μ L of water with 0.1% TFA and 500 μ L of acetonitrile with 0.1% TFA) was used as the matrix for MALDI-TOF analysis. MALDI Analysis was performed about 5 minutes after spotting.

4.4.4. UV-Melting Experiments

MP γ PNA–RNA duplexes were hybridized by mixing stoichiometric amount of each oligomer strand in physiologically relevant ionic strength (10 mM NaPi, 150 mM KCl, 2 mM MgCl₂; pH 7.4) and incubated at 90 °C for 5 min, followed by a gradual cooling to room temperature. UV-absorption was monitored at 260 nm as the function of temperatures from 25 to 95 °C at the rate of 1 °C/min. Both the heating and cooling runs were recorded in order to assess the reversibility of the hybridization process. All recorded spectra were smoothed using a 5-point adjacent averaging algorithm. The first derivative of the melting curve was taken to determine the melting temperature of the duplex.

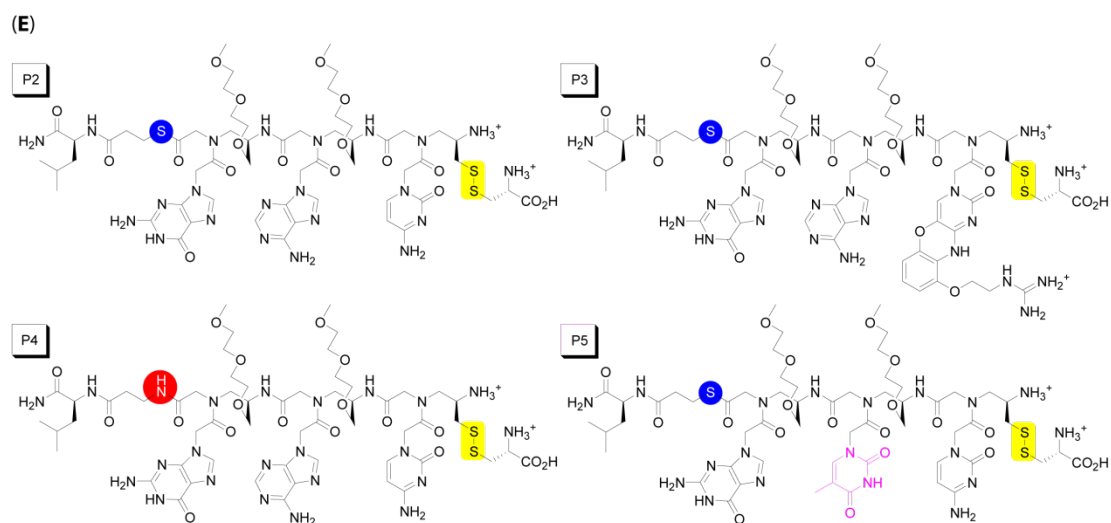
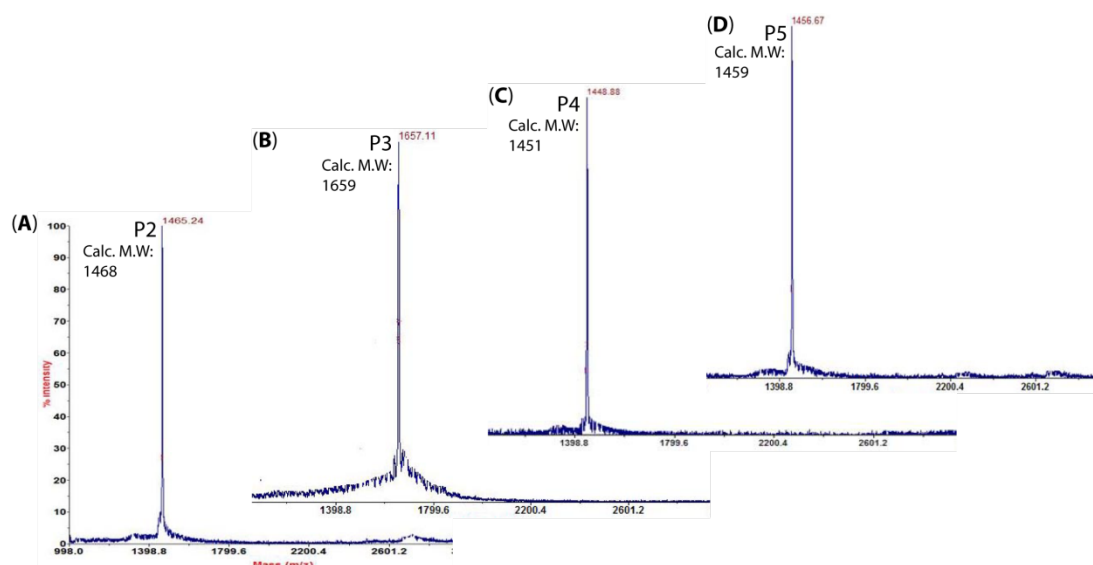
4.5. Appendices

Appendix IV- 1. Synthesis of cysteine-containing C and X monomers.

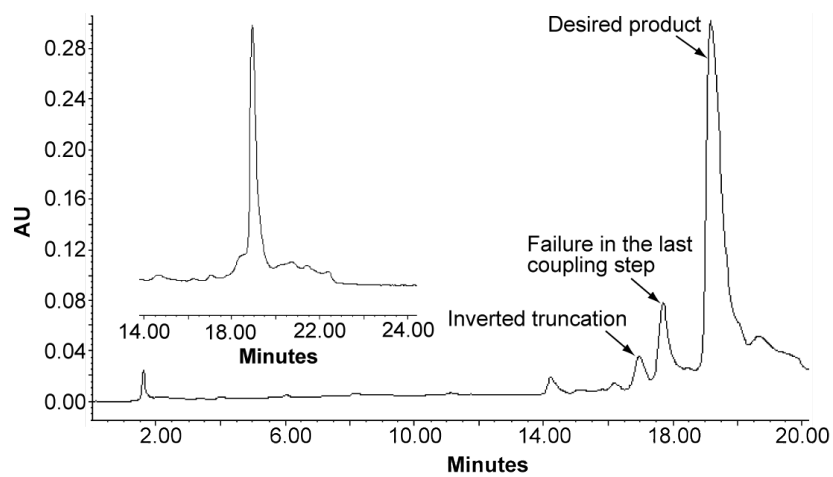


Reagents and conditions: (a) Isobutyl chloroformate, NaBH₄, NMM, DME, 0 °→ rt; (b) DIAD, (2-nitrosulfonyl)glycine ethyl ester, TPP, THF, 0 °→ rt; (c) Cs₂CO₃, thiophenol, THF, rt; (d) HBTU, NMM, DMF, rt; (e) 2 N NaOH/THF (1:1), 0 °C.

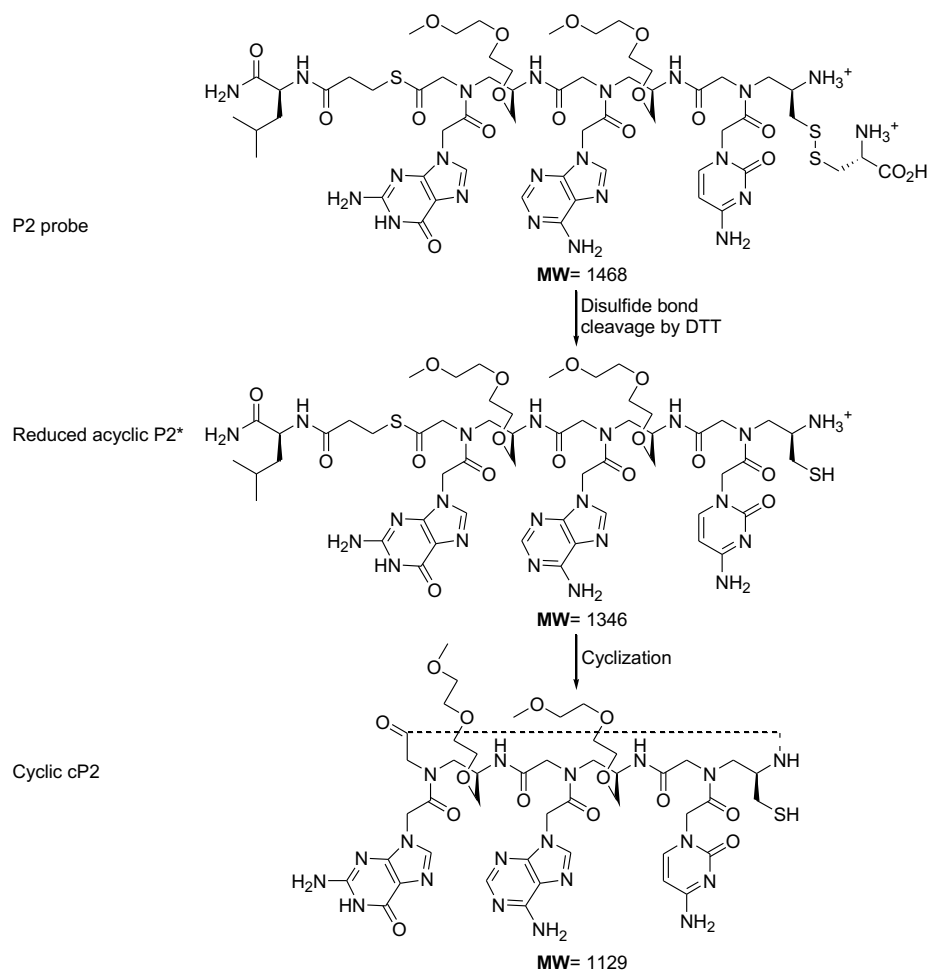
Appendix IV- 4. MALDI-TOF spectra of (A) P2, (B) P3, (C) P4, and (D) P5. (E) Chemical structures of P2 through 5. Calc. M.W. (M.W. found): P2, 1468 Daltons (1465 Daltons); P3, 1659 (1657); P4, 1451 (1448); and P5, 1459 (1457).



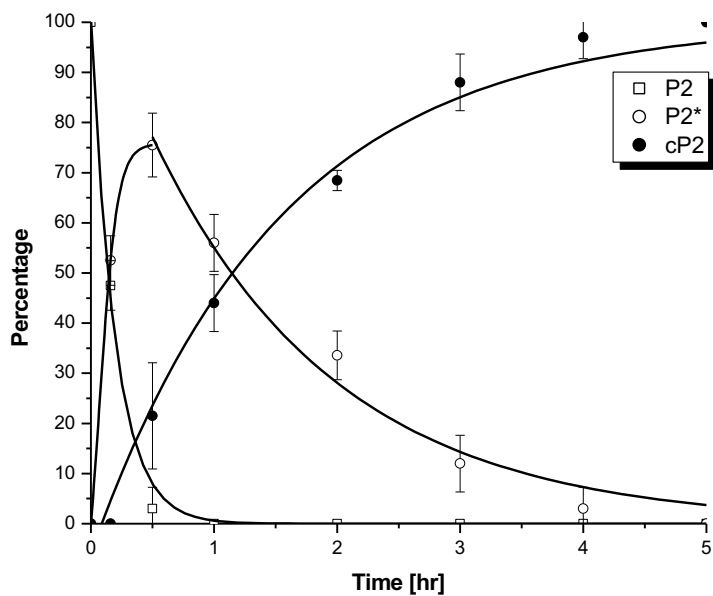
Appendix IV- 5. HPLC trace of crude P2. *Inset:* reinjection of purified P2.



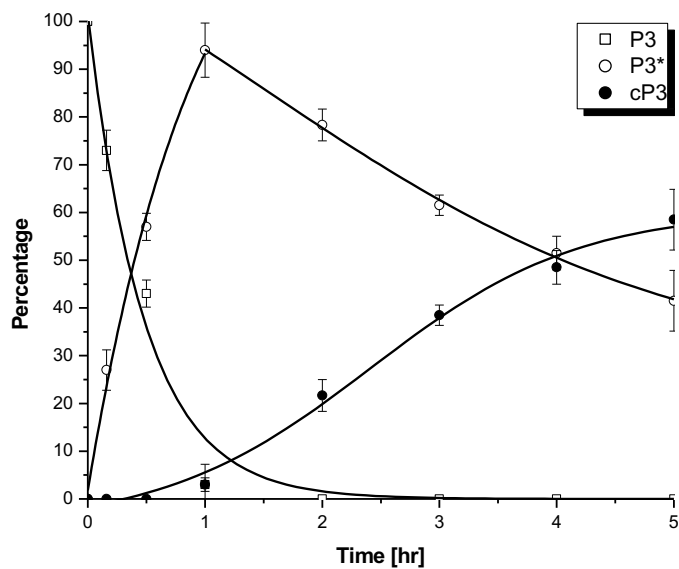
Appendix IV- 6. Reaction sequence of P2 probe.



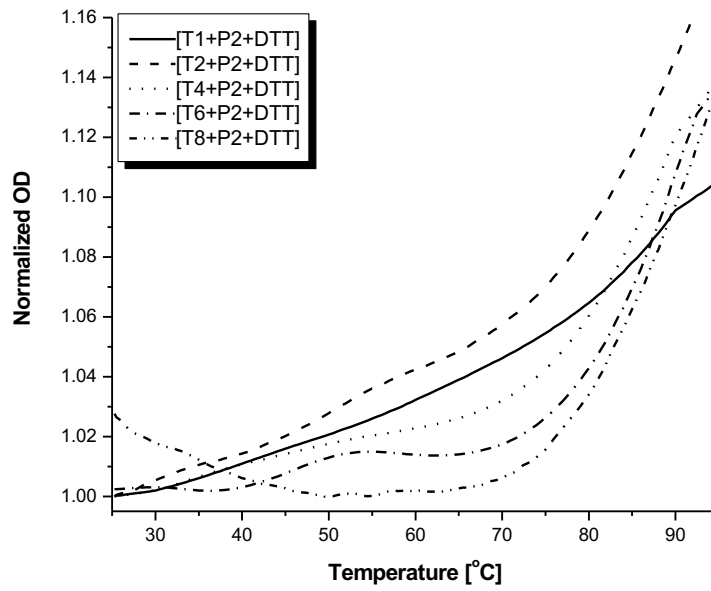
Appendix IV- 7. Reaction progress of P2. P2, parent probe; P2*, reduced acyclic form of P2; cP2, cyclic product of P2. P2 and P2* (with the latter starting from 0.5 hr) followed exponential decays, and cP2 followed exponential growth. Square, opened circle, and filled circle: experimental data, line: curve-fitting.



Appendix IV- 8. Reaction progress of P3. P3, parent probe; P3*, reduced acyclic form of P3; cP3, cyclic product of P3. P3 followed exponential decay, and P3* (starting from 1 hr) and cP3 followed sigmoidal decay and growth profiles, respectively. Square, opened circle, and filled circle: experimental data, line: curve-fitting.



Appendix IV- 9. UV-melting profiles of RNAs with P2 and DTT. The concentration of RNAs were: 12 μM (T1), 6 (T2), 3 (T4), 1.5 (T8), and 1 (T12); and that of P2 and DTT were 12 μM and 100 μM , respectively. The mixtures were incubated at 37 $^{\circ}\text{C}$ for 1 hr prior to subjecting to UV-melting analyses.



4.6. References

- (1) Li, X.; Liu, D. R. DNA-Templated Organic Synthesis: Nature's Strategy for Controlling Chemical Reactivity Applied to Synthetic Molecules. *Angew. Chem. Int. Ed. Engl.* **2004**, *43* (37), 4848–4870.
- (2) Gorska, K.; Winssinger, N. Reactions Templated by Nucleic Acids: More Ways to Translate Oligonucleotide-Based Instructions Into Emerging Function. *Angew. Chem. Int. Ed. Engl.* **2013**, *52* (27), 6820–6843.
- (3) Pedersen, C. J. Cyclic Polyethers and Their Complexes with Metal Salts. *J. Am. Chem. Soc.* **1967**, *89* (10), 2495–2496.
- (4) Dietrich, B.; Lehn, J. M.; Sauvage, J. P. Diaza-Polyoxa-Macrocycles Et Macrobicycles. *Tetrahedron Lett.* **1969**, *10* (34), 2885–2888.
- (5) Cram, D. J. The Design of Molecular Hosts, Guests, and Their Complexes. *Science* **1988**, *240* (4853), 760–767.
- (6) Gartner, Z. J.; Tse, B. N.; Grubina, R.; Doyon, J. B.; Snyder, T. M.; Liu, D. R. DNA-Templated Organic Synthesis and Selection of a Library of Macrocycles. *Science* **2004**, *305* (5690), 1601–1605.
- (7) Zhang, Z.; Zaworotko, M. J. Template-Directed Synthesis of Metal-Organic Materials. *Chem. Soc. Rev.* **2014**, *43* (16), 5444–5455.
- (8) Zhao, H.; Zhou, M.; Wen, L.; Lei, Y. Template-Directed Construction of Nanostructure Arrays for Highly-Efficient Energy Storage and Conversion. *Nano Energy* **2015**, *13*, 790–813.
- (9) Orgel, L. E. Unnatural Selection in Chemical Systems? *Acc. Chem. Res.* **1995**, *28*, 109–118.
- (10) Mansy, S. S.; Schrum, J. P.; Krishnamurthy, M.; Tobe, S.; Treco, D. A.; Szostak, J. W. Template-Directed Synthesis of a Genetic Polymer in a Model Protocell. *Nature* **2008**, *454* (7200), 122–125.
- (11) Higgs, P. G.; Lehman, N. The RNA World: Molecular Cooperation at the Origins of Life. *Nat. Rev. Genet.* **2015**, *16* (1), 7–17.
- (12) Gartner, Z. J.; Liu, D. R. The Generality of DNA-Templated Synthesis as a Basis for Evolving Non-Natural Small Molecules. *J. Am. Chem. Soc.* **2001**, *123* (28), 6961–6963.
- (13) Gartner, Z. J.; Kanan, M. W.; Liu, D. R. Expanding the Reaction Scope of DNA-Templated Synthesis. *Angew. Chem. Int. Ed. Engl.* **2002**, *41* (10), 1796–1800.
- (14) Dragulescu-Andrasi, A.; Rapireddy, S.; Frezza, B. M.; Gayathri, C.; Gil, R. R.; Ly, D. H. A Simple Gamma-Backbone Modification Preorganizes Peptide Nucleic Acid Into a Helical Structure. *J. Am. Chem. Soc.* **2006**, *128* (31), 10258–10267.
- (15) Verona, M. D.; Verdolino, V.; Palazzesi, F.; Corradini, R. Focus on PNA Flexibility and RNA Binding Using Molecular Dynamics and Metadynamics. *Sci. Rep.* **2017**, *7*, 42799.
- (16) Yeh, J. I.; Shivachev, B.; Rapireddy, S.; Crawford, M. J.; Gil, R. R.; Du, S.; Madrid, M.; Ly, D. H. Crystal Structure of Chiral γ PNA with Complementary DNA Strand: Insights Into the Stability and Specificity of Recognition and

- Conformational Preorganization. *J. Am. Chem. Soc.* **2010**, *132* (31), 10717–10727.
- (17) Wengel, J. Synthesis of 3'-C- and 4'-C-Branched Oligodeoxynucleotides and the Development of Locked Nucleic Acid (LNA). *Acc. Chem. Res.* **1998**, *32* (4), 301–310.
- (18) Dawson, P. E.; Muir, T. W.; Clark-Lewis, I.; Kent, S. B. Synthesis of Proteins by Native Chemical Ligation. *Science* **1994**, *266* (5186), 776–779.
- (19) Giriat, I.; Muir, T. W. Protein Semi-Synthesis in Living Cells. *J. Am. Chem. Soc.* **2003**, *125* (24), 7180–7181.
- (20) Yeo, D. S. Y.; Srinivasan, R.; Chen, G. Y. J.; Yao, S. Q. Expanded Utility of the Native Chemical Ligation Reaction. *Chem. Eur. J.* **2004**, *10* (19), 4664–4672.
- (21) Miller, J. W.; Urbinati, C. R.; Teng-Umnuay, P.; Stenberg, M. G.; Byrne, B. J.; Thornton, C. A.; Swanson, M. S. Recruitment of Human Muscleblind Proteins to (CUG)(N) Expansions Associated with Myotonic Dystrophy. *EMBO J.* **2000**, *19* (17), 4439–4448.
- (22) Wheeler, T. M.; Sobczak, K.; Lueck, J. D.; Osborne, R. J.; Lin, X.; Dirksen, R. T.; Thornton, C. A. Reversal of RNA Dominance by Displacement of Protein Sequestered on Triplet Repeat RNA. *Science* **2009**, *325* (5938), 336–339.
- (23) Sahu, B.; Sacui, I.; Rapireddy, S.; Zanotti, K. J.; Bahal, R.; Armitage, B. A.; Ly, D. H. Synthesis and Characterization of Conformationally Preorganized, (R)-Diethylene Glycol-Containing Gamma-Peptide Nucleic Acids with Superior Hybridization Properties and Water Solubility. *J. Org. Chem.* **2011**, *76* (14), 5614–5627.
- (24) Maher, P. The Effects of Stress and Aging on Glutathione Metabolism. *Ageing Res. Rev.* **2005**, *4* (2), 288–314.
- (25) Chenna, V.; Rapireddy, S.; Sahu, B.; Ausin, C.; Pedroso, E.; Ly, D. H. A Simple Cytosine to G-Clamp Nucleobase Substitution Enables Chiral Γ -PNAs to Invade Mixed-Sequence Double-Helical B-Form DNA. *Chembiochem* **2008**, *9* (15), 2388–2391.
- (26) Santoro, S. W.; Joyce, G. F. A General Purpose RNA-Cleaving DNA Enzyme. *Proc. Natl. Acad. Sci. U.S.A.* **1997**, *94* (9), 4262–4266.
- (27) Tian, B.; White, R. J.; Xia, T.; Welle, S.; Turner, D. H.; Mathews, M. B.; Thornton, C. A. Expanded CUG Repeat RNAs Form Hairpins That Activate the Double-Stranded RNA-Dependent Protein Kinase PKR. *RNA* **2000**, *6* (1), 79–87.
- (28) Yin, Y.; Zhao, X. S. Kinetics and Dynamics of DNA Hybridization. *Acc. Chem. Res.* **2011**, *44* (11), 1172–1181.
- (29) Li, X.; Zhan, Z.-Y. J.; Knipe, R.; Lynn, D. G. DNA-Catalyzed Polymerization. *J. Am. Chem. Soc.* **2002**, *124* (5), 746–747.
- (30) Heemstra, J. M.; Liu, D. R. Templated Synthesis of Peptide Nucleic Acids via Sequence-Selective Base-Filling Reactions. *J. Am. Chem. Soc.* **2009**, *131* (32), 11347–11349.
- (31) Vázquez, O.; Seitz, O. Templated Native Chemical Ligation: Peptide Chemistry Beyond Protein Synthesis. *J. Pept. Sci.* **2014**, *20* (2), 78–86.